" INVESTIGATION OF A SQUARE-BASED PYRAMIDAL-SHEET ROOF SYSTEM "

Thesis presented to the Faculty of Engineering in the University of London for the Degree of Doctor of Philosophy.

By

G. C. Wong Kong Ming, B.Sc.(Eng.), D.I.C.

Department of Civil Engineering,

Imperial College of Science & Technology. August, 1964.

ABSTRACT

This thesis describes an experimental and theoretical investigation of the stresses and deformations in a square-based pyramidal-sheet roof.

Four perspex pyramids were tested, and one beam of five perspex pyramids and one of seven pyramids. A larger steel model of seven pyramids was also tested to give a better idea of the behaviour of the thin metal structure.

Single pyramids were loaded at the apex, and strains and deflections measured when the base was fixed and simply-supported. Deflection measurements were taken with perspex trusses. The stress distributions in a pyramid of the steel truss and its base plate were obtained from strain measurements; the position of this pyramid in the span being varied. Deflections of the truss were also measured.

The theoretical work was divided into three parts,

(i) an approximate method was used to calculate the deformations of single pyramids and trusses. In this method, an equivalent skeletal system was used to replace the actual structure.

(ii) the stress distributions in a single pyramid having its base simply-supported and fixed and subjected to a vertical load at its apex were calculated. In both cases, the walls

were considered as plane stress problems having certain assumed boundary conditions.

(iii) an approximate method for calculating the buckling load limits of a pyramid was suggested. The pyramid wall was treated as a trapezoidal plate uniformly compressed along its two parallel edges.

The calculated deflections for the five exploratory models and the steel truss compared well with measured values. The theoretical stress distributions in the simply-supported pyramid were close to the experimental distributions but were less accurate in the fixed pyramid. The buckling load calculated for a pinned trapezoidal plate compared well with that obtained from test on one of the exploratory models.

ACKNOWLEDGEMENTS

I wish to express my deepest gratitude to Prof. S. R. Sparkes for his kindness in allowing me to work in his department and for his valuable advice, guidance and encouragement throughout the course of my work.

I owe special thanks to Dr. Z. S. Makowski for introducing me to the subject and for his help in the early stages of this work.

I also wish to thank Messrs. J. Neale and N. Scott and their staff of the Structures Laboratory and Workshop for their help in the preparation for the experimental work and the construction of the steel model, and Miss J. Gurr for taking the photographs.

I gratefully acknowledge the financial assistance received from the Scholarships Committee of the University of London in the form of a Postgraduate Studentship Award.

CONTENTS

CHAPTER 1

Introduction

1.1 Various types of hipped-plate or folded-plate structures have been in use for many years and their methods of analysis have become more and more sophisticated. A review of the different types of such structures together with their present methods of analysis is contained in a book by Born (1).

In recent years, however, a whole series of roof systems which may largely be called hipped-plate structures have been developed. These are the so-called stressed-skin space grids (2), in which a large number of three-dimensional sheet units are connected to a skin at their bases and to a plane grid system at their tops.

The roof system described in this thesis is a particular type of stressed-skin space grid. It consists of identical square-based pyramidal sheet units connected to a base plate and to a skeletal square grid at their apexes, Fig.1.1. Although two such roofs have actually been built, one for a hotel in Lagos, Nigeria (3), and the other, a temporary one, for the Architectural Congress building erected in London in 1961 (4), no attempt has so far been made to study its behaviour in any detail.

It should be mentioned that other variations of this roof system would basically be the same problem so long as the connecting units are symmetrical in form because the behaviour of a triangular plate is considered and this is common to all systems whether on a triangular, square or hexagonal base.

1.2 Advantages of these Sheet Roofs

The main reasons for using these roof systems may be enumerated as follows :-

i) Great rigidity. This means that greater clear spans can be covered and materials of low Young's modulus may be used. Sheets made from aluminium alloys have successfully been used (3,4) and there is little doubt that other materials, for example, structural plastics, plywood, etc. can also be used to advantage.

ii) Membrane action. Most of the applied loads are resisted by the pyramid walls by membrane action, bending being small.

iii) Great flexibility in use. The roof may be constructed either way up and may also be curved in elevation like a barrel vault, this being achieved by shortening or lengthening the members of the skeletal grid.

iv) No extra cover needed. This depends on the material used whether it is weather resistant and if not, whether it can be made so.

v) Easily manufactured, transported, stored and erected. This is because there are only three different parts to form the roof, namely, the pyramids, the base plate (which may be made up from smaller identical plates) and the grid members. The node connectors are also all identical.

vi) Unusual in form. The geometric patterns formed in these roofs by using different pyramid connectors are readily accepted by progressive architects and engineers who are always searching for the "new look" in buildings.

These and other advantages have already been mentioned by Makowski (2).

1.3 Considerations in design

The various factors to be considered in the design of a roof of the type under discussion are as follows:-

i) size and thickness of base plate,

ii) shape, size and wall thickness of connecting pyramidal units, and

iii) shape, size and length of top grid members.

The node connector needs only be sufficiently strong and stiff to transfer the load from the bars to the pyramid or vice versa. The method of connecting the bases of the pyramids to the base sheet depends on the material used in their construction. Glueing, riveting, welding, etc. may be used to give effective connections from the point of view of strength and rigidity.

Let us now look at the various parts of the roof in greater detail.

i) Base Plate.

The size of the base plate will obviously be fixed by the area of floor to be covered by the roof. In practice, this area will be too large for a single base plate to be used. But this can be overcomed by having it made up from smaller regular sheets so long as they are connected to act as though it is just one sheet. This implies that they have to be connected by lap joints.

The thickness of the base plate depends on which way up the roof is to be used. If the plate is in tension then its strength will be the criterion, but if it is in compression then buckling will probably control its thickness. The buckling criterion will depend on the size of the pyramids used since each base plate panel is governed by the size of the pyramid base. Practical considerations impose limits on the plate thickness also.

ii) Connecting Pyramids.

The shape of the pyramids may be said to be defined by the value of the angle of inclination of their walls to the horizontal i.e. by angle α in Fig.1.2. This together with the size of the base i.e. the value of b_2 determine the size of the pyramid.

The shape of a pyramid is an important factor since it controls the strength and buckling load of the pyramid as well as the overall rigidity of the roof. It controls the pyramid strength because the magnitudes of the components of any load applied at the apex of the pyramid in the planes of the walls depend on the angle α. Also, for a given value of b_2, the buckling load of the pyramid will decrease with increasing value of angle α. Finally, the rigidity of the roof varies as its height which in turn varies as the angle α for a given value of b_2.

The best shape for the pyramids, therefore, depends on whether strength, buckling or rigidity is the controlling factor in the design. These in turn depend on whether the pyramid walls are "thick" or "thin". If the walls are "thick" then strength considerations prevail while if the walls are "thin" buckling may be the controlling factor. Rigidity is seldom the criterion.

In Fig. 1.2, the plot of k (the ratio of height of the pyramid to its base dimension) versus β (the angle of inclination of the sloping edges of the walls to their bases) defines the shape of a pyramid. The angle β can only lie between 45 and 90 degrees. The straight portion of this graph may be taken to give good shapes for the pyramid since they appear to be well proportioned. In this research, a value of $\beta = 63^\circ\ 26'$ or b_2=h (i.e. $\alpha = 60^\circ$) has been chosen as the shape of the pyramids. This value of β is very nearly the mean value in the linear range.

Having decided on a "reasonable" shape for the pyramid, it is then possible to select a "reasonable" number of pyramids, which will be equivalent to choosing a size for the pyramids, as follows:-
Let the size of the roof be L x B (Fig. 1.3). Since a whole number of pyramids must be used, λ = L/B must be a whole number. For the shape chosen, the height of the pyramid H= $0.866b_2$. If n is the number of pyramids, then $B = nb_2$ so that H = 0.866B/n. The curve of H versus 1/n for a fixed value of B is shown in Fig.1.3. From this curve, it is seen that if B = 10 feet, and if n = 8, then H $\simeq$ 1.08 feet and b_2 = 1.25 feet. This seems a good H/B value considering that the height of the roof from the ground may be of the order of 15 feet, say. However, if B = 100 feet, then using the same number of pyramids, H = 10.8 feet and b_2 = 12.5 feet. Even allowing for the fact that the height of the roof from the ground for a roof of this size may be 30 feet or so, this depth of roof is clearly excessive. Hence, it is clear that as B increases, the

H/B value should decrease. For more realistic values of H for practical cases, the curve of H versus B given in Fig.1.3 is suggested. This gives H = 4.33 feet for B = 100 feet and n = 20. This H/B value of 0.043 may be considered small and a higher value may be suggested as a better alternative, but it should be remembered that with a larger roof and for a certain method of supporting it, the loads on the pyramids are greater and they are more likely to suffer from instability.

In considering the thickness of the pyramid walls, the material of the walls will decide whether they are to be "thick" or "thin". For example, if structural plastics or plywood were used then the walls will be "thick," while if aluminium sheets were used, they will be "thin." For "thick" walls, strength will be the primary consideration while for "thin" walls, stability will be important.

iii) Grid Members.

The length of these members depends on the size of the pyramids. Their shape is not important but in general, tubes may be used if they are in compression and solid bars if in tension. Strength is the main consideration in the determination of their cross-sections since buckling is unlikely even if they are in compression as they are usually short. However, if they are in compression, the lower compressive stress has to be used in their design.

1.4 Design Procedure

Given a rectangular area to be covered by the roof, the shape and size of the pyramids to be used are chosen as outlined in section 1.3(ii). The roof is then replaced by an equivalent skeletal system whereby the areas of the walls of the pyramids and base plate panels are assumed to be concentrated at their junctions to form skeletal members (Chapter 2). This equivalent system is considered to be pin-connected. The method of supporting the roof may introduce redundancies but so long as the roof itself is statically determinate it is a simple matter to calculate the forces in the skeletal members.

The grid member sustaining the heaviest load is then designed. All the other grid members will be made identical to it. The thickness of the base plate can then be designed by considering the strength or stability of the most critically loaded panel assuming it to be biaxially uniformly loaded together with uniform shears along the edges. For the pyramid walls, since the loads at its apex are known, the most heavily loaded pyramid can also be designed for strength and stability. Finally, the maximium deflection of the roof can then be checked by reverting to the equivalent system since the areas of all the members are now known.

1.5 Aims Of Research Work

In view of what was said in the last section, the research programme was designed to investigate the following issues:-

i) Validity of the skeletal system analogy.

A method of calculating the cross-sectional areas of the members of the equivalent system was suggested. Certain assumptions were made. Experimental results would verify whether the analogy could be used to predict forces in the grid members and the deflections of the roof. Models of single pyramids and "trusses" of an exploratory nature as well as an accurate large-scale steel model were tested for this purpose.

ii) Strength of pyramids.

In this connection, the load distribution in the pyramid walls were determined experimentally as well as by an approximate theory. Tests on single pyramids having simply-supported and fixed base conditions subjected to vertical as well as horizontal loading at their apexes were carried out. In addition, the stresses in a pyramid having the same base boundary conditions as those in the complete system were measured, the model used being the steel model mentioned in (i). These investigations would serve to indicate where the maximum stresses occurred in the pyramid walls.

iii) Buckling of pyramids.

It was hoped that some approximate method would be arrived at to calculate the initial buckling load of a pyramid. An exploratory model was used to supply a comparison with the theory. Accurate buckling tests were not envisaged as such tests would be difficult to control.

CHAPTER 2

Exploratory Models

2.1 Small-scale models were made and tested for the following reasons,

i) to get a feel for the problem. The roof being a three dimensional folded-plate structure was difficult to visualise. The various junctions between the walls, base plate and bars were complicated.

ii) to study the general behaviour of single pyramid and truss units. This would give a good indication of the way in which these units would behave when they were part of a whole roof.

iii) to obtain an indication of a probable method of analysis. This suggested the possibility of treating the roof as an equivalent skeletal space system in the estimation of deflections (see section 2.5).

The experience obtained with these exploratory models helped towards the making and testing of future models in the way that they were most useful for the objectives under consideration.

These exploratory models investigations were important because this type of roof system has not been studied in any detail before. The only available experimental work consisted of the loading of an aluminium sheet pyramid to failure by a horizontal load at its apex, its base being fixed (4).

2.2 Description of models

Five small-scale models were made in perspex, three of single pyramids and two of a strip of the sheet roof (a truss), Figs. 2.1 to 2.5. Perspex was used because it was well suited since its properties and behaviour under load was well known. Also, it was easily cut to size and then glued together with Tensol cement No. 7 to form the models. Finally, it was easily available in various sizes and thicknesses and, more important, with sufficient flatness required in the models.

All the models had pyramids of the same shape since as stated in Chapter 1, this research was to be concerned with pyramids of one shape only; this shape being a good and convenient shape for the pyramids. The size of the pyramids, however, were not all the same so that the effect of size on their behaviour could be studied. Also, the base boundary conditions were not the same in all models.

These models were simple models, which were easily made with sufficient accuracy for the purposes they were required to serve. Their dimensions had been chosen arbitrarily but each differed from another in the way that they served different purposes as discussed later in this chapter.

The models may briefly be described as follows:-

Model A - (Fig. 2.1) shows a pyramid with a 3 inch square base and 0.04 inch thick walls, glued to a 0.04 inch thick base sheet.

Model B - (fig. 2.2) shows a pyramid of the same dimensions as Model A but is connected to a 0.25 inch thick base plate.

Model C - (Fig. 2.3) shows a pyramid with a 4 inch square base and 0.04 inch thick walls, joined to a 0.04 inch thick base plate.

Model D - (Fig. 2.4) shows a truss consisting of seven 3 inch pyramids with 0.04 inch thick walls connected to a base plate 0.04 inch thick and to a 1/3" x 1/16" flat at their apexes. The top flat was later replaced by six short strips of the same size to span between the apexes of the pyramids. This modified model will be referred to as Model D'.

Model E - (Fig. 2.5) shows a truss of five 4 inch pyramids with 0.04 inch thick walls connected to a 0.04 inch thick base plate and a 3/4" x 1/4" beam. There was a total of ten resistance strain gauges on the model.

2.3 Model tests

Model A. Vertical loads were applied to the apex of the pyramid by means of dead weights as shown in Fig.2.6. Vertical deflections corresponding to these loads were measured by using a dial gauge capable of reading to an accuracy of ten thousandth of an inch. During the test, the model rested on a thick steel beam whose deflections were negligible compared with those of the pyramid itself. The load/deflection curves for the test are shown in Fig.2.7.

Model B was loaded in the same way as Model A. The relation between load and deflection for the apex of the pyramid is shown in Fig.2.7. In addition, the model was later tested to destruction in the loading device shown in Fig.3.5 of Chapter 3. The load/deflection curve is shown in Fig.2.8.

Model C was loaded in the same way as Model A. Vertical deflections of the apex were measured and the load/deflection graph is shown in Fig.2.7.

Model D was simply supported on a knife edge and a roller at its ends over a span of 22.75 inches; firstly with the pyramids pointing upwards (the normal position) and then with them pointing downwards. In each position, two loading cases were considered. The loading cases were,

Case 1 - Pyramids pointing upwards with central point load, Fig.2.9.

Case 2 - Pyramids pointing downwards with central line load, Fig.2.10.

Case 3 - Pyramids pointing upwards with two equal point loads on third pyramids from each end. Fig. 2.11.

Case 4 - Pyramids pointing downwards with equal line loads on third pyramids from each end. Fig.2.12.

The general set-up of the tests and the method of loading and measurement of deflections by dial gauges were similar to that used in the tests on Model E as shown in Figs.2.14 and 2.15. The load/deflection graphs for the above four loading cases are given in Figs.2.9 to 2.12.

Model D' was tested in exactly the same way as that of case 2 for Model D. However, downward deflections were measured at two points only as shown in Fig.2.13 which also shows their load/deflection graphs.

Model E was tested on a simply supported span of 21.5inches.

The loading cases were as follows,

Case 1 - Pyramids pointing upwards with two equal point loads on second pyramids from each end, Fig.2.16.

Case 2 - Pyramids pointing downwards with two equal line loads on second pyramids from each end, Fig.2.17.

The set-up for the tests and loading cases 1 and 2 are shown in Figs.2.14 and 2.15. respectively. The load/deflection graphs for the positions whose downward displacements were measured are shown in Figs.2.16 and 2.17. In addition, the surface strains at the five positions on the model were measured and their load/stress curves are given in Figs.2.18 and 2.19.

2.4 Comments on results

Fig.2.7 - The deflection was much the same in each of the three models. For a load of 20 lbs., the deflections were as follows,

Model	A	B	C	
Deflection	1.8	1.5	1.9	($\times 10^{-3}$ ins.)

The deflections in Models A and C were therefore the same as predicted by approximate theory in section 2.5.

Fig.2.8 - The load/deflection graph was linear till buckling occurred at a load of 195 lbs. at point A. The graph continued to be linear but with a reduced slope due to buckling. More of the load was being shedded from the centre portions of the walls to their edges due to shear lag until point B was reached when there was a stiffening effect due to tensile stresses being developed in the middle part of the walls. The top of the model crushed inwards

when a load of about 367 lbs. was reached. In Chapter 6, an attempt was made to estimate the buckling load for this model.

Figs.2.9 and 2.10 ·· The deflections at the points shown due to a central load of 10 lbs. were as follows,

Point	1	2	3		
Defln.	23	20	13	(x 10^{-3} ins.)	Case 1
"	34	25	17	"	Case 2

The deflections for the corresponding points in case 2 were larger because of both the force of the dial gauge spindles and the buckling of the panels since the deflections were measured at mid-panel and the panels were in compression.

Figs.2.11 and 2.12 ·· For loads of 5 lbs. each, the deflections measured at the various points were,

Point	1	2	3	4	5		
Defln.	19	17	5	18	-	(x10^{-3} ins)	Case 3
"	27	20	24	12	24	"	Case 4

The deflection of point 2 in case 4 was very nearly the same as that for point 1 in case 3 because the effect due to the force of the dial gauge spindle was compensated by the upward buckling of the panel brought about by the action of the loads on adjacent panels. On the other hand, the much larger deflection at point 1 in case 4 over that at point 2 in case 3 was due to the dial gauge spindle force as well as buckling of the panel. In case 4, the deflection at point 5 would have been greater than that at point 3 but for the compression of the walls of the middle pyramid.

Fig.2.13 - For a central load of 10 lbs., the deflections were,

Point	1	2	
Deflection	74	66	(x 10^{-3} ins.)

The deflection at point 1 was more than twice that for the corresponding point in Model D, Fig.2.10. This was due to the connecting member being smaller in size and consisting of separate members. The bending strain energy therefore became much more significant in this case. In section 2.5, the deflection calculated for this point neglecting bending strain energy was only about half the experimental value.

Figs.2.16 and 2.17 - The non-linearity of the load/deflection graphs shows that in this model, the base panel of the central pyramid was initially curved. The force of the dial gauge spindle in this case had greater effect on the deflection since the panel was greater in size. In case 2, the deflection at the mid-point of the central panel was much greater than in case 1 because of buckling. The deflections at the other points for loads of 5 lbs. each were,

Point	1	2	3	4	5		
Defln.	7	6	3	6	-	(x10^{-3}ins)	Case 1
"	-	8	4	8	2	"	Case 2

In both cases, deflection at point 4 would have been greater than that at point 2 but for the shortening of the pyramids. The deflections were smaller than in corresponding cases for Model D because of the shorter span of the model and the bigger connecting member.

Figs.2.18 and 2.19 - Due to the symmetrical loading, there was no stress at point 5 in both cases. In case 1, there was a greater difference in surface stresses at low loads at point 4 which again showed that the central panel was initially curved. In case 2, the large differences in the surface stresses at this point showed that this panel was buckled. The mid-plane stresses at the various points for loads of 5 lbs. each were as follows,

Point	1	2	3	4	5	
Stress (p.s.i)	-78	72	-55	24	0	Case 1
"	79	-70	55	-24	0	Case 2

At point 4 in case 2, although the panel was buckled the mid-plane stress was equal in magnitude to that in case 1. In each case, the magnitudes of the stresses at points 1 and 2 were very nearly equal as they were expected to be. In section 2.5, some simple calculations were made to estimate the mid-plane stresses at these points for comparison.

2.5 Approximate Calculations For Models

(a) Vertical deflection of a single pyramid due to a vertical point load at its apex.

A single square-based sheet pyramid is shown in Fig.2.20(a). The walls and base of the pyramid are assumed to be initially flat. Since the wall and base thicknesses are small compared with the overall dimensions of the pyramid, the greater part of the applied vertical load at the apex will be taken by the junctions between the walls and transferred to the junctions between the walls and base plate. This suggests the use of an "equivalent skeletal system" of the type shown in Fig.2.20(b) for an approximate estimation of deflections. The stresses in the pyramid are mainly membrane stresses and bending is negligible. Therefore, in the equivalent system, only direct strain energy will be considered in calculating deflections. This means that the equivalent system can be considered as pin-connected.

The forces in the members of the equivalent system can then be determined. In order to estimate the cross-sectional areas of these members, the stress distribution in the walls and base plate of the pyramid must be known so that an effective breadth concept may be applied. That is to say that it will then be possible to calculate the distance from the junction which will be sufficient to sustain the component of the computed force in the direction of the vertical stresses in the wall. The stress distributions in the walls of the single 12 inch perspex model tested in Chapter 3 show that for this shape of pyramid, the amount of shedding of the load to the junctions of the walls were insufficient to call for the exclusion of any part of the walls as ineffective. There is no available stress distribution in the base plate but it will also be assumed that the whole plate will be effective. Having assumed that all the area of the walls and base plate are to be considered in working out the size of the members of the equivalent system, it seems most convenient to distribute this area as shown in Fig.2.20.

That is, 2/3 of the material of each wall will be considered to make up a diagonal member while 1/3 and 1/4 of the material of the wall and base plate respectively will form a base member.

Calculations

Referring to Fig.2.20;

Let cross-sectional area of inclined members be A_i.

Let cross-sectional area of base member be A_b.

Then,
$$A_i = \frac{(2 \times \text{area } ADB) h_w}{\text{length } AB}$$

and
$$A_b = \frac{(\text{area } BDC \times h_w) + (\text{area } BOC \times h_b)}{\text{length } BC}$$

Since areas ADB and BDC are each assumed to be equal to 1/3 the area of a wall and area BOC as 1/4 the area of the base plate, then

$$A_i = \frac{2}{3\sqrt{5}} L h_w \qquad \text{———} \quad (1)$$

and
$$A_b = \frac{1}{12} L h_w \left(2 + 3\frac{h_b}{h_w}\right) \qquad \text{———} \quad (2)$$

Force in inclined members,

$$F_i = -\frac{\sqrt{5}}{4\sqrt{3}} P \qquad \text{(i.e. compression)}$$

and, force in base members,

$$F_b = \frac{1}{4\sqrt{3}} P \qquad \text{(i.e. tension)}$$

If V = the total direct strain energy in the structure, then the vertical deflection of the apex of the pyramid due to the applied load P is given by

$$\delta_v = \frac{\partial V}{\partial P} = \Sigma \frac{Fl}{AE} \cdot \frac{dF}{dP}$$

where F is the force in a member of length l, cross-sectional area A and Young's modulus E.

Substituting for the forces and cross-sectional areas obtained above,

$$\delta_v = \frac{P}{Eh_w}\left\{1.56 + \frac{1}{(2+3\lambda)}\right\} \qquad \text{——} \quad (3)$$

where $\lambda = h_b/h_w$

The deflection is therefore independent of the size of the pyramid. It should be restated that this will only be true for the shape of pyramid considered and if there is no buckling of the walls of the pyramid. As far as the shape of the pyramid is concerned, it is very probable that it has little effect on the calculated deflection except when it differs from the above shape very significantly.

Comparison with measured deflections for Models A, B and C:

For all three models,

Young's modulus, E = 4.5×10^5 p.s.i.

$h_w = 0.04$ in.

For Models A and C, $h_b = 0.04$ in. $\therefore \lambda = 1.$

For Model B, $h_b = 0.25$ in., $\therefore \lambda = 6.25$ i.e. the second term in expression (3) can be neglected.

For a load of 20 lbs., i.e. P = 20 lbs., the deflections calculated by using expression (3) for the models are,

	Calculated δ_v (in.)	Measured δ_v (in.)
Model A	0.0020	0.0018
" B	0.0017	0.0015
" C	0.0020	0.0019

(b) Deflection of a pyramidal truss unit.

The equivalent skeletal system method will also be used in calculating the deflections of a pyramidal truss unit. The space frames shown in Figs.2.21 and 2.22 are the equivalent systems for Models D and D' and Model E respectively. The cross-sectional areas of the various members of the frames are calculated in the same way as before. Only direct strain energy will be considered so that the frames are assumed to be pin-connected.

The expressions for calculating the vertical deflection of the apex of the central pyramid in each model for various loading conditions are as follows,

Model D

Case 1. $\delta = \frac{P}{Eh_\omega}(9.33a + 22.94)$

Case 2. $\delta = \frac{P}{Eh_\omega}(9.33a + 20.68)$ — also for Model D'.

Case 3. $\delta = \frac{P}{Eh_\omega}(16.67a + 36.83)$

Case 4. $\delta = \frac{P}{Eh_\omega}(16.67a + 35.83)$

Model E

Case 1. $\delta = \frac{P}{Eh_\omega}(5.33a + 16.58)$

Case 2. $\delta = \frac{P}{Eh_\omega}(5.33a + 15.98)$

where,

$a = Lh_\omega/A_1$, L = width of truss, h_ω = pyramid wall thickness,

A_1 = cross-sectional area of bar.

Note that the cross-sectional areas of diagonal members, longitudinal and end transverse base members, and internal transverse base members are $\frac{2}{3\sqrt{5}}Lh_\omega$, $\frac{5}{12}Lh_\omega$ and $\frac{7}{12}Lh_\omega$ respectively from expressions

(2.1) and (2.2) when $l_w = l_b$.

For a total load of 10 lbs. on the models, the calculated deflections compare with the measured values as follows,

Model D	Case 1	Case 2	Case 3	Case 4
Cald. Defln.	0.021"	0.019"	0.017"	0.017"
Exptl. Defln.	0.023"	-	0.019"	0.024"

Model D' - Case 2 - Calculated deflection = 0.042".

Model E	Case 1	Case 2
Cald. Defln.	0.006"	0.006"
Exptl. Defln.	0.007"	0.008"

The large percentage differences between the experimental and calculated deflections in case 4 for Model D and case 2 for Model E are due mainly to the buckling of the pyramid base panels thereby causing a reduction in the effective area of the members which was not taken into account. For Model D', the deflection at point 2 (Fig.2.13) should be nearly equal to the calculated value given above but it was more than 50% larger. This could not have been due to buckling alone and it is most likely to have been due to the large amount of bending strain energy in the separate bars joining the pyramid apexes having been neglected.

(c) Forces in a pyramid truss.

These forces can easily be estimated by considering the truss as a plane skeletal frame, pin-connected at its nodes. With these assumptions, the forces in various parts of Model E corresponding to the positions of the various strain gauges for a total load of

10 lbs. are compared with the measured stresses as follows,

Case 1	Pt. 1	Pt. 2	Pt. 3	Pt. 4	Pt. 5
Cald. Force (lb)	-5.8	5.8	-9.4	9.4	0
" Mean Stress (p.s.i)	-97	97	-50	50	0
Exptl. " " "	-78	72	-55	24	0

For point 4, the experimental stress was only half the calculated value. This was to be expected since more load was taken by the junctions between the base plate and the pyramid walls. All the other stresses agreed quite well with the calculated mean values since the gauges were placed towards the apexes of the pyramids.

2.6 Conclusions.

Good approximations to the deflections of a sheet roof can be obtained by treating it as an equivalent skeletal system provided that there is no buckling in the base panels or in the pyramid walls and the bars have the same order of cross-sectional area as the base plate.

The forces in the sheet roof can be approximated to, although to a less accurate extent, by treating each pyramid truss as a plane truss, instead of as a space truss used in calculating deflections.

CHAPTER 3

Tests On A Single Pyramid

3.1 In a roof system, the boundary conditions at the base in any pyramid will depend on the thickness of the base plate, the size of the base and the position the pyramid occupies in the roof. The boundary will lie somewhere between the "simply-supported" and "fixed" conditions and tests on a single pyramid were carried out in which these two limiting conditions were realised. The pinned condition was obtained by resting the pyramid on a smooth base so that the base of the walls were allowed to spread freely under a vertical point load at its apex. The fixed base condition was achieved by fixing the base of each wall to a flange and the flanges in turn fixed to a thick base slab.

3.2 Description of model

The model was made from 3/16 inch thick clear perspex sheets and had the dimensions shown in Fig.3.1(a). The different parts were glued together with Tensol cement No. 7 which had an ultimate bond strength of 6,600 p.s.i. This strength, although lower than that of the perspex in tension, flexure or shear, was nevertheless more than adequate for the order of stresses that were likely to be imposed on the joints during testing.

The model was made from four identical trapezoidal sheets forming the walls and a small piece of the same material forming the cap at the apex. The four edges of each of the walls were bevelled so that they could be glued to the top cap, Fig.3.1(b), and to each other along the sloping edges as shown in Fig.3.1(c). The top cap was provided so that the applied loading was transferred evenly to the tops of the four walls.

With the model in this condition, the simply-supported pyramid was tested with a vertical point load at the apex. The model was then modified so that it could be tested as a fixed pyramid, subjected to both a vertical as well as a horizontal load at the apex. Figs.3.2 (a) and (b) show these additions to the model and consisted of four "flanges" glued to the bases of the pyramid walls and a block for loading purposes glued to the top cap. The new additions were also made of perspex. The top block had two horizontal through holes, at right angles to each other thereby allowing horizontal loads in two perpendicular directions to be applied to the pyramid, Fig.3.14. The four flanges each had four holding-down screws to a thick plate which in turn could be bolted down at the corners.

3.3 "Simply-Supported" Pyramid Experiment

(a) Strain Measurements.

The strains at various points over half of a wall of the pyramid were measured by means of inductive displacement transducers (type F16), which were produced by the Bolton Paul Aircraft Electronics Department, in conjunction with one of their Peneford Multimeters (Type C21). At places where these transducers could not be used, for example, near the sloping edge and towards the top and bottom of the wall, Tepic resistance strain gauges (1/2 inch paper type) were employed.

Fig.3.3 shows the method of fixing the transducers to the pyramid wall. A transducer was held at two fixing points, the cylinder end at one point and the soft iron rod threaded through a 3/8 inch nylon ball at the other. At each fixing point there were two 3/8 inch Terry spring clips fixed to the pyramid wall by means of a 10BA bolt and nut. The extension or compression of the wall over the gauge length of the two fixing points for the transducers could thus be measured on both sides of the wall. The transducer fixing points were on a $1\frac{1}{2}$ inch grid over half a wall of the pyramid as shown in Fig.3.4. As the Terry clips could be rotated to any direction, strains in two directions at right angles could be measured. In the experiment, strains were measured in a direction parallel to the centre line of the wall (called the vertical direction) and in a direction at right angles to it (called the horizontal direction). With the positions of the fixing points shown in Fig.3.4, it was possible to measure the vertical strains at 12 points and the horizontal strains at 9 points.

Most of the resistance strain gauges were placed as near as possible to the edges of the wall and on both surfaces of it, Fig.3.4, and some gauges were placed along the centre line of one of the two adjacent walls for control purposes.

(b) Loading Arrangement.

A general view of the loading arrangement for this test is shown in Fig.3.5, while a close-up of the model itself under load is seen in Fig.3.6.

The loading frame was a square rigid closed frame made from steel angle sections. The model rested on a 3/4 inch perspex plate which in turn rested on a larger 1/2 inch steel plate supported at four points by adjustable steel blocks. The model was brought up to the right height for loading by means of two concrete blocks and a made-up steel section. Before loading commenced, the steel plate was levelled and molybdenum disulphide grease (moly slip) was applied to the contact surface between the model and the supporting perspex plate in order to reduce friction.

The vertical point load was applied to the apex of the pyramid by means of a loading screw measured by a 2000 lb. proving ring. Changes of temperature were measured but they were small enough not to affect readings significantly.

Figs.3.5 and 3.6 show a number of Metzger gauge points along a sloping edge of the model but the strains were too small to be measured by this method.

(c) Procedure For Testing.

The model was placed as centrally as possible under the loading screw by eye. A load equal to about half the maximum load was applied and a transducer was used on the outside to measure the strain at a point where there were gauges at a similar point on the control gauges wall. By this means it was possible to check that in fact the model was centrally loaded.

Four increments of load each of 100 divisions of the proving ring dial gauge, that is 141.3 lbs., were applied for each test. The maximum load applied was 565.2 lbs.

When taking readings with transducers, strains at one point only could be measured at a time. Two readings were taken for each load. After each test, the two transducers had to be moved to a new position which involved removing the proving ring and model because of the inside transducer. This process was tedious and time consuming and was discarded in the next experiment on the fixed pyramid.

A maximum of 24 strain gauges could be read at a time by using a 24-way strain gauge switch box and a Peekel register. Two readings were taken at each load to obtain an average value. All tests were repeated twice at different times so that the final results were average values of three readings.

On the most sensitive range, the Multimeter read to the nearest 1×10^{-6} inch and the Peekel read to the nearest micro-strain.

(d) Reduction of Readings.

For transducer readings, the extensions or compressions measured were divided by the gauge length of $1\frac{1}{2}$ inches to obtain strains.

For each point of the wall, the surface strains were plotted against load and graphs were drawn through the experimental points to get mean values. The values of the mean strains, both in the vertical and horizontal directions, for a load of 500 lbs. were read off from these graphs, and having thus obtained the strains at the measured points, those for points on a 1 inch grid were deduced by interpolation.

Finally, using the elastic stress-strain relations, the vertical and horizontal stresses at points on the 1 inch grid were calculated. Young's modulus and Poisson's ratio were determined from tests on tensile specimens taken from the same perspex sheet that was used for the model.

The modulus of elasticity, E, was 4.42×10^5 p.s.i.

Poisson's ratio, ν, was 0.35.

The vertical stress was thus $\sigma_v = \frac{E}{(1-\nu^2)}(\varepsilon_v + \nu\varepsilon_h)$

and the horizontal stress $\sigma_h = \frac{E}{(1-\nu^2)}(\varepsilon_h + \nu\varepsilon_v)$

That is $\sigma_v = 5.037 \times 10^5(\varepsilon_v + 0.35\varepsilon_h)$

and $\sigma_h = 5.037 \times 10^5(\varepsilon_h + 0.35\varepsilon_v)$

where ε_v and ε_h are vertical and horizontal strains.

The vertical and horizontal stresses on the outer and inner surfaces, and at the mid-plane of the wall are tabulated in Table 3.1 and plotted in Fig.3.8.

The bending moment in the vertical and horizontal directions for the grid points were calculated as follows, assuming plane sections remaining plane; see Fig.3.9.

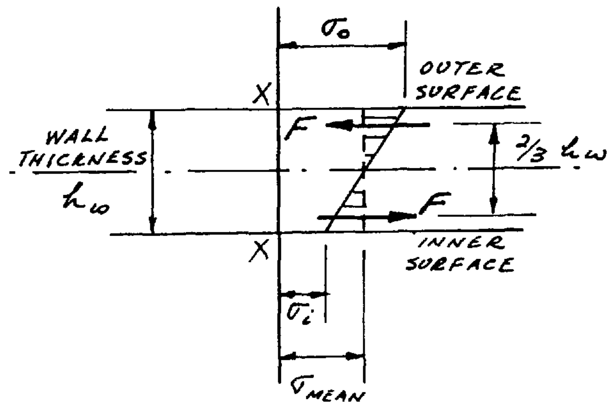

FIG. 3.9

σ_o = outside surface stress in p.s.i.

σ_i = inside surface stress in p.s.i.

Force F = $\frac{1}{8} h_w \; (\sigma_o - \sigma_i)$ p.s.i.

Bending moment M = $\frac{1}{12} h_w^2 \; (\sigma_o - \sigma_i)$ lb.-in./in.

For $h_w = 3/16''$, $M = 0.00293\,(\sigma_o - \sigma_i)$ lb.in./in.

The vertical and horizontal bending moments are given in Table 3.1 and plotted in Fig.3.10.

(e) Principal Stress Directions.

It was mentioned earlier that as the Terry clips used to support the transducers could be rotated to any direction as required, the strains in other directions could be measured as shown in Fig.3.11(a). Therefore, there were ten points at which strains in a third direction were measured. The gauge length in this case was 3.35 inches.

Knowing the strains in three directions at these ten points, it was therefore possible to calculate the principal stresses and their directions by means of Mohr's strain circles.

By symmetry, the centre line and sloping edges of the pyramid wall were principal stress directions and in between these lines, the principal stress directions fanned out from the apex towards the base. There were not sufficient points whose principal stress directions were known to allow for an accurate plot of the principal stress direction loci over the whole area of the wall but a good indication of them could be obtained as shown in Fig.3.11(b). The base and top of the wall also formed principal stress directions since there were no shears on these edges.

Table 3.2 shows the values of the principal stresses and directions at the points considered.

(f) Shear Stresses.

At the ten points where strains in three directions were measured, the shear stresses could be calculated by considering the equilibrium of the wedge element shown in Fig.3.12.

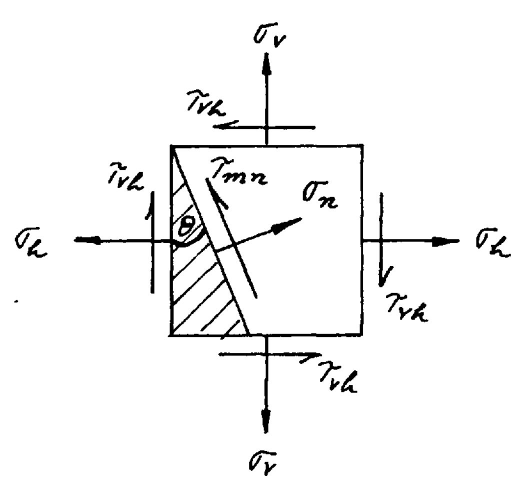

FIG. 3.12

The shear stress required is τ_{vl} and it is given by the expression

$$\tau_{vl} = \frac{E}{2(1-\nu^2)}\left\{\varepsilon_v(\tan\theta + \nu\cot\theta - \nu\sec\theta\,\mathrm{cosec}\,\theta) + \varepsilon_l(\nu\tan\theta + \cot\theta - \nu\sec\theta\,\mathrm{cosec}\,\theta) - (1-\nu)\varepsilon_n\sec\theta\,\mathrm{cosec}\,\theta\right\}$$

where E = modulus of elasticity,

ν = Poisson's ratio,

ε_v, ε_l & ε_n were the measured strains, and

θ specified the direction in which ε_n was measured.

For E = 4.42×10^5 p.s.i.

and $\nu = 0.35$,

$$\tau_{vl} = 94.52 \times 10^3(3\varepsilon_v + \varepsilon_l - 4\varepsilon_n) \qquad \text{for} \quad \theta = 60^\circ$$

and $$\tau_{vl} = 94.52 \times 10^3(\varepsilon_v + 3\varepsilon_l - 4\varepsilon_n) \qquad \text{for} \quad \theta = 30^\circ$$

The shear stresses calculated from these expressions are given in Table 3.2 and are compared with theoretical values in Fig.4.15.

3.4 Fixed Pyramid Experiment

(a) Strain Measurements.

It was mentioned earlier that the use of displacement transducers to measure strains in the experiment on the "Simply-Supported" Pyramid was both tedious and time consuming. This was due to the fact that strains could only be measured at one point at any one time and the transducers had to be moved to a new point and the whole loading procedure had to be repeated. Also, once the transducers were moved, they had to be reset before they could be reused. It took 30 minutes to measure the strains at any point of the wall.

Twenty new Tepic strain gauges similar to the old ones were employed in place of the transducers in order to measure the strains at sufficient points to allow accurate interpolation. The positions of these new gauges are shown in Fig.3.13 which also shows those of the old gauges.

Since only half of a wall was fitted with strain gauges, it was necessary, in the case of a horizontal load applied at the apex of the pyramid, to rotate the pyramid so that this wall occupied three different positions in relation to the applied load. This had the effect of being able to measure the strains in three walls of the pyramid due to a horizontally applied load. In the normal way, four times as many strain gauges would have been required to give the same results.

(b) Loading Arrangements.

(i) Vertical load.

A vertical load was applied to the apex of the pyramid in exactly the same manner as was used in the case of the simply-supported pyramid test. Fig.3.5 therefore shows the loading arrangement for this test also except that transducers were not used.

(ii) Horizontal load.

A horizontal load was applied to the apex of the pyramid in the way shown in Fig.3.14. Use was made of part of an existing loading frame as a base for the model. The perspex base of the model was bolted to a steel plate which was in turn dogged to the underside of the top flanges of the two channels forming part of the loading frame. This was sufficient to stop the model from moving in the direction of the applied horizontal load under its maximum value of 250 lbs. The steel plate was provided as an even base for the base of the model.

(c) Procedure for testing and results obtained.

(i) Vertical load.

As in the simply-supported pyramid test, four equal load increments of 100 divisions of the proving ring dial gauge (i.e. 141.32 lbs.) were applied so that the maximum load was 565.28 lbs. Again each load was applied twice with the corresponding zero values.

In this case, the loading procedure had to be repeated three times only since the maximum number of strain gauges that could be read was 24 and there were altogether 52 gauges.

The results of stresses and bending moments are shown in Table 3.3 and plotted in Figs.3.15 and 3.16.

(ii) Horizontal Load.

For each position of the model, Fig.3.14 shows the model in the position in which the wall with the strain gauges was nearest the load pulley, the loading procedure had to be performed three times for all the strain gauges to be read. In each loading sequence, there were five increments of 50 lbs. each giving a maximum horizontal load of 250 lbs. Each load was applied and removed twice and a mean result was obtained.

The other three positions of the model were obtained by rotating it through 90, 180 and 270 degrees from the position shown in Fig.3.14.

The results of stresses and bending moments are shown in Tables 3.4 to 3.6 and plotted in Figs.3.17 to 3.24.

3.5 Comments On Results.

(a) Simply- supported pyramid case. (Figs.3.8 & 3.10)

The general patterns of the stress distribution over the walls were of the type which were expected. That is to say, the vertical stresses were higher towards the top of the wall where the cross-sectional area was smaller, and towards the bottom more of the load was taken by the junctions of the walls resulting in higher stresses there. The force as given by the area of the stress diagram at each horizontal section of the wall was different at each section. This was because the interaction between the walls along the junctions gave rise to "extra" external forces on each wall, these forces having some unknown distribution and acting at right angles to the sloping edges of the wall. This is discussed more fully in Chapter 4. It is of interest to note that the middle portions of the wall nearest the base were in tension in the vertical direction. For the horizontal stresses, the large tensile stresses towards the base were anticipated. The vertical section along the centre line of the wall should have had a zero stress resultant since there were no shears on the base of the wall.

This was not so probably because the strains were small and the accuracy therefore was not very great especially over the middle portion of the wall.

The bending moments over most of the wall were small and were only of some significance at the top and lower portions. In Fig.3.9, these moments have been plotted to a large scale so that their magnitudes appear exaggerated.

(b) Fixed pyramid case.

(i) Vertical load. (Figs.3.15 & 3.16)

Vertical stresses were more uniform than in the simply-supported pyramid. There was no tension in any part of the wall. At the fixed base, the stress was again largest towards the corner. The force at each horizontal section was again different due to interaction at junctions of the walls. The horizontal stresses were much smaller than those for the simply-supported pyramid especially towards the base. The bending moments were also insignificant except at the top of the wall.

(ii) Horizontal load. (Figs. 3.17 to 3.24)

The vertical stresses in Wall 'A' were compressive and those in Wall 'C' were tensile. The general shapes of the curves at each horizontal section were much the same in these walls except that the signs were different. The compressive force at each section in Wall 'A' was greater than the tensile force for the same section in Wall 'C' but this was compensated by the greater tensile force over the compressive force in Wall 'B'.

The horizontal stresses in all three walls were small as in the case of the vertical load.

The bending moments in Wall 'A' were small in most parts but tended to be significant towards the base, whereas in Wall 'C' the vertical moments were significant over most of the wall but the horizontal moments remained small. The vertical moments in Wall 'B' were significant only at the lower part of the side nearest to the junction with Wall 'C'. The horizontal moments were once more negligibly small.

CHAPTER 4

Approximate Solutions For The Stress Distributions In The Walls Of A Symmetrically-Loaded Sheet Pyramid

4.1 A general solution for the stresses in the walls of any sheet pyramid with arbitrary base boundary conditions acted on by any system of loading is obviously a very difficult problem. It would have to take into account the exact deformation of the pyramid which in itself is difficult to determine in general terms.

The solutions attempted are therefore only particular solutions; the shape of the pyramid being that used in the experimental models, the base boundary conditions being either "simply-supported" or "fixed" as in the model in Chapter 3 and the load being a single vertical point load applied at its apex. Further, they are only approximate solutions since various simplifying assumptions are made. The object of these calculations is to provide a comparison with the stresses obtained experimentally in Chapter 3.

The general approach in these approximate solutions is to consider each individual wall of the pyramid as a plane stress problem. The actual boundary conditions at the edges of the wall are not known but various assumptions are made based upon the experimental results. There is in fact some bending in the walls but it is not significant and one is justified in ignoring it.

4.2 Simply-Supported Pyramid

A simply-supported pyramid with general dimensions is shown in Fig.4.1(a). Due to symmetry of the load, all the walls are similarly stressed so that one wall only requires to be analysed. The wall is analysed as a plane stress problem whose boundary conditions are assumed as follows:-

(a) Top Edge.

This edge is always short so that the component of the applied load may be considered to act uniformly on it. The normal stress on this edge is therefore uniform and compressive and is due to the component of the applied load in the plane of the wall, Fig.4.1(b). The shear stress is zero at the middle of the edge and is small over most of it so that it is reasonable to assume zero shear along this edge.

(b) Bottom Edge.

Short of a rigorous treatment of the whole pyramid in which the displacement of this edge may be calculated, the best assumption for the normal stress distribution here must be the actual distribution taken from the experimental results. It is however not possible to express this experimental curve in the form of a simple equation so that an approximate curve must be used. The limacon of Pascal (5) seems to be the only curve which satisfies the condition of zero stress and zero slope at the middle of the edge and still represents the experimental curve closely. A fourth order curve is easier to handle but it will not

satisfy the zero stress condition mentioned before. It is felt that this discrepancy will not affect the stresses in the wall to any appreciable extent so that this curve will be used in the analysis to compare with the results obtained with the limacon of Pascal. Since this edge was allowed to slide freely over the supporting slab in the experiment, there can be no shear along it.
(c) Sloping Edges.

This is the most difficult assumption to make. The presence of inplane forces of some distribution is due to the bending of the two adjacent walls under the action of the components of the quarter loads in the directions normal to their planes, Fig.4.1(b). However, in choosing an arbitrary load distribution, there are two points to consider, namely, (i) this distribution must have a zero resultant because, as can be seen from Fig.4.1(c), the stress distribution at the section along the centre lines of the two walls must be self-balancing since there are no horizontal reactions on the base of the pyramid, and (ii) the top part of the wall must be under compression and the lower part under tension. The linear normal stress distribution shown in Fig.4.2 satisfies these two conditions. However, the distribution is more likely to be non-linear and the effect of the loads producing it more localised. Therefore, the third order curve shown dotted in Fig.4.2 will also be considered as a possible distribution.

Because of symmetry, the shear stress along these edges is zero.

Calculation of Boundary Loading.

(a) Top Edge. Fig.4.1(b).

Component of applied load in plane of wall = $\frac{P}{4} \sin\alpha$

$$\therefore \text{ Mean stress, } \quad \sigma_{xk} = \frac{1}{4} \cdot \frac{P\sin\alpha}{b_1 t} \qquad — \quad (1)$$

$$\text{Shear stress, } \quad \tau_{xy_k} = 0 \qquad — \quad (2)$$

(b) Bottom Edge.

The limacon of Pascal and the fourth order curve assumptions consists of two constants which can be calculated from vertical equilibrium of the pyramid and by assuming the experimental stress value at the ends of the edge. The latter condition can be expressed in the form of a concentration factor.

(i) Limacon of Pascal assumption. Fig.4.3.

The equation of this curve is given in polar co-ordinates as $\rho = b + a\cos\theta$ (where a < b) and a and b are the constants to be determined. The part of the curve to be used is from $\theta = 90°$ to $270°$.

To satisfy the vertical equilibrium condition, we must have

$$(A_3 - A_2) = \frac{1}{8} \sin\alpha \cdot \eta \cdot \lambda_L \cdot \lambda_S \qquad — \quad (3)$$

where $\eta = P/t$,

λ_L = linear scale factor

and λ_S = stress " "

But $$(A_3 - A_2) = (A_3 + A_1) - (A_1 + A_2)$$
$$= b(b-a) - \int_{\pi/2}^{\pi} \tfrac{1}{2}\rho^2\, d\theta$$
$$= b^2(1-\tfrac{\pi}{4}) - \tfrac{\pi}{8}a^2$$

Also, $$b = \tfrac{1}{2} b_2 \lambda_L ,$$

Therefore, substitution in equation (3) gives

$$a^2 = \tfrac{2}{\pi} b_2^2 \lambda_L^2 (1-\tfrac{\pi}{4}) - \tfrac{1}{\pi}\sin\alpha .\, \eta \lambda_L \lambda_s \qquad -(4)$$

Further, if the stress concentration factor is n, where

$$n = \frac{\text{stress at ends of edge}}{\text{mean stress on edge}}$$

then

$$(b-a) = \frac{1}{4} \cdot \frac{n . \eta . \sin\alpha}{b_2} \cdot \lambda_s$$

Substituting for b, this gives

$$a^2 = \left(\tfrac{1}{2} b_2 \lambda_L - \frac{n\eta\sin\alpha}{4b_2}\lambda_s\right)^2 \qquad -(5)$$

From (4) and (5), we obtain the relationship between λ_L and λ_s in the equation

$$\left(\tfrac{3}{4}-\tfrac{2}{\pi}\right)b_2^2\lambda_L^2 + \left(\tfrac{1}{\pi}-\tfrac{n}{4}\right)\eta\sin\alpha .\,\lambda_s\lambda_L + \left(\frac{n\eta\sin\alpha}{4b_2}\right)^2\lambda_s^2 = 0 \qquad -(6)$$

This means that only one scale can be chosen arbitrarily; so that a and b can be calculated as soon as λ_L or λ_s is chosen.

(ii) Fourth order curve assumption.

The equation of the curve is taken as

$$\sigma_{x_0} = a y^4 + b$$

where the co-ordinate axes are as shown in Fig.4.2.

From the vertical equilibrium condition, we have,

$$\int_0^{\frac{1}{2}b_2} \sigma_{x_0}\, dy = \frac{1}{8}\eta \sin\alpha$$

giving $$\frac{b_2^4}{80} a + b = \frac{\eta \sin\alpha}{4 b_2} \qquad — (7)$$

For a stress concentration factor of n,

$$\left(\frac{b_2}{2}\right)^4 a + b = \frac{n \eta \sin\alpha}{4 b_2} \qquad — (8)$$

Equations (7) and (8) give

$$\left.\begin{aligned} a &= \frac{5 \eta \sin\alpha}{b_2^5}(n-1) \\ \text{and} \quad b &= \frac{\eta \sin\alpha}{16 b_2}(5-n) \end{aligned}\right\} \qquad — (9)$$

Whatever the normal stress assumption along this edge is, the shear stress $\tau_{xy_0} = 0.$ — (10)

(c) Sloping Edges.

The unknown ordinate at the ends of the assumed linear or cubic curve normal stress distributions can be found by considering the rotational equilibrium of the adjoining walls. This is because the loading along the edges of these walls normal to their planes is the inplane normal loading on the wall under consideration.

(i) Linear Distribution Assumption.

The equation of the distribution is taken as

$$\sigma_t = c_1 \left(s - \frac{s_1}{2} \right)$$

where the axes s and t are shown in Fig.4.2.

Rotational equilibrium of an adjoining wall, Fig.4.4, gives

$$c_1 = \frac{3 \eta h \cos\alpha}{2 s_1^3 \sin\beta}$$

or
$$c_1 = \frac{3 \eta \cos\alpha . \sin^2\beta}{2h^2} \qquad \text{--- (11)}$$

The assumed distribution becomes

$$\sigma_t = \frac{c_1}{\sin\beta} \left(x - \frac{h}{2} \right) . \qquad \text{--- (12)}$$

when referred to the x - y axes.

(ii) Cubic Curve Distribution Assumption.

The assumed curve is given by (Fig.4.2)

$$\sigma_t = c_1 \left(s - \frac{s_1}{2} \right)^3$$

Rotational equilibrium of an adjoining wall, Fig.4.4, now gives

$$c_1 = \frac{10 \eta \cos\alpha . \sin^4\beta}{h^4} \qquad \text{--- (13)}$$

The cubic equation, if referred to the x - y axes, becomes

$$\sigma_t = \frac{c_1}{\sin^3\beta} \left(x - \frac{h}{2} \right)^3 \qquad \text{--- (14)}$$

Shear stress $\tau_{st} = 0.$ — (15)

Solution Of The Plane Stress Problem.

Having thus assumed all the required force boundary conditions for the wall, the solution for the stresses can be obtained by the usual elasticity principles. The governing equation in the solution of two-dimensional problems of this nature when body forces are absent or are constant is

$$\nabla^4 \phi = \frac{\partial^4 \phi}{\partial x^4} + 2\frac{\partial^4 \phi}{\partial x^2 \partial y^2} + \frac{\partial^4 \phi}{\partial y^4} = 0 \qquad \text{—— (16)}$$

where ϕ is Airy's stress function and x, y are rectangular co-ordinates in the plane. In practice, in all but the very simple cases of boundary conditions and shapes of plates, it is not always possible, or if so it is usually difficult, to solve the resulting fourth order equations even assuming these can be obtained.

In the present problem, due to the complexity of the boundary conditions and the shape of the wall, it is felt that it will be easier to obtain the solution by finite difference techniques. With the help of a high speed digital computer, it will be possible to use a finite difference net of sufficient fineness to obtain a solution of good accuracy.

Finite Difference Solution.

The finite difference equivalent of the biharmonic equation (16) for a square net is

$$20\phi_0 - 8(\phi_1 + \phi_2 + \phi_3 + \phi_4) + 2(\phi_6 + \phi_8 + \phi_{10} + \phi_{12}) + (\phi_5 + \phi_7 + \phi_9 + \phi_{11}) = 0 \qquad \text{—— (17)}$$

where the grid points are numbered as shown in Fig. 4.5.

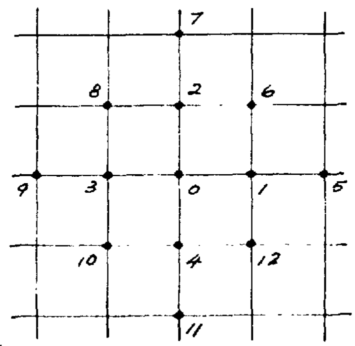

FIG. 4.5 - SQUARE NET

Before equation (17) can be used, the values of ϕ and its derivaties $\partial\phi/\partial x$ and $\partial\phi/\partial y$ at the boundaries must be calculated from the boundary conditions so that the ϕ values which may be required outside the wall can be calculated.

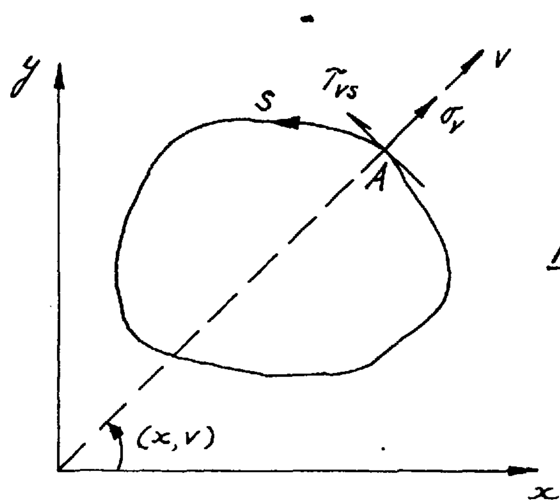

FIG. 4.6.

With reference to Fig.4.6, it can be shown (6) that

$$\left.\begin{aligned} \frac{\partial\phi}{\partial x} &= -\int \tau_{vy}\, ds \\ \frac{\partial\phi}{\partial y} &= \int \tau_{vx}\, ds \end{aligned}\right\} \quad \text{--- (18)}$$

and $$\phi = \int\left\{ \frac{\partial \phi}{\partial y}\cos(x,\nu) - \frac{\partial \phi}{\partial x}\sin(x,\nu)\right\} ds \qquad \text{— (19)}$$

at point A where the normal and shear stresses are known. These are therefore the boundary conditions which the stress function ϕ has to satisfy at this point.

The expressions for ϕ and its first derivatives at the boundaries will now be obtained. Only one half of the wall is considered because of symmetry.

Top Edge.

By definition,

$$\frac{\partial^2\phi}{\partial y^2} = \sigma_{x_h} \quad \text{and} \quad \frac{\partial^2\phi}{\partial x\,\partial y} = -\tau_{xy_h} = 0 \qquad \text{(Fig.4.2)}$$

Integrating these with respect to y,

$$\partial\phi/\partial y = \sigma_{x_h}\cdot y + a$$
$$\phi = \tfrac{1}{2}\sigma_{x_h}\cdot y^2 + a.y + b$$
$$\partial\phi/\partial x = c$$

At $y = 0$, $\partial\phi/\partial y = 0$ by symmetry, $\therefore$ $a = 0$.

b and c are arbitrary constants. Therefore, let $b = c = 0$.

Then,
$$\left.\begin{aligned} \partial\phi/\partial y &= \sigma_{x_h}\cdot y \\ \phi &= \tfrac{1}{2}\sigma_{x_h}\cdot y^2 \\ \partial\phi/\partial x &= 0 \end{aligned}\right\} \qquad \text{— (20)}$$

Sloping Edge.

(i) Linear distribution for σ_t.

From (18) and (12),

$$\partial\phi/\partial x = -\int c_1 \left(x - \frac{h}{2}\right) ds$$

$$\partial\phi/\partial y = \int c_1 \cot\beta \left(x - \frac{h}{2}\right) ds$$

Substituting for $ds = -dx/\sin\beta$, Fig. 4.7,

$$\frac{\partial\phi}{\partial x} = \int \frac{c_1}{\sin\beta}\left(x - \frac{h}{2}\right) dx$$

$$\frac{\partial\phi}{\partial y} = -\int \frac{c_1}{\sin\beta} \cot\beta \left(x - \frac{h}{2}\right) dx$$

Performing the integration,

we have,

$$\left.\begin{aligned} \frac{\partial\phi}{\partial x} &= \frac{c_1}{2\sin\beta}\left(x - \frac{h}{2}\right)^2 + d \\ \frac{\partial\phi}{\partial y} &= -\frac{c_1}{2\sin\beta}\cot\beta\left(x - \frac{h}{2}\right)^2 + e \end{aligned}\right\} -(21)$$

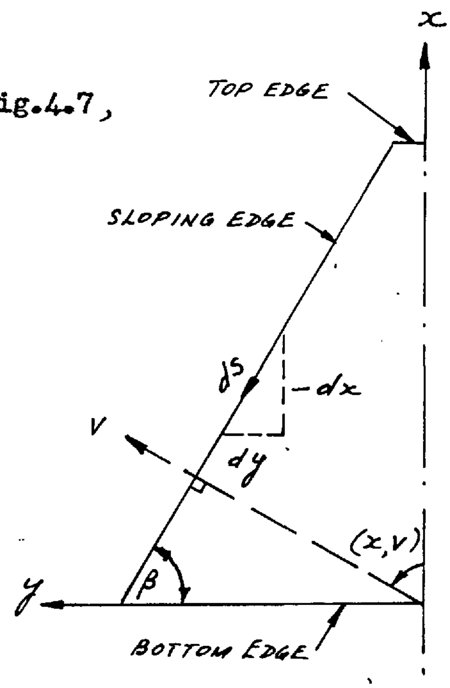

FIG. 4.7

Now using (19) and (21),

$$\phi = \int\left[\left\{-\frac{c_1 \cot\beta}{2\sin\beta}\left(x - \frac{h}{2}\right)^2 + e\right\}\cos\beta - \left\{\frac{c_1}{2\sin\beta}\left(x - \frac{h}{2}\right)^2 + d\right\}\sin\beta\right]\left(-\frac{dx}{\sin\beta}\right)$$

so that, $$\phi = \frac{c_1}{6\sin^3\beta}\left(x - \frac{h}{2}\right)^3 + (d - e\cot\beta)x + f \qquad -(21)$$

The constants d, e and f can be found from the condition that $\frac{\partial\phi}{\partial x}$, $\frac{\partial\phi}{\partial y}$ and ϕ must have the same values at the point of intersection of this edge with the top edge i.e. at $x = h$, $y = \frac{1}{2} b_1$.

At this point,

$$\partial\phi/\partial x = 0 = \frac{c_1}{2\sin\beta}\left(\frac{h}{2}\right)^2 + d$$

$$\partial\phi/\partial y = \tfrac{1}{2}b_1\sigma_{xh} = -\frac{c_1\cot\beta}{2\sin\beta}\left(\frac{h}{2}\right)^2 + e$$

$$\phi = \tfrac{1}{8}b_1^2\sigma_{xh} = \frac{c_1}{6\sin^3\beta}\left(\frac{h}{2}\right)^3 + (d - e\cot\beta)h + f$$

so that,

$$\left.\begin{aligned} d &= -\frac{c_1}{2\sin\beta}\left(\frac{h}{2}\right)^2 \\ e &= \tfrac{1}{2}b_1\sigma_{xh} + \frac{c_1\cot\beta}{2\sin\beta}\left(\frac{h}{2}\right)^2 \\ f &= \tfrac{1}{2}b_1\sigma_{xh}\left(\tfrac{1}{4}b_h + h\cot\beta\right) + \frac{5c_1}{6\sin^3\beta}\left(\frac{h}{2}\right)^3 \end{aligned}\right\} \quad -(22)$$

(ii) Cubic curve distribution for σ_t.

Following the same procedure as that for the linear distribution for σ_t in (i), we obtain,

$$\left.\begin{aligned} \partial\phi/\partial x &= \frac{c_1}{4\sin^3\beta}\left(x - \frac{h}{2}\right)^4 + d \\ \partial\phi/\partial y &= -\frac{c_1\cot\beta}{4\sin^3\beta}\left(x - \frac{h}{2}\right)^4 + e \\ \phi &= \frac{c_1}{20\sin^5\beta}\left(x - \frac{h}{2}\right)^5 + (d - e\cot\beta)x + f \end{aligned}\right\} \quad -(23)$$

where

$$\left.\begin{aligned} d &= -\frac{c_1}{4\sin^3\beta}\left(\frac{h}{2}\right)^4 \\ e &= \frac{c_1\cot\beta}{4\sin^3\beta}\left(\frac{h}{2}\right)^4 + \tfrac{1}{2}b_1\sigma_{xh} \\ f &= \frac{9c_1}{20\sin^5\beta}\left(\frac{h}{2}\right)^5 + \tfrac{1}{2}b_1\sigma_{xh}\left(\tfrac{1}{4}b_h + h\cot\beta\right) \end{aligned}\right\} \quad -(24)$$

Bottom Edge.

(i) Limacon of Pascal distribution for σ_{x_0}.

It is not possible to express σ_{x_0} explicitly in rectangular co-ordinates so that it is not possible to obtain ϕ in the form of an expression. However, the individual values of ϕ at any node point on this boundary can be obtained by numerical integration. At the point of intersection of this edge with the sloping edge i.e. at $x = 0$, $y = \frac{1}{2} b_2$, the ϕ value obtained by numerical integration must be made equal to that given by expression (21) or (23) by adding a constant. This constant will then have to be added to all the ϕ values along this bottom boundary.

The value of $\partial\phi/\partial x$ at co-ordinate ($0, \frac{1}{2}b_2$) is zero from expression (21) or (23) and must therefore be zero all along the boundary.

(ii) Fourth order curve distribution for σ_{x_0}.

The equation for the stress distribution is

$$\sigma_{x_0} = a y^4 + b$$

where a and b are given by expression (9).

From (10),

$$\tau_{xy_0} = 0$$

$$\therefore \quad \partial^2\phi/\partial y^2 = a y^4 + b$$

and

$$\partial^2\phi/\partial x \partial y = 0$$

Integrating with respect to y,

$$\partial\phi/\partial y = \tfrac{1}{5} a y^5 + by + g$$

$$\phi = \tfrac{1}{30} a y^6 + \tfrac{1}{2} b y^2 + gy + h$$

$$\partial\phi/\partial x = i$$

Equating these values at $x = 0$, $y = \tfrac{1}{2}b_2$ with those for the sloping edge gives

$$\left.\begin{aligned} i = g &= 0 \\ h &= \frac{2c_1}{3\sin^3\beta}\left(\frac{h}{2}\right)^3 + \tfrac{1}{2} b_1 \sigma_{xh}\left(\tfrac{1}{4} b_1 + h\cot\beta\right) - \tfrac{1}{30} a \left(\frac{b_2}{2}\right)^6 - \tfrac{1}{2} b \left(\frac{b_2}{2}\right)^2 \end{aligned}\right\} \quad -(25)$$

for linear distribution of σ_t, and

$$\left.\begin{aligned} i = g &= 0 \\ h &= \frac{2c_1}{5\sin^5\beta}\left(\frac{h}{2}\right)^5 + \tfrac{1}{2} b_1 \sigma_{xh}\left(\tfrac{1}{4} b_1 + h\cot\beta\right) - \tfrac{1}{30} a \left(\frac{b_2}{2}\right)^6 - \tfrac{1}{2} b \left(\frac{b_2}{2}\right)^2 \end{aligned}\right\} \quad -(26)$$

for cubic curve distribution for σ_t.

There are therefore four cases to be considered corresponding to the different boundary assumptions. These are

Case 1 ;- Limacon of Pascal distribution for σ_{x_0} and linear distribution for σ_t.

Case 2 :- Fourth order curve distribution for σ_{x_0} and linear distribution for σ_t.

Case 3 :- Limacon of Pascal distribution for σ_{x_0} and cubic curve distribution for σ_t.

Case 4 ;- Fourth order curve distribution for σ_{x_0} and cubic curve distribution for σ_t .

The appropriate expressions (20) to (26) are used to obtain the values of ϕ , $\partial\phi/\partial x$ and $\partial\phi/\partial y$ for each of the four cases.

Numerical Calculations For The 12 inch Perspex Model Tested In Chapter 3.

The dimensions of the model were

$b_1 = 0.7835''$, $b_2 = 11.7835''$, $h = 11''$ and $t = 3/16''$

and the experimental results were obtained for a load of P = 500 lbs.

Therefore, $\alpha = 60^\circ$, $\sin\beta = \frac{2}{\sqrt{5}}$, $\cos\beta = \frac{1}{\sqrt{5}}$, $\eta = \frac{8000}{3}$.

Also, n was approximately equal to 8.

Top Edge :-

$$\sigma_{x_h} = 736.89 \quad p.s.i.$$

$$\tau_{xy_0} = 0$$

Botton Edge :-

(i) Limacon of Pascal Assumption.

Choosing a stress scale of $1'' \equiv 100$ p.s.i.

i.e. $\lambda_s = 1/100$ and using n = 8, equation (6) gives

$$\lambda_L = 1.9 \quad \text{or} \quad 0.48$$

For convenience, let $\lambda_L = 2$ i.e. a linear scale of $1'' \equiv 2$ ins., then using equation (6) again but assuming n to be unknown gives $n = 8.3$.

This is acceptable.

For $\lambda_c = 2$, $b = 12"$.

Also, equation (4) gives , $a = 8"$.

Therefore, the equation for σ_{x_o} is given by the polar equation $\rho = 12 + 8 \cos \theta$. This equation is plotted in Fig.4.8 to compare with the experimental curve.

(ii) Fourth order curve assumption.

Equations (9) give, for $n = 8$,

$a = 0.3308$ and $b = -36.75$.

The equation for the normal stress is therefore

$$\sigma_{x_o} = 0.3308\, y^4 - 36.75$$

This is also plotted in Fig.4.8 to compare with the experimental curve.

The shear stress for this edge , $\tau_{xy_o} = 0$.

Sloping Edge.

Expressions (11) and (13) give

$c_1 = 13.22$ for linear distribution of σ_t , and

$c_1 = 0.5828$ for cubic curve distribution of σ_t ,

so that their respective equations are

$$\sigma_t = 14.78\,(x - 5.5) \qquad \text{from (12)}$$

and $$\sigma_t = 0.6759\,(x - 5.5)^3 \qquad \text{from (14)}$$

Shear stress $\tau_{st} = 0$.

The expressions for ϕ , $\frac{\partial \phi}{\partial x}$ and $\frac{\partial \phi}{\partial y}$ which are required for calculating the ϕ values on and outside the boundaries can now be found for the four cases under consideration.

Case 1.

$$\left.\begin{aligned} \phi &= 368.45\, y^2 \\ \partial\phi/\partial x &= 0 \end{aligned}\right\} \text{for top edge.} \quad -(27)$$

$$\left.\begin{aligned} \phi &= 3.08(x-5.5)^3 - 423.85x + 4206.43 \\ \partial\phi/\partial x &= 7.392(x-5.5)^2 - 223.61 \\ \partial\phi/\partial y &= -3.695(x-5.5)^2 + 400.48 \end{aligned}\right\} \text{for sloping edge} \quad -(28)$$

ϕ values are obtained by adding 3794 to the values found by numerical integration as shown in Fig.4.9

$$\partial\phi/\partial x = 0$$

} for bottom edge. -(29)

Case 2.

Expressions are the same as (27) and (28) for the top edge and sloping edge respectively.

$$\left.\begin{aligned} \phi &= 0.011\, y^6 - 18.375\, y^2 + 3870.48 \\ \partial\phi/\partial x &= 0 \end{aligned}\right\} \text{for bottom edge.} \quad -(30)$$

Case 3.

Expressions are the same as (27) for the top edge,

$$\left.\begin{aligned}\phi &= 0.0509(x-5.5)^5 - 377.23\,x + 3949.81\\ \partial\phi/\partial x &= 0.2036\,(x-5.5)^4 - 186.31\\ \partial\phi/\partial y &= -0.1018\,(x-5.5)^4 + 381.83\end{aligned}\right\}\quad \text{for sloping edge.} \quad -(31)$$

ϕ values are obtained by adding 3793.64 to the values found by numerical integration as shown in Fig.4.9.

$$\partial\phi/\partial x = 0$$

for bottom edge. –(32)

Case 4.

Expressions are the same as (27) and (31) for the top edge and sloping edge respectively.

$$\left.\begin{aligned}\phi &= 0.011\,y^6 - 18.375\,y^2 + 3870.12\\ \frac{\partial\phi}{\partial x} &= 0\end{aligned}\right\}\quad \text{for bottom edge.} \quad -(33)$$

A square net is used for one half of the wall as shown in Fig.4.10 and the required values of ϕ on and outside the boundaries are also shown. It should be mentioned that in calculating the ϕ values outside the sloping edge, the following approximations, with reference to Fig.4.11, are used for point 4,

$$\phi_{4x} = \phi_0 + \delta\left(\frac{\partial\phi}{\partial x}\right)_0$$

$$\phi_{4y} = \phi_5 + \delta\left(\frac{\partial\phi}{\partial y}\right)_5$$

and

$$\phi_{4xy} = \tfrac{1}{2}(\phi_{4x} + \phi_{4y})$$

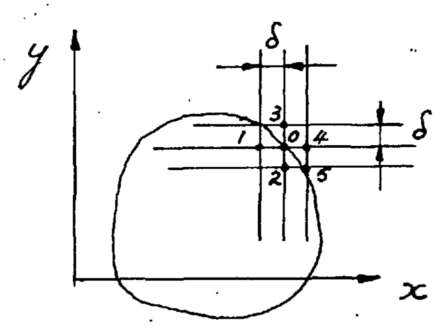

FIG. 4.11

In applying the finite difference equation (17) to point 1, say, the value of ϕ at point 4 is taken as ϕ_{4_x} while for point 3, $\phi_{3_{xy}}$ is used. ϕ_{3_y} will be used in considering the equation at point 2. The ϕ values outside the bottom edge are assumed to be equal to the corresponding values on the edge itself while that for point 35 (Fig.4.10) is assumed to be zero since this will give a value of σ_x there which is close to the experimental value.

Applying the finite difference equation (17) to the 34 mesh points at which the ϕ values are to be determined, we obtain a 34 x 34 matrix (Fig.4.12), which is the main matrix of the problem.

Computer Programme.

The programme is written in the Autocode System (7) for running on the Ferranti Mercury computer belonging to the Computer Unit of the University of London. This computer has special functions to facilitate matrix operations which are made use of by the programme.

The programme is in two parts. The first part reads in the main matrix (Fig.4.12) and boundary ϕ values from the data tape, forms the 34 x 4 load matrix and then solves for the ϕ values at the 34 mesh points. The second part makes use of these ϕ results to calculate the σ_x , σ_y and τ_{xy} stresses for these points. These stresses are printed out from the output tape and are shown in Tables 4.1 to 4.3. The stress distributions in the wall are plotted in Figs.4.13 to 4.15 and compared with the experimental results.

It should be mentioned that this computer programme is not a general programme but has been specially written to solve this particular numerical problem. However, so long as the same square net is used, it is possible to cater for any amount of loading cases with only slight changes in the data tape.

Comments On Results And Conclusions

Generally, the theoretical and experimental stresses compare well. There are various places especially near the boundaries where the differences are significant. This is only to be expected since firstly the assumed stress distributions for the boundaries are by no means the actual distributions, and secondly a numerical solution of this nature has inherent inaccuracies due to the size of the mesh, and the approximations used in obtaining the ϕ values outside the boundaries.

There is little difference between the stresses obtained in the four cases considered in the theory, because the assumed boundary stress distributions are not very different fom each other. In solving another problem of this type, one will therefore use only one case out of the four considered and obviously case 2 is the one to be considered since it is the simplest to handle even though the base boundary stress assumption is not correct at the middle portion of the boundary. Cases 1 and 3 which have the limacon of Pascal curve assumption for the bottom boundary stress are tedious to work out since they involved numerical integration. They were considered only because this was the most accurate assumption for the base stress distribution and also to show that the fourth order curve assumption was in fact accurate enough. Case 4 contained the third order curve assumption for the stress distribution along the sloping edge and was considered so that a comparison might be made with case 2.

Therefore, it seems that the actual boundary conditions need not be known so long as the general nature of them may be guessed. Then, a numerical solution of the type used here will give results which can be accepted as sufficiently accurate.

4.3 Fixed Pyramid

This problem is solved in the same way as the simply-supported case. That is to say that the wall is considered as a plane stress problem with certain assumptions made for the boundary conditions. However, there is the difference that while the wall in the simply-supported case had only one type of boundary conditions i.e. traction conditions, the wall in this case has both traction and displacement boundary conditions. This is because the base of the wall in this case is fixed and the displacements along this boundary must therefore be zero. For the top and sloping edges, it is still easier to assume traction, rather than displacement, boundary conditions as before.

Calculation Of Boundary Loading.

Top Edge.

The normal stress distribution here is assumed to be uniform and compressive as before. With the same dimensions for the pyramid as shown in Fig. 4.1(a), this stress is

$$\sigma_{xh} = \frac{1}{4} \cdot \frac{P \sin \alpha}{b_1 t} \qquad \text{from (1)}$$

The shear stress is again assumed to be zero all along this edge, i.e. $\tau_{xy_h} = 0$

Sloping Edge.

Experimental results for σ_x distribution suggest that the normal stress distribution along this edge is of the type shown in Fig.4.16(a). The stresses are compressive towards the top and base with tensile stresses in between. Also, the top compression is greater than that at the bottom. This type of stress distribution may be guessed at when one considers the way in which opposite walls of the pyramid have to deform, Fig.4.16(b).

This type of stress distribution is therefore assumed, as shown in Fig.4.17(a) in the form of three linear distributions. Just as in the simply-supported pyramid case, having thus allowed for the bending of the adjoining walls in this way by the assumption of these side loadings, we consider now the equilibrium of a flat wall, Fig.4.17.

The maximum stresses a, b and c in the three stress distributions can be found by considering horizontal equilibrium and the assumptions of zero moments at three sections in the wall, say at A, B and C. These conditions give three equations as follows,

$$\left.\begin{aligned} 6a - 12b - 8c &= -3N \\ 2a - 6b - 5c &= -3N \\ 4a - 8b - 4c &= -4H/P\cos\alpha.\sin\alpha \end{aligned}\right\} \qquad (34)$$

where $$N = \frac{P\cos\alpha.\sin\beta}{t.h}$$

Further, the condition that there should be no bending in the wall means that the resultant of H and P/4 forces must act in its plane; so that,

$$H = \frac{P}{4}\cot\alpha \qquad (35)$$

Solution of equations (34) and (35) gives

$$\left.\begin{aligned} a &= \frac{3N}{4\sin^2\alpha} \\ b &= \frac{N}{4}\left(\frac{7}{2\sin^2\alpha} - 3\right) \\ c &= \frac{3N}{4}\left(2 - \frac{1}{\sin^2\alpha}\right) \end{aligned}\right\} \qquad (36)$$

Due to symmetry, the shear stress along this edge is zero.

Solution Of The Mixed Boundary Conditions Plane Stress Problem.

Plane stress problems with mixed boundary conditions like the problem here are best solved in terms of displacements rather than in terms of a stress function. To do this, the given boundary tractions are expressed in terms of displacements, with the use of the stress-strain relations, and then they are applied in order to solve the governing simultaneous equations (8).

The governing equations are

$$\left.\begin{aligned} \frac{\partial}{\partial x}\left(\frac{\partial u}{\partial x}+\frac{\partial v}{\partial y}\right)+\frac{1-\mu}{1+\mu}\,\nabla^2 u &= 0 \\ \frac{\partial}{\partial y}\left(\frac{\partial u}{\partial x}+\frac{\partial v}{\partial y}\right)+\frac{1-\mu}{1+\mu}\,\nabla^2 v &= 0 \end{aligned}\right\} \quad (37)$$

when body force is absent or is constant and where u and v are the displacements in the x and y directions respectively; and μ is Poisson's ratio.

At any point on the boundary where the traction is specified as T_{vx} and T_{vy} (Fig.4.6), these can be expressed in terms of displacements by the equations

$$\left.\begin{aligned} 2\,\frac{(1-\mu^2)}{E}\,T_{vx} &= 2\left(\frac{\partial u}{\partial x}+\mu\frac{\partial v}{\partial y}\right)\cos(x,v)+(1-\mu)\left(\frac{\partial v}{\partial x}+\frac{\partial u}{\partial y}\right)\sin(x,v) \\ 2\,\frac{(1-\mu^2)}{E}\,T_{vy} &= 2\left(\frac{\partial v}{\partial y}+\mu\frac{\partial u}{\partial x}\right)\sin(x,v)+(1-\mu)\left(\frac{\partial v}{\partial x}+\frac{\partial u}{\partial y}\right)\cos(x,v) \end{aligned}\right\} \quad (38)$$

where E is Young's modulus.

The governing equations (37) together with the boundary equations (38) define the problem completely. Due to the complicated nature of these equations, these types of problems are best solved by numerical methods and this particular problem is solved by the finite difference method.

Finite Difference Solution.

For any given mesh, there are twice as many equations in this type of solution as there are in the ϕ solution. This is because there are two unknowns in u and v at each node instead of one unknown ϕ. Therefore, to obtain a solution of the same accuracy as before, a mesh of greater fineness has to be used. To use a square net as the one used before (Fig.4.10) means that 60 equations have to be solved. However, before doing this, it is wise to use a coarser net to test the accuracy of the boundary conditions assumptions. For this a coarser rectangular net is used.

For a general rectangular net of mesh size $\delta_1 \times \delta_2$, Fig.4.18, the finite difference equivalents of the equations (37) are

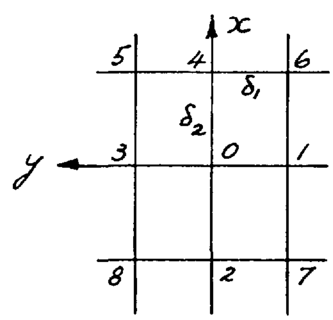

FIG. 4.18.

$$\left.\begin{aligned} -\frac{16\lambda^2+8(1-\mu)}{\lambda(1+\mu)}u_0 + \frac{4(1-\mu)}{\lambda(1+\mu)}(u_1+u_3) + \frac{8\lambda}{(1+\mu)}(u_2+u_4) \\ + (v_5 - v_6 + v_7 - v_8) = 0 \\ -\frac{16+8\lambda^2(1-\mu)}{\lambda(1+\mu)}v_0 + \frac{8}{\lambda(1+\mu)}(v_1+v_3) + \frac{4\lambda(1-\mu)}{(1+\mu)}(v_2+v_4) \\ + (u_5 - u_6 + u_7 - u_8) = 0 \end{aligned}\right\} \quad (39)$$

where $\lambda = \delta_1/\delta_2$.

Therefore, for a rectangular net where $r = 1/2$, equations (39) become

$$\left.\begin{aligned} -(2k_1+8k_2)u_0 + k_1(u_2+u_4) + 4k_2(u_1+u_3) + (v_5-v_6+v_7-v_8) &= 0 \\ -(8k_1+2k_2)v_0 + 4k_1(v_1+v_3) + k_2(v_2+v_4) + (u_5-u_6+u_7-u_8) &= 0 \end{aligned}\right\} \quad (40)$$

and for a square net i.e. $r = 1$, they become

$$\left.\begin{aligned} -4(k_1+k_2)u_0 + 2k_1(u_2+u_4) + 2k_2(u_1+u_3) + (v_5-v_6+v_7-v_8) &= 0 \\ -4(k_1+k_2)v_0 + 2k_1(v_1+v_3) + 2k_2(v_2+v_4) + (u_5-u_6+u_7-u_8) &= 0 \end{aligned}\right\} \quad (41)$$

where $k_1 = \dfrac{4}{1+\mu}$ and $k_2 = \dfrac{2(1-\mu)}{1+\mu}$

<u>Numerical Calculations For The 12 inch Perspex Model Tested In Chapter 3.</u>

The dimensions of this model have already been given on page 51. Also for perspex, $\mu = 0.35$.

Therefore, for $p' = \dfrac{P}{1000\,t}$, the boundary tractions are

$$\left.\begin{aligned} \sigma_{x_h} &= -276.3401\,p' \\ \tau_{xy_h} &= 0 \end{aligned}\right\} \text{ for the top edge.}$$

and,

$$\left.\begin{aligned} &\left.\begin{aligned} a &= 40.6552\,p' \\ b &= -16.9397\,p' \\ c &= -20.3276\,p' \end{aligned}\right\} \text{ from (36)} \\ &\tau_{st} = 0 \end{aligned}\right\} \text{ for the sloping edge.}$$

σ_t can be found from the three stress distributions with the values of a, b and c given above.

(a) Rectangular Net Solution. (Fig.4.19)

$$k_1 = 2.963 , \qquad k_2 = 0.963.$$

Equations (40) become

$$\left.\begin{aligned} -13.630\,u_0 + 2.963\,(u_2+u_4) + 3.852\,(u_1+u_3) + (v_5 - v_6 + v_7 - v_8) = 0 \\ -25.630\,v_0 + 11.852\,(v_1+v_3) + 0.963\,(v_2+v_4) + (u_5 - u_6 + u_7 - u_8) = 0 \end{aligned}\right\} (42)$$

Boundary Conditions.

Substitution of the required numerical values in equations (38) gives

$$\left.\begin{aligned} \frac{\partial u}{\partial x} + 0.35\,\frac{\partial v}{\partial y} &= k\,\sigma_{x_k} \\ \frac{\partial v}{\partial x} + \frac{\partial u}{\partial y} &= 0 \end{aligned}\right\} \text{ for the top edge} - (43)$$

and

$$\left.\begin{aligned} \left(\frac{\partial u}{\partial x} + 0.35\frac{\partial v}{\partial y}\right) + 0.65\left(\frac{\partial v}{\partial x} + \frac{\partial u}{\partial y}\right) &= \sqrt{5}\,k\,\sigma_t \\ \left(\frac{\partial v}{\partial y} + 0.35\frac{\partial u}{\partial x}\right) + 0.1625\left(\frac{\partial v}{\partial x} + \frac{\partial u}{\partial y}\right) &= 0 \end{aligned}\right\} \text{ for the sloping edge} - (44)$$

where $k = \dfrac{1-\mu^2}{E}$

The values of σ_t at points a to f on the boundaries are

Point	a	b	c	d	e	f
$\sigma_t\ (\times p')$	-5.8519	5.2358	8.9318	-9.5478	-28.0274	-276.3401

Boundary Displacements.

These are calculated in terms of displacements at internal points as follows,

Point C. The approximations are made that

$$\left(\frac{\partial u}{\partial x}\right)_c = \frac{1}{2}(u_c - u_9) \qquad \left(\frac{\partial u}{\partial y}\right)_c = (u_c - u_{12})$$

$$\left(\frac{\partial v}{\partial x}\right)_c = \frac{1}{2}(v_c - v_9) \qquad \left(\frac{\partial v}{\partial y}\right)_c = (v_c - v_{12})$$

Substitution of these expressions into (44) gives

$$u_c = 1.0646\sqrt{5}\,k\,\sigma_{t_c} + 0.4160\,u_9 + 0.2920\,v_9 + 0.5840\,u_{12} - 0.2920\,v_{12}$$

$$v_c = -0.3323\sqrt{5}\,k\,\sigma_{t_c} + 0.0320\,u_9 - 0.0160\,v_9 - 0.0320\,u_{12} + 1.0148\,v_{12}$$

In a similar manner, we obtain the expressions for u and v at points a, b, d and e.

Displacements Of Points Outside The Boundary.

These are found from the assumption that there is a linear continuation of u and v outside the field, so that

$$u_{c'} = u_6 + u_c - 0.5\,u_5 - 0.5\,u_{12}$$

$$v_{c'} = v_6 + v_c - 0.5\,v_5 - 0.5\,v_{12}$$

Similar expressions are obtained for u and v at points b', d' and e'.

The displacements of points f and f' are calculated as follows :-

The approximations are made that

$$u_{f'} = u_e + u_{f''} - 0.5\,u_{14} - 0.5\,u_f$$

$$v_{f'} = v_e + v_{f''} - 0.5\,v_{14}$$

and

$$\left(\frac{\partial u}{\partial x}\right)_{f''} = (u_f - u_{15}) \qquad \left(\frac{\partial u}{\partial y}\right)_{f''} = 2(u_{f''} - u_f)$$

$$\left(\frac{\partial v}{\partial x}\right)_{f''} = (v_{f''} - 0.5\,v_e) \qquad \left(\frac{\partial v}{\partial y}\right)_{f''} = 2\,v_{f''}$$

Substitution into (38) gives

$$u_f = k\sigma_{x_L} + 0.2326\sqrt{5}\,k\,\tau_{t_e} - 0.0224\,u_{14} + 0.3612\,v_{14} + 1.0224\,u_{15}$$

$$u_{f'} = 0.5\,k\sigma_{x_L} + 0.4\sqrt{5}\,k\,\tau_{t_e} - 0.1032\,u_{14} + 0.7266\,v_{14} + 1.1032\,u_{15}$$

$$v_{f'} = -0.6646\sqrt{5}\,k\,\tau_{t_e} + 0.0640\,u_{14} - 1.0320\,v_{14} - 0.0640\,u_{15}$$

Having obtained the required displacements on and outside the boundaries in this way, equations (42) are now applied to points 1 to 14 to obtain 24 equations. For point 15, a modified set of finite difference equations are used since it is bounded by an irregular mesh. These modified equations are

$$-14.667\,u_0 + 2.963\,(u_2 + 2\,u_4) + 2.889\,(u_1 + u_3) + (v_5 - v_6 + v_7 - v_8) = 0$$

$$-20.667\,v_0 + 8.889\,(v_1 + v_3) + 0.963\,(v_2 + 2\,v_4) + (u_5 - u_6 + u_7 - u_8) = 0$$

The resulting 25 equations are solved directly by means of a computer.

Computer Programme.

This is similar to the one used in the simply-supported case in that the first part solves for the displacements u and v at the 15 mesh points while the second part makes use of these values to solve for σ_x , σ_y and τ_{xy} . In working out the stresses from the displacements, the elastic relations used are

$$k\sigma_x = \frac{\partial u}{\partial x} + \mu \frac{\partial v}{\partial y}$$

$$k\sigma_y = \frac{\partial v}{\partial y} + \mu \frac{\partial u}{\partial x}$$

$$k\tau_{xy} = \frac{1-\mu}{2}\left(\frac{\partial v}{\partial x} + \frac{\partial u}{\partial y}\right)$$

The results of σ_x , σ_y and τ_{xy} are given in Table 4.4 and plotted in Figs.4.20 to 4.22.

(b) Square Net Solution. (Fig.4.23)

As before, $k_1 = 2.963$ and $k_2 = 0.963$.

Equations (41) become

$$\left.\begin{aligned} -15.704u_0 + 5.926(u_2+u_4) + 1.926(u_1+u_3) + (v_5 - v_6 + v_7 - v_8) &= 0 \\ -15.704v_0 + 5.926(v_1+v_3) + 1.926(v_2+v_4) + (u_5 - u_6 + u_7 - u_8) &= 0 \end{aligned}\right\} \quad (45)$$

The boundary conditions for the top and sloping edges are given by (43) and (44) respectively.

The values of σ_t for points a to l on the boundaries are

Point	a	b	c	d	e	f
$\sigma_t\ (\times p')$	-11.3958	-5.8519	-0.3080	5.2358	10.7798	8.9318

Point	g	h	i	j	k, l
$\sigma_t\ (\times p')$	-0.3080	-9.5478	-18.7877	-28.0274	-276.3401

Boundary Displacements.

Point d. The approximations are made that (8)

$$\left(\frac{\partial u}{\partial x}\right)_d = 1.5\,u_d - 2u_{16} + 0.5u_{11} \qquad \left(\frac{\partial u}{\partial y}\right)_d = 1.5\,u_d - 2u_{20} + 0.5\,u_{19}$$

$$\left(\frac{\partial v}{\partial x}\right)_d = 1.5\,v_d - 2v_{16} + 0.5\,v_{11} \qquad \left(\frac{\partial v}{\partial y}\right)_d = 1.5\,v_d - 2v_{20} + 0.5\,v_{19}$$

Substitution of these expressions into (44) gives

$$u_d = 0.5514\sqrt{5}\,k\,\sigma_{td} - 0.1927\,u_{11} - 0.1407\,v_{11} + 0.7707\,u_{16} + 0.5626\,v_{16}$$
$$- 0.1407\,u_{19} + 0.1407\,v_{19} + 0.5626\,u_{20} - 0.5626\,v_{20}.$$

$$v_d = -0.2431\sqrt{5}\,k\,\sigma_{td} - 0.0154\,u_{11} + 0.0154\,v_{11} + 0.0617\,u_{16} - 0.0617\,v_{16}$$
$$+ 0.0154\,u_{19} - 0.3488\,v_{19} - 0.0617\,u_{20} + 1.3949\,v_{20}.$$

Similar expressions are obtained for u and v at points b, f and h.

Point j. Approximations used are

$$\left(\frac{\partial u}{\partial x}\right)_j = 1.5\,u_j - 2u_{34} + 0.5\,u_{32} \qquad \left(\frac{\partial u}{\partial y}\right)_j = u_j - u_{35}$$

$$\left(\frac{\partial v}{\partial x}\right)_j = 1.5\,v_j - 2v_{34} + 0.5\,v_{32}, \qquad \left(\frac{\partial v}{\partial y}\right)_j = v_j$$

so that from (44) we obtain

$$u_j = 0.7054\sqrt{5}k\,\sigma_{t_j} - 0.2212\,u_{32} - 0.1682\,v_{32} + 0.8848\,u_{34} + 0.6728\,v_{34} + 0.3364\,u_{35}$$

$$v_j = -0.3914\sqrt{5}k\,\sigma_{t_j} - 0.0184\,u_{32} + 0.0276\,v_{32} + 0.0737\,u_{34} - 0.1106\,v_{34} - 0.0553\,u_{35}.$$

Displacements Of Points Outside Boundary.

There are two types of such points, namely, points a', c', e', g' and i' and points b', d', f', h' and j'. For the first type, the boundary conditions at the corresponding points on the boundary are used to obtain their displacements, while for the second type, a parabolic continuation of u and v outside the field is assumed. (8)

Point i'. It is assumed that at point i,

$$\left(\frac{\partial u}{\partial x}\right)_i \doteq \left(\frac{\partial u}{\partial x}\right)_{34} = 0.5u_j - 0.5u_{32} \qquad \left(\frac{\partial u}{\partial y}\right)_i = u_{i'} - u_{34}$$

$$\left(\frac{\partial v}{\partial x}\right)_i \doteq \left(\frac{\partial v}{\partial x}\right)_{34} = 0.5v_j - 0.5v_{32} \qquad \left(\frac{\partial v}{\partial y}\right)_i = v_{i'} - v_{34}$$

so that substitution into (44) gives

$$u_{i'} = -0.3257\sqrt{5}k\,\sigma_{t_j} + 1.6862\sqrt{5}k\,\sigma_{t_i} + 0.9126\,u_{32} + 0.6107\,v_{32} + 0.3087\,u_{34} - 0.4423\,v_{34} - 0.2214\,u_{35}$$

$$v_{i'} = -0.0387\sqrt{5}k\,\sigma_{t_j} - 0.2740\sqrt{5}k\,\sigma_{t_i} + 0.0669\,u_{32} + 0.0092\,v_{32} - 0.0485\,u_{34} + 0.9631\,v_{34} - 0.0184\,u_{35}$$

In the same way, at point c' we obtain,

$$u_{c'} = 1.6862\sqrt{5}k\,\sigma_{t_c} - 0.2864\sqrt{5}k\,\sigma_{t_d} + 0.8896\,u_{11} + 0.5964\,v_{11} + 0.3988\,u_{16} - 0.3855\,v_{16} + 0.0964\,u_{19} + 0.0703\,v_{19} - 0.3855\,u_{20} - 0.2811\,v_{20}$$

$$v_{c'} = -0.2740\sqrt{5}k\,\sigma_{t_c} - 0.0302\sqrt{5}k\,\sigma_{t_d} + 0.0654\,u_{11} + 0.0077\,v_{11} - 0.0422\,u_{16} + 0.9692\,v_{16} + 0.0077\,u_{19} - 0.0077\,v_{19} - 0.0308\,u_{20} + 0.0308\,v_{20}$$

Similar expressions for u and v are obtained for points a', e' and g'.

Parabolic continuation of u and v outside the wall means that at point f', say, we have,

$$u_{f'} = 3u_{24} - 3u_{19} + u_{13}$$

$$v_{f'} = 3v_{24} - 3v_{19} + v_{13}$$

The displacements at points b', d', h' and j' are found in a similar way.

The displacements at points k and l are found with the help of the following approximations;

At point l, let

$$\left(\frac{\partial u}{\partial x}\right)_l = 1.5u_l - 2u_{35} + 0.5u_{33} \qquad \left(\frac{\partial v}{\partial y}\right)_l = 2v_k$$

while at point k, let

$$\left(\frac{\partial u}{\partial x}\right)_k = u_k - 0.5u_j - 0.5u_{35} \qquad \left(\frac{\partial u}{\partial y}\right)_k = u_{k'} - u_l$$

$$\left(\frac{\partial v}{\partial x}\right)_k = v_k - 0.5v_j \qquad \left(\frac{\partial v}{\partial y}\right)_k = v_{k'}$$

These expressions together with $\left(\frac{\partial u}{\partial y}\right)_l = \left(\frac{\partial v}{\partial x}\right)_l = 0$ when substituted into (43) for points k and l give

$$u_l = 0.3210k\sigma_{xh_l} + 0.3457k\sigma_{xh_k} + 0.4807\sqrt{5}k\sigma_{t_j} - 0.1093u_{32} - 0.0953v_{32} - 0.1605u_{33} + 0.2643u_{34} + 0.4418v_{34} + 1.0054u_{35}$$

$$u_{k'} = -0.4198k\sigma_{xh_l} + 1.0863k\sigma_{xh_k} + 1.3153\sqrt{5}k\sigma_{t_j} - 0.3526u_{32} - 0.2858v_{32} + 0.2099u_{33} + 0.8674u_{34} + 1.3334v_{34} + 0.2754u_{35}$$

$$v_{k'} = 0.7408k\sigma_{xh_l} - 0.7407k\sigma_{xh_k} - 1.4218\sqrt{5}k\sigma_{t_j} + 0.2158u_{32} + 0.2319v_{32} - 0.3704u_{33} - 0.4927u_{34} - 1.5575v_{34} + 0.6470u_{35}$$

Having obtained these boundary displacements in this way, the governing finite-difference equations (45) are now applied to points 1 to 35 to obtain 60 equations in u and v. These equations are solved directly by a computer programme similar to the one used for the rectangular net case. The resulting values of σ_x , σ_y and τ_{xy} at the 35 mesh points are given in Table 4.5 and plotted in Figs.4.20 to 4.22.

Comments On Results And Conclusions.

In general, the theoretical results of σ_x and σ_y do not compare at all well with the experimental results. The distributions of the calculated σ_x stresses towards the bottom edge of the wall seems to suggest that the assumption of zero displacements there is wrong. It appears that there is in fact some displacement of this edge which is caused by the bending of the wall near the edge. If, in the theoretical solution, this bottom edge is assumed to have some u displacement, the distributions at the various sections, especially those nearest the bottom edge, will have smaller values towards the centre line, and therefore due to equilibrium, the σ_x values towards the sloping edge will be greater.

There is also the possibility that the normal stress distributions along the sloping edge have been wrongly assumed.

However, although the values of these stresses may have been smaller than the actual values, the type of distribution seems unlikely to be very far wrong since it was suggested by experimental evidence.

The solution due to the coarser net is better than that due to the finer net so far as comparison with the experimental results is concerned. This supports the suggestion that some boundary condition must have been badly assumed. It should be mentioned, however, that the solution of mixed boundary conditions problems of this type have inherent inaccuracies in themselves so that some errors in this solution must have been due to this fact.

It is just possible that a better solution to the problem may be obtained if the bottom edge is assumed to have a form of u displacement with a maximum value at $y = 0$ and zero values at $y = \pm \frac{1}{2}b_2$. The solution of σ_x stresses can then be found in terms of this one unknown u value. To find this u value, one could consider equilibrium of forces in the x direction along this bottom edge.

CHAPTER 5

Tests On A Steel Pyramidal Truss Model.

5.1 Description Of Model.

The boundary condition at the base of a pyramid in an actual roof was realised in a large scale steel model. The model consisted of seven pyramids and a base made from 1/12 inch bright mild steel plates connected by a mild steel bar, Fig.5.1. The various parts of the model were welded together, Fig.5.2.

It was important that the walls of the pyramids and their base plates were to be flat after construction so that they would not buckle as soon as the model was loaded. The 1/12 inch bright mild steel plates were sufficiently flat when obtained and thick enough so that the model could be welded with little distortion. Even so, great care had to be exercised in the welding process and a special jig, Fig.5.3, was constructed for this. Fig.5.4 shows the set-up for the welding of a pyramid to its base.

5.2 Measurement Of Strains And Deflections.

The strains in two directions and on both surfaces of two half- and one whole-wall of a pyramid and half of its base were measured by means of 1/2 inch Huggenberger (paper-backed type) resistance strain gauges, (Fig.5.5). Four strain gauges were placed on the bar, two on either side of the apex of the above pyramid. The total number of strain gauges used was 192.

The strain gauges on the inside of the walls and base nearest the welds had to be placed $1\frac{1}{4}$ inches away so that they were not affected by the welding. This minimum distance had been determined from separate tests. The wires from the internal gauges were taken out through two 1/2 inch diameter holes in the base.

Vertical deflections were measured at various points of the models using dial gauges capable of reading to the nearest ten thousandth of an inch. The places at which deflections were measured are shown in Fig. 5.6.

5.3 Loading Cases.

The model was tested as a simply-supported beam with a central point load. The span was changed so that the pyramid with the strain gauges occuppied three different positions in the span corresponding to the three loading cases shown in Fig.5.6.

In loading case 1, this pyramid was in the centre of the five-pyramid span so that it was symmetrically loaded by a vertical point load. The horizontal force, as measured by the strain gauges in the bar, was not zero but was negligible when compared with the vertical force.

In loading case 2, the pyramid was at one end of the five-pyramid span so that it was subjected to a large shearing force. At its apex, it was subjected to a large horizontal force.

In loading case 3, the pyramid was in a different position in the seven-pyramid span but it was again subjected to a large horizontal force at its apex. It was not however subjected to a heavy shear so that this case was somewhat between the two extreme cases above.

5.4 Description Of Tests.

The general arrangements for the test are shown in Figs. 5.7 and 5.8. The model was simply-supported on two rollers. Two stools were used to raise the model from the reaction beam so that dial gauges could be placed below the model to measure deflections. The point load was supplied by a 10 ton hydraulic jack, the load being measured by a 5000 p.s.i. pressure dial gauge. Strain measurements were made using a high speed automatic strain recorder manufactured by 'Solartron'. This apparatus was capable of reading 300 strain gauges at a time with a speed of 50 per second. The printer used to print out the results however had a speed of only 10 per second. In the tests, since only 50 dummy gauges were available, only 50 active gauges could be read at a time at a speed of 10 per second. Even so, this was very fast and temperature correction was unnecessary.

The load was applied in increments of 250 p.s.i. of the pressure gauge (corresponding to 0.53 ton) up to a maximum of 2000 p.s.i. (corresponding to 4.24 tons). Each load increment was put on twice and strain and deflection readings were taken at these loads and the corresponding zero loads.

In changing from one loading case to another, the model with the rollers and stools were moved while the loading frame was left in position.

5.5 Results.

The strains in two directions and on both surfaces of the walls and base of the pyramid on a 2 in. x 1 in. grid for the walls and a 2 in. x 3 in. grid for the base were obtained from the mean measured values by interpolation. The stresses at these points were then calculated using the elastic relations. The values of Young's modulus and Poisson's ratio were obtained from tensile tests and were 29.48×10^{6} p.s.i. and 0.304 respectively. These surface stresses together with the mid-plane stresses are given in Tables 5.1 to 5.12 and plotted in Figs. 5.10 to 5.24.

Load/deflection graphs are shown in Figs. 5.25 to 5.27 for the measured points.

5.6 Approximate Calculation Of Deflections.

Using the equivalent skeletal system technique (see Chapter 2), the deflections of the model can be estimated with a good degree of accuracy. With this method, therefore, the vertical deflections at the loading point in Cases 1, and 2 and in Case 3 are given by the expressions

$$\delta_p = \frac{4PL}{E}\left\{\frac{5}{6A_1} + \frac{23}{48A_2} + \frac{25\sqrt{5}}{96A_3}\right\}$$

and $$\delta_p = \frac{4PL}{E}\left\{\frac{14}{6A_1} + \frac{60}{48A_2} + \frac{35\sqrt{5}}{96A_3}\right\}$$ respectively,

where P = point load, L = truss width, E = Young's modulus, and A_1, A_2 and A_3 are the cross-sectional areas of the bar, base and diagonal members respectively.

Distributing the material of the pyramid walls and bases to the diagonal and base members as before,

$$A_2 = \frac{5}{12} L h \qquad \text{and} \qquad A_3 = \frac{2}{3\sqrt{5}} L h$$

where h = thickness of walls and bases.

For this model, $L = 12''$, $h = 1/12''$, $A_1 = 1$ sq. in. and $E = 29.48 \times 10^6$ p.s.i.

Therefore, for $P = 4$ tons,

$$\delta_p = 0.058'' \qquad \text{for Cases 1 and 2,}$$

and

$$\delta_p = 0.118'' \qquad \text{for Case 3.}$$

5.7 Comments On Results.

(a) The deflections of the model at the points shown in Fig.5.6 due to a central load of 4 tons were found from Figs. 5.24 to 5.26 to be as follows,

Point	1	2	3	4	5
Case 1	0.065"	–	0.045"	0.027"	0.049"
" 2	0.062"	0.045"	0.046"	0.027"	0.049"
" 3	0.118"	–	0.096"	0.041"	0.102"

The deflection at the load point can be obtained by assuming a parabolic deflection curve. This gives δ_p for Cases 1, 2 and 3 as 0.066, 0.062 and 0.120 inches respectively; compared with the calculated values of 0.058, 0.058 and 0.118 inches. The deflections at point 5 in each case were less than δ_p due to shortening of the loaded pyramid. The measured deflections in Cases 1 and 2 compare well as they should. However, in Case 1, the non-linearity of the load/deflection graph for point 2 shows that the base of the pyramid with the strain gauges was initially curved. This was also the case with the base of the central pyramid.

(b) The bending moments in the pyramid walls for all three cases of loading were negligibly small except at their junctions with the base plate. These can be seen from the plotted surface stresses in Figs. 5.9 to 5.23. Because of this, bending moment diagrams were felt to be unnecessary. In the base plate, however, there were great differences between the outside and inside surface stresses at a number of points but this was mainly because this base plate was not initially flat.

The horizontal stresses in Walls A and C were mainly small since there were no transverse load on the model in all cases. Those in Wall B were quite appreciable since the wall could stretch in the longitudinal direction causing tension towards the base.

In Case 1, the stress distributions in Walls A and C were much the same because of symmetry of the loading. In Wall

B, the vertical stress distribution is seen to be symmetrical about the centre line. The horizontal stress distribution was also symmetrical over most of the wall except towards the base. It was suspected that one of the measured horizontal strains in the right side of the wall towards the base was too large. There is no direct comparison between the stress distributions here with those described in Chapter 3 due to the different boundary conditions at the base of the walls. However, Walls A and C had boundary conditions approaching those of a "fixed" pyramid while Wall B had those similar to a "simply-supported" pyramid.

In Cases 2 and 3, since the horizontal loads were very nearly the same, the stress distributions in the walls were very similar. Towards the top of the walls, at any horizontal cross-section, the compression in Wall A was equal to the tension in Wall C so that the stress distribution in Wall B was symmetrical about the centre line. Towards the base of the walls, however, the compression in Wall A became larger than the tension in Wall C so that the stress distribution in Wall B was no longer symmetrical but there was more tension than compression. This was also evident in Chapter 3 in the case of the "fixed" pyramid subjected to a horizontal load.

In the base plate, because of the initial curvature, it is difficult to deduce anything from the stress distributions. In Case 1, where the stress distributions should have been symmetrical about the centre lines, they were not so especially in the longitudinal direction. However, the stress distributions for Cases 1 and 3 were very similar since the bending moment at the pyramid in each case was the same thereby causing the same tension in the base plate. In Case 2, the longitudinal stresses were small because the pyramid was taking a large shear but a small bending moment.

CHAPTER 6

Approximate Theory For The Buckling Of A Single Pyramid

6.1 One criterion in the behaviour of the pyramid structure is the buckling characteristics of the walls. From purely stress considerations, the pyramid walls can be very thin, but the usual problems governing the behaviour of thin plates then arise. If the plates are absolutely flat, it is reasonable to expect a theory of buckling to apply. In all practical cases however, perfectly flat plates cannot be obtained, and the sudden increase in deflection of the plate at buckling load does not occur. The characteristic behaviour of a thin plate with initial deviations from flatness is that deflections occur from first application of load, and there is an acceleration of deflection with increasing load until membrane action is important. A design limitation is therefore likely to be one of deflection rather than the buckling stress of a perfectly flat plate.

A study of the general behaviour of plates with different initial deformations is not likely to be fruitful in any practical application, but as purely comparative criteria, the buckling load of perfectly flat plates forming the sides of a pyramid under different edge restraints has been assessed, and the results compared with a single test on a 3" perspex pyramid.

6.2 The calculation of this initial buckling load is based mainly on a paper by Klein (9) in which he approximately calculated the initial buckling load of a simply-supported trapezoidal plate subjected to uniform uni-axial compression on the two parallel edges and uniform shear on the sloping edges, Fig.6.1. He used the method of collocation with the points for collocation taken at

$$\left(\frac{y-h_1}{h}\right) = \frac{1}{3},\ \frac{1}{2}\ \text{and}\ \frac{2}{3} \qquad \text{on the } y\text{-axis.}$$

The function he chose to represent the deflected shape at buckling was

$$\omega = F(y)\cos\left(\frac{\pi k x}{2y}\cot\theta\right), \qquad k = 1, 3, 5, \ldots$$

where

$$F(y) = a_1 \sin(n-1)\pi\left(\frac{y-h_1}{h}\right) + a_2 \sin n\pi\left(\frac{y-h_1}{h}\right) + a_3 \sin(n+1)\pi\left(\frac{y-h_1}{h}\right) \ldots\ldots \qquad n = 2, 3, 4, \ldots$$

This chosen deflection function satisfied the deflection boundary conditions exactly along the edges but not the moment conditions, which were satisfied at some points along the sloping edges, and at $x = 0$ on the parallel edges. Even so, Klein's solution when applied to the case of a square plate shows that his result is the same as that given by other methods. The nature of the shapes of the curves obtained by him shows that they were accurate enough for practical purposes.

6.3 Initial Buckling Of "Clamped" Trapezoidal Plates.

In considering the buckling of the walls of a pyramid, the boundary conditions of the edges are not known. Therefore, it will be useful to derive the buckling load for the case of the fixed plate so that with Klein's solution for the pinned plate, the two limiting cases are known. Then it will be possible, with the help of the experimental result available, to see whether the boundary conditions of the walls are nearer the pinned or clamped case.

Klein's method of solution will be followed closely in this clamped plate solution. The deflection function must however be different and the following function is adopted;

$$w = F(y)\cos\left(\frac{\pi k x}{2y}\cot\theta\right), \quad k = 1, 3, 5 \ldots \qquad -(6.1)$$

where

$$F(y) = \alpha_1 F_1 + \alpha_2 F_2 + \alpha_3 F_3$$

with

$$F_1 = \sin^2(n-1)\pi\left(\frac{y-b_1}{h}\right)$$

$$F_2 = \sin(n-1)\pi\left(\frac{y-b_1}{h}\right)\sin n\pi\left(\frac{y-b_1}{h}\right)$$

$$F_3 = \sin(n-1)\pi\left(\frac{y-b_1}{h}\right)\sin(n+1)\pi\left(\frac{y-b_1}{h}\right),$$

$$n = 2, 3, 4 \ldots\ldots$$

The three points chosen for collocation are

$\left(\frac{y-h_1}{h}\right) = \frac{1}{3}, \frac{1}{2}$ and $\frac{2}{3}$ along the y - axis.

For $n = 2$;

at $\left(\frac{y-h_1}{h}\right) = \frac{1}{3}$,

$$\left.\begin{aligned}
F &= \frac{3}{4}(\alpha_1 + \alpha_2) \\
\frac{dF}{dy} &= \frac{\sqrt{3}}{2}\left(\frac{\pi}{h}\right)(\alpha_1 - \frac{1}{2}\alpha_2 - 3\alpha_3) \\
\frac{d^2F}{dy^2} &= -\left(\frac{\pi}{h}\right)^2(\alpha_1 + \frac{19}{4}\alpha_2 + 3\alpha_3) \\
\frac{d^4F}{dy^4} &= \left(\frac{\pi}{h}\right)^4(4\alpha_1 + \frac{163}{4}\alpha_2 + 60\alpha_3)
\end{aligned}\right\} \quad (6.2)$$

at $\left(\frac{y-h_1}{h}\right) = \frac{1}{2}$,

$$\left.\begin{aligned}
F &= (\alpha_1 - \alpha_3) \\
\frac{dF}{dy} &= -2\left(\frac{\pi}{h}\right)\alpha_2 \\
\frac{d^2F}{dy^2} &= -2\left(\frac{\pi}{h}\right)^2(\alpha_1 - 5\alpha_3) \\
\frac{d^4F}{dy^4} &= 8\left(\frac{\pi}{h}\right)^4(\alpha_1 - 17\alpha_3)
\end{aligned}\right\} \quad (6.3)$$

at $\left(\frac{y-h_1}{h}\right) = \frac{2}{3}$,

$$\left.\begin{aligned} F &= \frac{3}{4}(\alpha_1 - \alpha_2) \\ \frac{dF}{dy} &= -\frac{\sqrt{3}}{2}\left(\frac{\pi}{h}\right)\left(\alpha_1 + \frac{1}{2}\alpha_2 - 3\alpha_3\right) \\ \frac{d^2F}{dy^2} &= -\left(\frac{\pi}{h}\right)^2\left(\alpha_1 - \frac{19}{4}\alpha_2 + 3\alpha_3\right) \\ \frac{d^4F}{dy^4} &= \left(\frac{\pi}{h}\right)^4\left(4\alpha_1 - \frac{163}{4}\alpha_2 + 60\alpha_3\right) \end{aligned}\right\} \quad (6.4)$$

Similar expressions may be written for other values of n .

The derivatives of ω at $x = 0$ are

$$\left.\begin{aligned} \frac{\partial^2\omega}{\partial x^2} &= -F(y)\left(\frac{\rho}{y}\right)^2 \\ \frac{\partial^2\omega}{\partial y^2} &= \frac{\partial^2 F}{\partial y^2} \\ \frac{\partial^4\omega}{\partial x^4} &= F(y)\left(\frac{\rho}{y}\right)^4 \\ \frac{\partial^4\omega}{\partial y^4} &= \frac{\partial^4 F}{\partial y^4} \\ \frac{\partial^4\omega}{\partial x^2\partial y^2} &= \left\{\frac{-6F}{y^2} + \frac{4}{y}\left(\frac{\partial F}{\partial y}\right) - \left(\frac{\partial^2 F}{\partial y^2}\right)\right\}\left(\frac{\rho}{y}\right)^2 \end{aligned}\right\} \quad (6.5)$$

where

$$\rho = \frac{\pi k \cot\theta}{2}$$

Substitution of expressions (6.5) into the buckling equation

$$\frac{\partial^4 \omega}{\partial x^4} + 2\frac{\partial^4 \omega}{\partial x^2 \partial y^2} + \frac{\partial^4 \omega}{\partial y^4} + \frac{N_x}{D}\cdot\frac{\partial^2 \omega}{\partial x^2} + \frac{N_y}{D}\cdot\frac{\partial^2 \omega}{\partial y^2} = 0$$

where D = flexural rigidity of plate, and N_x , N_y are positive when compressive, we obtain,

$$\left(\frac{y}{\rho}\right)^4 \frac{d^4F}{dy^4} - \frac{2}{\rho^2}\left(y^2\frac{d^2F}{dy^2} - 4y\frac{dF}{dy} + 6F\right)$$

$$+ \frac{N_y}{D}\left(\frac{y}{\rho}\right)^4\frac{d^2F}{dy^2} - \frac{N_x}{D}\left(\frac{y}{\rho}\right)^2 F + F = 0 \qquad \text{——}(6.6)$$

The values of N_x and N_y at the points of collocation are as follows,

$$\left.\begin{aligned}
N_x &= \tfrac{1}{4}(\lambda_1 N_1 \rho_4 - \lambda_2^2 N_2) && \text{at } \left(\tfrac{y-h_1}{h}\right) = \tfrac{1}{3}\\
&= (\lambda_1 N_1 - \lambda_2 N_2)\,\tfrac{\tan\theta}{2} && \text{"}\quad\text{"}\quad = \tfrac{1}{2}\\
&= \tfrac{1}{4}(-\lambda_1^2 N_1 - \lambda_2 N_2 \rho_5) && \text{"}\quad\text{"}\quad = \tfrac{2}{3}\\
N_y &= (2\lambda_1 N_1 + \lambda_2 N_2)\,\tfrac{1}{3\rho_1} && \text{at } \left(\tfrac{y-h_1}{h}\right) = \tfrac{1}{3}\\
&= (\lambda_1 N_1 + \lambda_2 N_2)\,\tfrac{1}{2\rho_3} && \text{"}\quad\text{"}\quad = \tfrac{1}{2}\\
&= (\lambda_1 N_1 + 2\lambda_2 N_2)\,\tfrac{1}{3\rho_2} && \text{"}\quad\text{"}\quad = \tfrac{2}{3}
\end{aligned}\right\}(6.7)$$

where

$$\lambda_1 = b_1/h\ ; \qquad \lambda_2 = b_2/h\ ;$$

$$p_1 = r_1 + \frac{2}{3}\tan\theta\,; \qquad p_2 = r_1 + \frac{4}{3}\tan\theta\,;$$

$$p_3 = r_1 + \tan\theta\,; \qquad p_4 = r_2 + 2\tan\theta\,;$$

$$p_5 = r_1 - 2\tan\theta\,.$$

Substitution of equations (6.2) to (6.4) and (6.7) into equation (6.6) gives the following set of three simultaneous equations;

at $\left(\frac{y-h_1}{h}\right) = \frac{1}{3}$,

$$A_{11} = \left\{4\left(\frac{p_1}{k}\right)^4 + 2\left(\frac{p_1}{k}\right)^2 + \frac{3}{4}\right\} + \frac{8\tan\theta}{\pi k^2}\left\{\sqrt{3}\,p_1 - \frac{9\tan\theta}{2\pi}\right\}$$

$$B_{11} = \left\{-r_1\,\frac{N_1}{N_2}\left(\frac{2}{3k^2} + \frac{3}{16}\cdot\frac{p_4}{p_1}\right) - r_2\left(\frac{1}{3k^2} - \frac{3}{16}\cdot\frac{r_2}{p_1}\right)\right\}\frac{p_1^3}{k^2}$$

$$A_{12} = \left\{\frac{163}{4}\left(\frac{p_1}{k}\right)^4 + \frac{19}{2}\left(\frac{p_1}{k}\right)^2 + \frac{3}{4}\right\} - \frac{8\tan\theta}{\pi k^2}\left\{\frac{\sqrt{3}}{2}\,p_1 + \frac{9\tan\theta}{2\pi}\right\}$$

$$B_{12} = \left\{-r_1\,\frac{N_1}{N_2}\left(\frac{19}{6k^2} + \frac{3}{16}\cdot\frac{p_4}{p_1}\right) - r_2\left(\frac{19}{12k^2} - \frac{3}{16}\cdot\frac{r_2}{p_1}\right)\right\}\frac{p_1^3}{k^2}$$

$$A_{13} = \left\{60\left(\frac{p_1}{k}\right)^4 + 6\left(\frac{p_1}{k}\right)^2\right\} - \frac{8\tan\theta}{\pi k^2}\cdot 3\sqrt{3}\,p_1$$

$$B_{13} = \left\{-r_1\,\frac{N_1}{N_2}\cdot\frac{2}{k^2} - r_2\cdot\frac{1}{k^2}\right\}\frac{p_1^3}{k^2}$$

The equation being

$$(A_{11}+B_{11}\beta)\alpha_1+(A_{12}+B_{12}\beta)\alpha_2+(A_{13}+B_{13}\beta)\alpha_3=0 \qquad -(6.8)$$

at $\left(\frac{y-h_1}{h}\right)=\frac{1}{2}$,

$$A_{21} = \left\{8\left(\frac{p_3}{k}\right)^4+4\left(\frac{p_3}{k}\right)^2+1\right\}-\frac{48\tan^2\theta}{k^2\pi^2}$$

$$B_{21} = \left\{-\lambda_1\frac{N_1}{N_2}\left(\frac{1}{k^2}+\frac{\tan\theta}{2p_3}\right)-\lambda_2\left(\frac{1}{k^2}-\frac{\tan\theta}{2p_3}\right)\right\}\frac{p_3^3}{k^2}$$

$$A_{22} = -\frac{32\,p_3\tan\theta}{k^2\pi}$$

$$B_{22} = 0$$

$$A_{23} = \left\{-136\left(\frac{p_3}{k}\right)^4-20\left(\frac{p_3}{k}\right)^2-1\right\}+\frac{48\tan^2\theta}{k^2\pi^2}$$

$$B_{23} = \left\{\lambda_1\frac{N_1}{N_2}\left(\frac{5}{k^2}+\frac{\tan\theta}{2p_3}\right)+\lambda_2\left(\frac{5}{k^2}-\frac{\tan\theta}{2p_3}\right)\right\}\frac{p_3^3}{k^2}$$

The equation being

$$(A_{21}+B_{21}\beta)\alpha_1+(A_{22}+B_{22}\beta)\alpha_2+(A_{23}+B_{23}\beta)\alpha_3=0 \qquad -(6.9)$$

at $\left(\frac{y-h_1}{h}\right) = \frac{2}{3}$,

$$A_{31} = \left\{4\left(\frac{p_2}{k}\right)^4 + 2\left(\frac{p_2}{k}\right)^2 + \frac{3}{4}\right\} - \frac{8\tan\theta}{\pi k^2}\left(\sqrt{3}\,p_2 + \frac{9}{2}\cdot\frac{\tan\theta}{\pi}\right)$$

$$B_{31} = \left\{-\lambda_1\frac{N_1}{N_2}\left(\frac{1}{3k^2} - \frac{3}{16}\cdot\frac{\lambda_1}{p_2}\right) - \lambda_2\left(\frac{2}{3k^2} + \frac{3}{16}\cdot\frac{p_5}{p_2}\right)\right\}\frac{p_2^3}{k^2}$$

$$A_{32} = \left\{-\frac{163}{4}\left(\frac{p_2}{k}\right)^4 - \frac{19}{2}\left(\frac{p_2}{k}\right)^2 - \frac{3}{4}\right\} - \frac{8\tan\theta}{\pi k^2}\left(\frac{\sqrt{3}}{2}p_2 - \frac{9}{2}\frac{\tan\theta}{\pi}\right)$$

$$B_{32} = \left\{\lambda_1\frac{N_1}{N_2}\left(\frac{19}{12k^2} - \frac{3}{16}\cdot\frac{\lambda_1}{p_2}\right) + \lambda_2\left(\frac{19}{6k^2} + \frac{3}{16}\frac{p_5}{p_2}\right)\right\}\frac{p_2^3}{k^2}$$

$$A_{33} = \left\{60\left(\frac{p_2}{k}\right)^4 + 6\left(\frac{p_2}{k}\right)^2\right\} + \frac{24\sqrt{3}\,p_2\tan\theta}{\pi k^2}$$

$$B_{33} = \left\{-\lambda_1\frac{N_1}{N_2}\left(\frac{1}{k^2}\right) - \lambda_2\left(\frac{2}{k^2}\right)\right\}\frac{p_2^3}{k^2}$$

The equation being

$$(A_{31} + B_{31}\beta)\alpha_1 + (A_{32} + B_{32}\beta)\alpha_2 + (A_{33} + B_{33}\beta)\alpha_3 = 0 \quad \text{—(6.10)}$$

In equations (6.8) to (6.10), $\beta = \frac{N_2 h^2}{\pi^2 D}$. These equations may be written in matrix form as

$$(A + B\beta)\alpha = 0$$

which corresponds to a standard eigenvalue problem in which β may be found by determining the characteristic equation and subsequently its lowest positive root. To be perfectly rigorous, both n and k should be varied in determining the lowest value of β .

It should be mentioned that the chosen deflection function (6.1), although satisfying the deflection boundary conditions exactly along all edges and the rotation boundary conditions at the parallel edges, did not satisfy the latter conditions along the sloping edges, and this will give rise to some inaccuracy. It may be pointed out that the buckling load of a clamped square plate calculated by this method is about 30% smaller than the actual value; whereas in the other limit of a right-angled isosceles triangular plate, the buckling load is only 10% smaller than that given by a data sheet published by the Royal Aeronautical Society (10).

6.4 Buckling Load For Model 'B' Of Chapter 2.

The model was loaded by a vertical load at its apex. In order to calculate a buckling load, the following assumptions have been made :-

(i) the compressive load in the plane of the wall due to the external load is uniformly spread along the top edge; this is justified since this edge is usually short,

(ii) there is no normal load on the sloping edges. This is not true as can be seen from Chapter 4 where a normal stress σ_t was assumed in working out the stress distributions in the walls of the pyramid. However, the stress is small compared with that acting on the top edge. Also, there is some tension in the middle portion of the edges which will tend to compensate for the compression as regards the buckling load; and

(iii) the load is uniform along the bottom edge. This again is not true but it is not expected to make much difference to the buckling load.

<u>Calculations</u>

The dimensions of the walls are as follows (ref. Fig.6.1);

$$b_1 = 3/8'', \quad b_2 = 3'', \quad h = 2\,5/8'', \quad t = 1/25''.$$

Young's modulus, $E = 4.5 \times 10^5$ p.s.i.

Poisson's ratio, $\mu = 0.35$.

$$\lambda_1 = 1/7, \quad \lambda_2 = 8/7, \quad \tan\theta = 1/2,$$

so that

$$p_1 = 0.4762, \; p_2 = 0.8095, \; p_3 = 0.6429, \; p_4 = 2.1428 \;\&\; p_5 = -0.8571.$$

Also,

$$N_1/N_2 = 8$$

and

$$D = \frac{Et^3}{12(1-\mu^2)} = 2.735 \quad \text{lb.-in.}$$

(i) If the edges of the wall are assumed to be <u>simply-supported</u>, then the characteristic equation may be written as

$$\begin{vmatrix} (0.493-0.094\beta) & (0.514-0.279\beta) & (-2.1) \\ (0.785-0.304\beta) & (-3.27) & (-21.135+2.736\beta) \\ (0.169-0.209\beta) & (-7.157+1.28\beta) & (3.574) \end{vmatrix} = 0$$

from which β = 5.15. This gives N_2 = 20.1 lb. so that the buckling load for the pyramid is

$$P_{crit.} = 208.6 \text{ lb.}$$

(ii) However, if the edges of the wall are assumed to be <u>fixed</u>, then the characteristic equation becomes

$$\begin{vmatrix} (1.548-0.201\beta) & (3.563-0.664\beta) & (1.295-0.370\beta) \\ (2.805-0.607\beta) & (-3.274) & (-31.280+3.037\beta) \\ (1.082-0.707\beta) & (-25.919+2.980\beta) & (35.051-1.819\beta) \end{vmatrix} = 0$$

from which β = 11.84. This gives N_2 = 46.2 lb. so that the buckling load is

$$P_{crit.} = 480 \text{ lb.}$$

The experimental buckling load for the model was ~~202~~ 195 lb. (see Fig.2.8, Chapter 2), which corresponds well with the value for pinned edges.

However, if the pyramid is loaded horizontally, Fig.6.2, the buckling load is

$H_{crit.} = 90.5$ lb.

for the pinned edges, and

$H_{crit.} = 208$ lb.

for the clamped edges,

due to the buckling of Wall A.

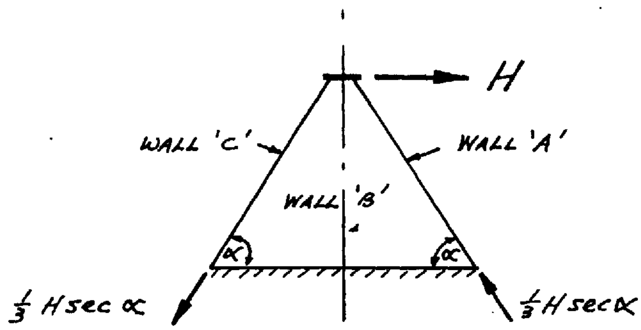

FIG. 6.2

There is no experimental result to show which case is the better approximation but it is likely, since Walls B are not likely to buckle before Wall A, that the actual buckling load will be nearer the clamped edges case.

6.5 Conclusions.

Although no rigorous method for calculating the buckling load of a pyramid seems possible, the very approximate method outlined seems to give reasonable estimates. Klein's solution may be used to obtain the buckling load of a symmetrically loaded pyramid although it should be mentioned that the good comparison with the experimental result should be accepted with reserve since buckling experiments of this sort are difficult to control. Again, the suggestion that for a horizontally loaded pyramid, the clamped edges case probably gives a better approximation is not backed by experimental evidence and is therefore not conclusive. However, the work done in this chapter is useful in that some idea of the buckling loads of sheet pyramids is possible even though they may be very approximate.

CHAPTER 7

Conclusions

7.1 The research has shown that within the limits normally expected with this type of structure, the square-based pyramidal roof behaves in a similar manner to a pinned skeletal system in which the area of each diagonal member is equivalent to two thirds of the area of the triangular plate on one side. On this basis the calculated and measured deformations agreed within about 10%. The stresses in the plate in the most stressed pyramid are not critical and any small tendency to buckling does not seriously reduce the performance of the system within the elastic range nor its ultimate load bearing capacity.

7.2 In the simply-supported single pyramid, the measured stresses in the plate agreed well with those obtained by plane stress theory assuming the edges to be simply-supported.

7.3 In the single pyramid with a fixed base the agreement between measured and theoretical stresses was not good because the assumption of zero displacement along the bottom edge of the wall was not valid. However this case is only of academic interest because the fixed base condition cannot realistically be achieved in practice.

7.4 The buckling load of a pyramid with fixed base subjected to a vertical load at its apex was calculated by considering the walls as pinned trapezoidal plates under uniform compression along their parallel edges. Calculated and measured values were in close agreement.

BIBLIOGRAPHY

1. Born, J. " Faltwerke." 1960. Verlag Konrad Wittwer, Stuttgart.

2. Makowski, Z. S. " Stressed Skin Space Grids." July, 1961. Architectural Design.

3. Makowski, Z. S. " Developments In Aluminium Sheet Space Structures." April, 1961. Light Metals.

4. Makowski, Z. S. " Aluminium Sheet Structure." July, 1961. Light Metals.

5. Larsen, H. D. " Rinehart Mathematical Tables, Formulas And Curves." Rinehart and Company, Inc., New York.

6. Allen, D. N. de G. " Relaxation Methods In Engineering And Science." McGraw-Hill Book Company, Inc., New York.

7. Brooker, R. A., etc. " Mercury Autocode Manual." Second Edition. Manchester University Computing Machine Laboratory.

8. Fox, L. " Mixed Boundary Conditions In The Relaxational Treatment Of Biharmonic Problems (Plane Strain Or Stress)" Proceedings of the Royal Society, A, 189, (1947).

9. Klein, B. " Buckling Of Simply Supported Plates Tapered In Planform." Journal of Applied Mechanics, June, 1956.

10. Aero. Data Sheet No. 02.04.06. " Initial Buckling Of Flat Isosceles Triangular Plates Under Combined Compression And Shear." Published by the Royal Aeronautical Society. May, 1957.

11. Timoshenko, S. P. and Goodier, J. N. " Theory Of Elasticity." Second edition. McGraw-Hill Book Company, Inc., New York.

12. Timoshenko, S. P. and Gere, J. M. " Theory Of Elastic Stability." Second edition. McGraw-Hill Book Company, Inc., New York.

13. Timoshenko, S. P. and Woinowsky-Krieger, S. " Theory Of Plates And Shells." Second edition. McGraw-Hill Book Company, Inc., New York.

FIG. 1.1 — DIAGRAMMATIC REPRESENTION OF A SQUARE-BASED PYRAMIDAL-SHEET ROOF

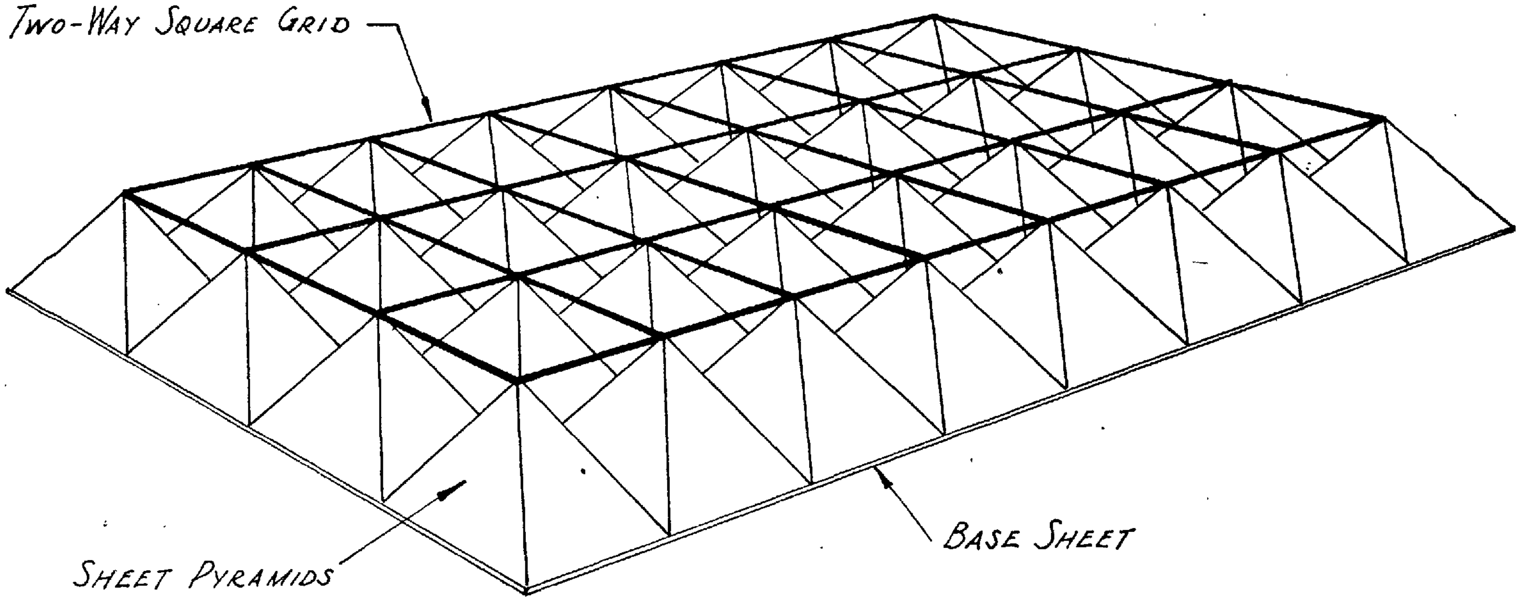

FIG. 1.2 — HEIGHT - BASE RELATIONSHIP OF PYRAMID

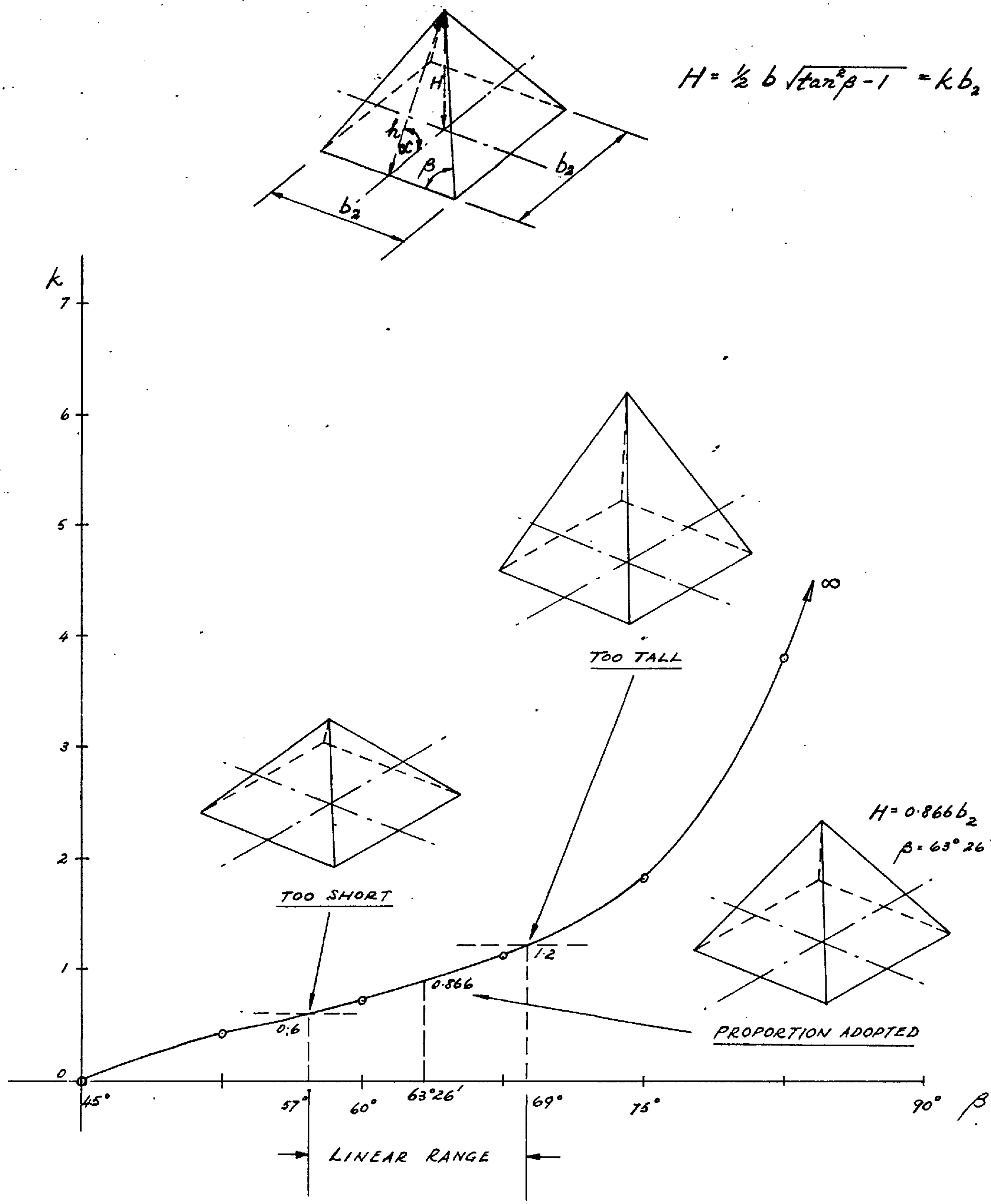

Fig. 1.3 — Suggested Curves For Determination Of Required Number Of Pyramids In A Roof Of Given Dimensions

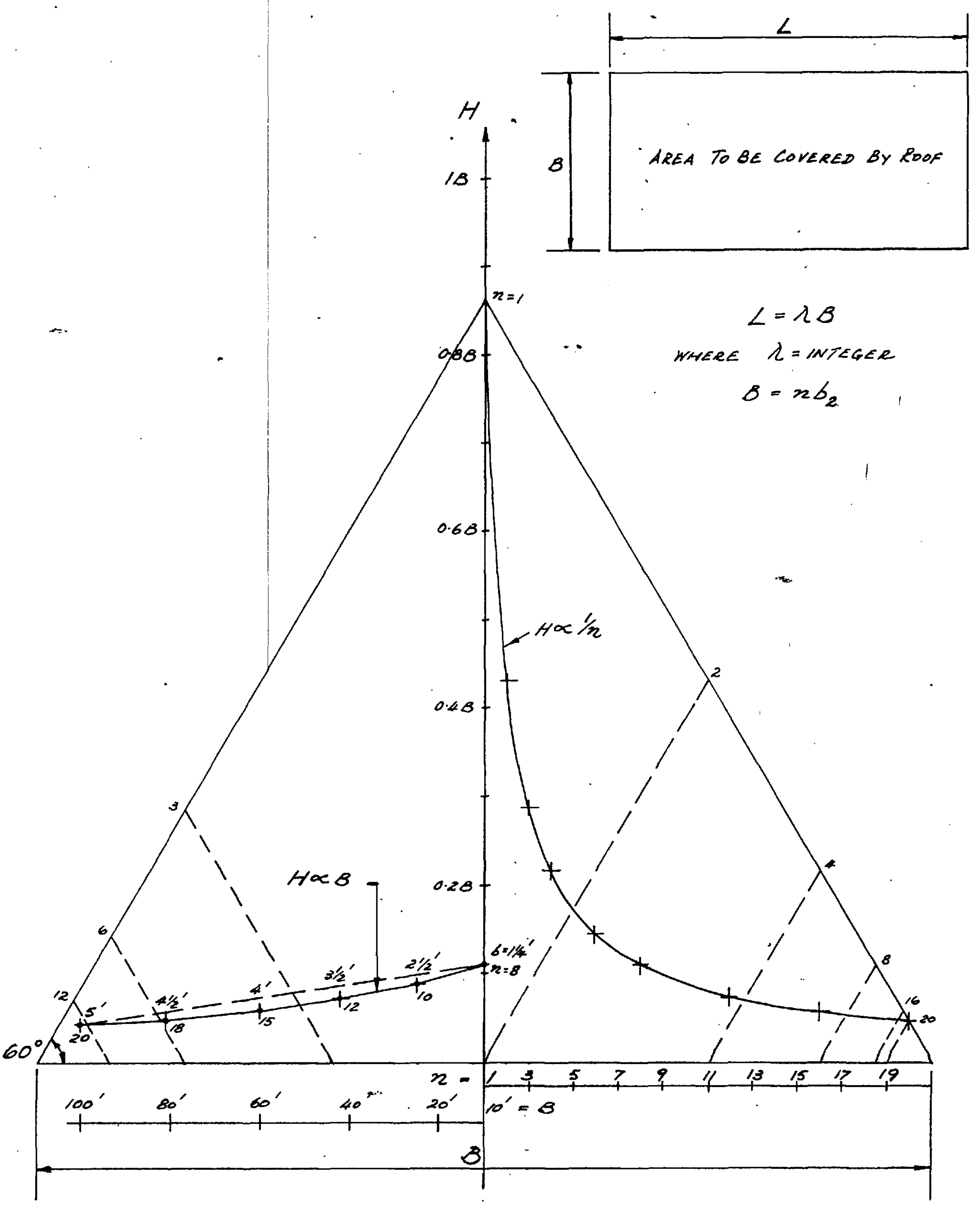

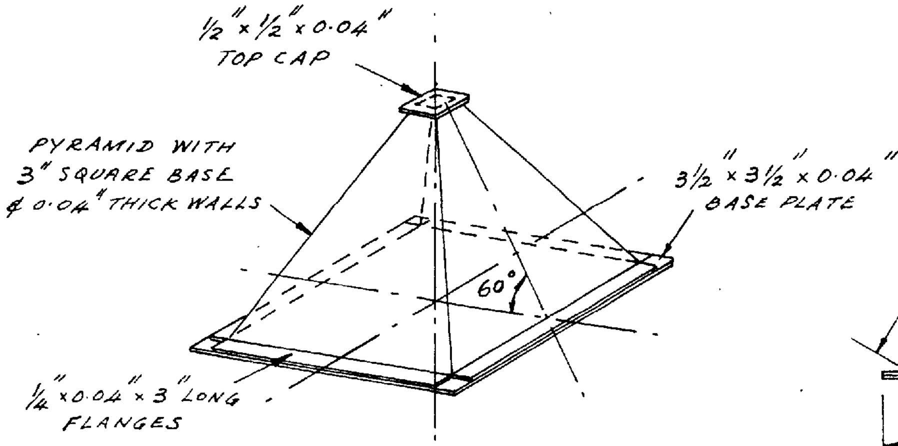

FIG. 2.1 — MODEL A

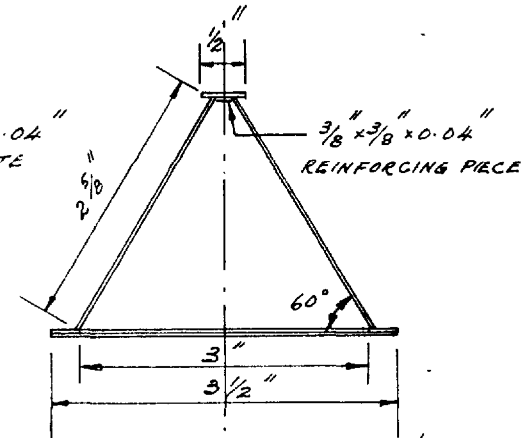

CROSS-SECTION THROUGH ℄

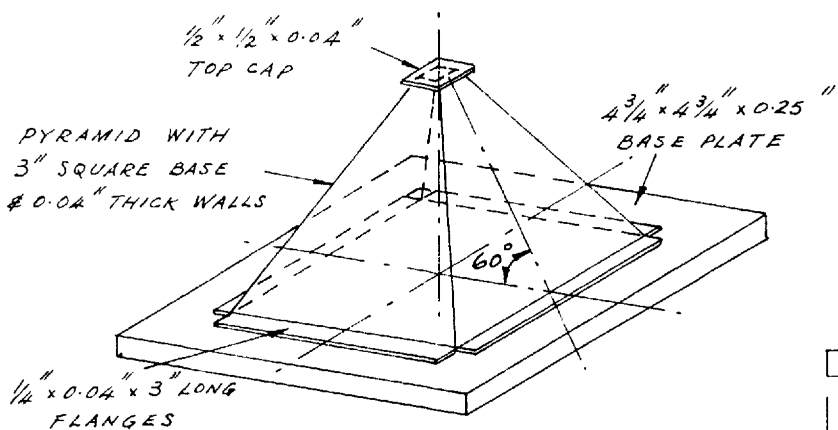

FIG. 2.2 — MODEL B

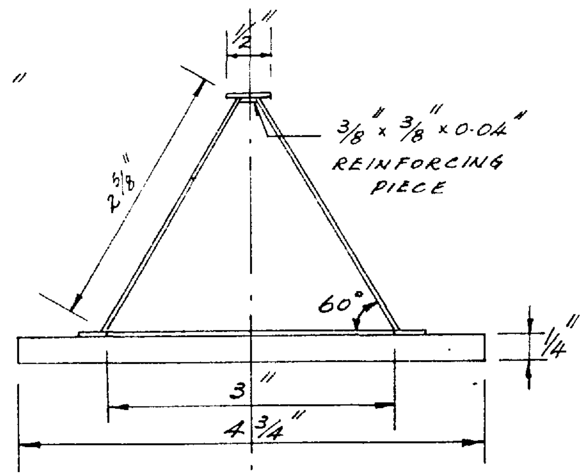

CROSS-SECTION THROUGH ℄

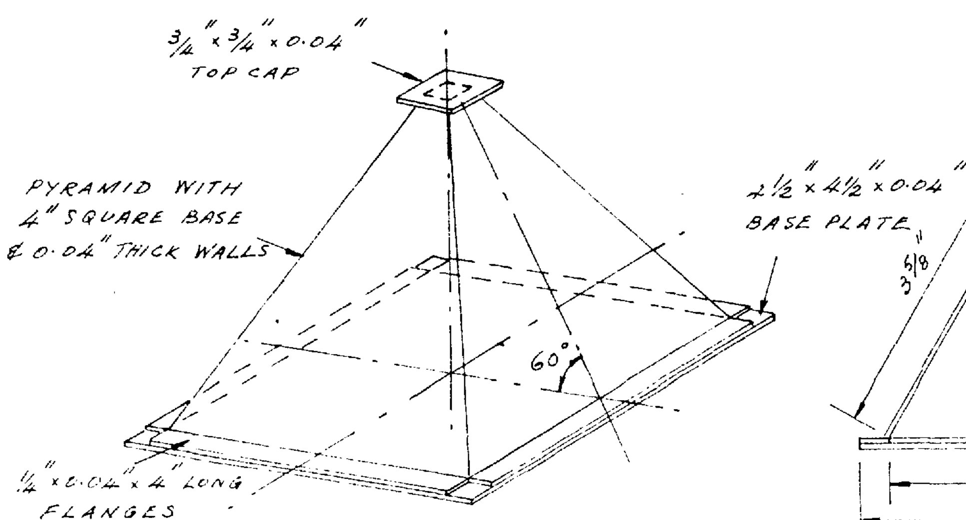

FIG. 2.3 — MODEL C

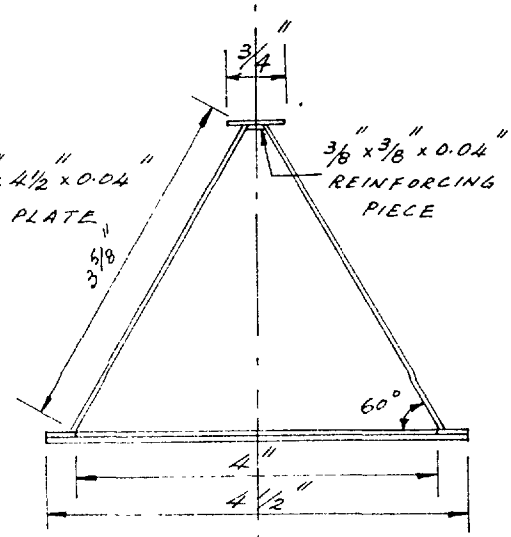

CROSS-SECTION THROUGH ℄

FIG. 2.4 MODELS D & D'

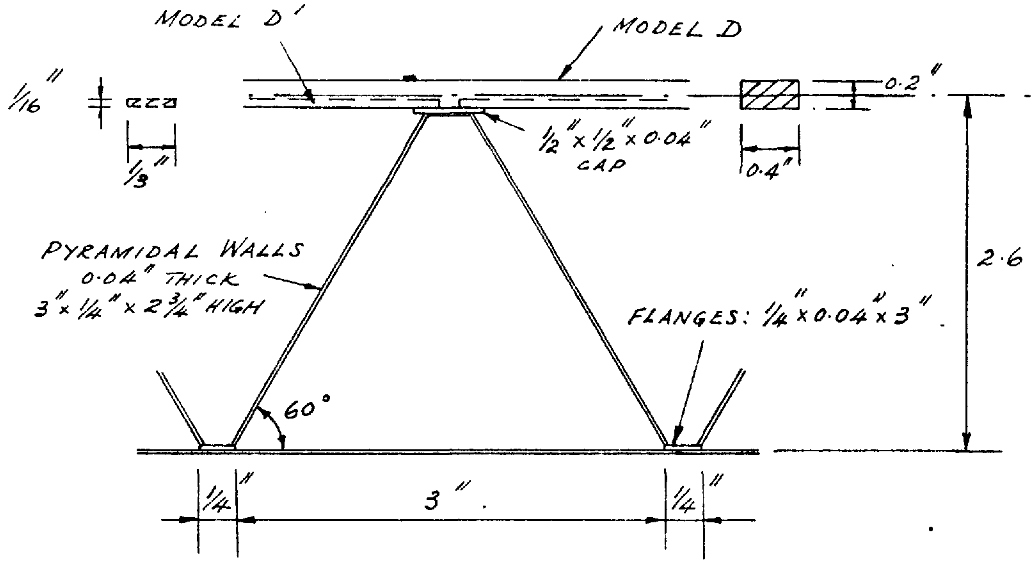

LONGITUDINAL SECTION

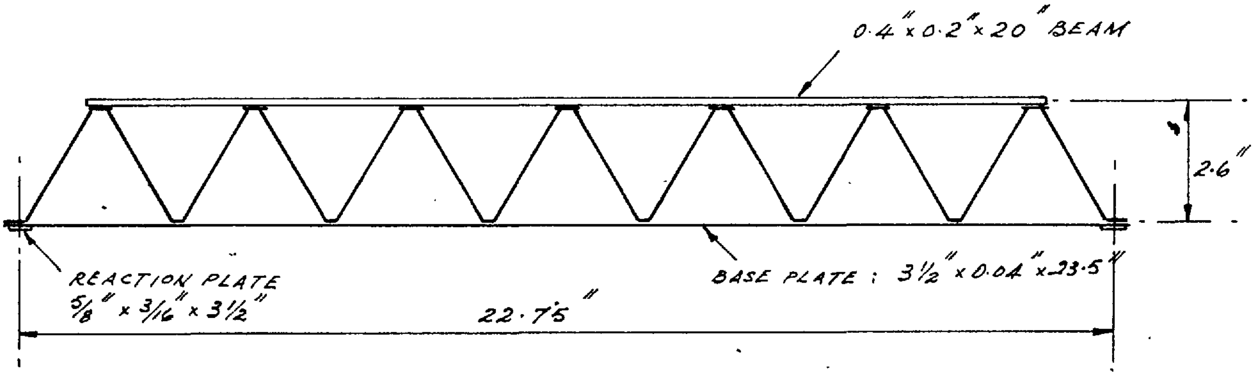

MODEL D

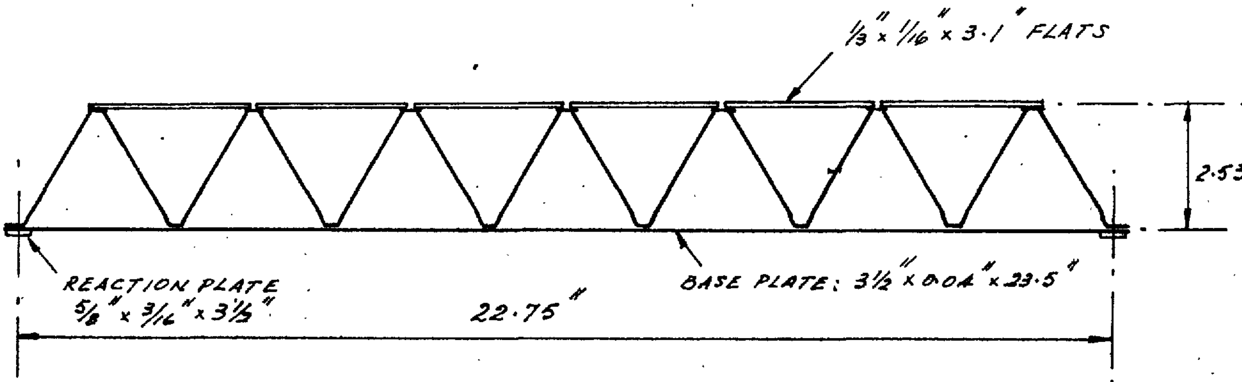

MODEL D'

FIG. 2.5 — MODEL E

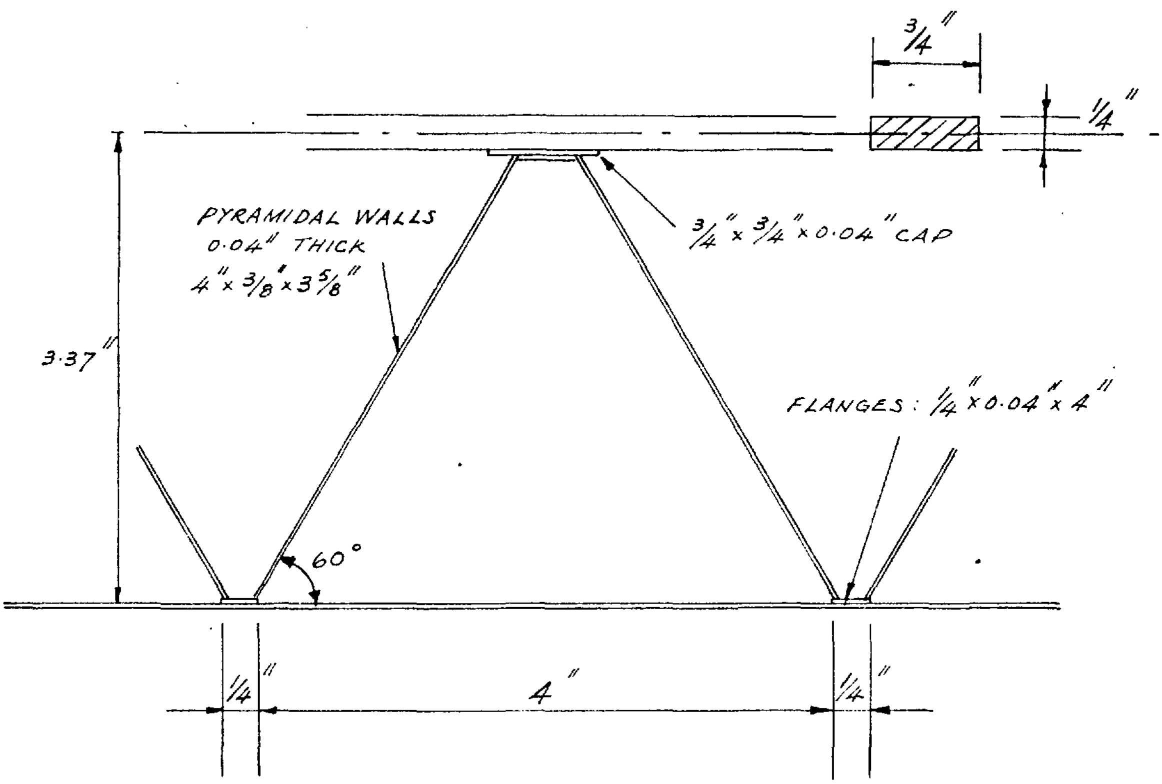

LONGITUDINAL SECTION

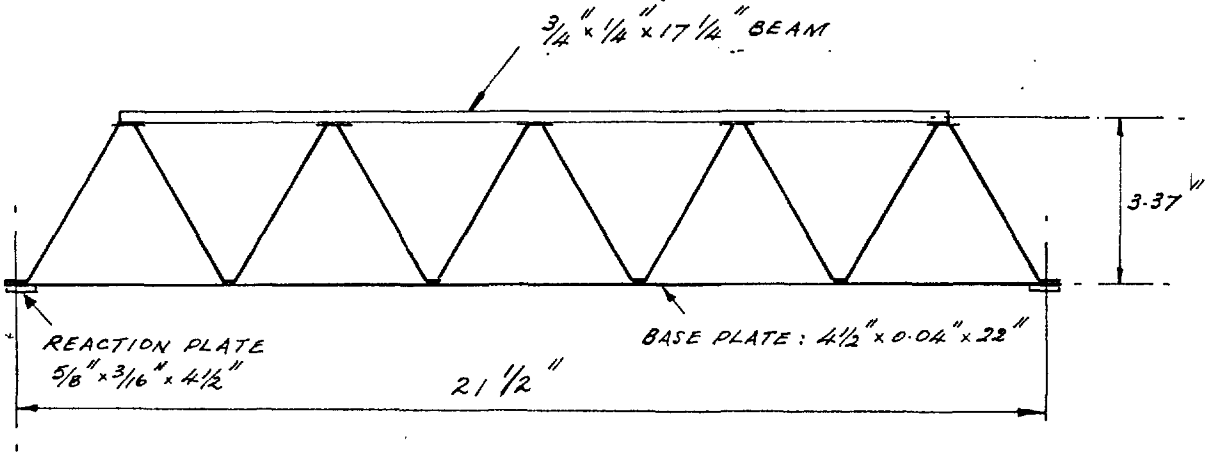

FIG. 2.6 LOADING ARRANGEMENT FOR TESTS ON MODELS A, B & C

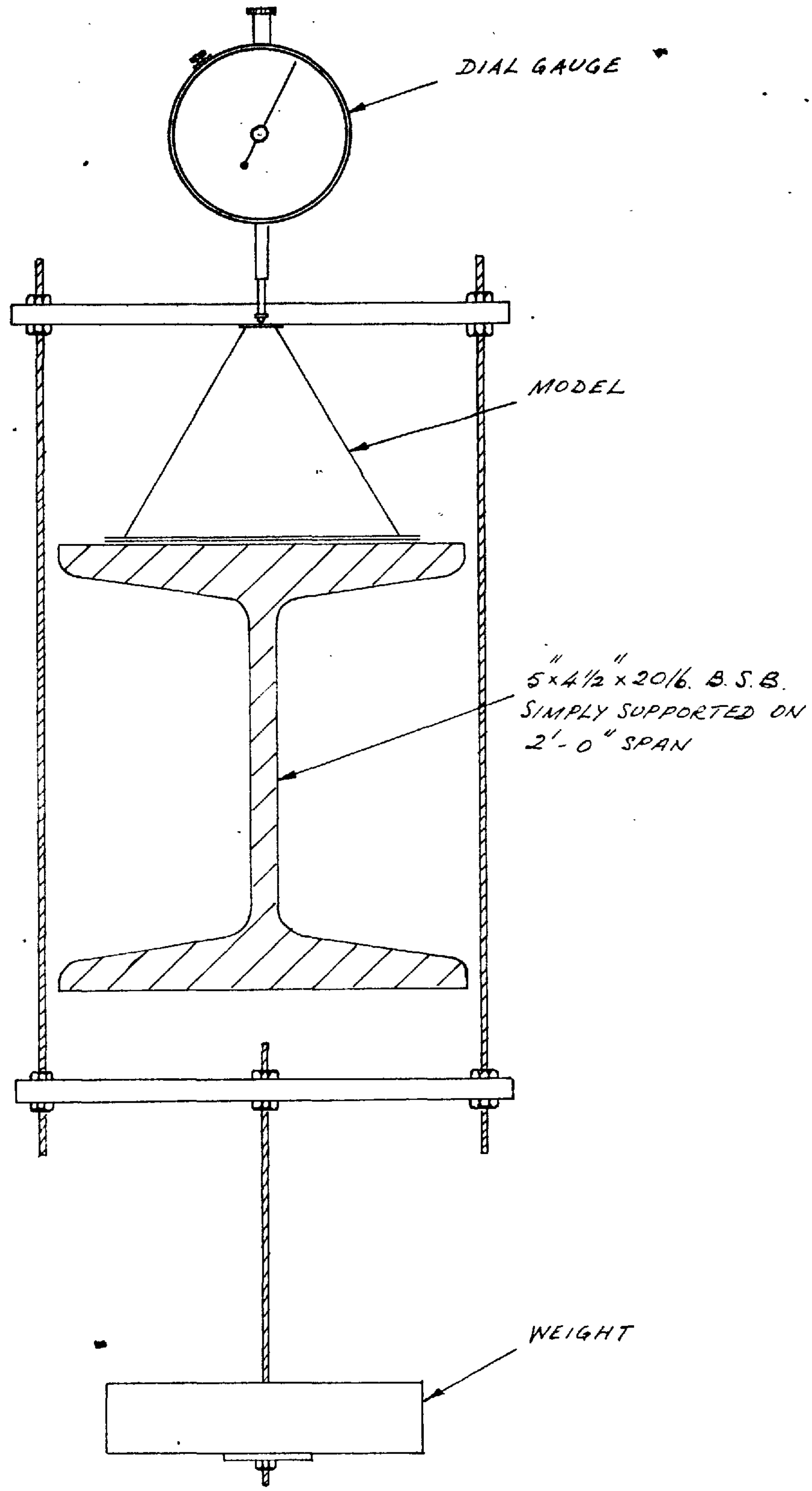

FIG. 2.7 – LOAD-DEFLECTION GRAPHS FOR SINGLE PYRAMIDS

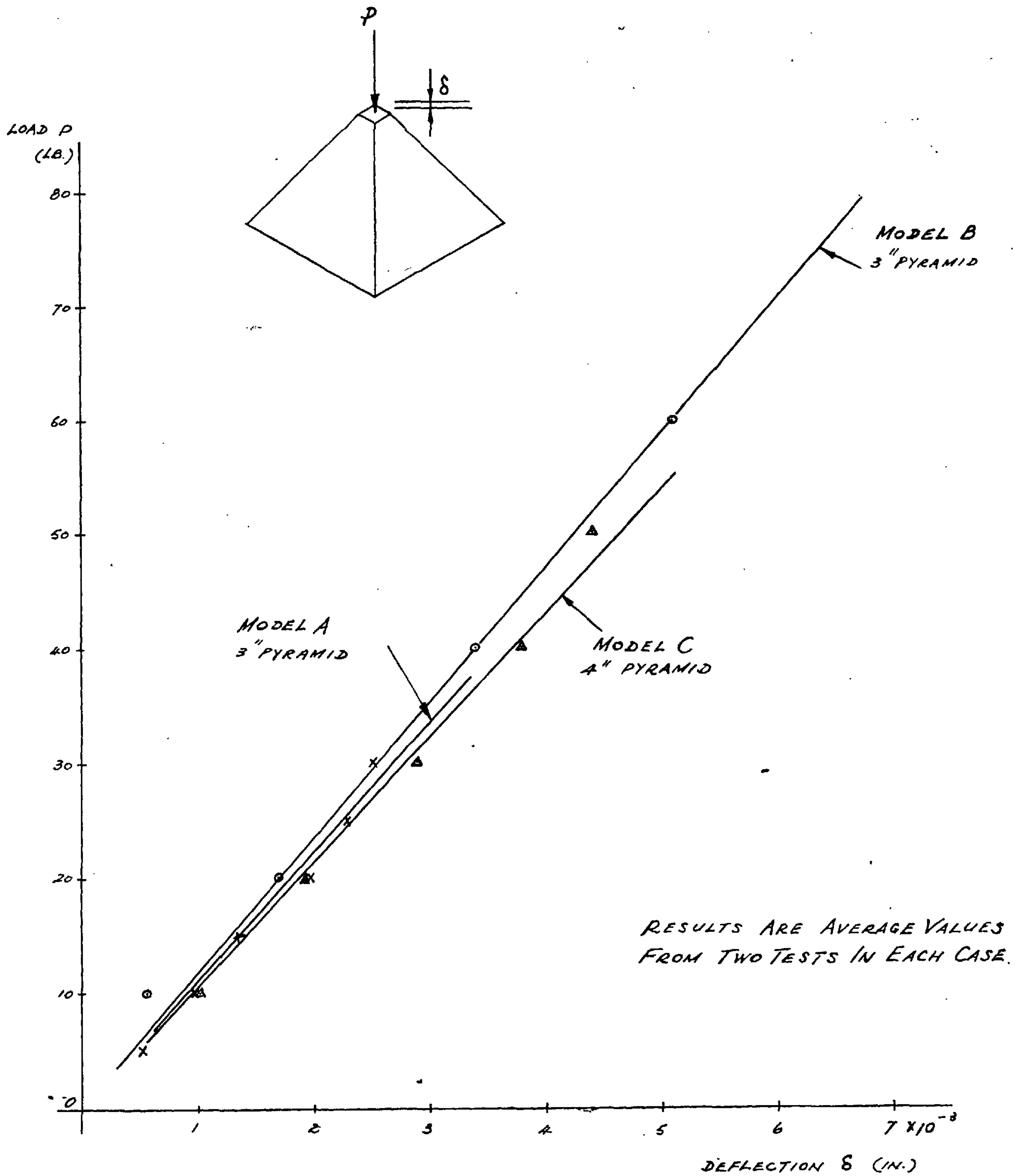

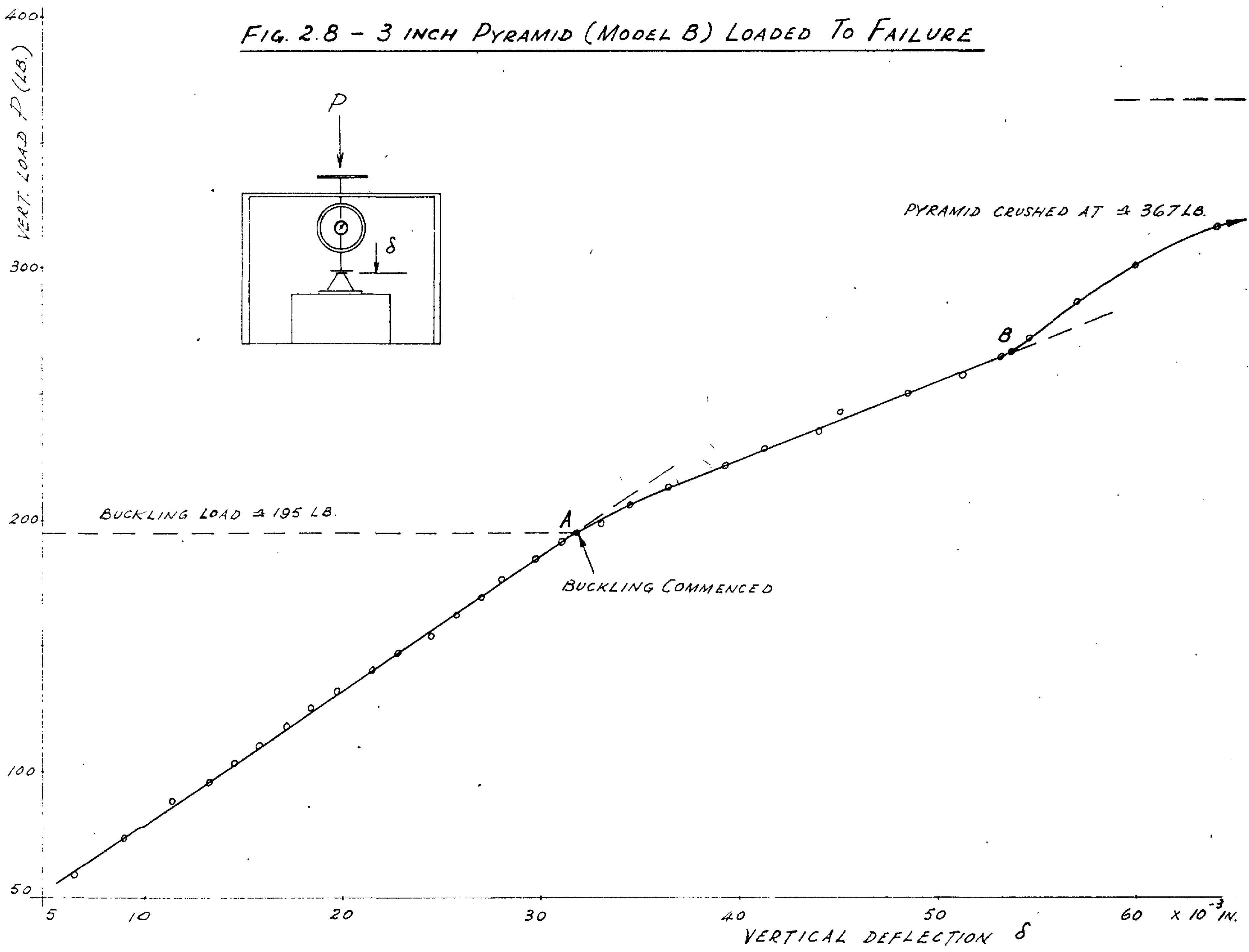
FIG. 2.8 – 3 INCH PYRAMID (MODEL B) LOADED TO FAILURE
VERT. LOAD P (LB.)
400
300
200
100
50
P
δ
PYRAMID CRUSHED AT ≙ 367 LB.
B
A
BUCKLING LOAD ≙ 195 LB.
BUCKLING COMMENCED
5
10
20
30
40
50
60
× 10⁻³ IN.
VERTICAL DEFLECTION δ

FIG. 2.9 — TEST ON MODEL D. (CASE 1)

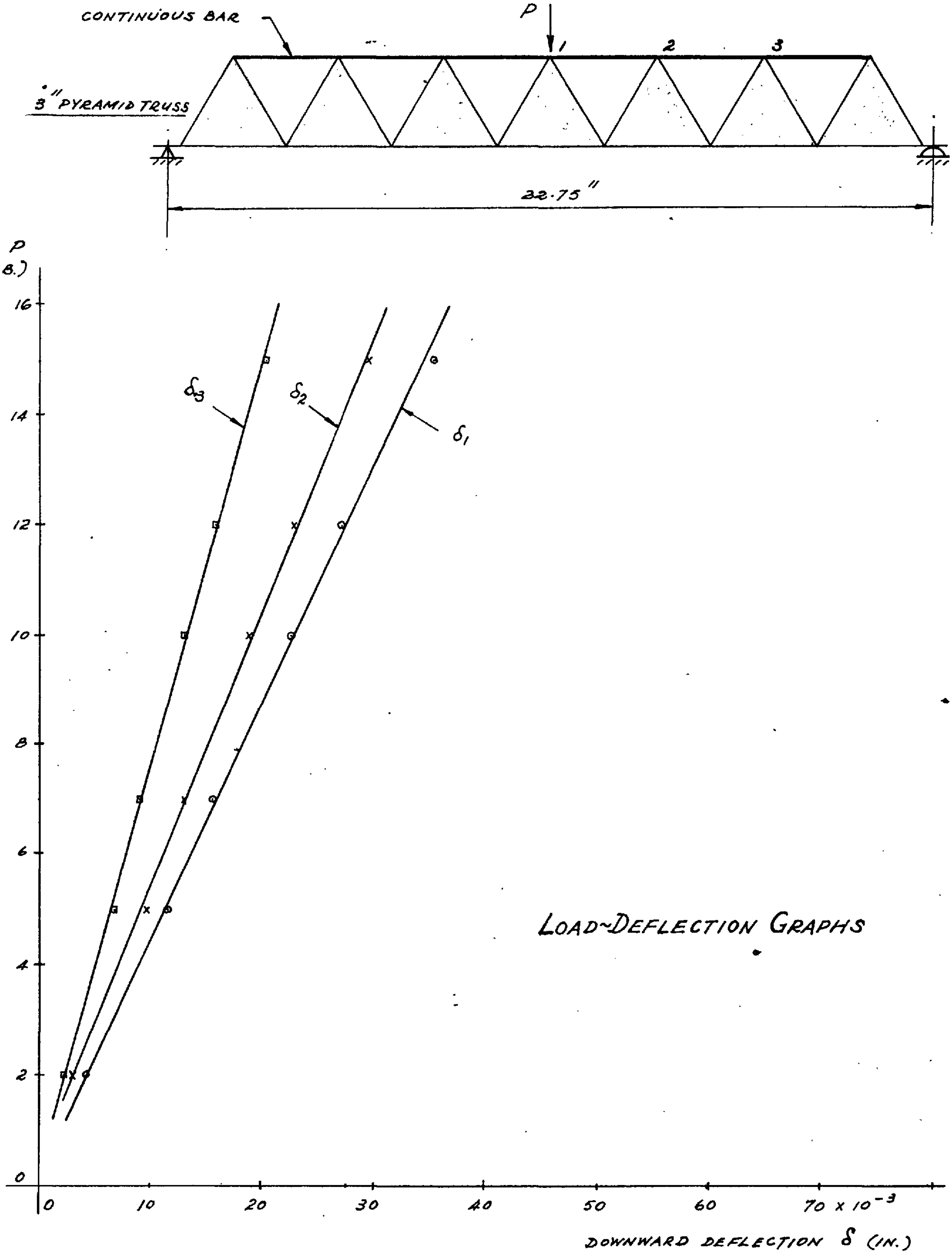

LOAD~DEFLECTION GRAPHS

FIG. 2.10. – TEST ON MODEL D. (CASE 2)

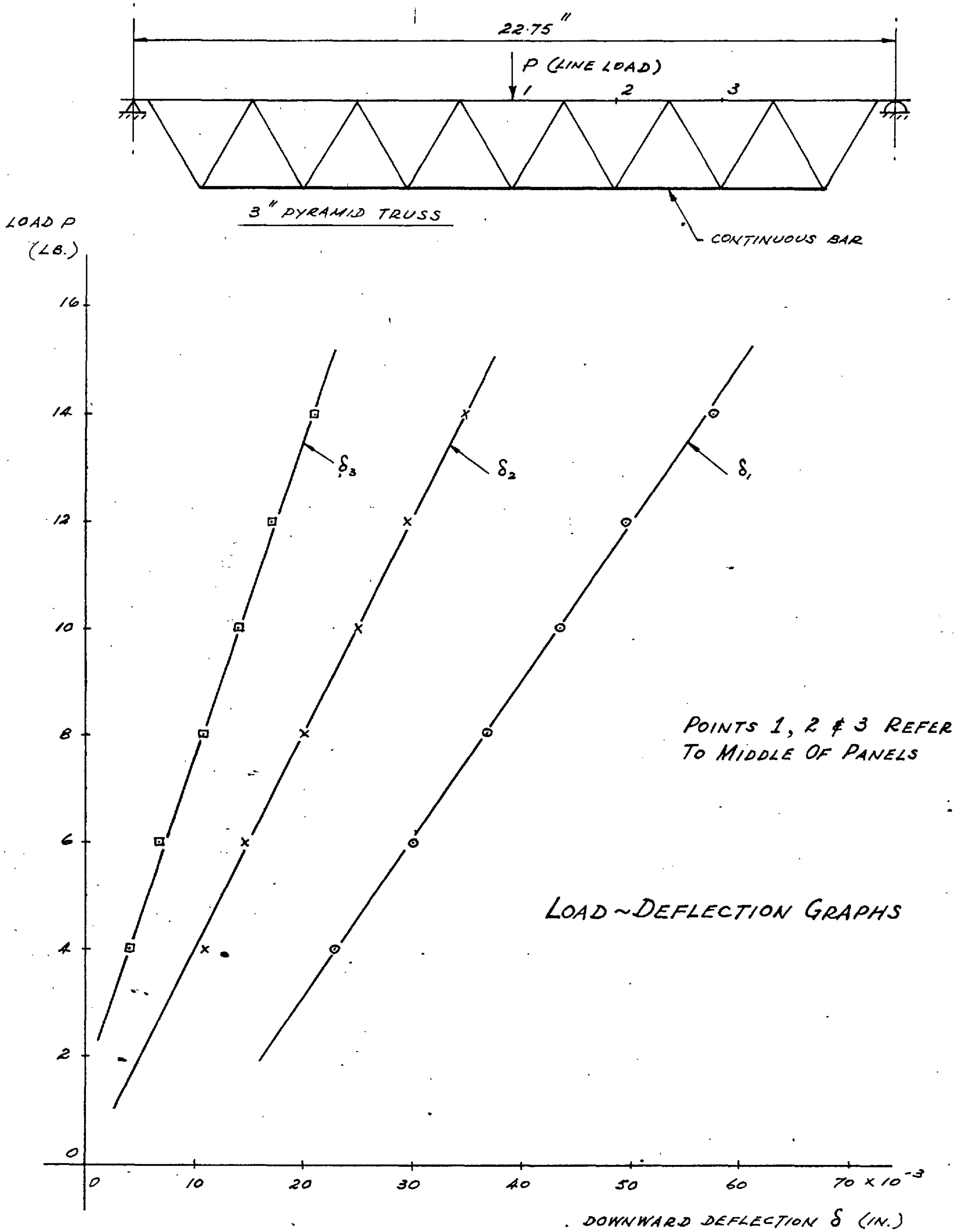

FIG. 2.11 – TEST ON MODEL D. (CASE 3)

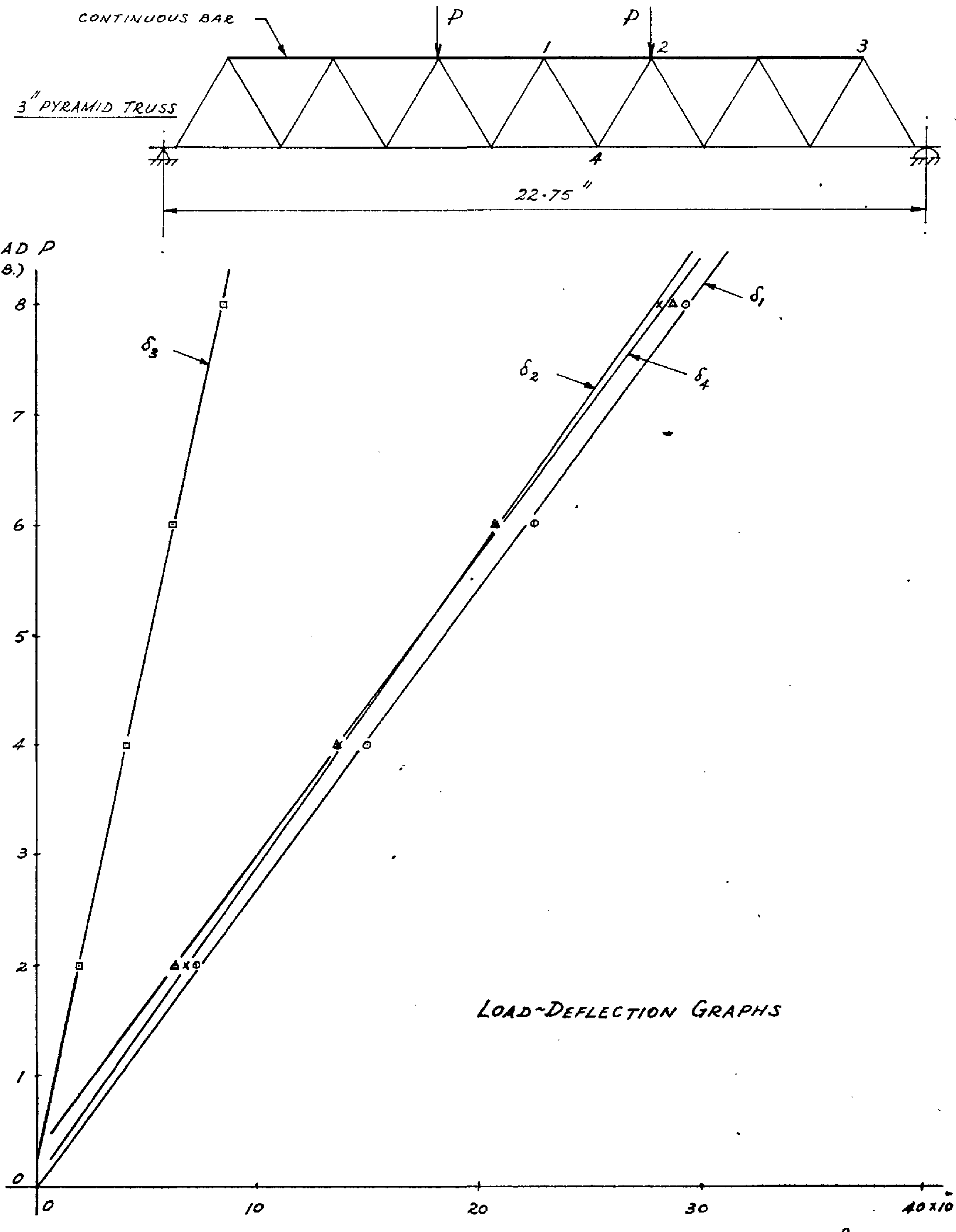

FIG. 2.12 – TEST ON MODEL D. (CASE 4)

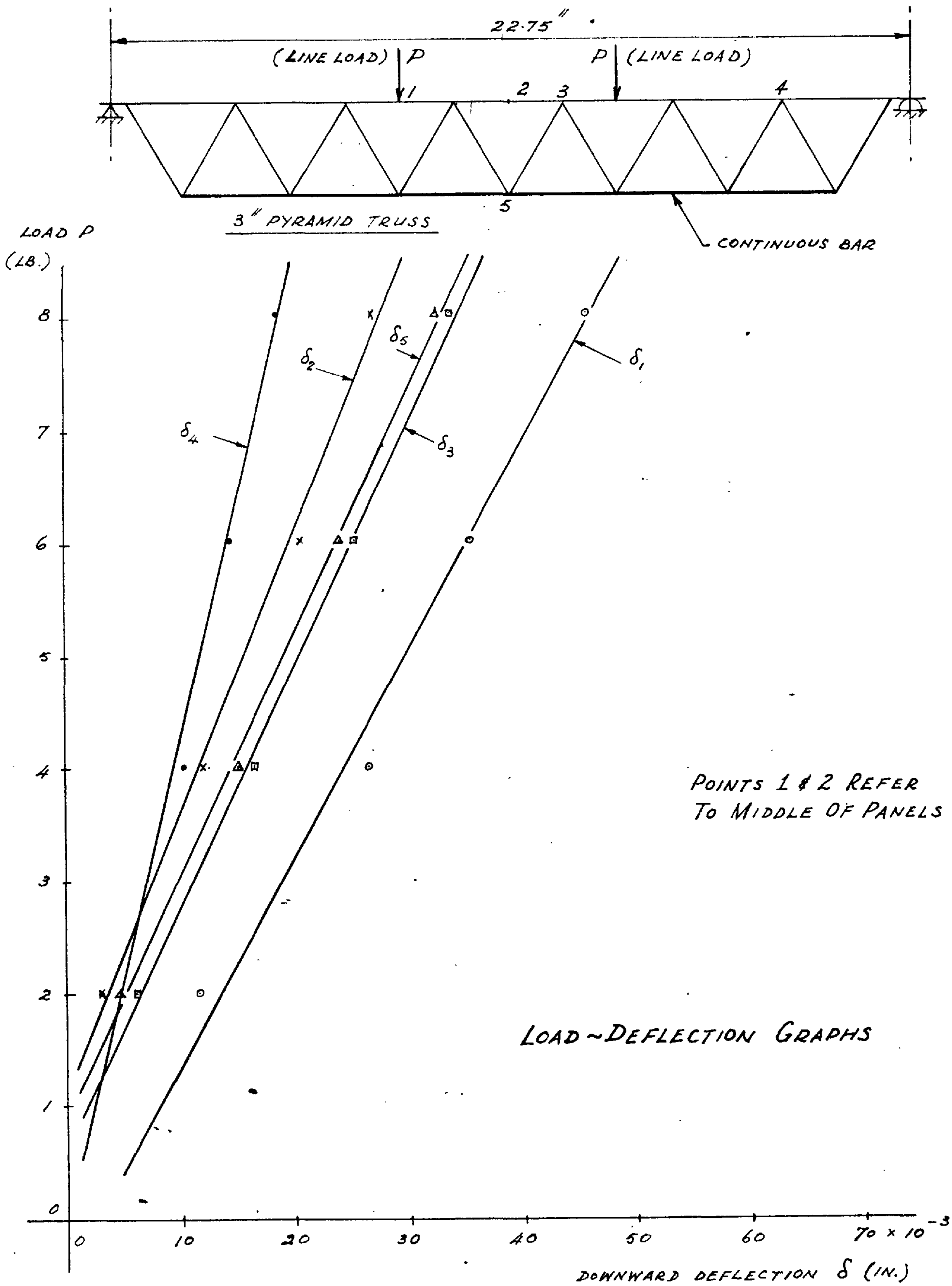

FIG. 2.13 — TEST ON MODEL D′

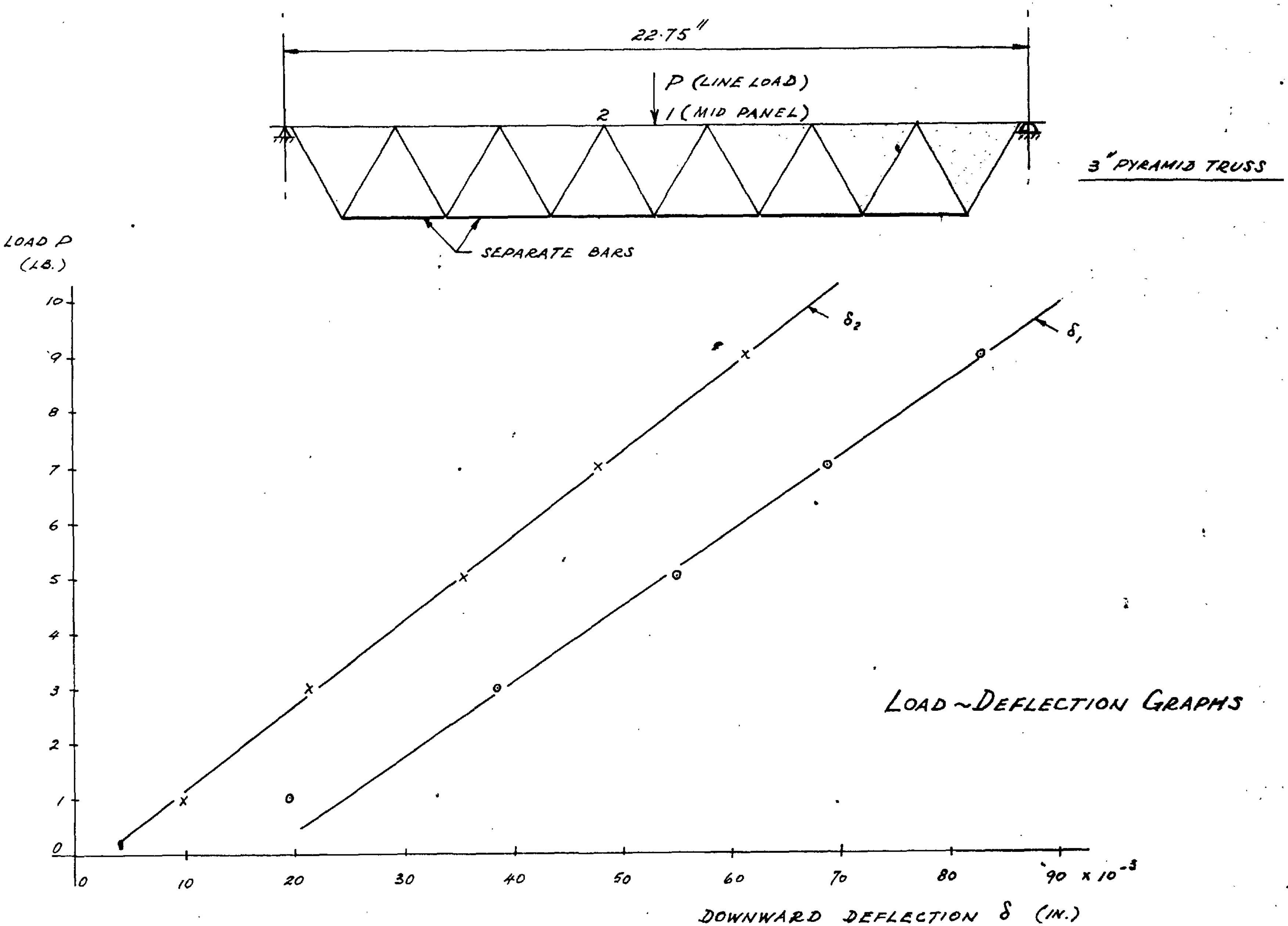

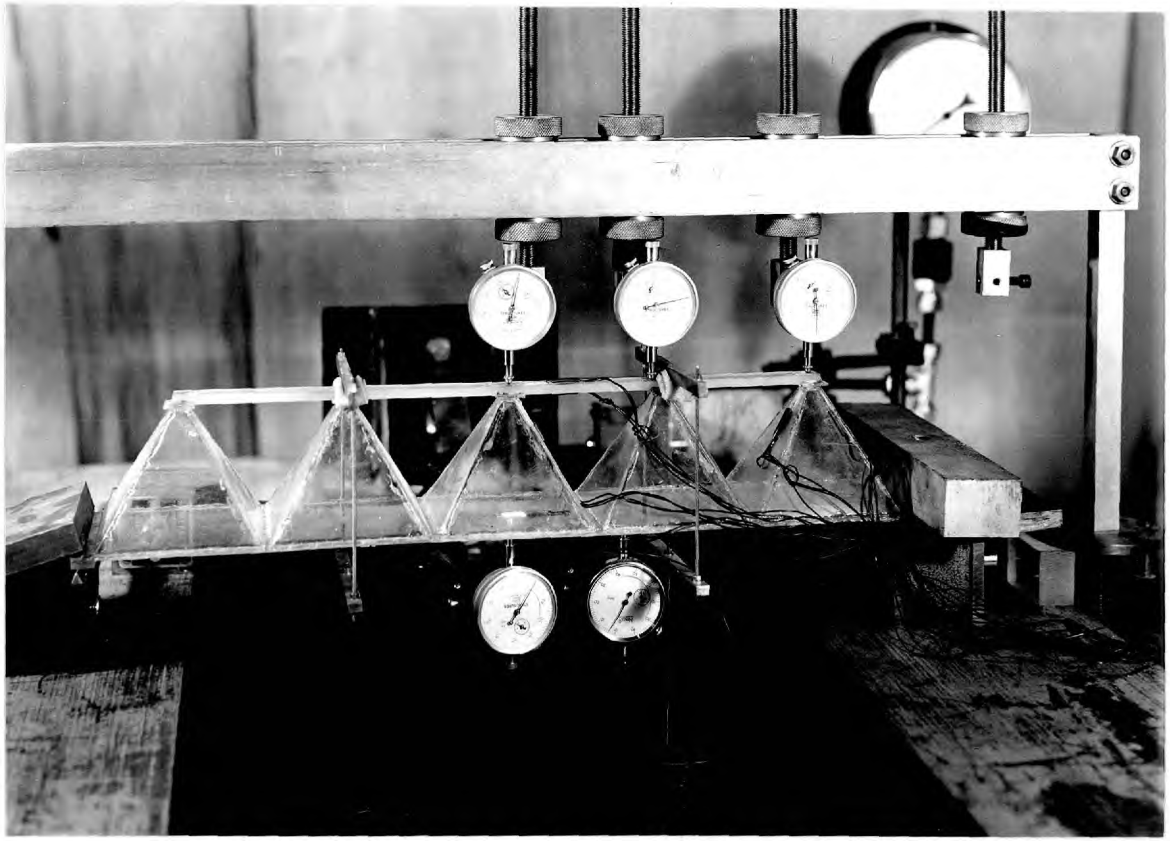

Fig. 2.14 - Model E ; Loading Case 1.

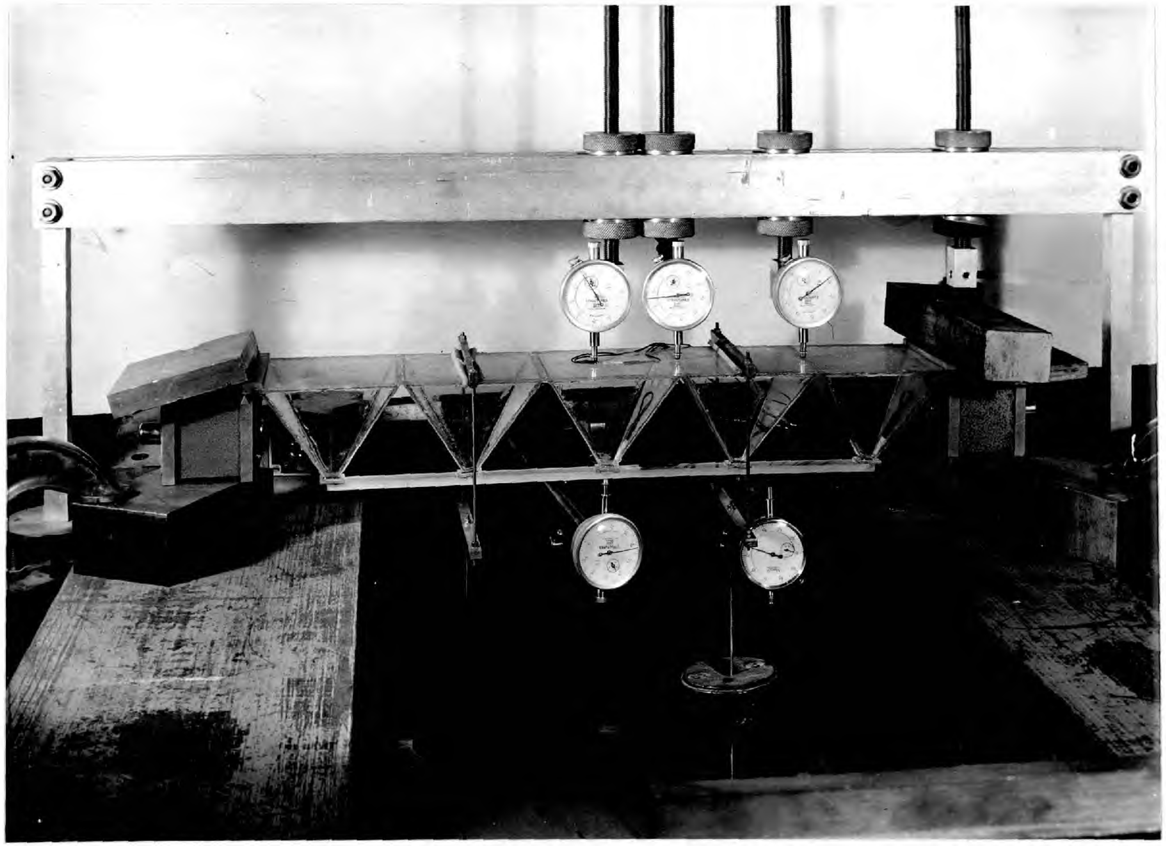

Fig. 2.15 - Model E ; Loading Case 2.

FIG. 2.16 – TEST ON MODEL E. (CASE 1)

LOAD ~ DEFLECTION GRAPHS

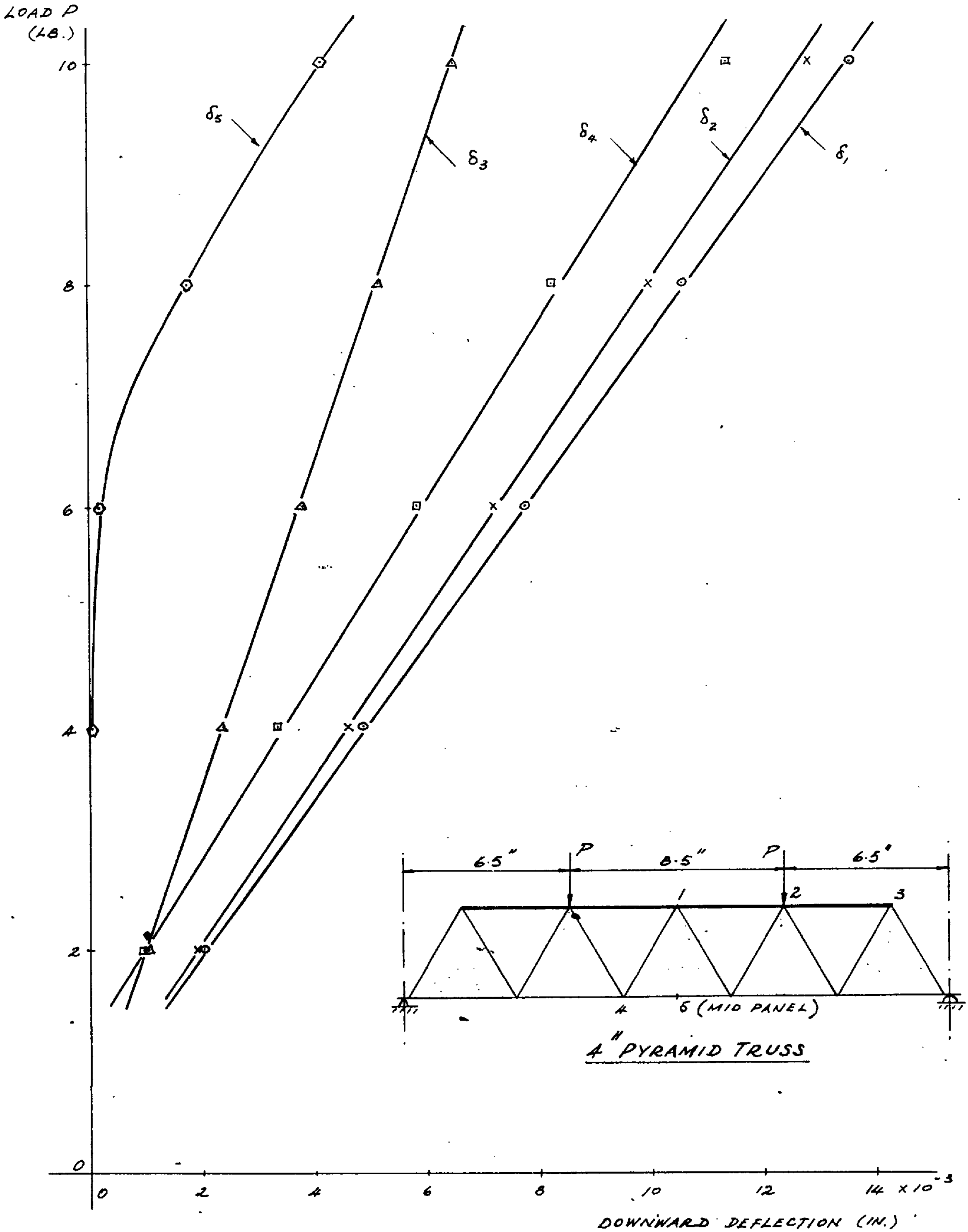

FIG. 2.17 – TEST ON MODEL E. (CASE 2)

LOAD ~ DEFLECTION GRAPHS

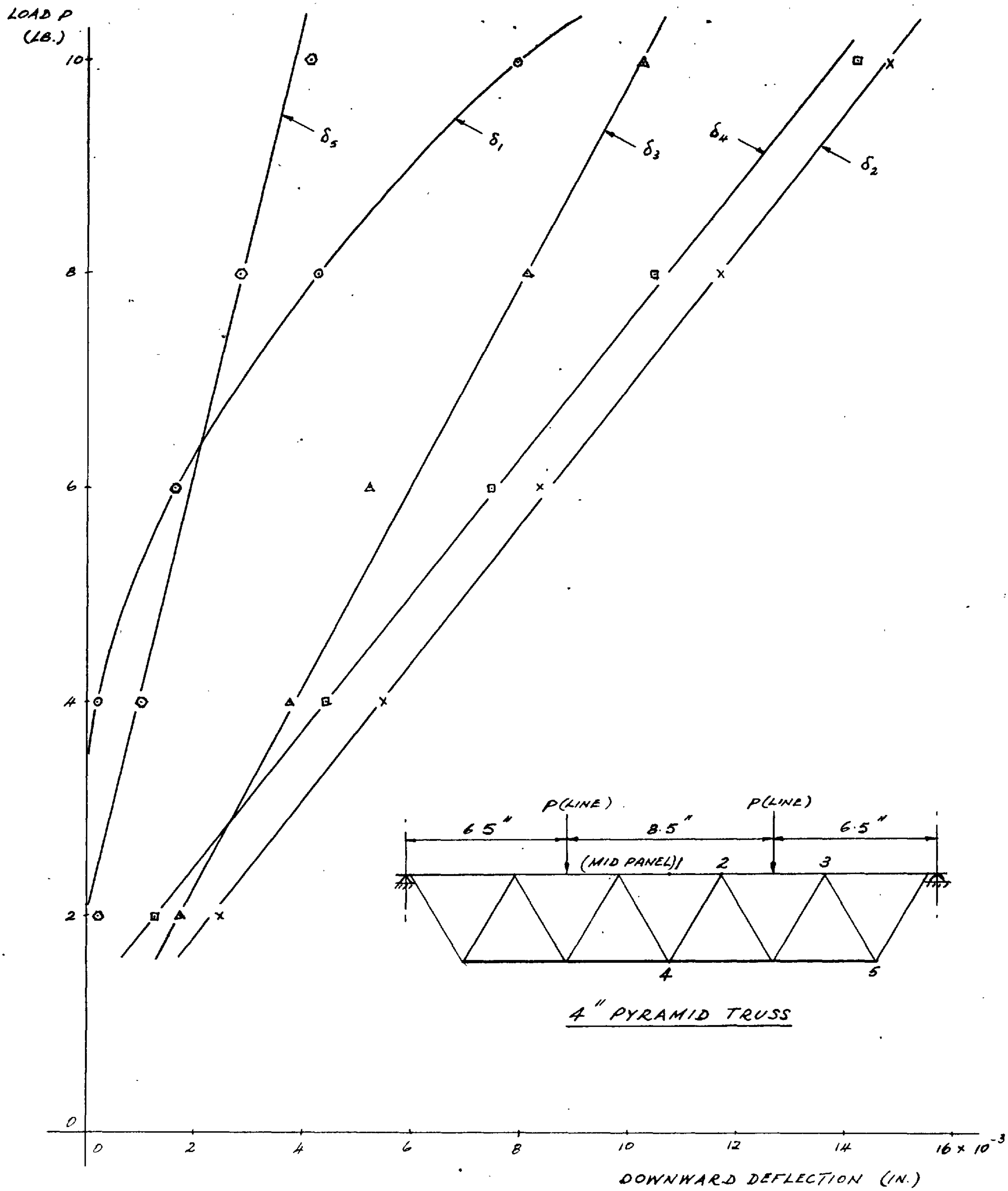

FIG. 2.18—TEST ON MODEL E (CASE 1)

LOAD ~ STRESS GRAPHS

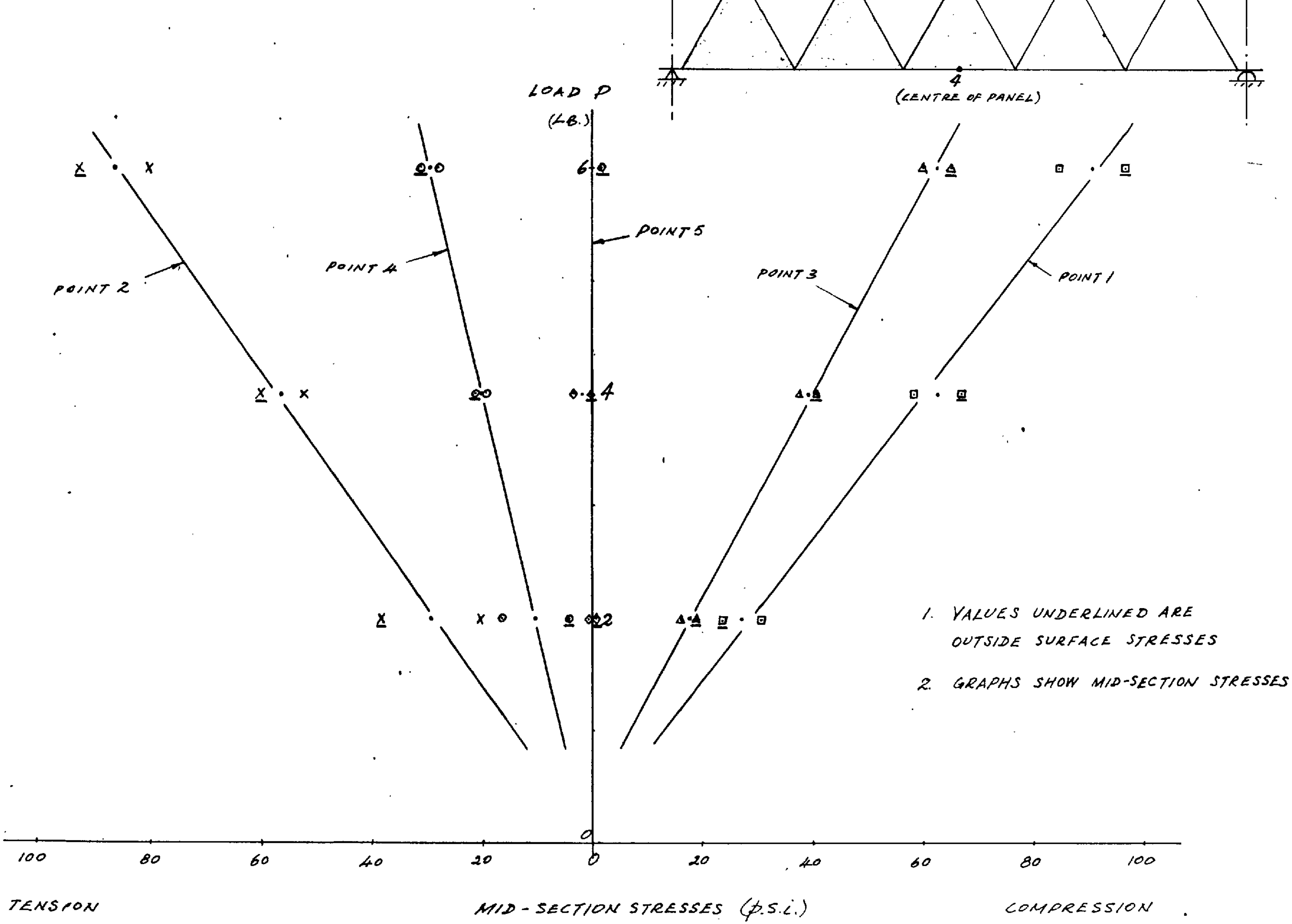

Fig. 2.19 – Test On Model E (Case 2)

Load ~ Stress Graphs

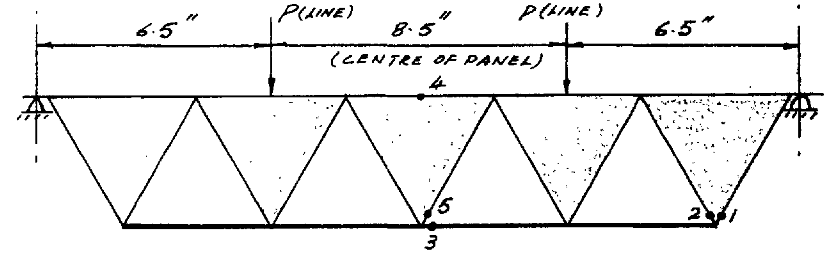

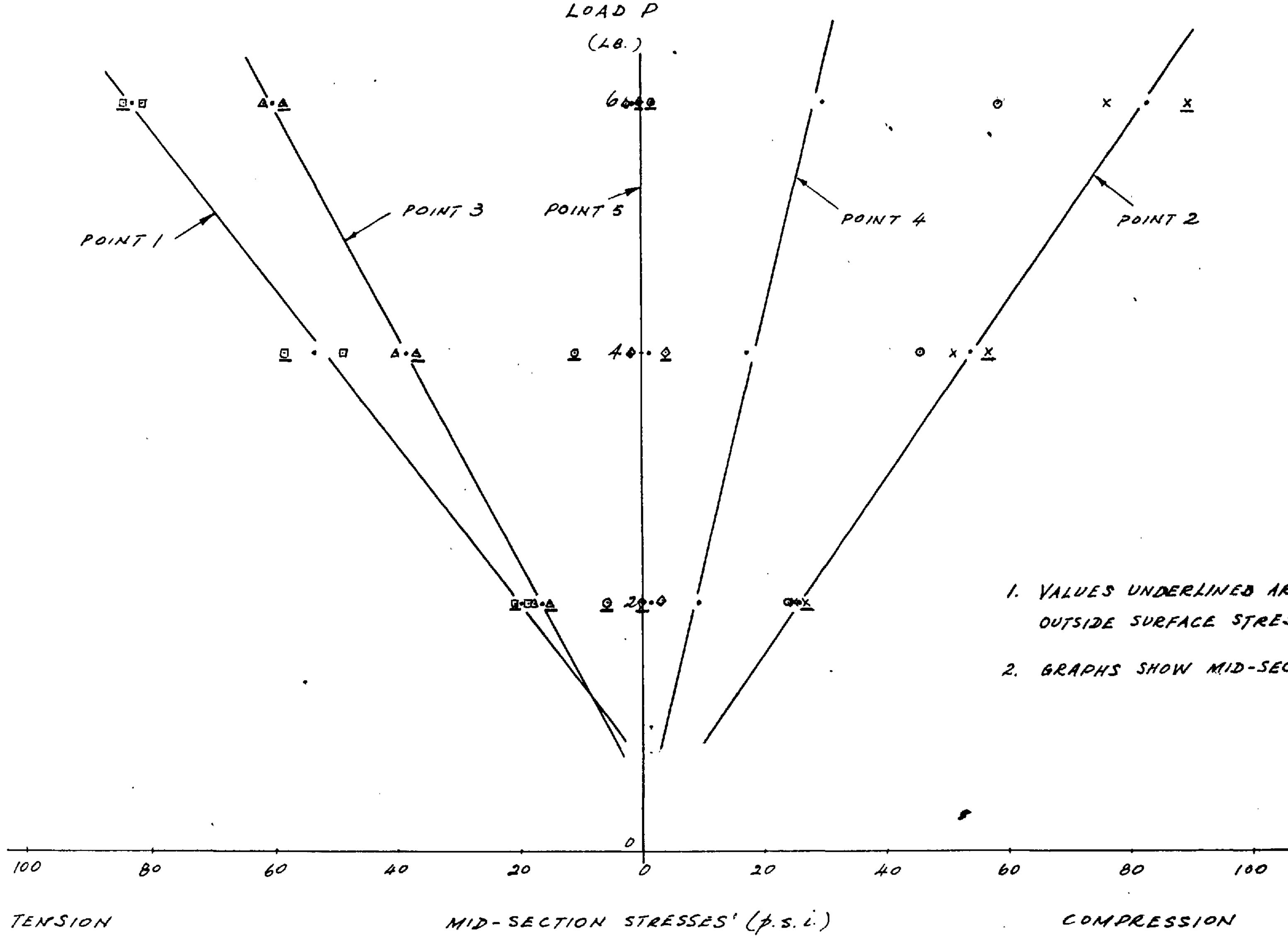

1. VALUES UNDERLINED ARE OUTSIDE SURFACE STRESSES.
2. GRAPHS SHOW MID-SECTION STRESSES

THICKNESS OF PYRAMID WALLS = h_w
" " " BASE = h_b

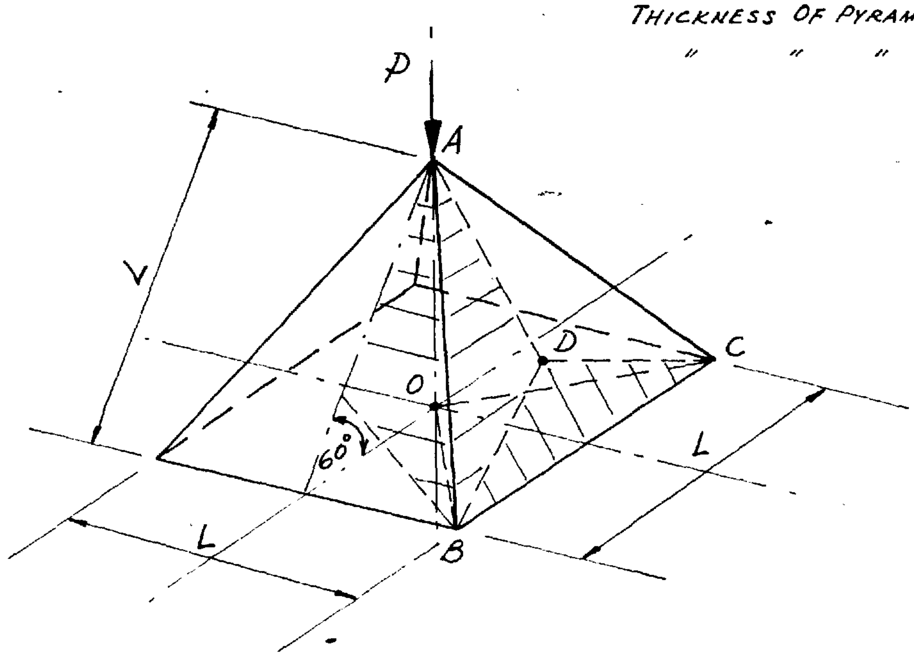

(a) A SQUARE-BASED SHEET PYRAMID

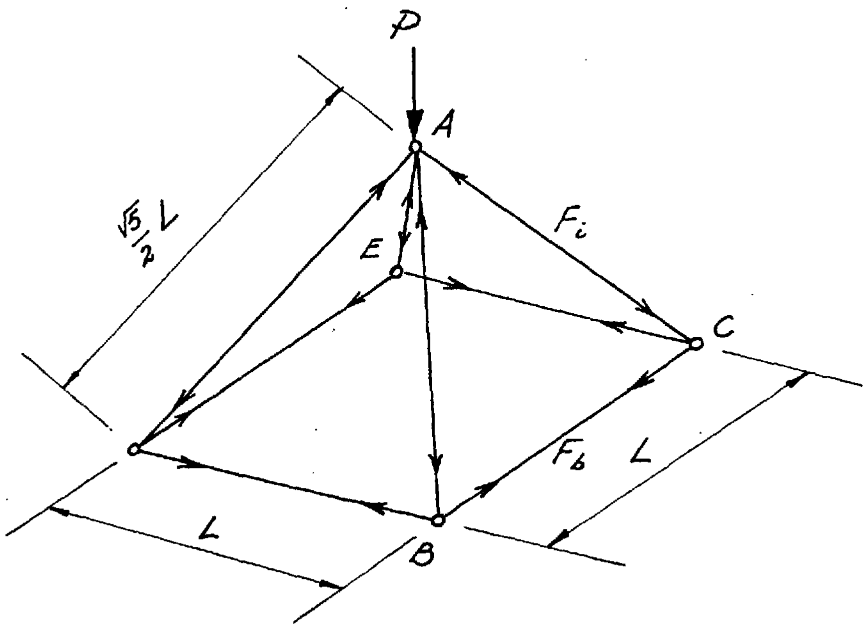

(b) EQUIVALENT SKELETAL SYSTEM

FIG. 2.20

FIG. 2.21 - EQUIVALENT SKELETAL SYSTEM OF MODELS D & D'

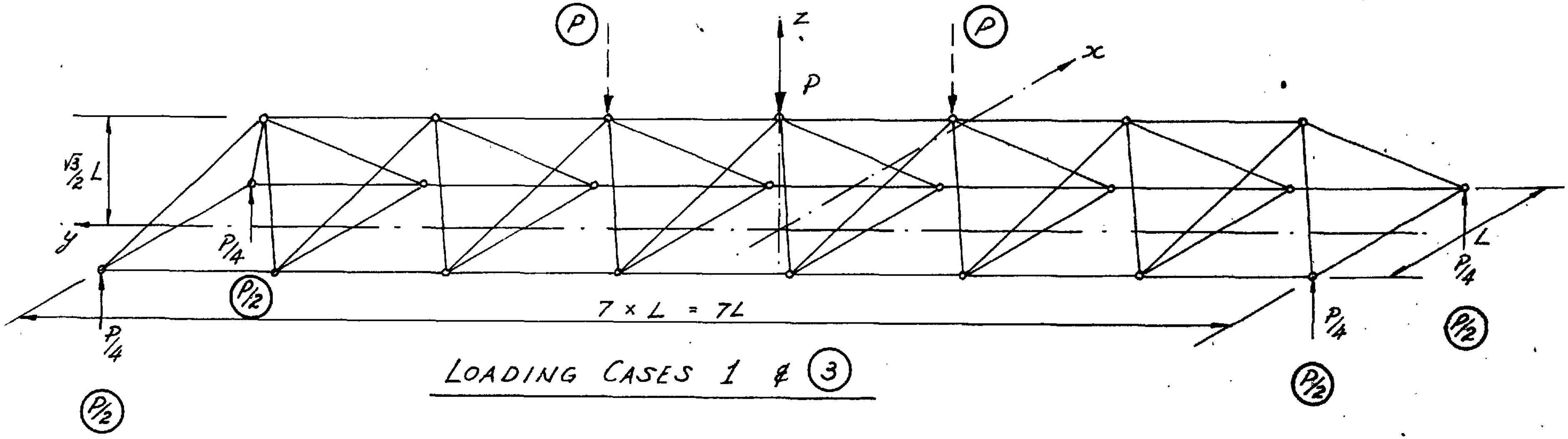

LOADING CASES 1 & 3

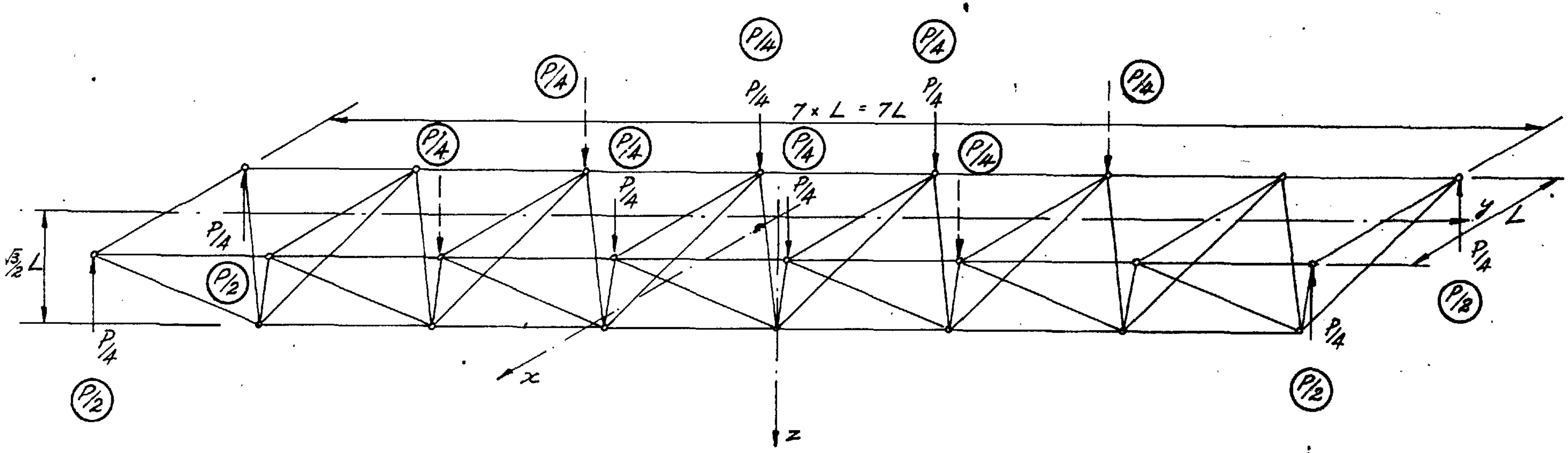

LOADING CASES 2 & 4

FOR MODEL D', ONLY CASE 2 APPLIES.

FIG. 222 - EQUIVALENT SKELETAL SYSTEM OF MODEL E

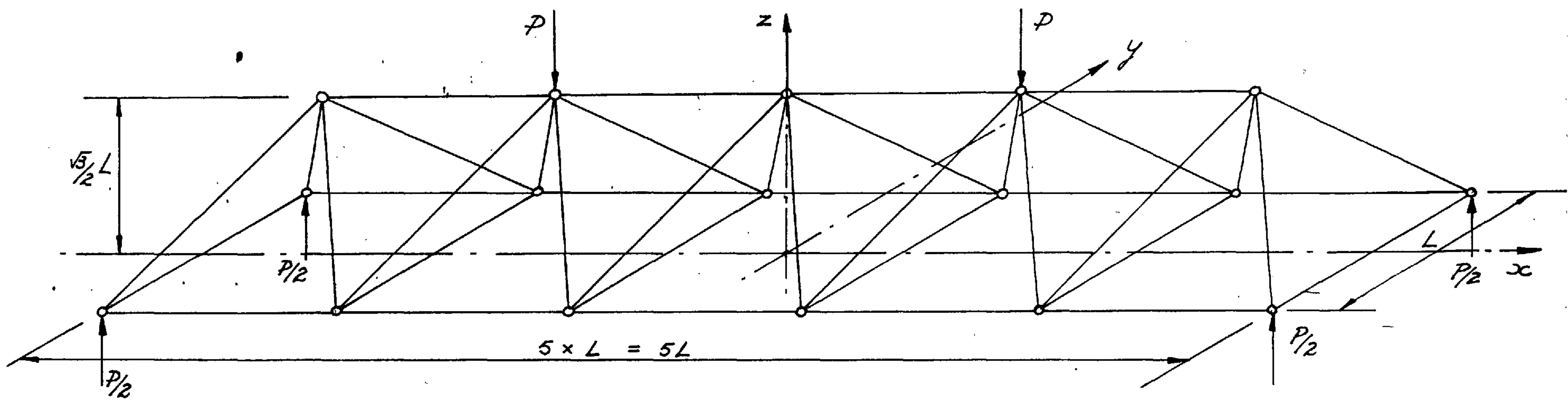

LOADING CASE 1

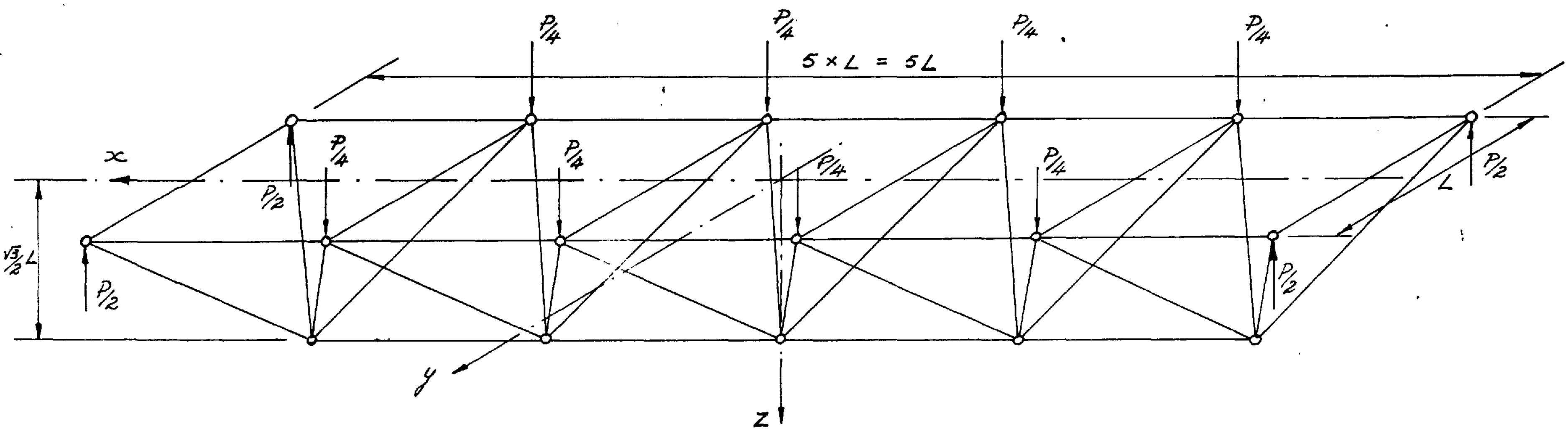

LOADING CASE 2

TABLE 3.1 - EXPERIMENTAL STRESSES & MOMENTS IN WALLS OF "SIMPLY-SUPPORTED" PYRAMID.

POINT (SEE FIG. 3.7)	OUTER SURFACE STRESS		INNER SURFACE STRESS		MID-PLANE STRESS		BENDING MOMENT	
	VERTICAL	HORIZONTAL	VERTICAL	HORIZONTAL	VERTICAL	HORIZONTAL	VERTICAL	HORIZONTAL
1A	609.12	237.49	254.88	-250.59	432.00	-6.55	1.04	1.43
2A	533.52	192.06	502.80	-54.76	518.16	68.65	0.09	0.72
2B	120.89	-46.09	205.21	-82.85	163.05	-64.47	-0.25	0.11
3A	321.51	104.17	321.21	-35.67	321.36	34.25	0	0.41
3B	125.82	-31.98	218.92	-13.56	172.37	-22.77	-0.27	-0.05
4A	224.85	55.31	219.61	7.45	222.23	31.38	0.02	0.14
4B	135.75	-9.92	198.21	29.36	166.98	9.82	-0.18	-0.12
4C	59.54	-113.94	183.24	92.88	121.39	-10.53	-0.36	-0.61
5A	175.79	54.05	158.27	26.65	167.03	40.35	0.05	0.08
5B	158.87	30.88	153.63	38.74	156.25	34.81	0.02	-0.02
5C	126.93	9.07	147.89	43.81	137.41	26.44	-0.06	-0.10
6A	129.70	48.51	85.48	38.33	107.59	43.42	0.13	0.03
6B	154.89	57.32	88.09	35.66	121.49	46.49	0.20	0.06
6C	152.72	57.42	119.08	44.84	135.90	51.13	0.10	0.04
6D	82.51	39.94	116.05	2.16	99.28	21.05	-0.10	0.11
7A	108.04	49.77	29.26	48.55	68.65	49.66	0.23	0
7B	128.75	58.83	28.81	35.27	78.78	47.05	0.29	0.07
7C	139.68	64.37	50.62	29.63	95.15	47.00	0.26	0.10
7D	144.06	76.97	112.02	23.27	128.04	50.12	0.09	0.16
8A	107.49	48.25	-16.01	43.93	45.74	46.09	0.36	0.01
8B	107.29	53.90	-23.87	32.74	41.71	43.32	0.38	0.22
8C	123.46	62.21	-16.58	15.87	53.44	39.04	0.41	0.14
8D	183.60	95.20	99.58	41.90	141.59	68.55	0.25	0.16
8E	260.41	144.21	161.09	59.89	210.75	102.05	0.29	0.25
9A	103.01	22.82	-38.93	31.48	32.04	27.15	0.42	-0.03
9B	120.28	27.96	-49.96	21.40	35.16	24.68	0.50	0.02
9C	166.22	58.18	-65.98	21.10	50.12	39.64	0.68	0.11
9D	196.64	88.30	-38.08	6.10	79.28	47.20	0.69	0.24
9E	197.95	104.67	60.35	21.97	129.15	63.32	0.40	0.24
10A	46.54	-132.22	-37.58	8.30	4.48	-62.96	0.25	-0.41
10B	76.56	-96.96	-44.12	-4.78	16.22	-50.87	0.35	-0.27
10C	131.72	-46.69	-54.16	20.79	38.78	-12.95	0.55	-0.20
10D	176.45	-1.01	-88.61	-7.95	43.92	-4.48	0.78	0.20
10E	183.75	32.49	33.25	31.99	108.50	32.24	0.44	0
10F	291.89	88.90	170.31	94.96	231.10	91.93	0.36	-0.02
11A	19.95	-189.24	-66.79	-207.28	-23.42	-198.26	0.25	0.05
11B	30.93	-189.39	-74.25	-197.05	-21.66	-193.22	0.31	0.02
11C	64.68	-168.74	-85.84	-192.22	-10.58	-180.48	0.44	0.07
11D	136.75	-114.34	-75.29	-129.36	30.73	-121.85	0.62	0.04
11E	249.33	-45.33	-44.83	-133.39	102.25	-89.36	0.86	0.26
11F	468.44	75.56	-25.00	-199.32	221.72	-55.21	1.45	0.81
12A	-10.07	-224.50	-52.69	-429.50	-31.38	-327.00	0.13	0.60
12B	-12.59	-225.41	-104.27	-451.97	-58.43	-338.69	0.27	0.66
12C	4.03	-228.43	-111.83	-463.45	-53.90	-345.94	0.34	0.69
12D	84.32	-232.56	-120.38	-527.02	-18.03	-379.79	0.60	0.86
12E	308.62	-128.44	-181.18	-578.36	63.72	-353.40	1.44	1.32
12F	648.92	-238.20	-238.20	-617.28	205.36	-297.18	2.60	1.88

TABLE 3.2 — PRINCIPAL AND SHEAR STRESSES

POINT. (SEE FIG. 3.11)	PRINCIPAL STRESS			SHEAR STRESS (p.s.i.)
	MAXIMUM (p.s.i.)	MINIMUM (p.s.i.)	DIRECTION (ANGLE FROM VERTICAL)	
a	196·24	5·04	18° 04′	60·97
b	142·50	38·38	16° 34′	31·57
c	91·87	29·92	49° 24′	25·90
d	42·76	4·84	52° 24′	16·45
e	146·98	20·95	30° 16′	47·64
f	82·46	−4·28	46° 05′	25·61
g	51·78	3·98	64° 00′	17·96
h	177·30	1·51	30° 20′	113·05
i	157·36	5·14	51° 30′	70·61
j	117·36	−11·94	49° 00′	60·02

COMPRESSIVE STRESS POSITIVE

Table 3.3 – Experimental Stresses and Moments in Walls of Vertically Loaded "Fixed" Pyramid

Point (see Fig. 3.7)	Outer Surface Vert. Stress (p.s.i)	Outer Surface Horiz. Stress (p.s.i)	Inner Surface Vert. Stress (p.s.i)	Inner Surface Horiz. Stress (p.s.i)	Mid-Plane Vert. Stress (p.s.i)	Mid-Plane Horiz. Stress (p.s.i)	Vert. Bending Moment (lb-in/in)	Horiz. Bending Moment (lb-in./in.)
1A	99·7	-96·1	643·0	77·4	371·3	-9·3	-1·59	-0·48
2A	137·5	-47·7	335·8	7·6	236·6	-20·0	-0·58	-0·16
2B	127·2	-7·5	118·7	-17·5	122·9	-12·5	0·02	0·03
3A	136·5	9·1	136·9	4·7	136·7	6·9	0	0·01
3B	113·2	14·7	105·0	2·6	109·1	8·6	0·02	0·04
3C	77·2	18·7	64·5	0·1	70·8	9·4	0·04	0·05
4A	70·9	0·7	77·0	0·3	73·9	0·5	-0·02	0
4B	75·2	13·0	69·3	3·5	72·2	8·2	0·02	0·03
4C	64·7	16·5	58·1	6·6	61·4	11·5	0·02	0·03
4D	48·5	16·9	54·4	12·8	51·4	14·8	-0·02	0·01
5A	42·8	3·4	42·4	-0·2	42·6	1·8	0	0·01
5B	40·4	8·3	35·3	-0·1	37·8	4·1	0·01	0·02
5C	40·3	8·6	36·5	4·5	38·4	6·5	0·01	0·01
5D	48·3	9·4	44·5	13·1	46·4	11·2	0·01	-0·01
5E	53·7	5·0	64·7	28·1	59·2	16·5	-0·03	-0·07
6A	37·5	11·1	30·2	6·4	33·8	8·7	0·02	0·01
6B	36·2	10·6	23·9	4·3	30·0	7·4	0·04	0·02
6C	28·5	7·9	21·1	3·2	24·8	5·5	0·02	0·01
6D	33·8	11·1	27·3	5·4	30·5	8·2	0·02	0·02
6E	38·2	9·2	50·2	13·8	44·2	11·5	-0·04	-0·01
6F	42·1	4·7	88·7	27·8	65·4	16·2	-0·14	0·07
7A	42·4	8·2	-9·7	-27·6	16·3	-9·7	0·15	0·10
7B	16·6	-3·8	-8·6	-24·6	4·0	-14·2	0·07	0·06
7C	8·5	-11·2	-0·6	-17·3	3·9	-14·2	0·03	0·02
7D	-2·8	-19·7	4·2	-11·8	0·7	-15·7	-0·02	-0·02
7E	61·4	9·0	15·8	-22·8	38·6	-6·9	0·13	0·09
7F	115·6	-13·8	51·3	5·0	83·4	-4·4	0·19	-0·06

TABLE 3.4 – EXPERIMENTAL STRESSES AND MOMENTS IN WALL "A" OF HORIZONTALLY LOADED "FIXED" PYRAMID

POINT (SEE FIG. 3.7)	OUTER SURFACE VERT. STRESS (p.s.i.)	OUTER SURFACE HORIZ. STRESS (p.s.i.)	INNER SURFACE VERT. STRESS (p.s.i.)	INNER SURFACE HORIZ. STRESS (p.s.i.)	MID-PLANE VERT. STRESS (p.s.i.)	MID-PLANE HORIZ. STRESS (p.s.i.)	VERT. BENDING MOMENT (lb-in./in.)	HORIZ. BENDING MOMENT (lb-in./in.)
1A	173·4	-98·6	336·8	-125·7	255·1	-112·2	-0·48	0·08
2A	262·7	-58·5	337·8	-72·1	300·3	-65·3	-0·22	0·04
2B	283·7	-62·3	302·3	-46·9	293·0	-54·6	-0·05	-0·05
3A	335·3	22·2	294·7	-12·0	315·0	5·1	0·12	0·10
3B	329·8	31·3	275·7	3·5	302·8	17·4	0·16	0·08
3C	247·5	31·4	230·7	38·6	239·1	35·0	0·05	-0·02
4A	250·7	38·9	224·7	10·1	237·7	24·5	0·08	0·08
4B	210·5	25·8	187·0	3·5	198·8	14·7	0·07	0·07
4C	200·0	21·8	155·7	8·4	177·9	15·1	0·13	0·04
4D	182·3	15·1	152·4	31·2	167·4	23·2	0·09	-0·05
5A	219·9	40·2	197·1	32·3	208·5	36·3	0·07	0·02
5B	175·9	28·4	117·8	8·1	146·9	18·3	0·17	0·06
5C	139·7	20·2	89·3	2·5	114·5	11·4	0·15	0·05
5D	144·0	19·4	101·7	18·8	122·9	19·1	0·12	0
5E	184·4	21·7	160·2	64·3	172·3	43·0	0·07	-0·12
6A	198·2	22·9	183·4	37·7	190·8	30·3	0·04	-0·04
6B	170·1	18·4	146·1	38·3	158·1	28·4	0·07	-0·06
6C	147·2	16·1	106·1	31·4	126·7	23·8	0·12	-0·04
6D	104·8	10·5	94·8	24·3	99·8	17·4	0·03	-0·04
6E	87·7	4·2	108·4	25·6	98·1	14·9	-0·06	0·06
6F	180·7	48·6	157·8	33·9	169·3	41·3	0·07	0·04
7A	174·1	-1·9	172·4	24·9	173·3	11·5	0	-0·08
7B	79·9	-24·2	149·2	59·7	114·6	17·8	-0·20	-0·25
7C	-56·2	-71·8	145·6	74·4	44·7	1·3	-0·59	-0·43
7D	-60·8	-85·5	139·9	58·7	39·6	-13·4	-0·59	-0·42
7E	126·0	-44·4	144·9	34·8	135·5	-4·8	-0·06	-0·23
7F	421·8	28·9	182·7	16·6	302·3	22·8	-0·70	0·04

TABLE 3.5 — EXPERIMENTAL STRESSES & MOMENTS IN WALL 'B' OF HORIZONTALLY LOADED "FIXED" PYRAMID

POINT (SEE FIG. 3.7)	OUTER SURFACE STRESS		INNER SURFACE STRESS		MID-PLANE STRESS		BENDING MOMENT	
	VERTICAL	HORIZONTAL	VERTICAL	HORIZONTAL	VERTICAL	HORIZONTAL	VERTICAL	HORIZONTAL
1A	-6.8	-15.7	19.6	13.9	6.4	-0.9	-0.08	-0.09
2B	212.3	44.3	217.2	57.4	214.8	50.9	0.01	-0.04
2A	-5.1	-7.1	-2.7	8.9	1.2	-0.9	-0.02	-0.05
2B′	-223.5	-45.1	-218.0	-54.2	-220.8	-49.7	-0.02	0.03
3C	122.6	14.0	122.9	-19.1	122.8	2.6	0	0.10
3B	85.0	15.1	86.3	25.3	85.7	20.2	0	-0.03
3A	-4.4	2.4	-5.2	7.9	-4.8	5.2	0	-0.02
3B′	-105.4	-8.2	-113.3	-20.2	-109.4	-14.2	0.02	0.04
3C′	-150.8	11.3	-130.0	-17.6	-140.4	-3.2	-0.06	0.08
4D	77.4	3.6	79.1	17.5	78.3	10.6	0	-0.04
4C	66.5	13.1	72.5	21.4	69.5	17.3	-0.02	-0.02
4B	43.6	10.8	48.8	19.3	46.2	15.1	-0.02	-0.02
4A	-3.0	6.5	-12.1	5.9	-7.6	6.2	0.03	0
4B′	-40.6	4.8	-62.3	-1.9	-51.5	1.5	0.06	0.02
4C′	-81.4	7.8	-95.3	-6.8	-88.4	0.5	0.04	0.04
4D′	-93.5	21.3	-103.8	-1.0	-98.7	10.2	0.03	0.07
5E	26.6	-6.2	45.6	29.2	36.1	11.5	-0.03	-0.10
5D	28.6	3.4	43.0	21.7	35.8	12.6	-0.04	0.05
5C	23.2	6.8	30.2	12.7	26.7	9.8	-0.02	-0.02
5B	11.6	5.4	12.0	6.4	11.8	5.9	0	0
5A	-12.0	1.1	-19.5	1.1	-15.8	1.1	0.02	0
5B′	-39.5	-4.1	-34.5	2.5	-37.0	-0.8	-0.01	-0.02
5C′	-53.7	-2.0	-47.3	3.8	-50.5	0.9	-0.02	-0.02
5D′	-69.3	4.0	-85.6	-10.9	-77.5	-3.5	0.05	0.04
5E′	-73.8	60.8	-137.0	-37.8	-105.4	11.5	0.19	0.29
6F	4.8	-11.6	34.6	28.1	19.7	8.3	-0.09	-0.05
6E	16.9	9.8	32.3	18.8	24.6	14.3	-0.05	-0.03
6D	19.5	7.7	24.9	10.5	22.2	9.1	-0.02	-0.01
6C	10.7	7.7	13.9	3.1	12.3	5.4	-0.01	0.01
6B	-10.3	-0.6	4.7	0.8	-2.8	0.1	-0.04	0
6A	-38.3	-13.4	-8.2	-0.7	-23.3	-7.1	-0.09	-0.04
6B′	-69.8	-27.7	-18.3	-5.5	-44.1	-16.6	-0.15	-0.07
6C′	-74.2	-22.4	-21.6	-4.9	-47.9	-13.7	-0.15	-0.05
6D′	-71.9	-9.7	-16.8	2.5	-44.4	-3.6	-0.16	-0.04
6E′	-67.8	8.6	-60.2	-3.8	-64.0	2.4	-0.02	0.04
6F′	-59.5	31.2	-139.7	-20.2	-99.6	5.5	0.23	0.15
7F	74.8	-1.3	-16.8	-22.7	29.0	-12.0	0.27	0.06
7E	60.2	7.8	-13.9	-18.1	23.2	-5.2	0.22	0.08
7D	4.7	0.8	8.5	-7.2	6.6	-3.2	-0.01	0.02
7C	-24.5	-0.7	5.4	-4.7	-9.6	-2.7	-0.09	0.01
7B	-56.4	-9.6	21.7	2.7	-17.4	-3.5	-0.23	-0.04
7A	-74.0	-20.5	31.2	7.0	-21.4	-6.8	-0.31	-0.08
7B′	-108.7	-33.3	103.9	31.5	-2.4	-0.9	-0.62	-0.19
7C′	-124.2	-35.1	160.0	52.9	17.9	8.9	-0.83	-0.26
7D′	-195.8	-54.8	197.4	74.0	0.8	9.6	-1.15	-0.38
7E′	-295.7	-86.7	247.7	108.0	-24.0	10.7	-1.59	-0.57
7F′	-373.8	-107.3	231.8	106.3	-71.0	-0.5	-1.77	-0.63

TABLE 3.6 — EXPERIMENTAL STRESSES AND MOMENTS IN WALL "C" OF HORIZONTALLY LOADED "FIXED" PYRAMID

POINT (SEE FIG. 3.7)	OUTER SURFACE VERT. STRESS (p.s.i)	OUTER SURFACE HORIZ. STRESS (p.s.i)	INNER SURFACE VERT. STRESS (p.s.i)	INNER SURFACE HORIZ. STRESS (p.s.i)	MID-PLANE VERT. STRESS (p.s.i)	MID-PLANE HORIZ. STRESS (p.s.i)	VERT. BENDING MOMENT (lb-in./in.)	HORIZ. BENDING MOMENT (lb-in./in.)
1A	−125.4	203.8	−364.4	58.2	−244.9	131.0	0.70	0.43
2A	−272.8	85.9	−358.4	24.9	−315.6	55.4	0.25	0.18
2B	−252.0	0.2	−250.5	42.8	−251.3	21.5	0	−0.12
3A	−335.0	−22.2	−309.7	−13.4	−322.4	−17.8	−0.07	−0.03
3B	−296.8	−26.5	−262.9	−17.7	−279.9	−22.1	−0.10	−0.03
3C	−186.6	−27.7	−178.2	−66.8	−182.4	−47.3	−0.02	0.11
4A	−207.4	−30.6	−199.7	−8.0	−203.6	−19.3	−0.02	−0.07
4B	−196.1	−29.7	−180.4	−10.1	−188.3	−19.9	−0.05	−0.06
4C	−165.8	−31.5	−149.7	−10.3	−157.8	−20.9	−0.05	−0.06
4D	−120.8	−35.7	−114.7	−18.0	−117.8	−26.9	−0.02	−0.05
5A	−175.3	−52.5	−141.7	−6.7	−158.5	−29.6	−0.10	−0.13
5B	−145.9	−37.8	−95.4	5.5	−120.7	−16.2	−0.15	−0.13
5C	−111.5	−21.8	−76.4	−2.9	−94.0	9.5	−0.10	−0.06
5D	−108.0	−24.1	−104.8	−27.9	−106.4	−26.0	−0.01	0.01
5E	−107.4	−27.7	−134.1	−69.6	−120.8	−48.7	0.08	0.12
6A	−178.4	−70.1	−33.0	19.4	−105.7	−25.4	−0.43	−0.26
6B	−162.1	−52.2	−24.8	14.4	−93.5	−18.9	−0.40	−0.20
6C	−135.7	−33.8	−33.1	6.6	−84.4	−13.6	−0.30	−0.12
6D	−95.3	−6.8	−26.8	−4.0	−61.1	−5.4	−0.20	−0.01
6E	−74.9	13.6	−84.1	−31.6	−79.5	−9.0	0.03	0.13
6F	−80.5	22.7	−259.3	−109.3	−169.9	−43.3	0.52	0.39
7A	−192.8	−45.4	140.0	71.1	−26.4	12.9	−0.98	−0.34
7B	−148.7	−7.8	132.5	62.3	−8.1	27.3	−0.82	−0.21
7C	−190.6	−13.6	153.9	60.5	18.4	23.5	−1.01	−0.22
7D	−292.0	−38.1	144.2	58.0	−73.9	10.0	−1.28	−0.28
7E	−416.0	−102.3	75.7	77.4	−170.2	−12.5	−1.44	−0.53
7F	−480.0	−132.6	−185.4	23.2	−332.7	−54.7	−1.95	−0.46

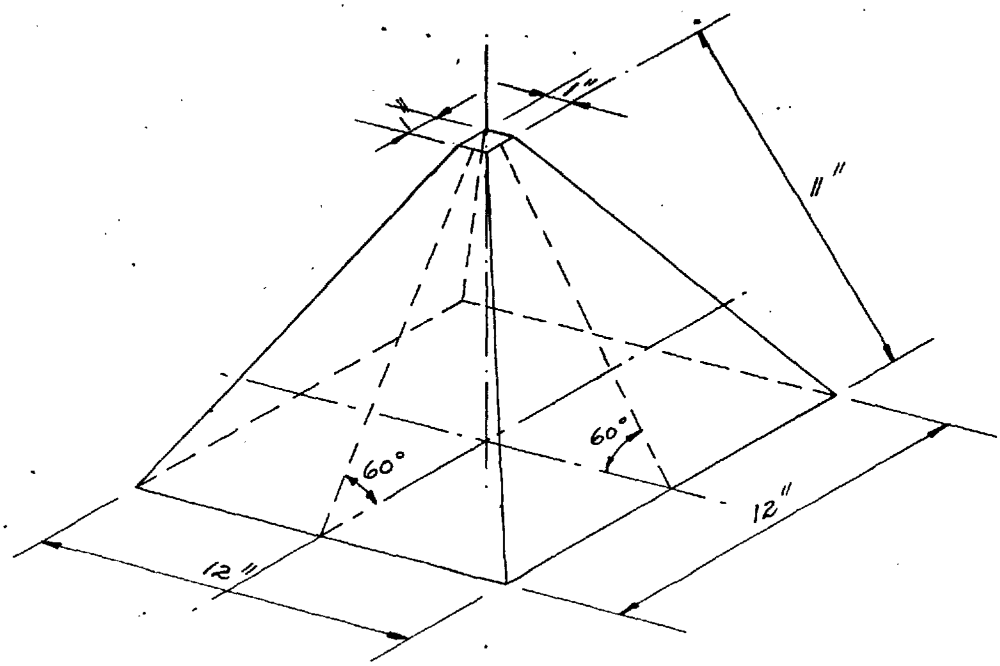

(a) OVERALL DIMENSIONS

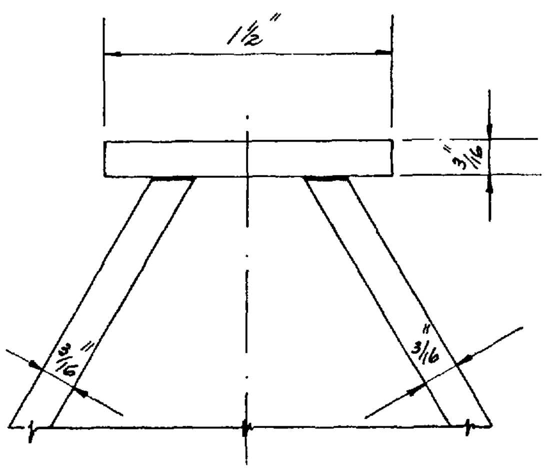

(b) TOP JOINT

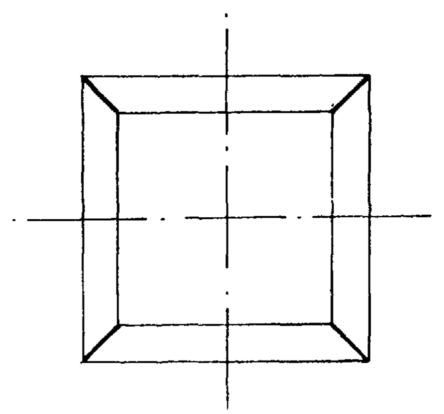

(c) SIDE JOINTS

FIG. 3.1 - 12 INCH PERSPEX MODEL
(STAGE I)

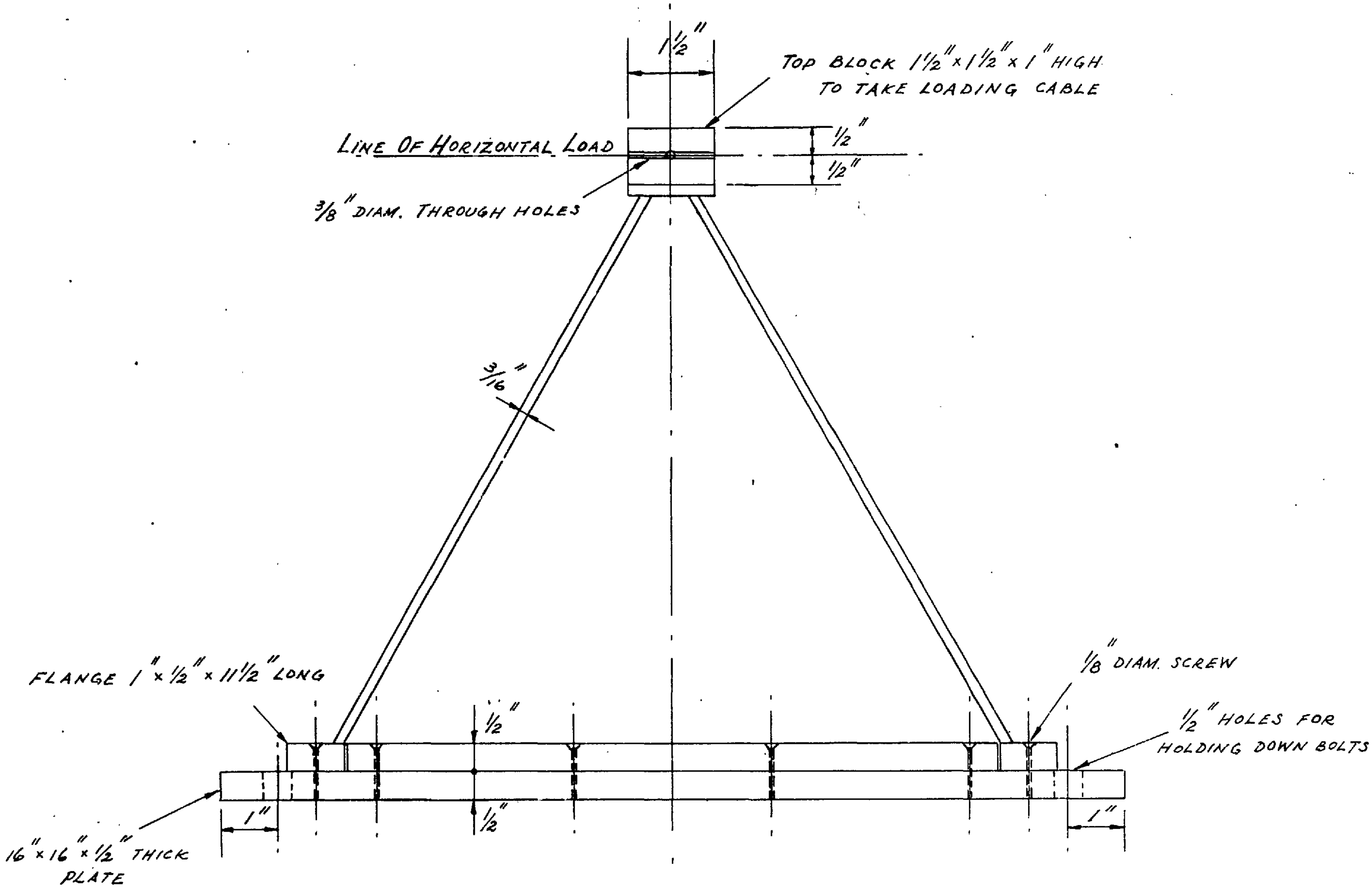

FIG. 3.2(a) — 12 INCH PERSPEX MODEL
(STAGE II)

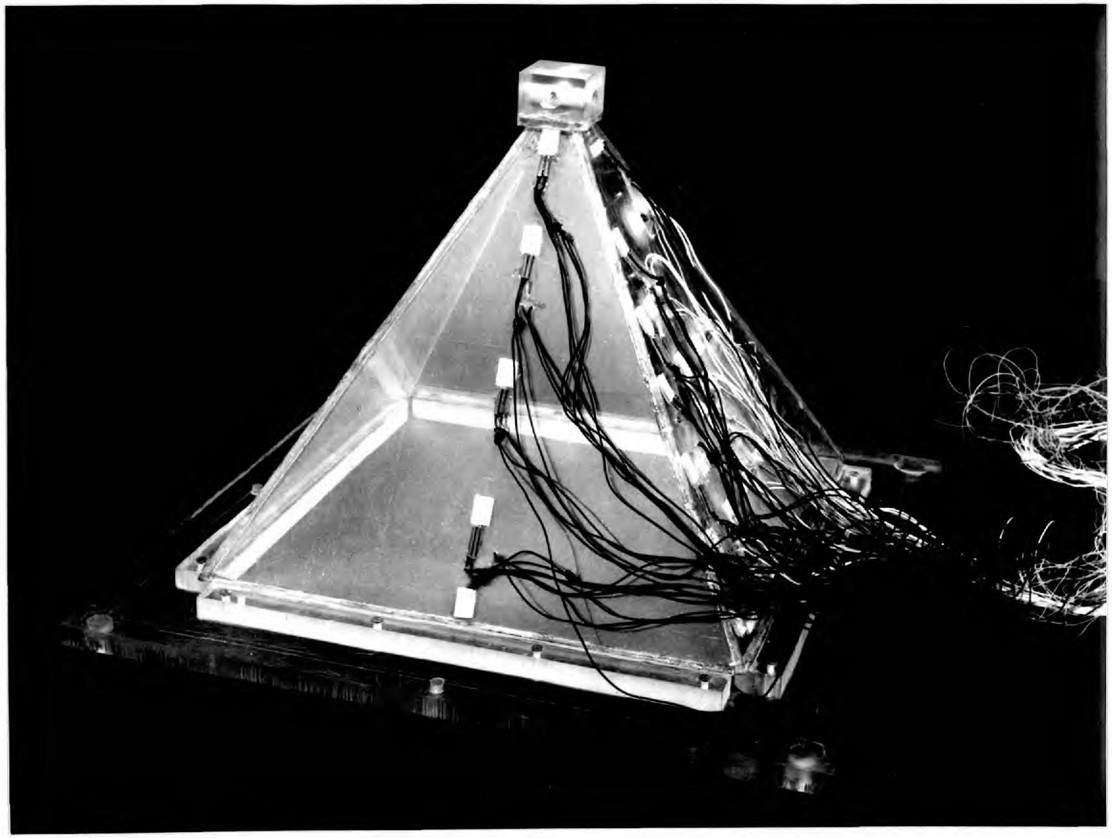

Fig. 3.2(b) - Fixed pyramid with strain gauges.

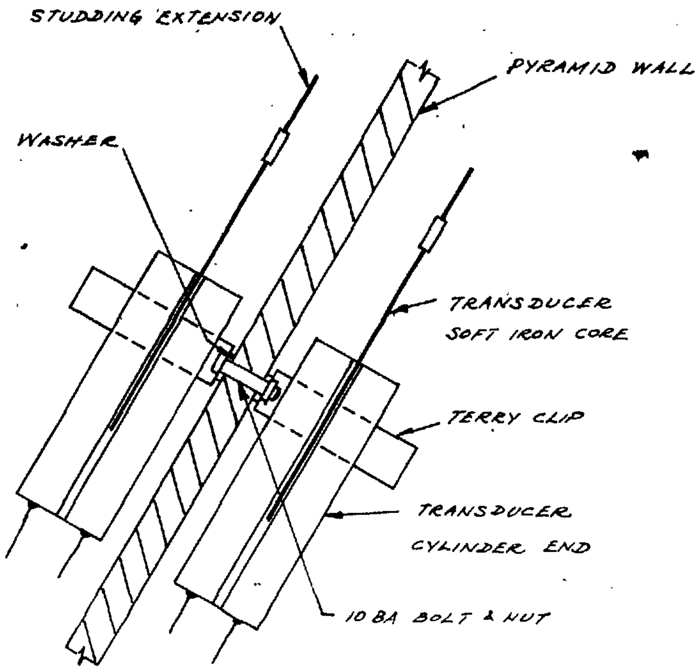

TRANSDUCER CYLINDER END

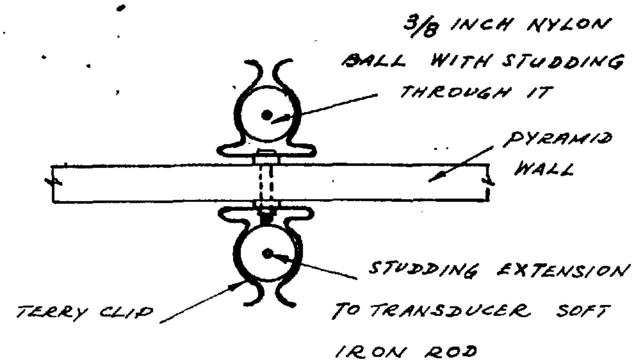

NYLON BALL END

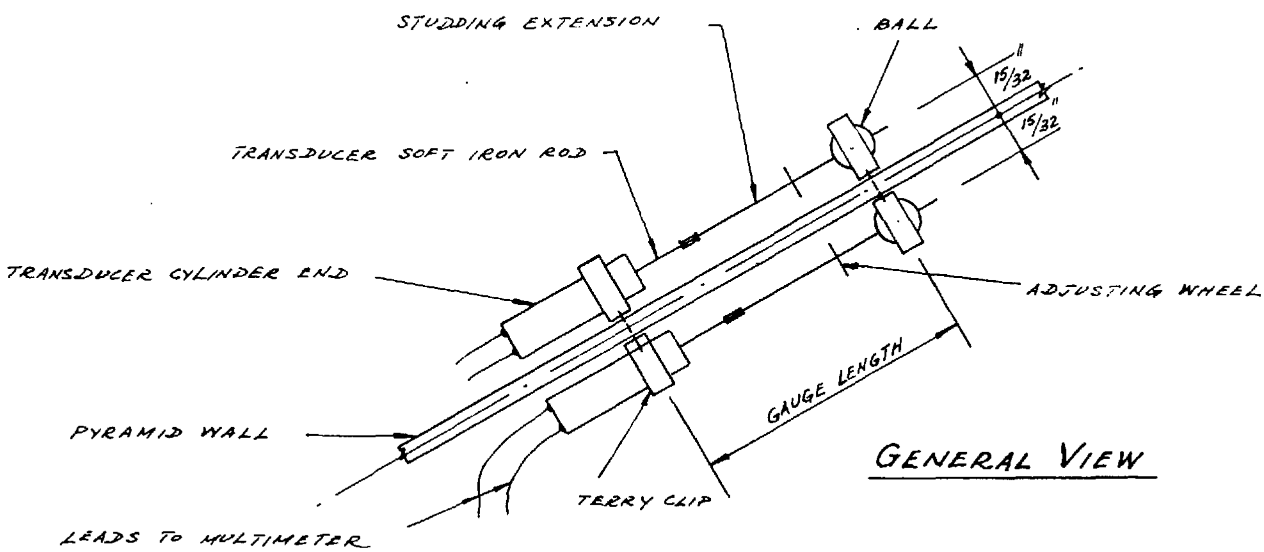

GENERAL VIEW

FIG. 3.3 – FIXINGS FOR DISPLACEMENT TRANSDUCERS

FIG. 3.4 — TRANSDUCER AND STRAIN GAUGE POSITIONS

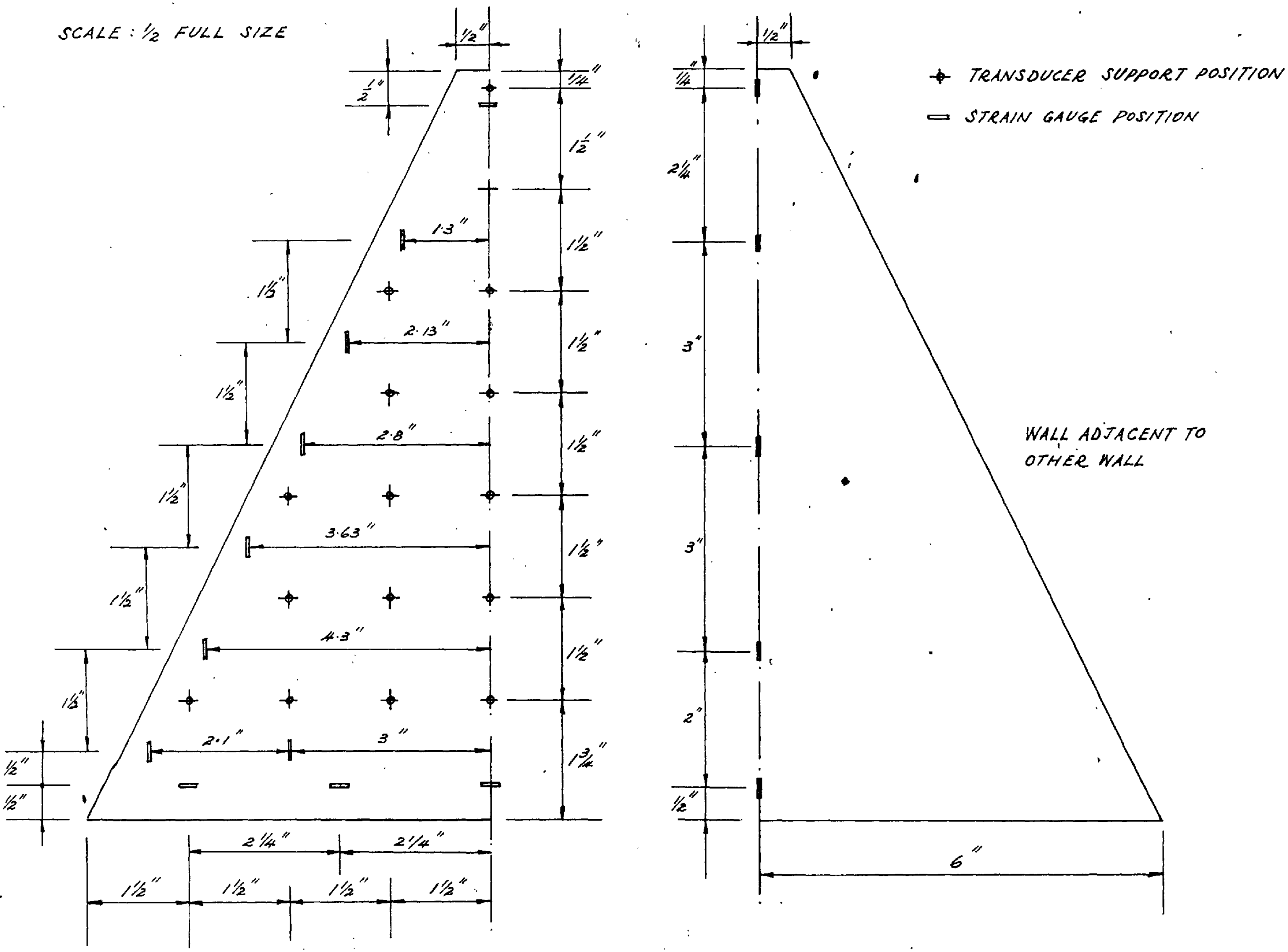

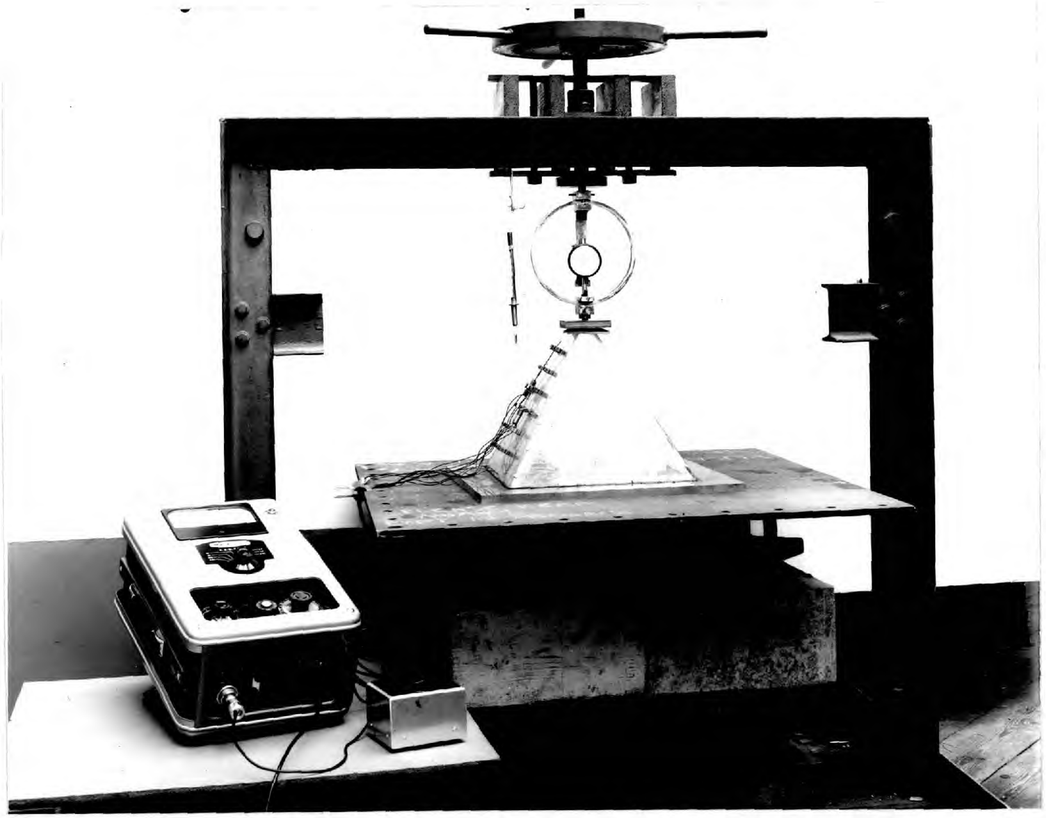

Fig. 3.5 - Loading arrangement for test on single pyramid.

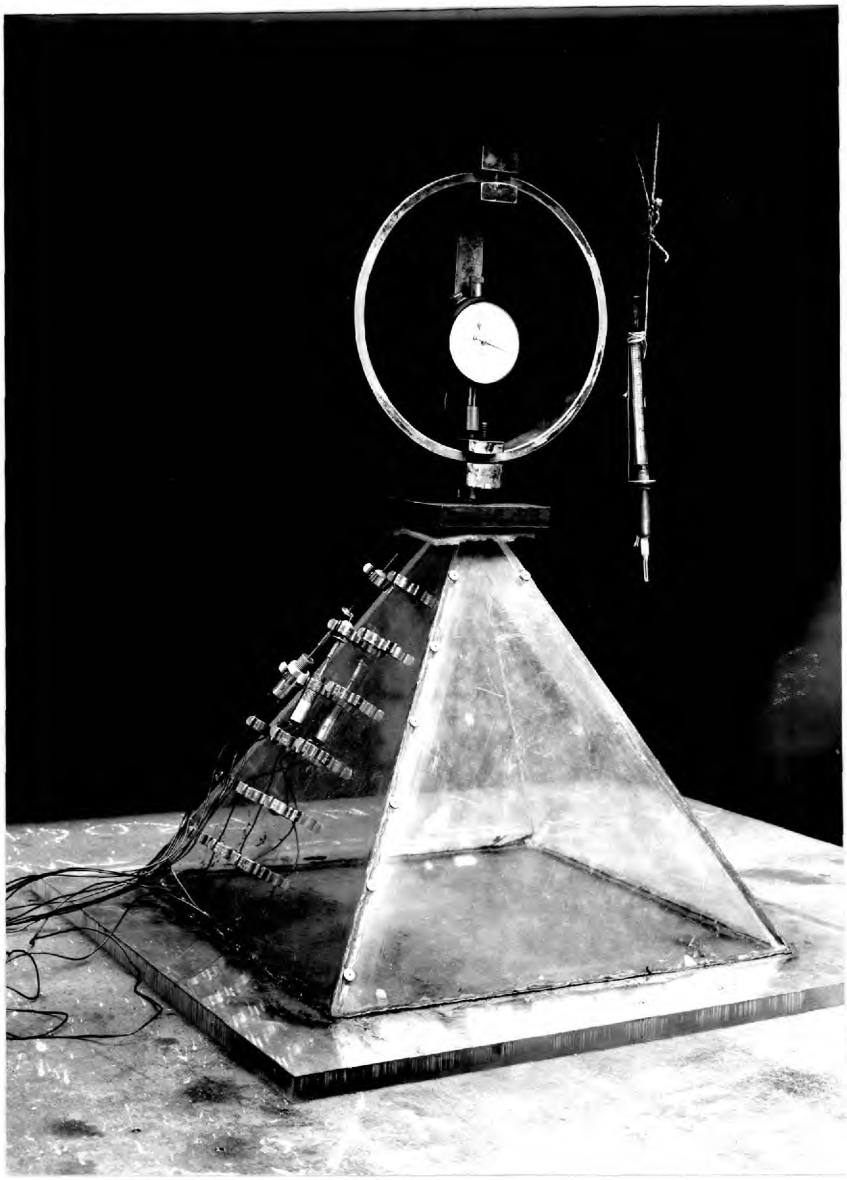

Fig. 3.6 - Simply-supported pyramid showing displacement transducers.

FIG. 3.7 — REFERENCE DIAGRAMS FOR TABLES 3.1 TO 3.6

SIGN CONVENTIONS

COMPRESSIVE STRESS + VE

OUTER FACE
INNER FACE
+ VE MOMENT

STRESSES IN lb/sq. in.

MOMENTS IN lb. in./in.

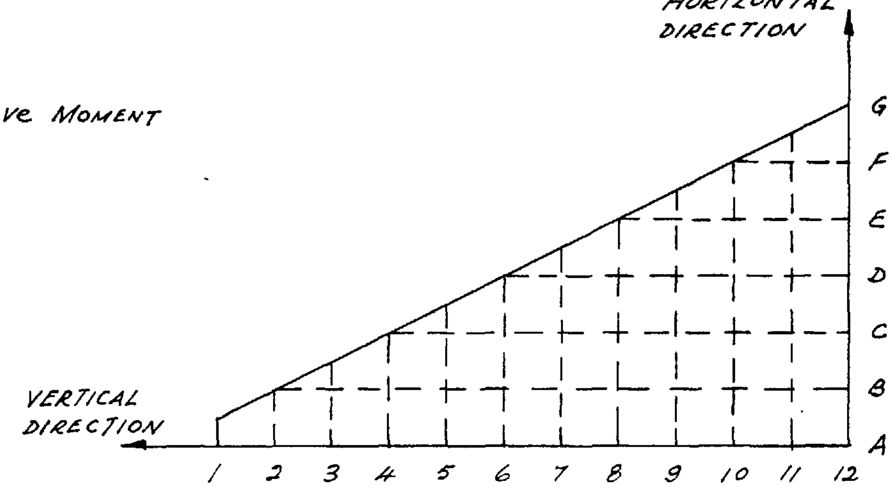

"SIMPLY - SUPPORTED" PYRAMID ONLY

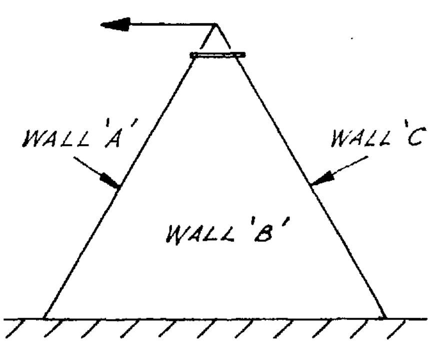

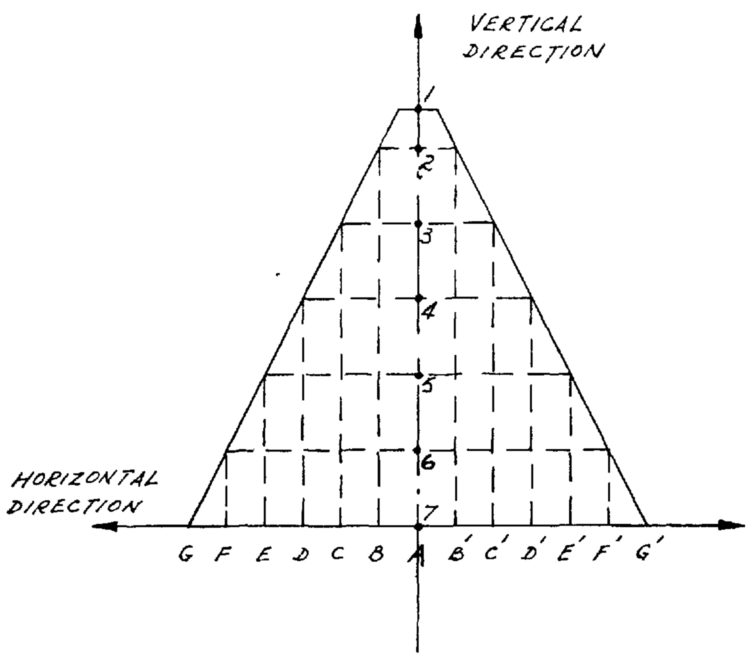

"FIXED" PYRAMID ONLY

Fig. 3.8 — Mid-Plane Stress Distribution In Walls Of Simply Supported Pyramid Under Vertical Load

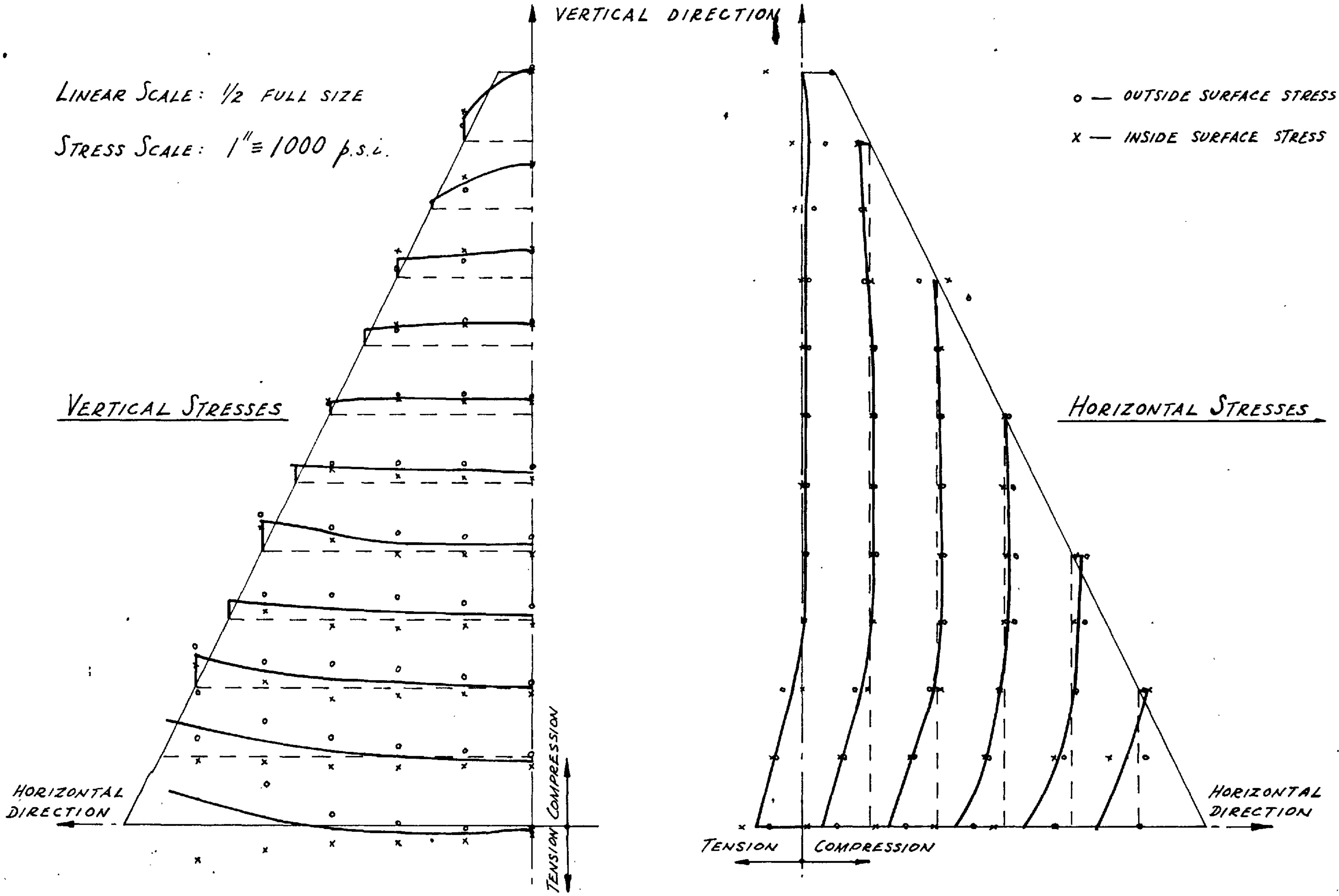

Fig. 3.10 – Bending Moments In Walls Of Simply Supported Pyramid Under Vertical Load

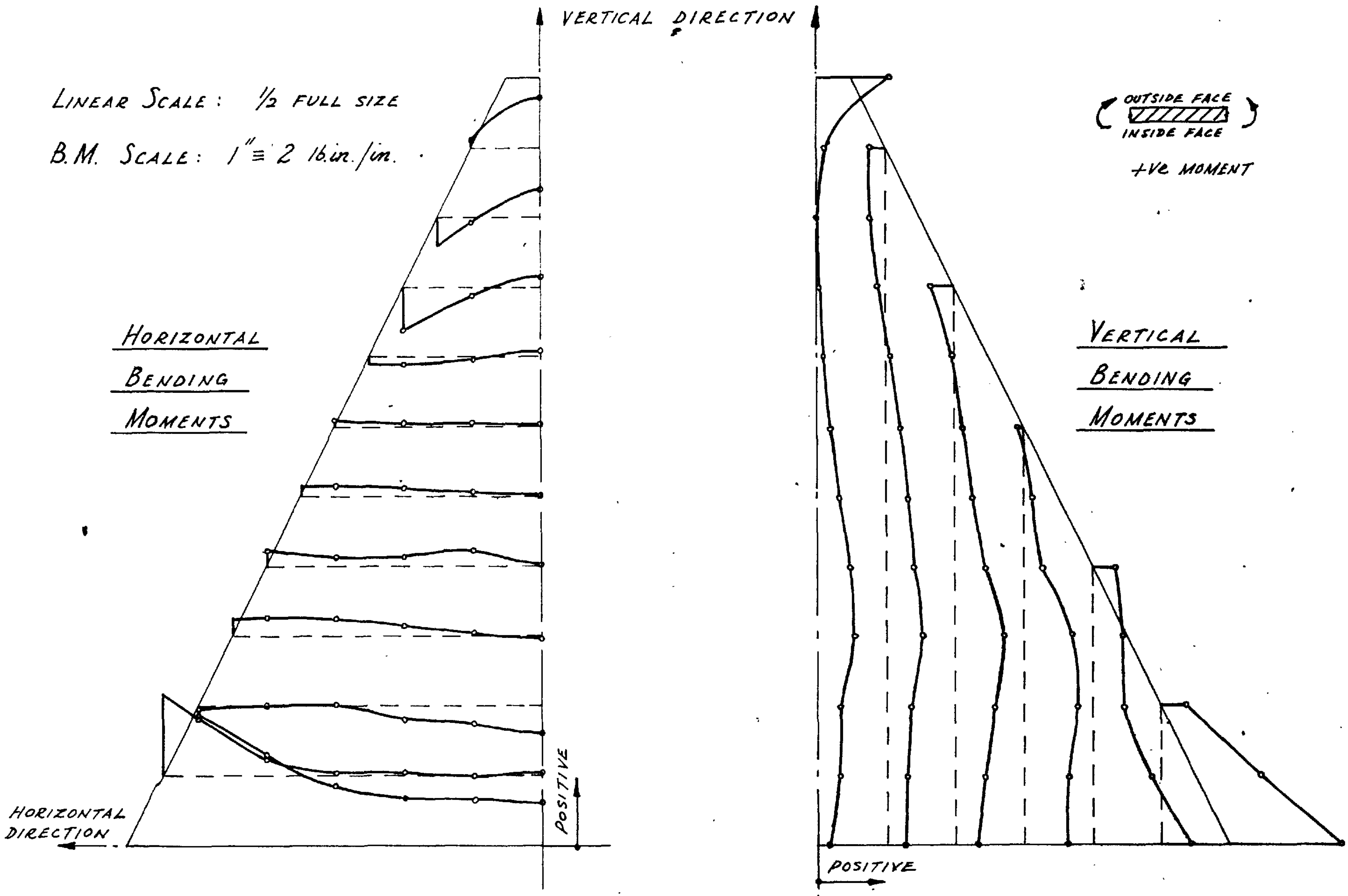

FIG. 3.11 - PRINCIPAL STRESS DIRECTIONS

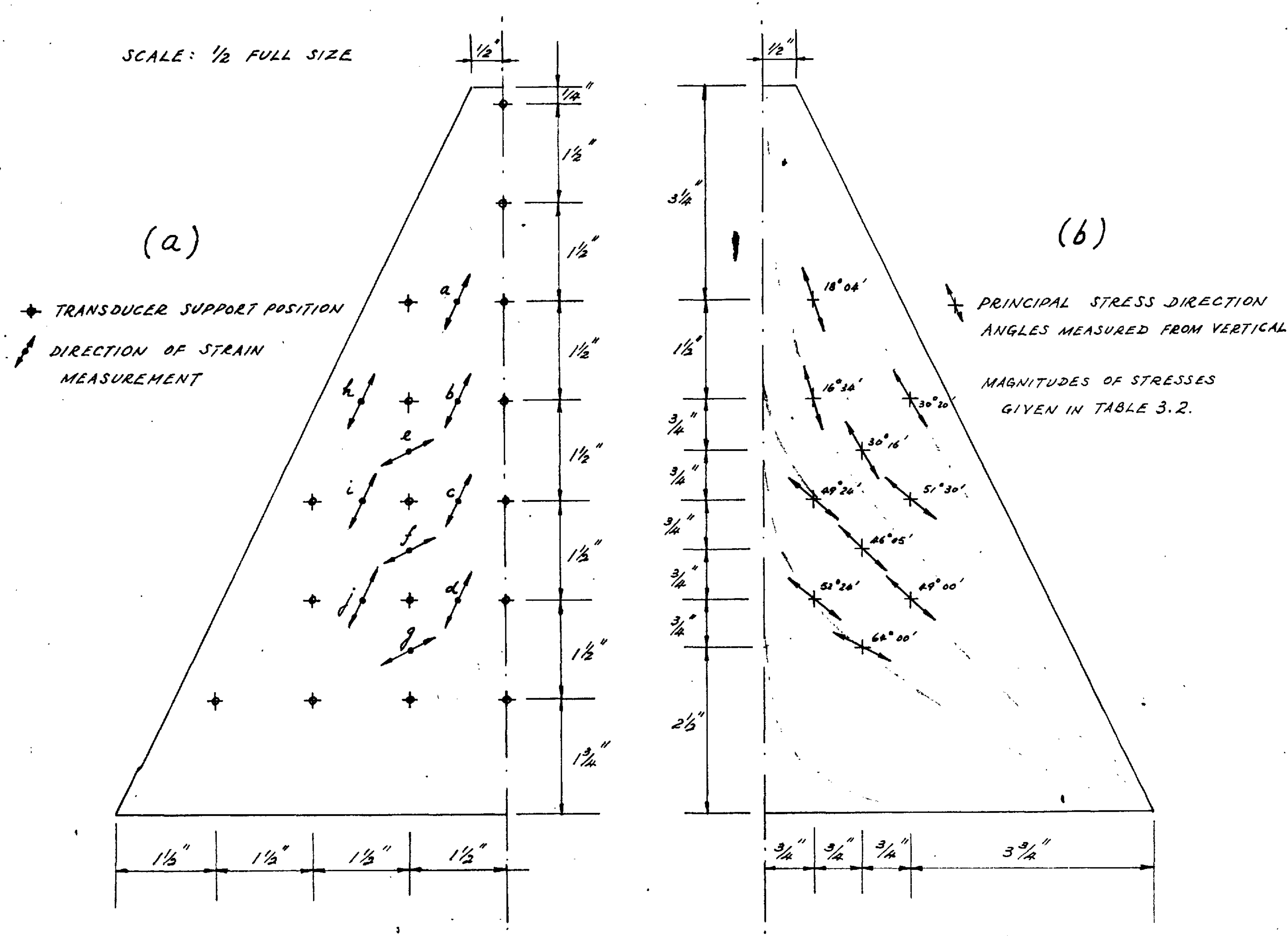

FIG. 3.13 – LOCATIONS OF STRAIN GAUGES

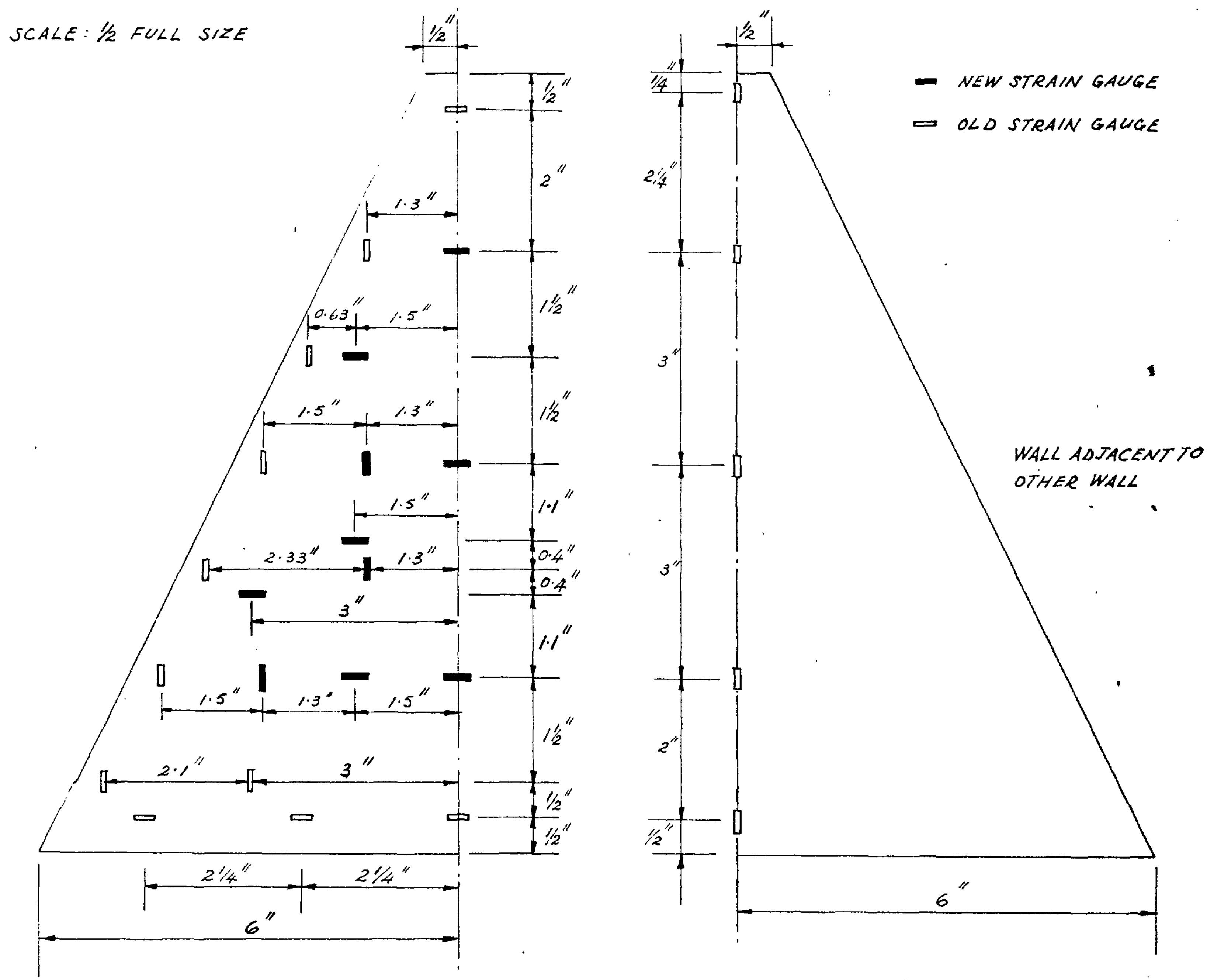

FIG. 3.14 - HORIZONTAL LOAD ON "FIXED" PYRAMID

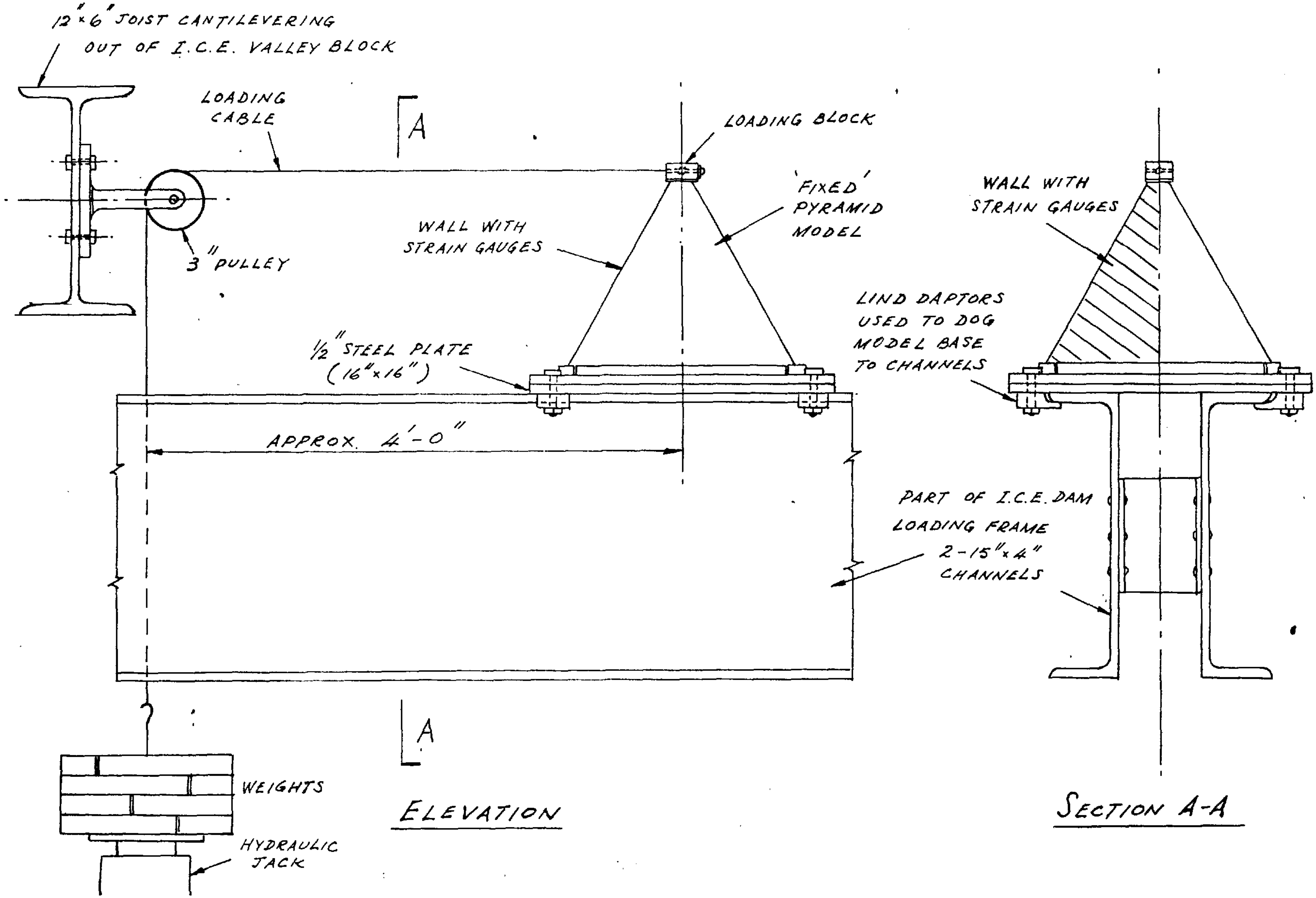

Fig. 3.15 – Mid-Plane Stress Distribution In Walls Of Fixed Pyramid Under Vertical Load

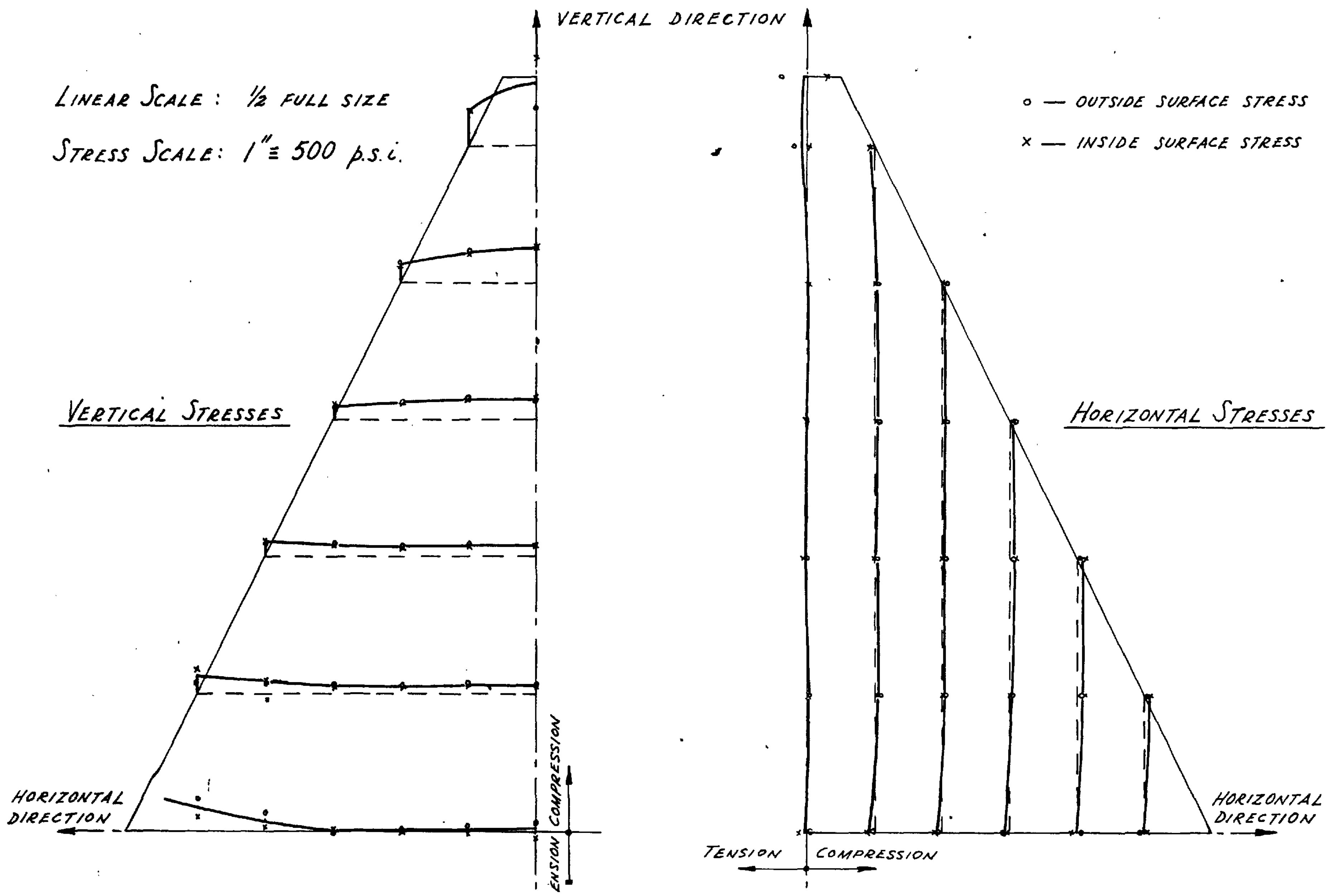

FIG. 3.16 - BENDING MOMENTS IN WALLS OF FIXED PYRAMID UNDER VERTICAL LOAD

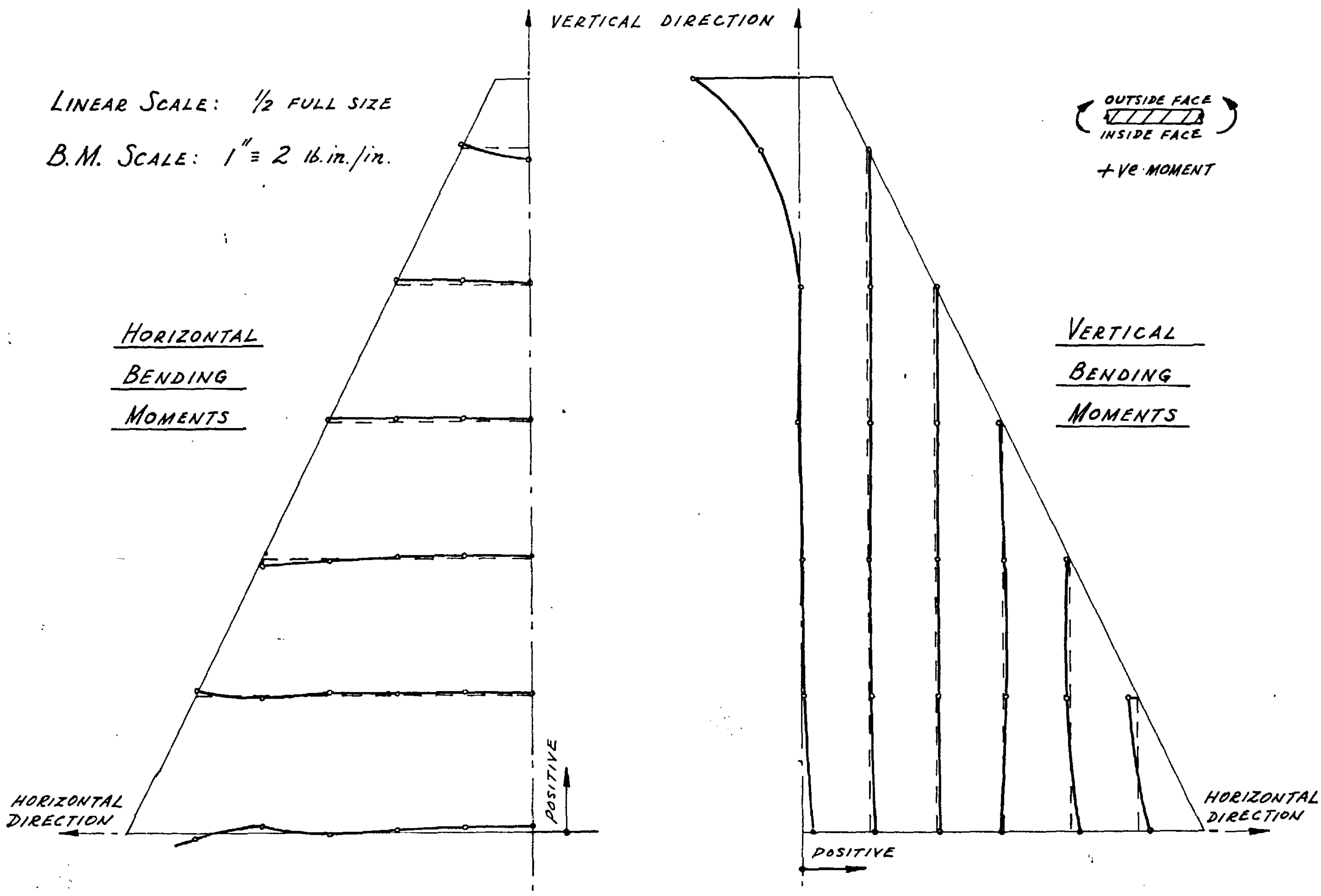

FIG. 3.17 - MID-PLANE STRESS DISTRIBUTION IN WALL "A" OF FIXED PYRAMID UNDER HORIZONTAL LOAD

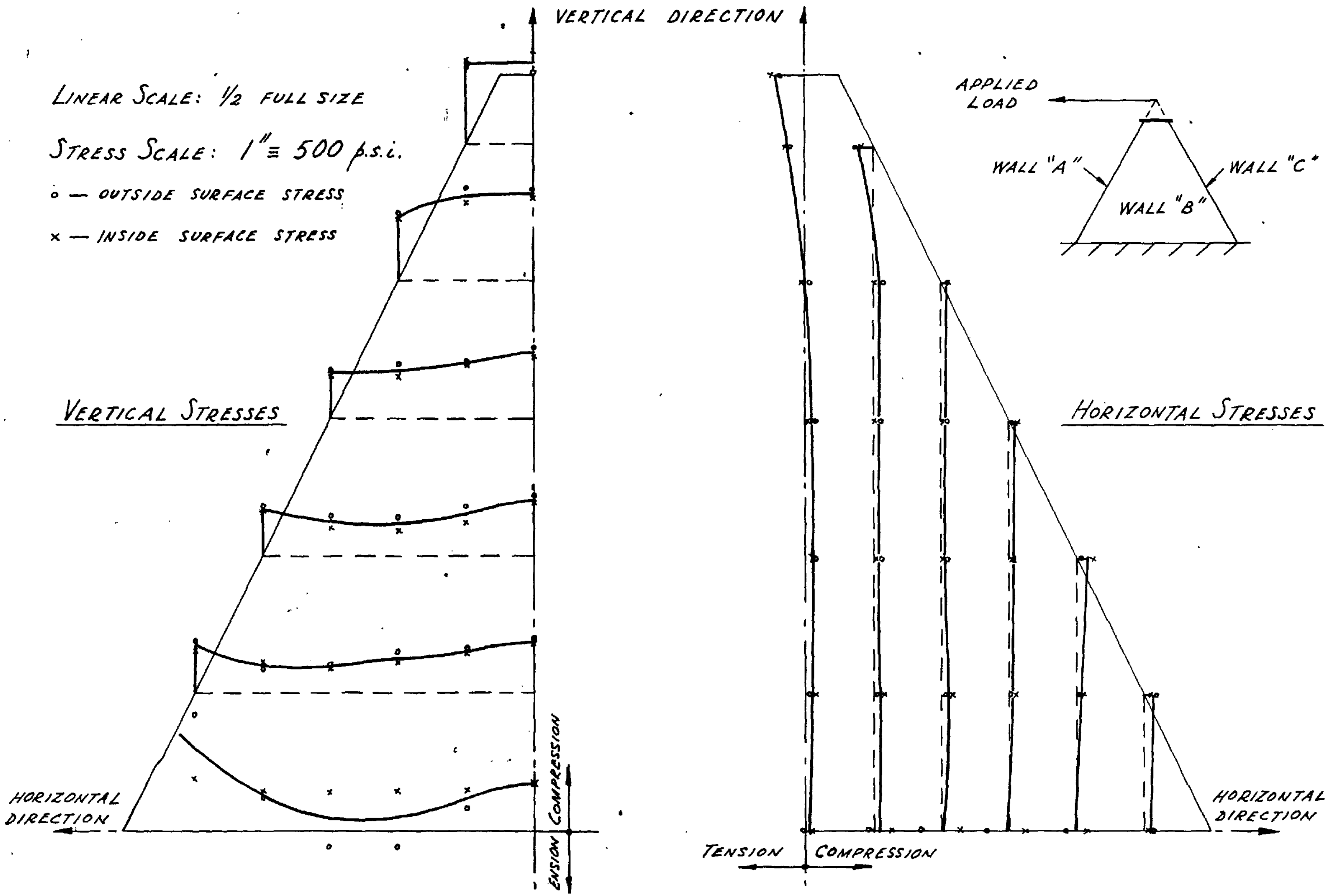

FIG. 3.18 – BENDING MOMENTS IN WALL "A" OF FIXED PYRAMID UNDER HORIZONTAL LOAD

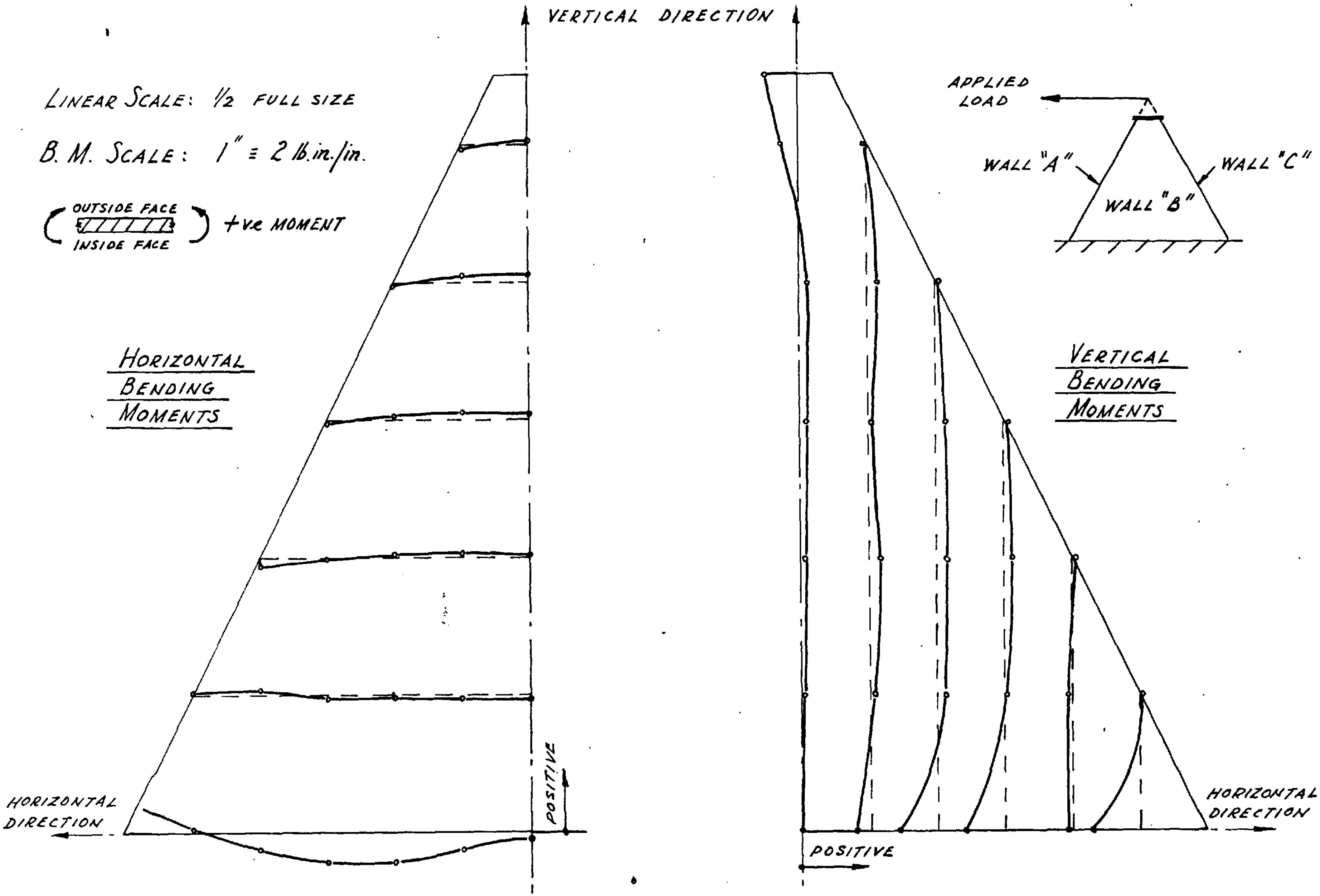

FIG. 3.19 - MID-PLANE STRESS DISTRIBUTION IN WALL "B" OF FIXED PYRAMID UNDER HORIZONTAL LOAD.

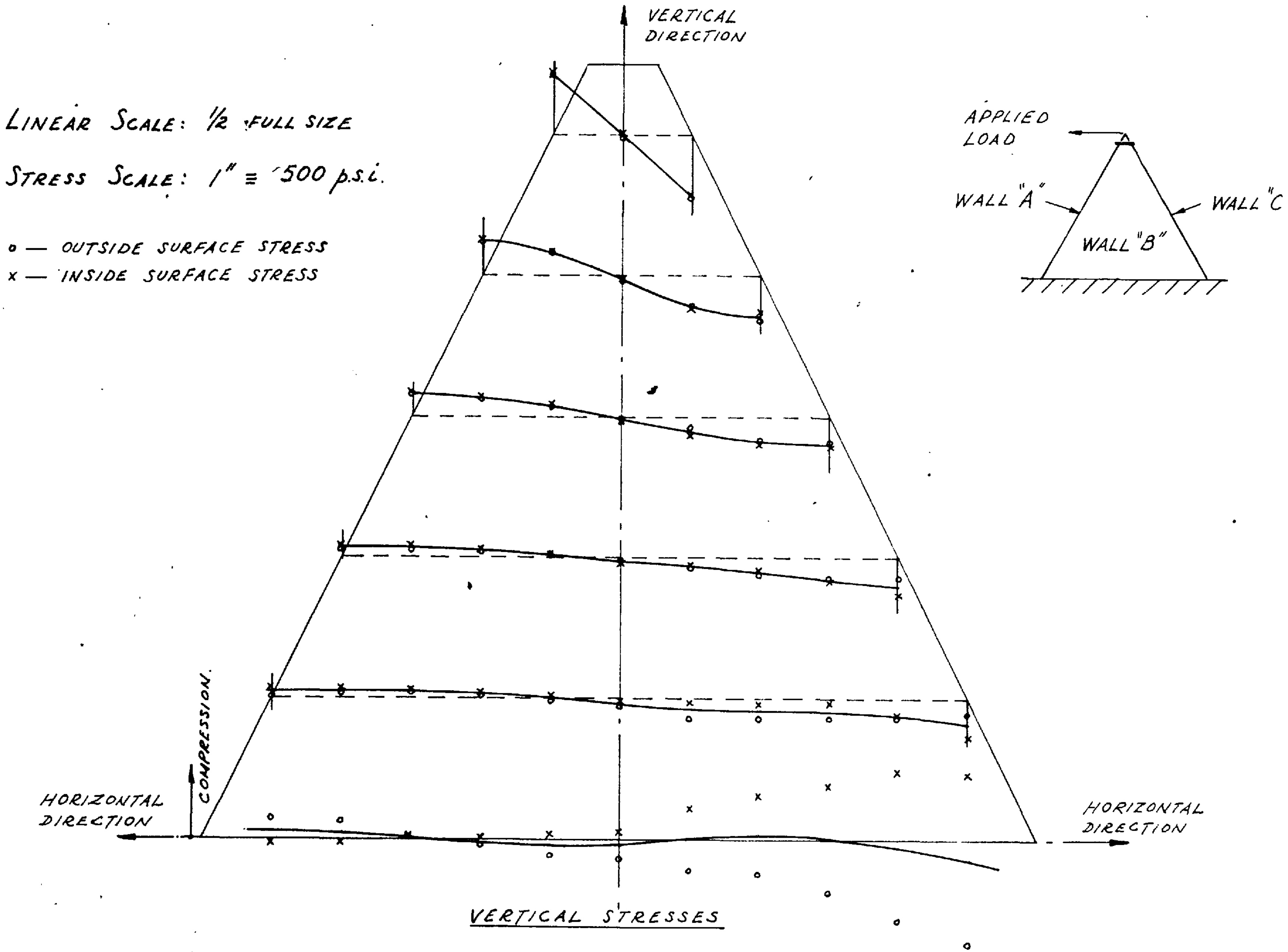

FIG. 3.20 - MID-PLANE STRESS DISTRIBUTION IN WALL "B" OF FIXED PYRAMID UNDER HORIZONTAL LOAD

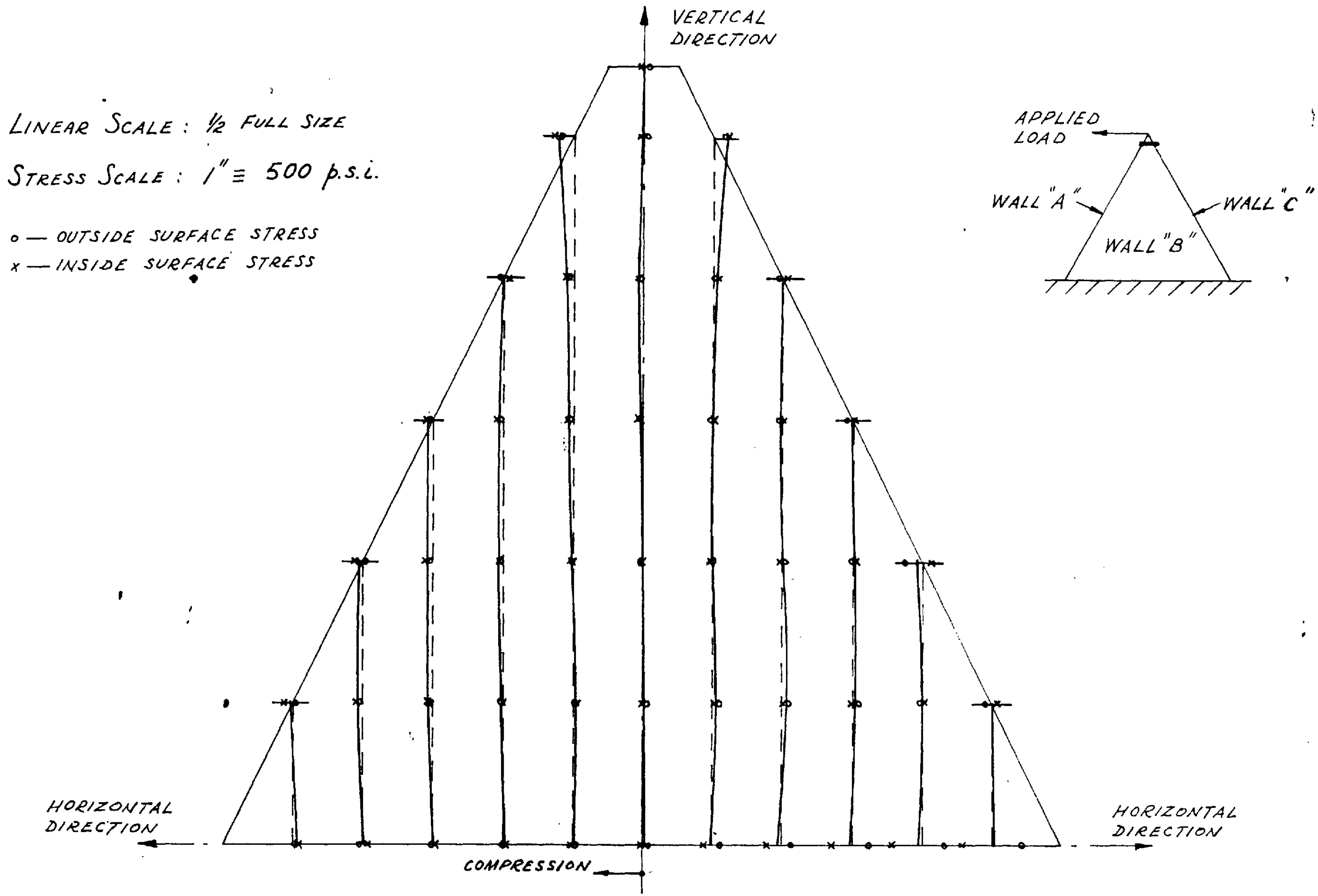

HORIZONTAL STRESSES

FIG. 3.21 – BENDING MOMENTS IN WALL "B" OF FIXED PYRAMID UNDER HORIZONTAL LOAD

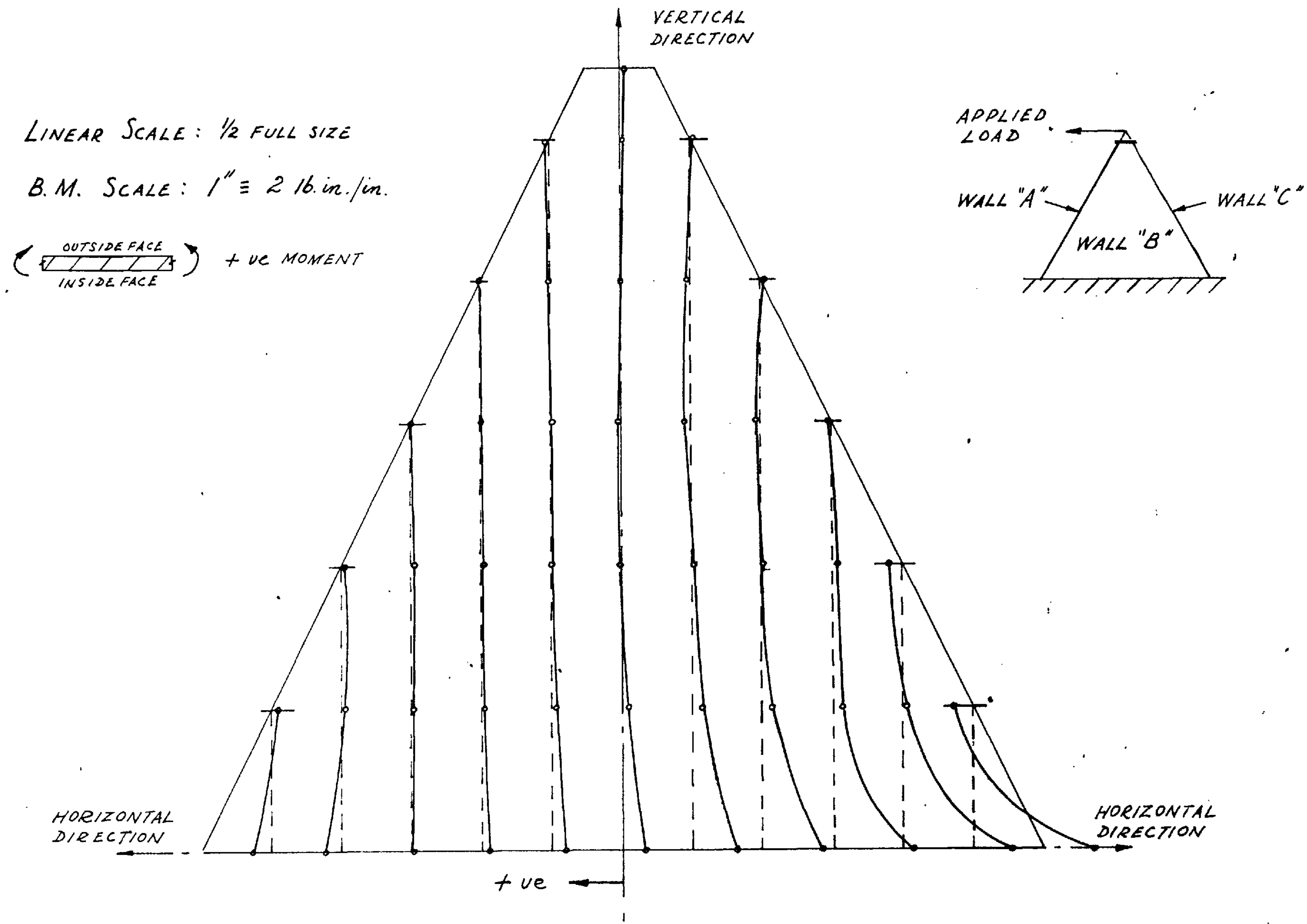

VERTICAL BENDING MOMENTS

FIG. 3.22 - BENDING MOMENTS IN WALL "B" OF FIXED PYRAMID UNDER HORIZONTAL LOAD

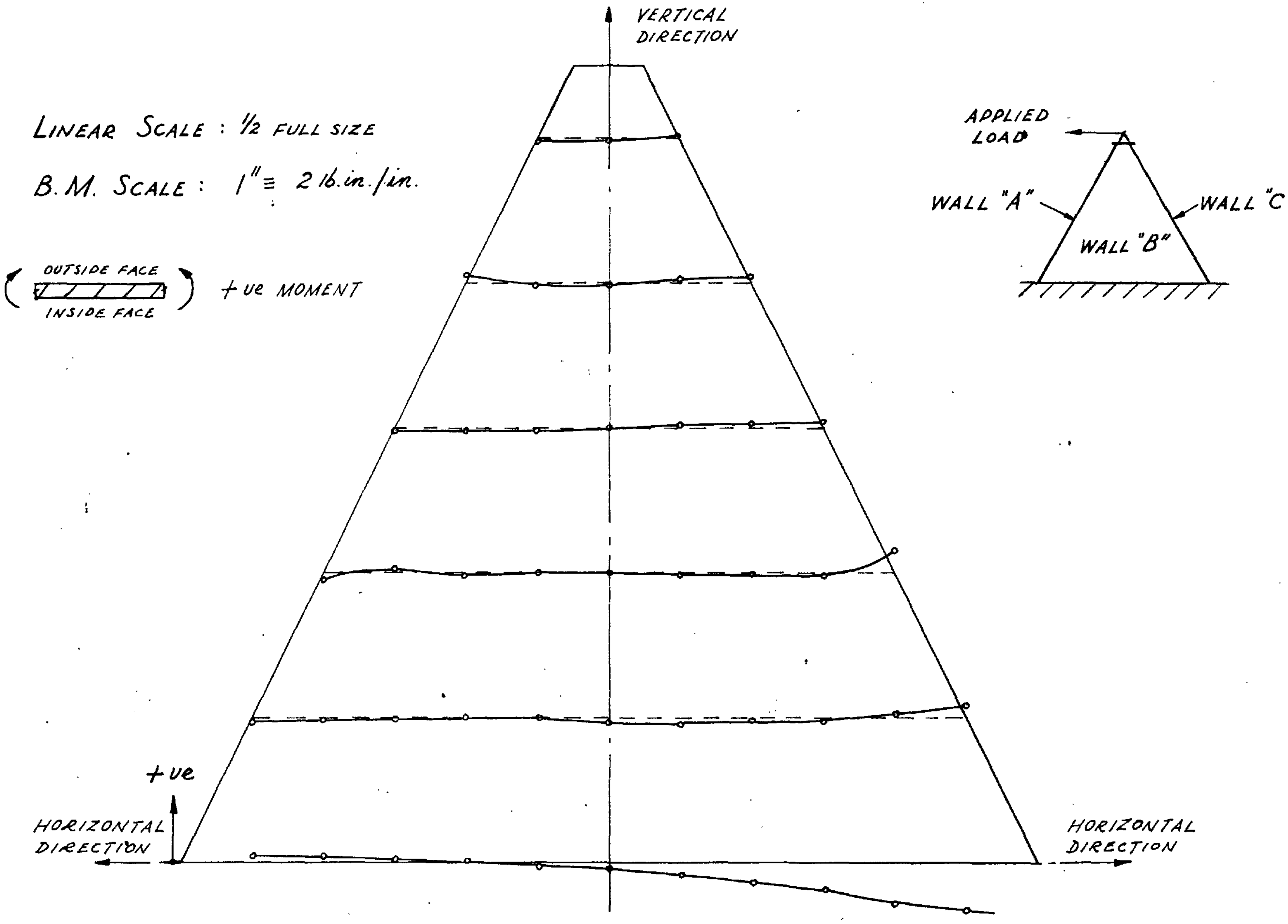

HORIZONTAL BENDING MOMENTS

Fig. 3.23 - Mid-Plane Stress Distribution In Wall "C" Of Fixed Pyramid Under Horizontal Load

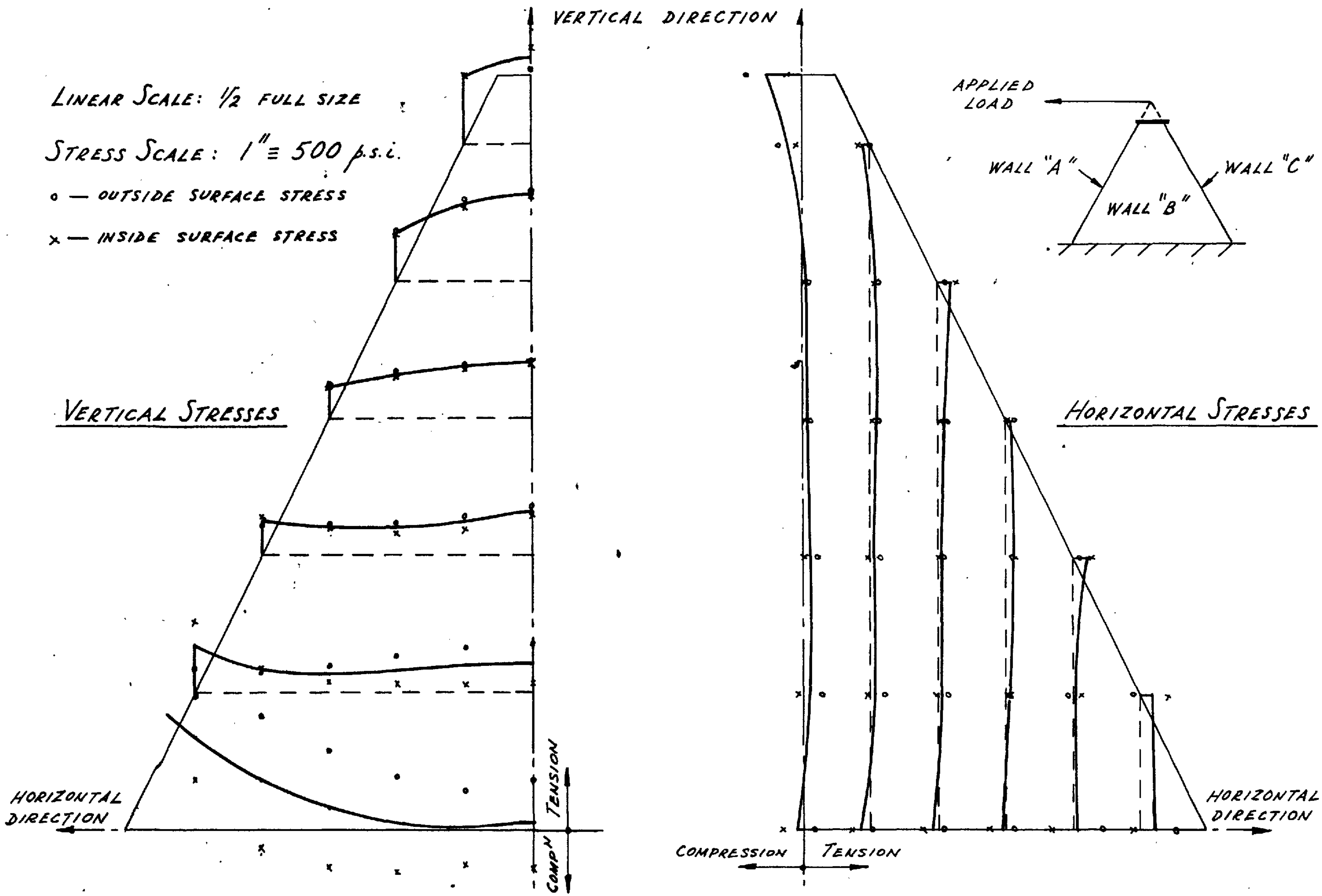

FIG. 3.24 - BENDING MOMENTS IN WALL "C" OF FIXED PYRAMID UNDER HORIZONTAL LOAD

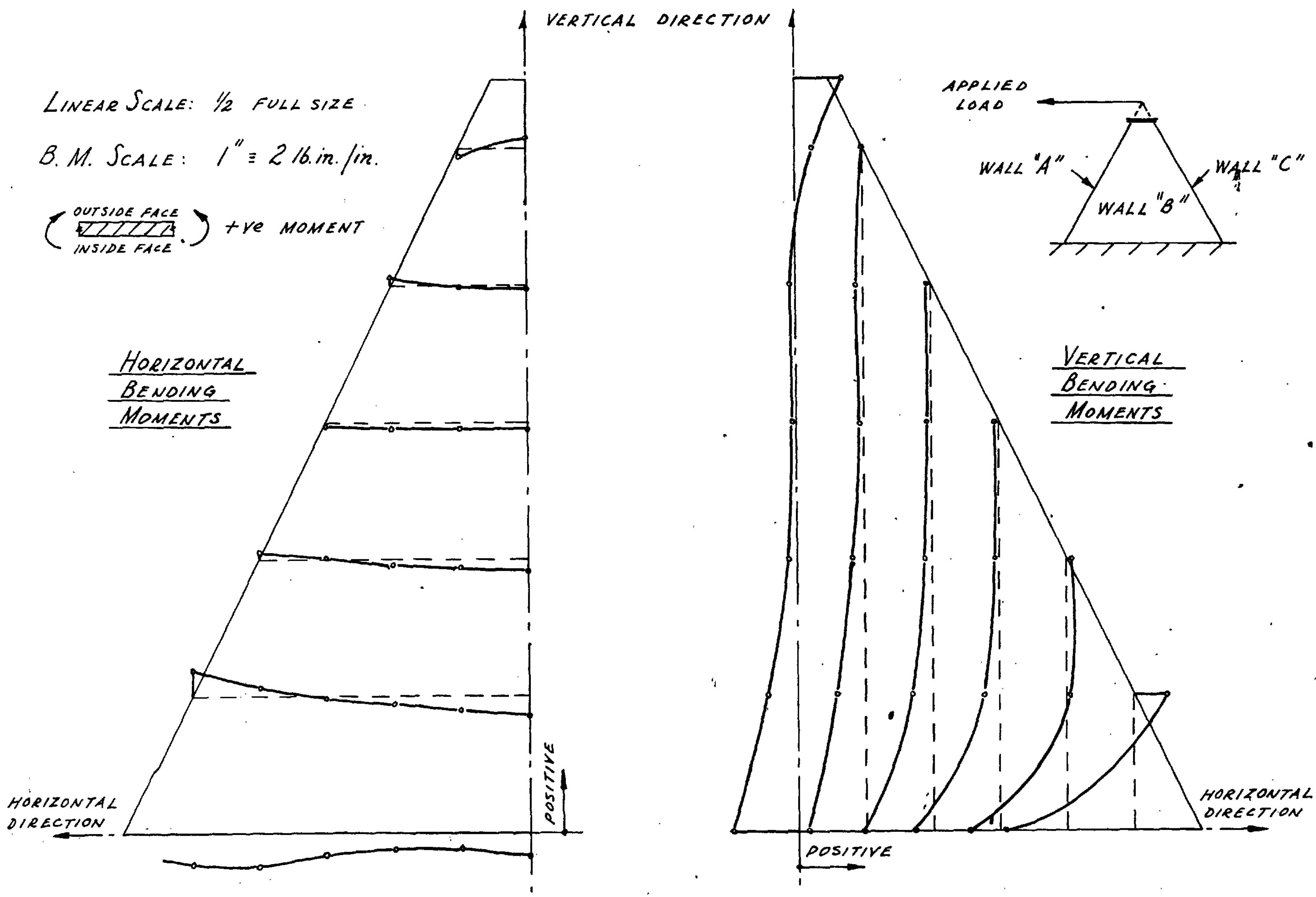

TABLE 4.1 – STRESSES IN SIMPLY-SUPPORTED PYRAMID. σ_x STRESSES.

POINT (SEE FIG. 4.10)	CASE 1	CASE 2	CASE 3	CASE 4
1	-15.98	-34.18	-18.16	-36.36
2	-23.14	-31.23	-25.41	-33.50
3	-22.67	-18.56	-25.05	-20.91
4	8.74	15.18	6.54	13.01
5	84.71	85.56	85.43	86.38
6	198.22	195.41	215.55	212.87
7	-10.68	-21.50	-15.66	-26.46
8	-10.07	-16.38	-15.00	-21.32
9	1.82	2.12	-2.87	-2.58
10	39.87	42.72	35.79	38.66
11	113.91	116.11	111.65	113.84
12	8.14	1.52	0.76	-5.86
13	12.52	7.97	5.29	0.74
14	31.33	30.58	25.20	24.46
15	76.76	78.83	73.87	75.94
16	162.73	166.59	158.29	162.13
17	35.92	31.76	27.02	22.86
18	40.92	37.81	31.62	28.52
19	59.18	58.39	49.31	48.50
20	97.37	98.87	89.59	91.11
21	69.26	66.70	61.78	59.22
22	73.45	71.54	65.31	63.40
23	91.58	91.29	83.02	82.73
24	125.60	127.32	119.86	121.58
25	103.86	102.36	100.02	98.52
26	101.58	100.45	95.73	94.60
27	107.42	107.36	98.21	98.15
28	147.22	146.48	149.88	149.14
29	133.10	132.66	131.03	130.59
30	127.73	127.96	119.54	119.78
31	202.84	202.56	215.02	214.72
32	147.61	147.44	148.08	147.93
33	317.64	317.60	343.98	343.94
34	143.75	143.74	143.76	143.75

N.B. STRESSES IN p.s.i. COMPRESSIVE STRESS +VE.

TABLE 4.2 - STRESSES IN SIMPLY-SUPPORTED PYRAMID. σ_Y STRESSES.

POINT (SEE FIG. 4.10)	CASE 1	CASE 2	CASE 3	CASE 4
1	-161.87	-162.70	-160.95	-161.79
2	-154.73	-157.64	-154.12	-157.03
3	-138.38	-142.55	-138.47	-142.64
4	-115.87	-118.35	-116.59	-119.14
5	-90.97	-88.73	-92.00	-89.94
6	-72.08	-60.89	-77.12	-66.43
7	-69.11	-66.69	-65.04	-62.61
8	-62.35	-61.52	-58.08	-57.26
9	-46.07	-46.85	-41.24	-42.03
10	-24.77	-24.40	-18.51	-18.09
11	2.29	6.62	13.05	17.48
12	-4.70	-1.48	1.76	4.98
13	-0.22	2.13	6.68	9.04
14	10.07	11.23	17.64	18.82
15	18.70	19.68	24.64	25.60
16	11.05	12.06	9.28	10.27
17	33.11	36.36	39.80	43.06
18	35.89	38.71	44.05	46.88
19	42.80	44.95	55.66	57.80
20	54.26	56.28	76.87	78.91
21	49.76	52.64	57.74	54.61
22	50.36	53.00	53.48	56.08
23	46.62	48.54	51.95	53.87
24	26.29	27.25	31.90	32.85
25	55.46	57.78	49.56	51.88
26	59.84	62.01	55.37	57.54
27	67.61	69.54	66.06	67.99
28	48.24	49.76	32.91	34.43
29	54.37	55.74	40.55	41.91
30	43.49	44.29	29.94	30.74
31	44.65	45.55	23.18	24.08
32	74.24	75.03	55.09	55.90
33	33.19	33.54	19.78	20.13
34	65.57	65.82	54.74	54.98

N.B. STRESSES IN p.s.i. COMPRESSIVE STRESS +ve.

Table 4.3 – Stresses in Simply-Supported Pyramid. τ_{xy} Stresses.

Point (see Fig. 4.10)	Case 1	Case 2	Case 3	Case 4
1	0	0	0	0
2	3.31	8.73	0.84	6.25
3	18.25	21.71	13.37	16.82
4	43.92	42.18	36.85	35.11
5	74.99	70.32	66.33	61.66
6	234.13	238.70	252.57	257.14
7	0	0	0	0
8	14.94	18.73	12.41	16.19
9	37.36	40.81	32.64	36.09
10	67.87	69.01	62.04	63.16
11	106.65	107.45	98.43	99.18
12	0	0	0	0
13	24.40	26.86	22.33	24.79
14	51.49	54.48	47.02	50.02
15	80.20	82.58	73.52	75.90
16	131.25	133.87	112.79	115.41
17	0	0	0	0
18	30.51	32.19	30.26	31.94
19	60.81	63.26	59.72	62.17
20	88.97	91.45	85.75	88.23
21	0	0	0	0
22	32.15	33.31	34.28	35.44
23	59.37	61.21	62.53	64.37
24	84.68	86.81	87.04	89.17
25	0	0	0	0
26	52.00	52.68	28.56	29.24
27	59.70	61.02	64.13	65.45
28	0	0	0	0
29	36.25	36.80	41.84	42.38
30	54.07	54.95	61.07	61.95
31	0	0	0	0
32	48.92	49.21	53.76	54.04
33	0	0	0	0
34	58.88	58.99	63.84	63.95

N.B. Stresses in p.s.i.

TABLE 4.4 – STRESSES IN FIXED PYRAMID
RECTANGULAR NET SOLUTION

POINT (SEE FIG. 4.19)	σ_x (p.s.i.)	σ_y (p.s.i.)	τ_{xy} (p.s.i.)
1	−102.59	−1.41	0
2	−98.08	−1.87	8.95
3	−83.52	0.83	16.22
4	−62.88	−3.79	18.85
5	−37.81	1.07	18.20
6	−124.24	−1.95	0
7	−120.85	−3.79	13.48
8	−102.83	−10.21	25.75
9	−72.72	−19.23	30.20
10	−166.75	−23.95	0
11	−162.11	−27.01	25.04
12	−146.83	−42.53	52.51
13	−235.76	−37.20	0
14	−222.13	−39.71	37.71
15	−347.00	−55.00	0

N.B. COMPRESSIVE STRESS −ve.

TABLE 4.5 – STRESSES IN FIXED PYRAMID: SQUARE NET SOLUTION.

POINT (SEE FIG. 4.23)	σ_x (p.s.i.)	σ_y (p.s.i.)	τ_{xy} (p.s.i.)
1	−106.56	−17.15	0
2	−102.37	−16.72	8.32
3	−88.29	−14.51	15.41
4	−69.71	−11.01	20.32
5	−55.23	−6.00	22.05
6	−48.12	−3.71	23.36
7	−114.20	−11.31	0
8	−109.10	−10.56	7.31
9	−83.50	−5.92	10.64
10	−62.90	−0.72	17.97
11	−52.60	1.09	29.49
12	−128.19	−19.95	0
13	−124.40	−26.35	13.25
14	−102.77	−3.52	24.35
15	−68.88	16.69	28.56
16	−48.45	10.67	28.99
17	−140.90	−0.93	0
18	−133.60	−0.32	19.23
19	−112.16	2.11	38.67
20	−59.81	18.00	42.69
21	−162.27	−2.03	0
22	−154.11	−3.28	20.40
23	−130.48	−9.81	40.96
24	−98.59	−14.85	49.07
25	−189.90	−14.85	0
26	−178.00	−16.83	27.65
27	−152.77	−22.99	56.08
28	−227.20	−18.51	0
29	−206.00	−20.80	40.03
30	−175.97	−23.01	83.39
31	−281.60	−17.68	0
32	−237.81	−18.93	54.05
33	−365.23	−35.23	0
34	−261.09	−14.40	71.55
35	−430.59	−52.53	0

N.B. COMPRESSIVE STRESS −ve.

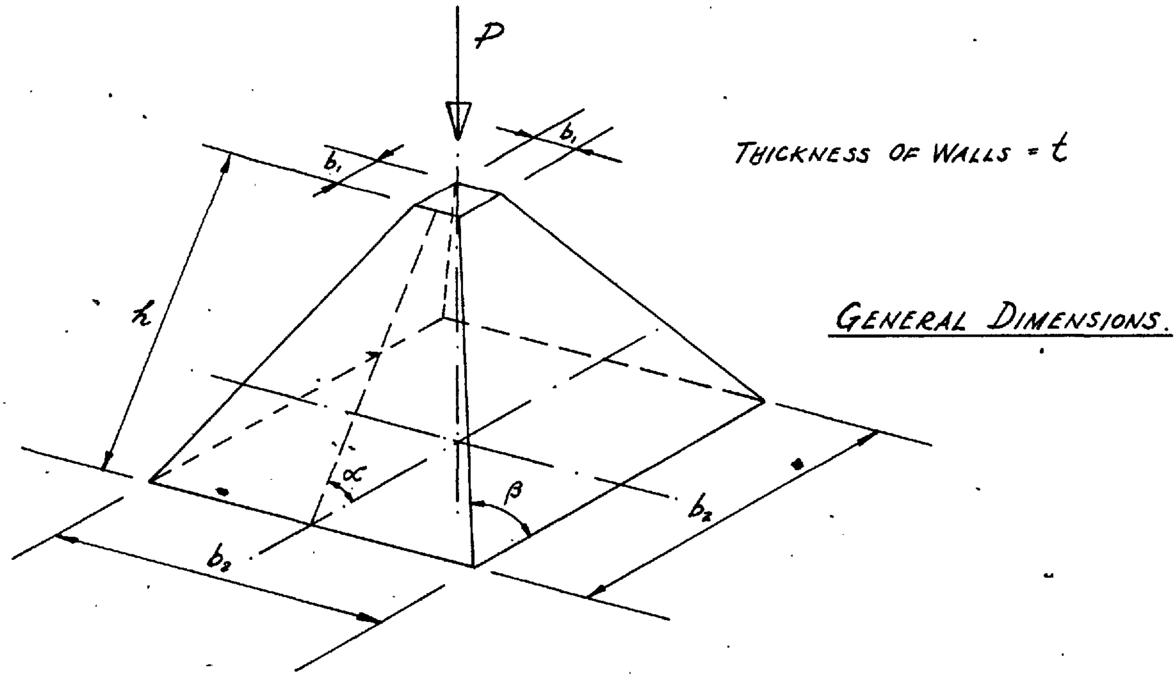

FIG. 4.1 (a)

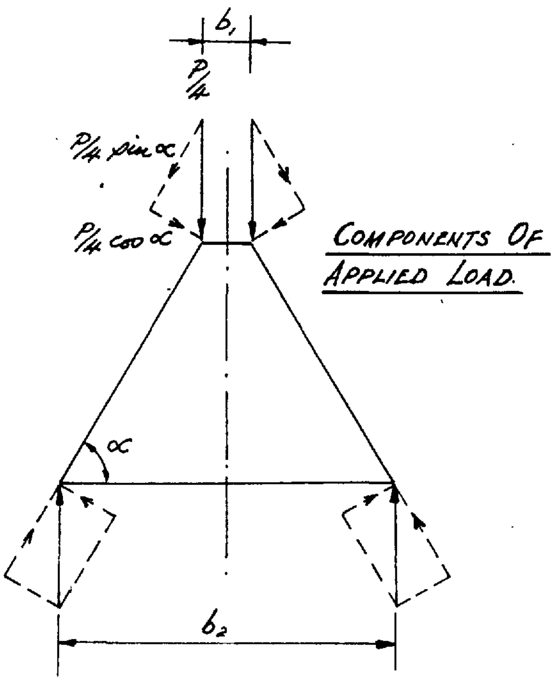

FIG. 4.1 (b)

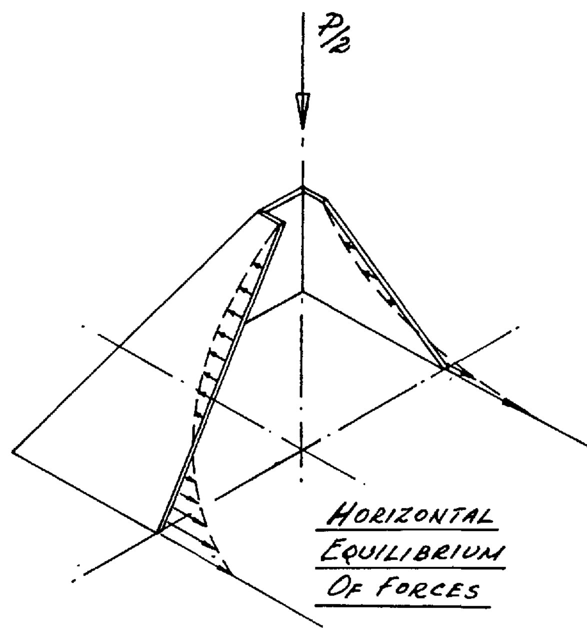

FIG. 4.1 (c)

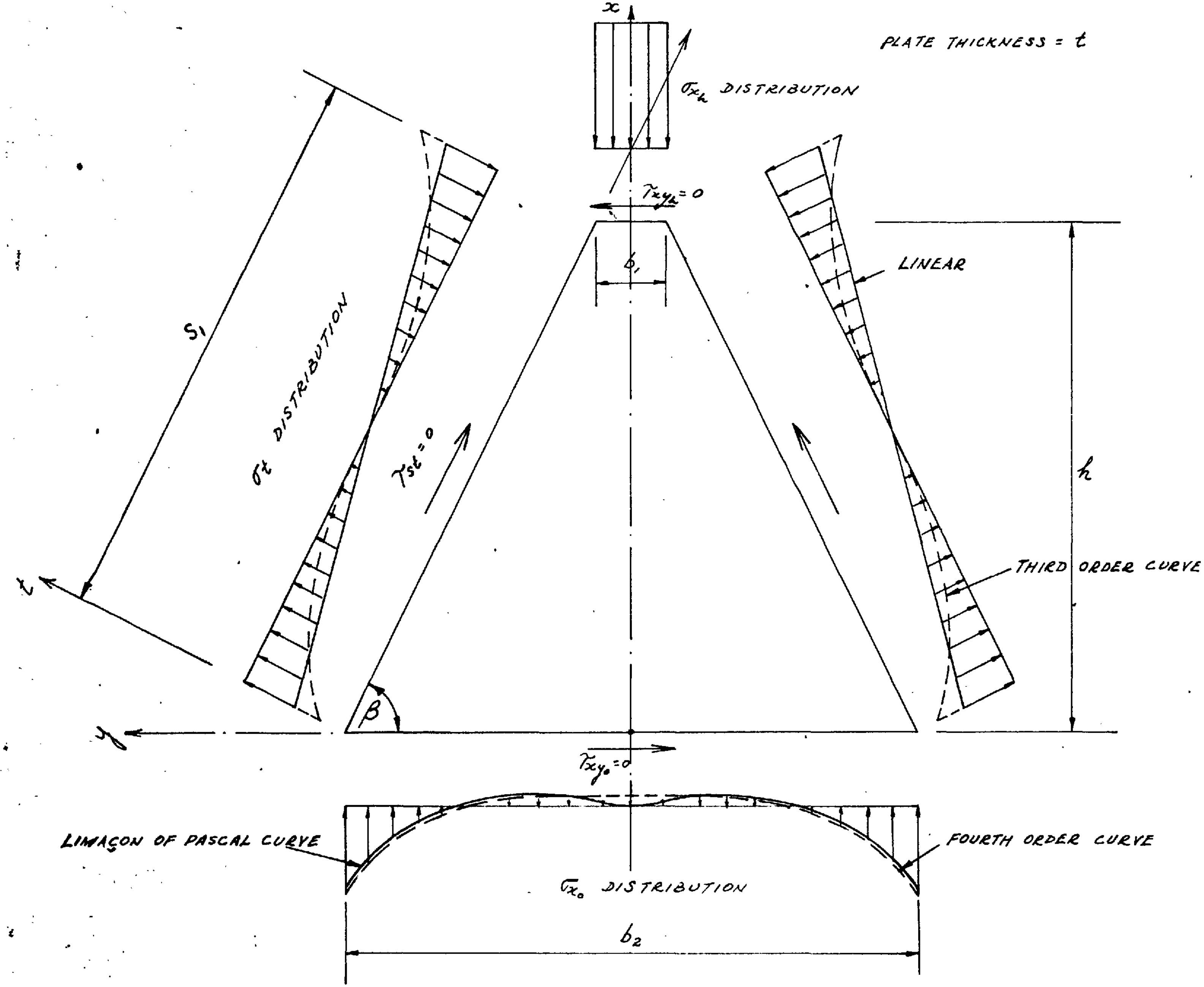

FIG. 4.2 — BOUNDARY TRACTION ASSUMPTIONS

FIG. 4.3 - LIMAÇON OF PASCAL ASSUMPTION FOR NORMAL STRESS DISTRIBUTION AT BOTTOM EDGE OF WALL

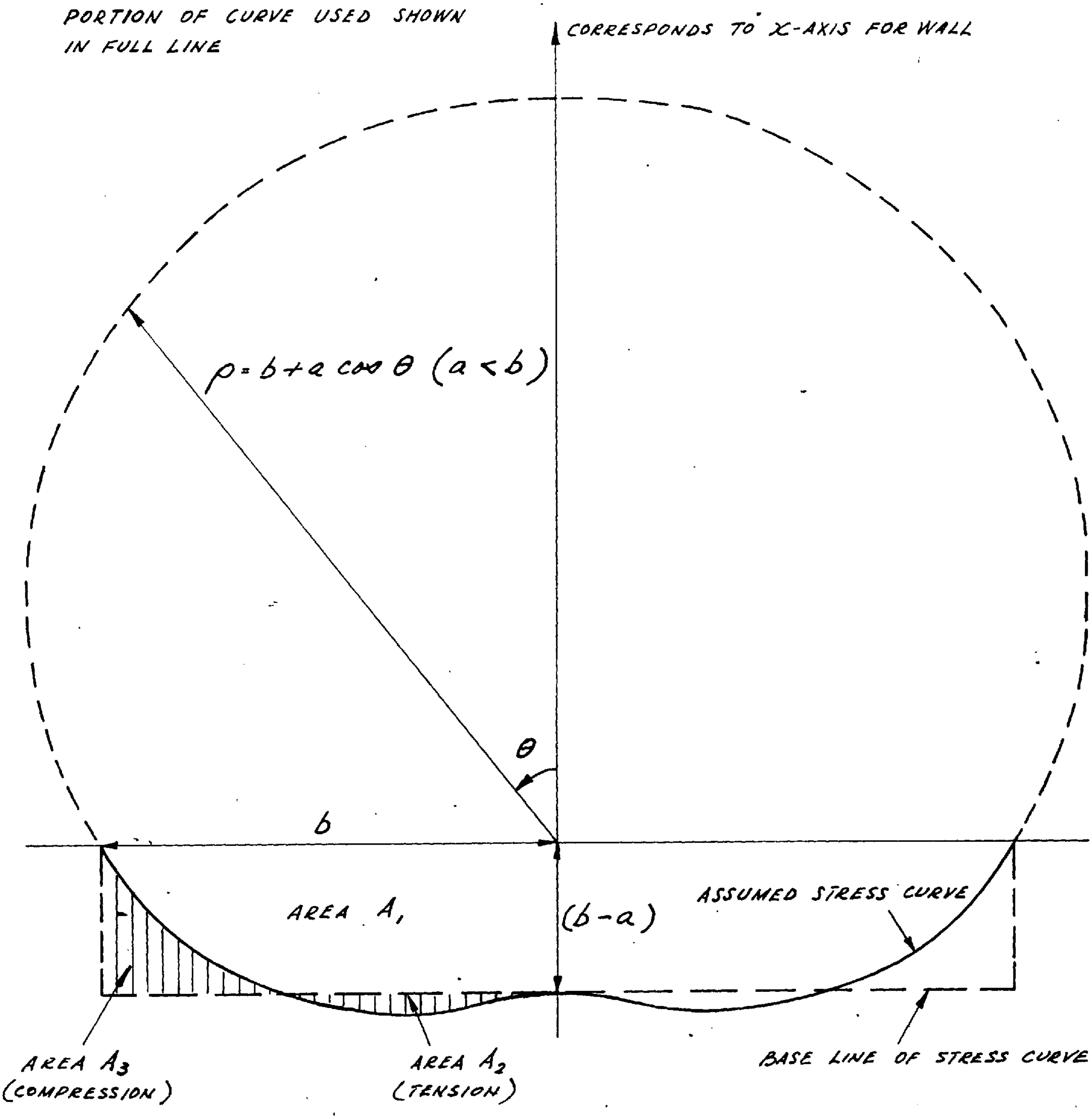

FIG. 4.4 — ROTATIONAL EQUILIBRIUM OF AN ADJOINING WALL

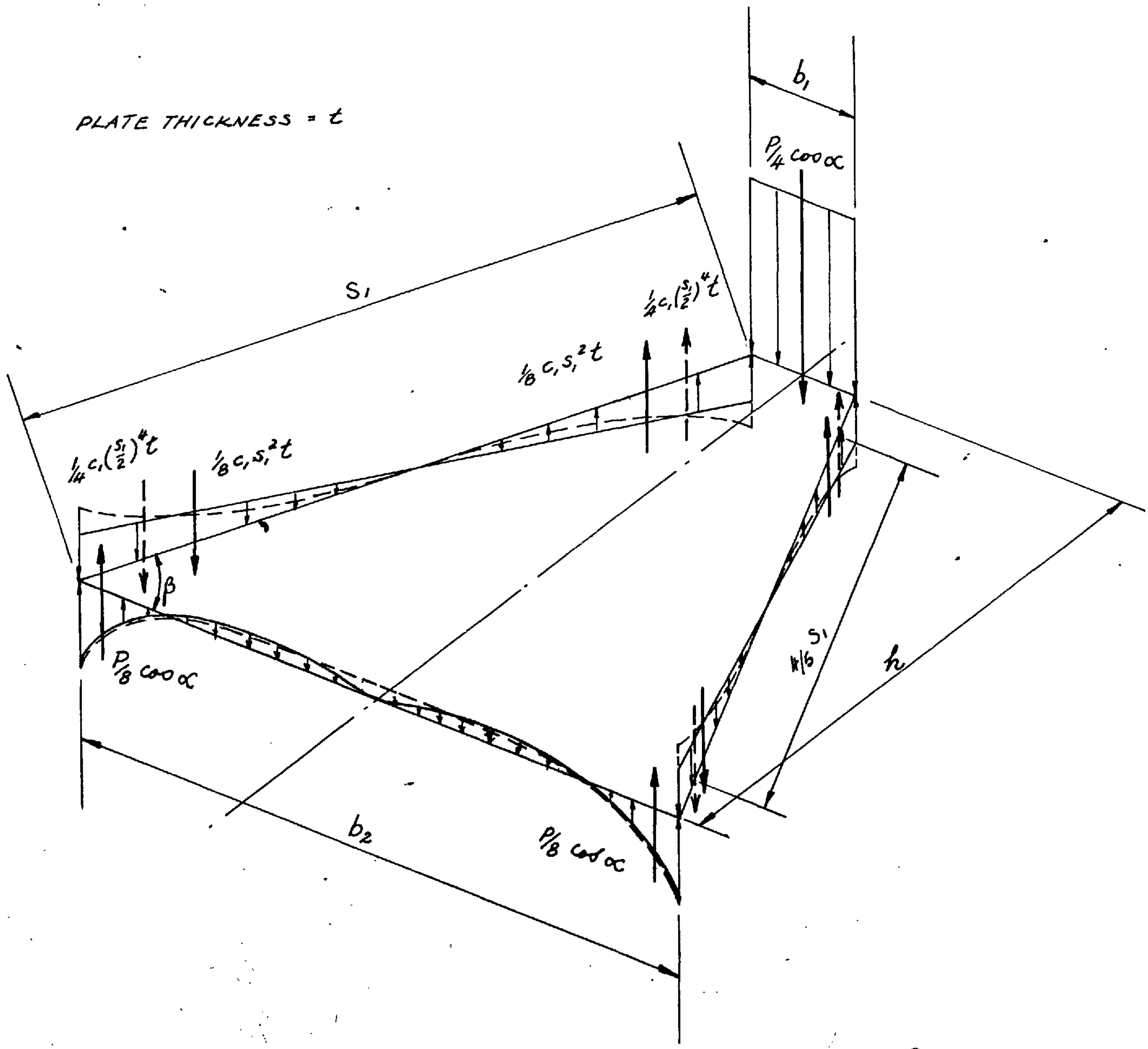

FIG. 4.8 - BOUNDARY TRACTION ASSUMPTIONS FOR BOTTOM EDGE OF WALL

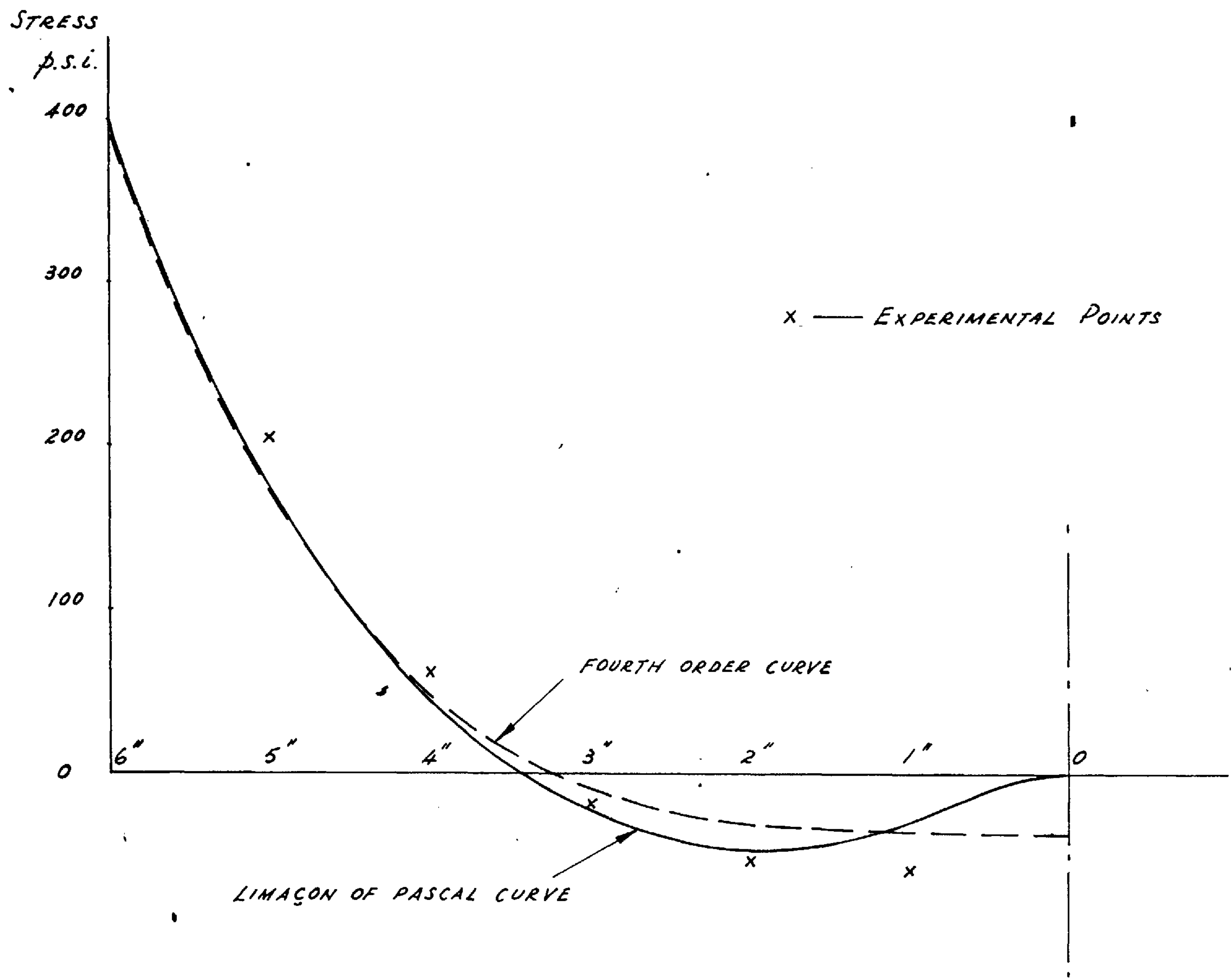

FIG. 4.9 – NUMERICAL INTEGRATION OF σ_{x_0}

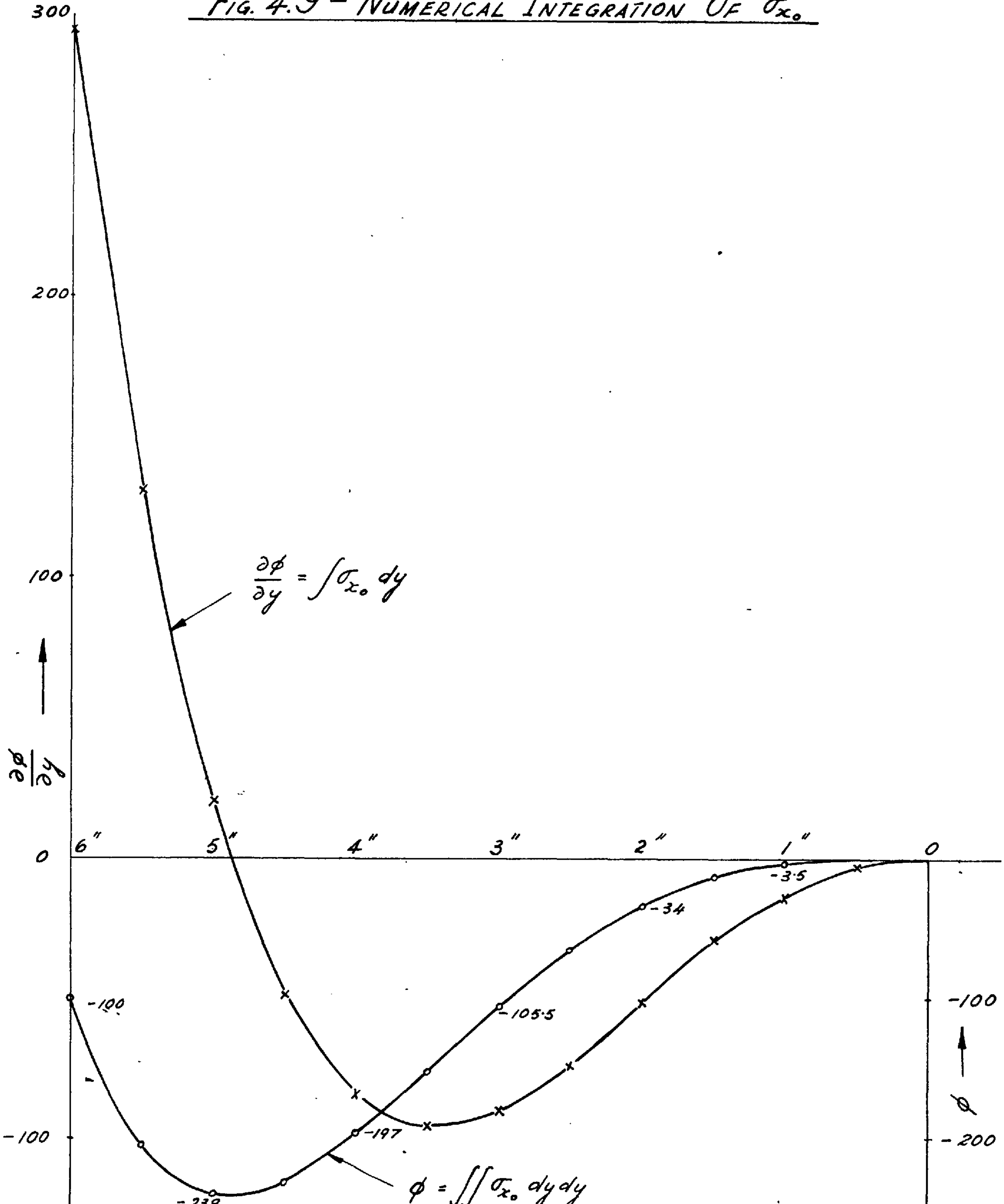

FIG. 4.10 - BOUNDARY φ VALUES

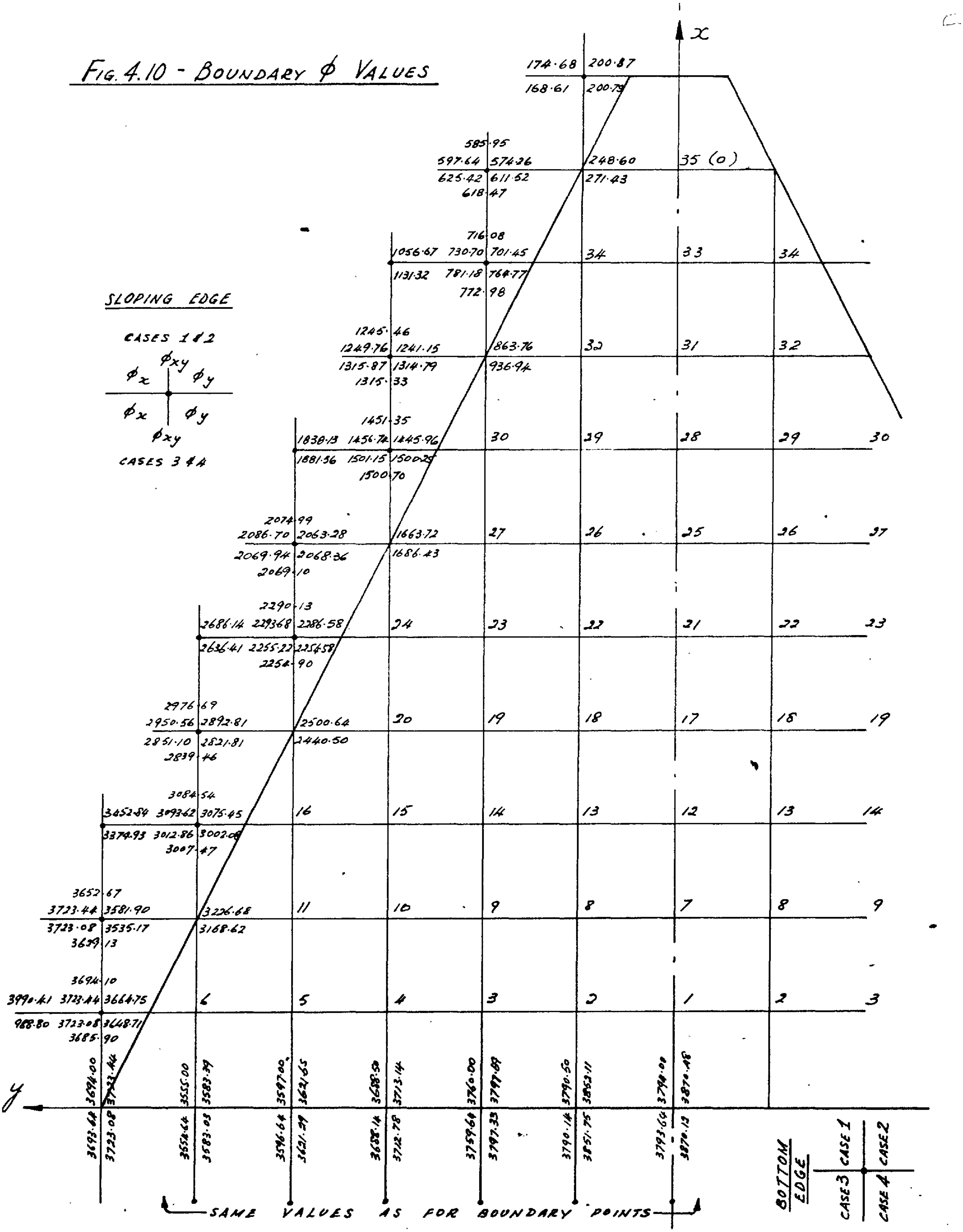

Fig. 4.12 – Main Matrix in Stress Function Solution

N.B. All empty spaces contain zero

ϕ_1	ϕ_2	ϕ_3	ϕ_4	ϕ_5	ϕ_6	ϕ_7	ϕ_8	ϕ_9	ϕ_{10}	ϕ_{11}	ϕ_{12}	ϕ_{13}	ϕ_{14}	ϕ_{15}	ϕ_{16}	ϕ_{17}	ϕ_{18}	ϕ_{19}	ϕ_{20}	ϕ_{21}	ϕ_{22}	ϕ_{23}	ϕ_{24}	ϕ_{25}	ϕ_{26}	ϕ_{27}	ϕ_{28}	ϕ_{29}	ϕ_{30}	ϕ_{31}	ϕ_{32}	ϕ_{33}	ϕ_{34}
10	-8	1				-4	2				0.5																						
-8	21	-8	1			2	-8	2				1																					
1	-8	20	-8	1			2	-8	2				1																				
	1	-8	20	-8	1			2	-8	2				1																			
		1	-8	20	-8				2	-8					1																		
			1	-8	20					2																							
-4	2					10	-8	1			-4	2				0.5																	
2	-8	2				-8	21	-8	1		2	-8	2				1																
	2	-8	2			1	-8	20	-8	1		2	-8	2				1															
		2	-8	2			1	-8	20	-8			2	-8	2				1														
			2	-8	2			1	-8	20				2	-8																		
0.5						-4	2				10	-8	1			-4	2			0.5													
	1					2	-8	2			-8	21	-8	1		2	-8	2			1												
		1					2	-8	2		1	-8	20	-8	1		2	-8	2			1											
			1					2	-8	2		1	-8	20	-8			2	-8				1										
				1					2	-8			1	-8	20				2														
						0.5					-4	2				10	-8	1		-4	2			0.5									
							1				2	-8	2			-8	21	-8	1	2	-8	2			1								
								1				2	-8	2		1	-8	20	-8		2	-8	2			1							
									1				2	-8	2		1	-8	20			2	-8										
											0.5					-4	2			10	-8	1		-4	2		0.5						
												1				2	-8	2		-8	21	-8	1	2	-8	2		1					
													1				2	-8	2	1	-8	20	-8		2	-8			1				
														1				2	-8		1	-8	20			2							
																0.5				-4	2			10	-8	1	-4	2		0.5			
																	1			2	-8	2		-8	21	-8	2	-8	2		1		
																		1			2	-8	2	1	-8	20		2	-8				
																				0.5				-4	2		10	-8	1	-4	2	0.5	
																					1			2	-8	2	-8	21	-8	2	-8		1
																						1			2	-8	1	-8	20		2		
																								0.5			-4	2		10	-8	-4	2
																									1		2	-8	2	-8	21	2	-8
																											0.5			-4	2	10	-8
																												1		2	-8	-8	21

FIG. 4.13 – THEORETICAL AND EXPERIMENTAL σ_x STRESS DISTRIBUTIONS IN WALLS OF SIMPLY-SUPPORTED PYRAMID

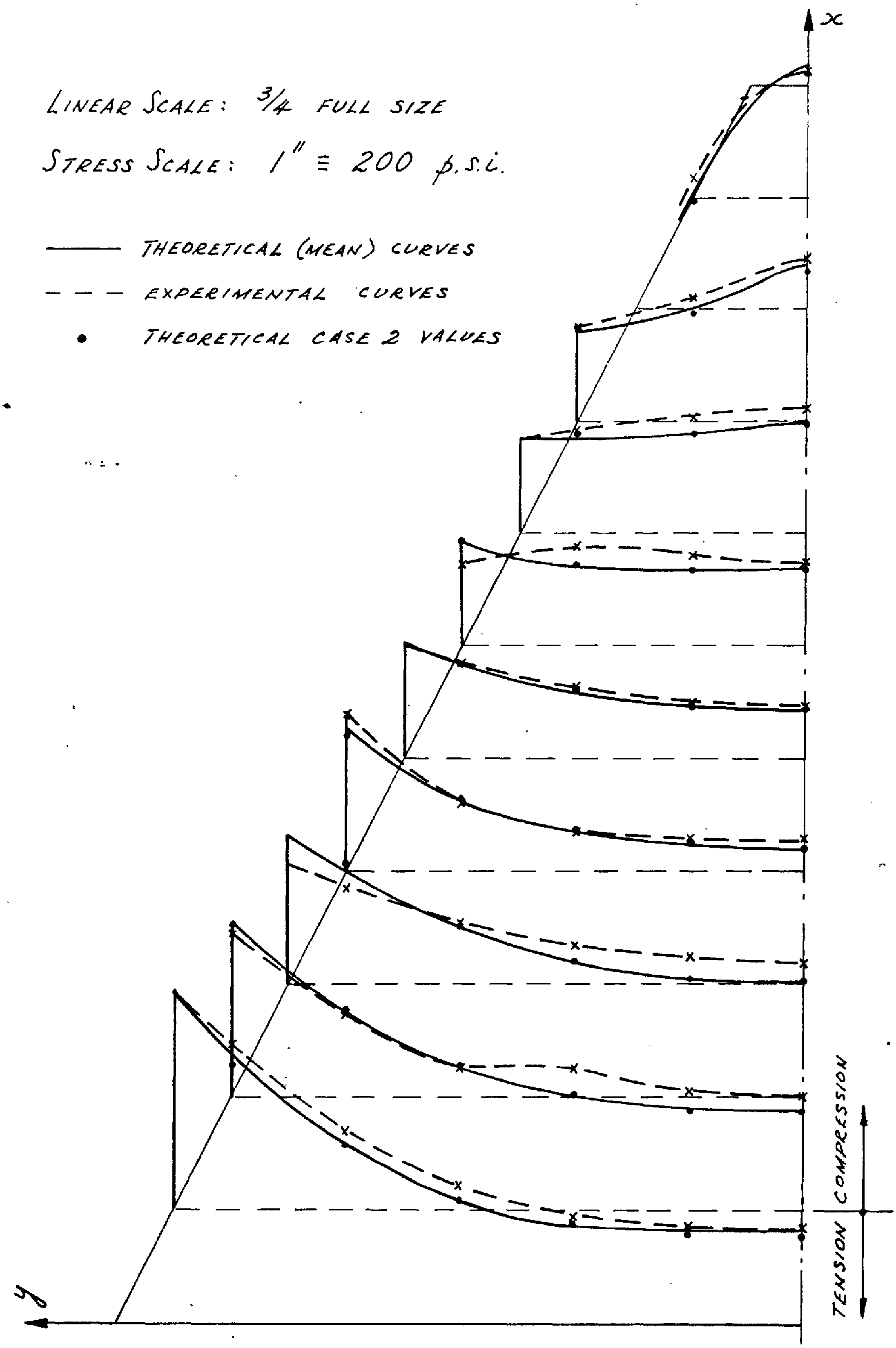

FIG. 4.14 - THEORETICAL AND EXPERIMENTAL σ_y STRESS DISTRIBUTIONS IN WALLS OF SIMPLY-SUPPORTED PYRAMID

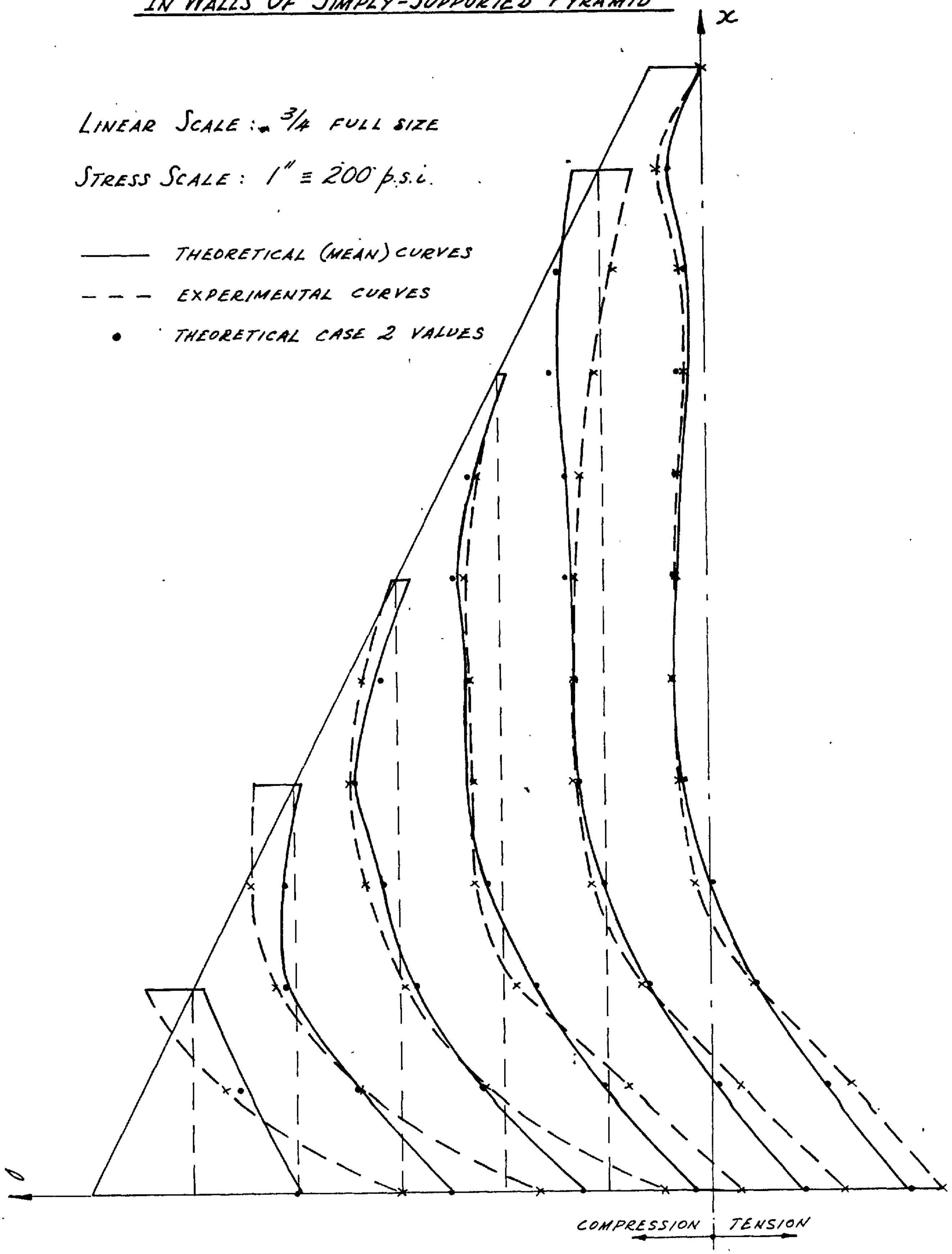

FIG. 4.15 – THEORETICAL AND EXPERIMENTAL τ_{xy} STRESS DISTRIBUTIONS IN WALLS OF SIMPLY-SUPPORTED PYRAMID

LINEAR SCALE : 3/4 FULL SIZE

STRESS SCALE : 1" ≡ 200 p.s.i.

—— THEORETICAL (MEAN) CURVES

x EXPERIMENTAL VALUES

• THEORETICAL CASE 2 VALUES

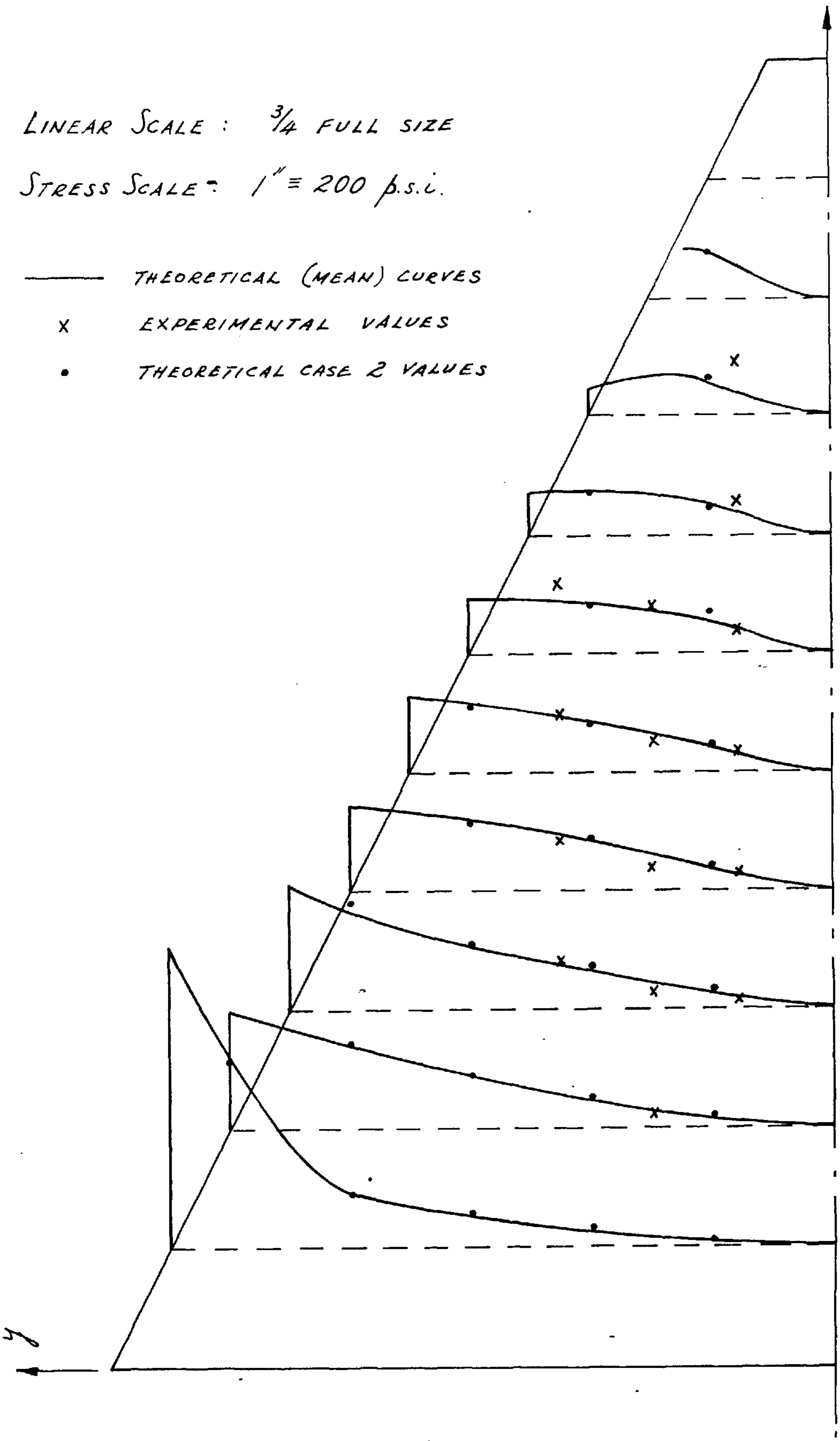

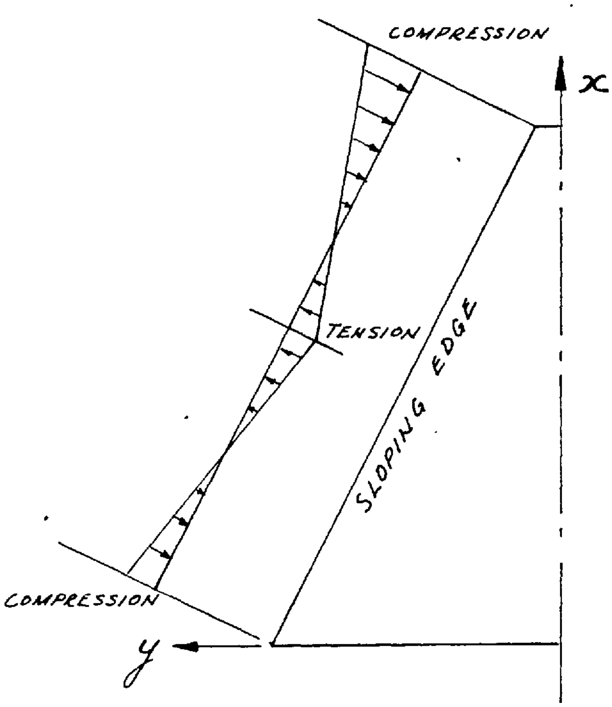

FIG. 4.16 (a)
TYPE OF SIDE LOADING SUGGESTED BY EXPERIMENTAL RESULTS

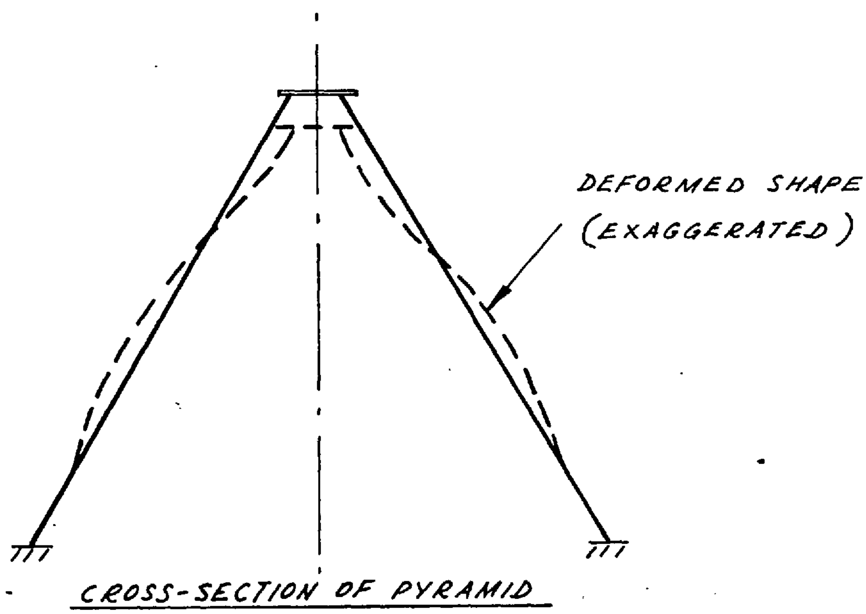

FIG. 4.16 (b) - DEFORMATION OF OPPOSITE WALLS

Fig. 4.17 – Equilibrium Of An Adjoining Wall

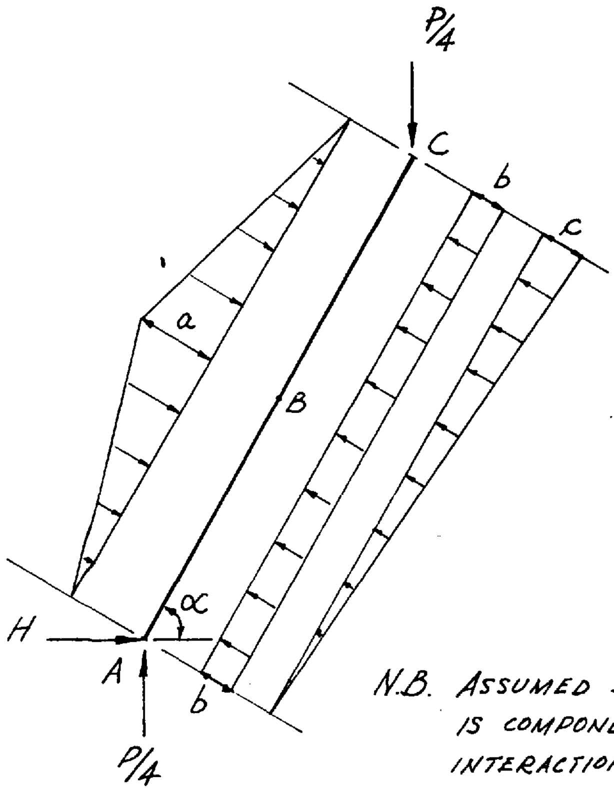

(a) Side Elevation

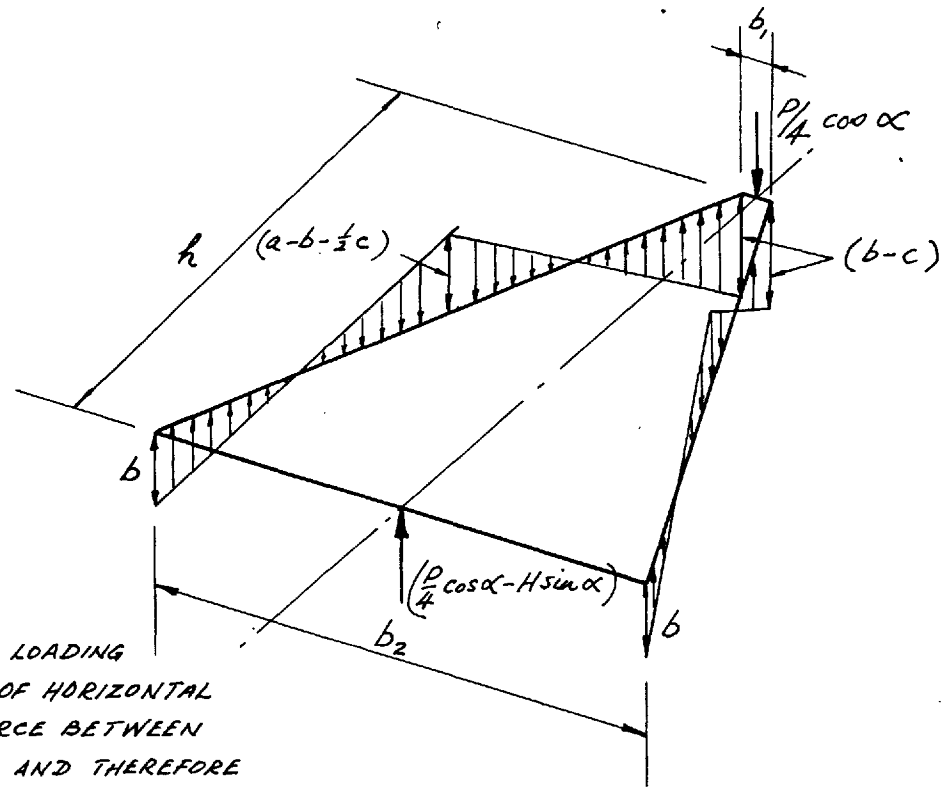

N.B. Assumed side loading is component of horizontal interaction force between wall junctions and therefore has no vertical component.

(b) Rotational Equilibrium

Fig. 4.19 - Rectangular Net For Mixed Boundary Problem

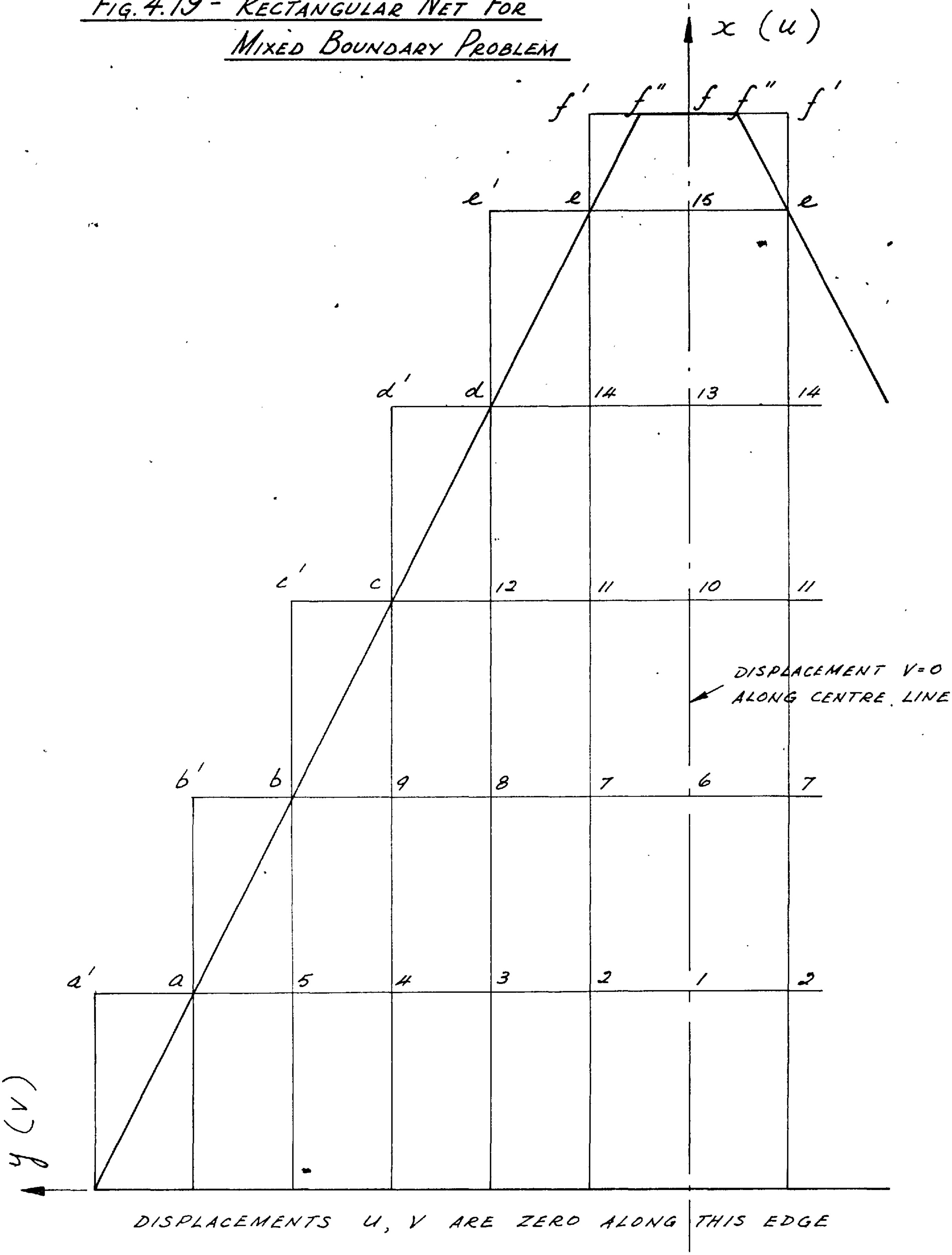

FIG. 4.20 - THEORETICAL AND EXPERIMENTAL σ_x STRESS DISTRIBUTIONS IN WALLS OF FIXED PYRAMID

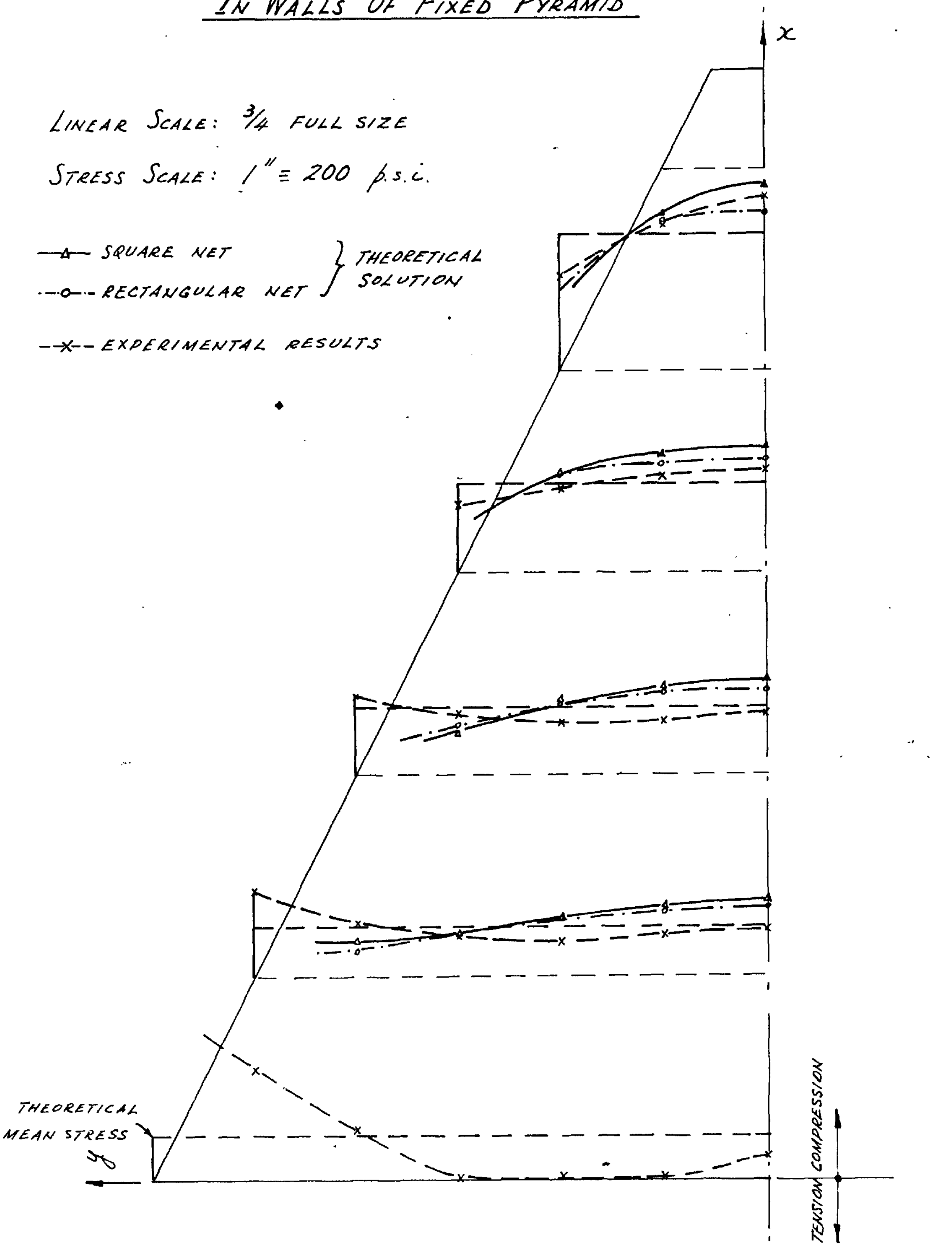

FIG. 4.21 - THEORETICAL AND EXPERIMENTAL σ_y STRESS DISTRIBUTIONS IN WALLS OF FIXED PYRAMID

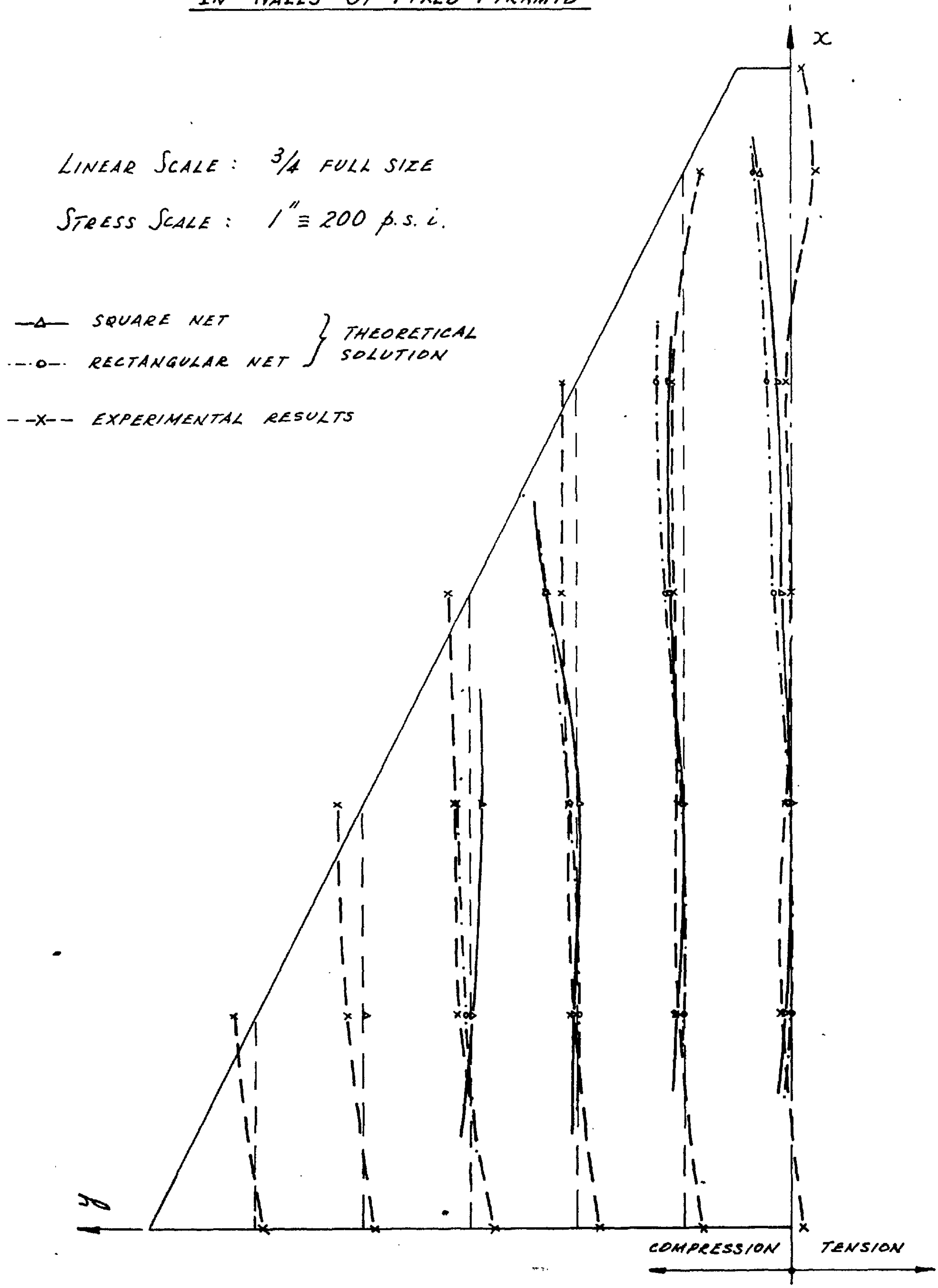

Fig. 4.22 - Theoretical τ_{xy} Stress Distribution In Walls Of Fixed Pyramid

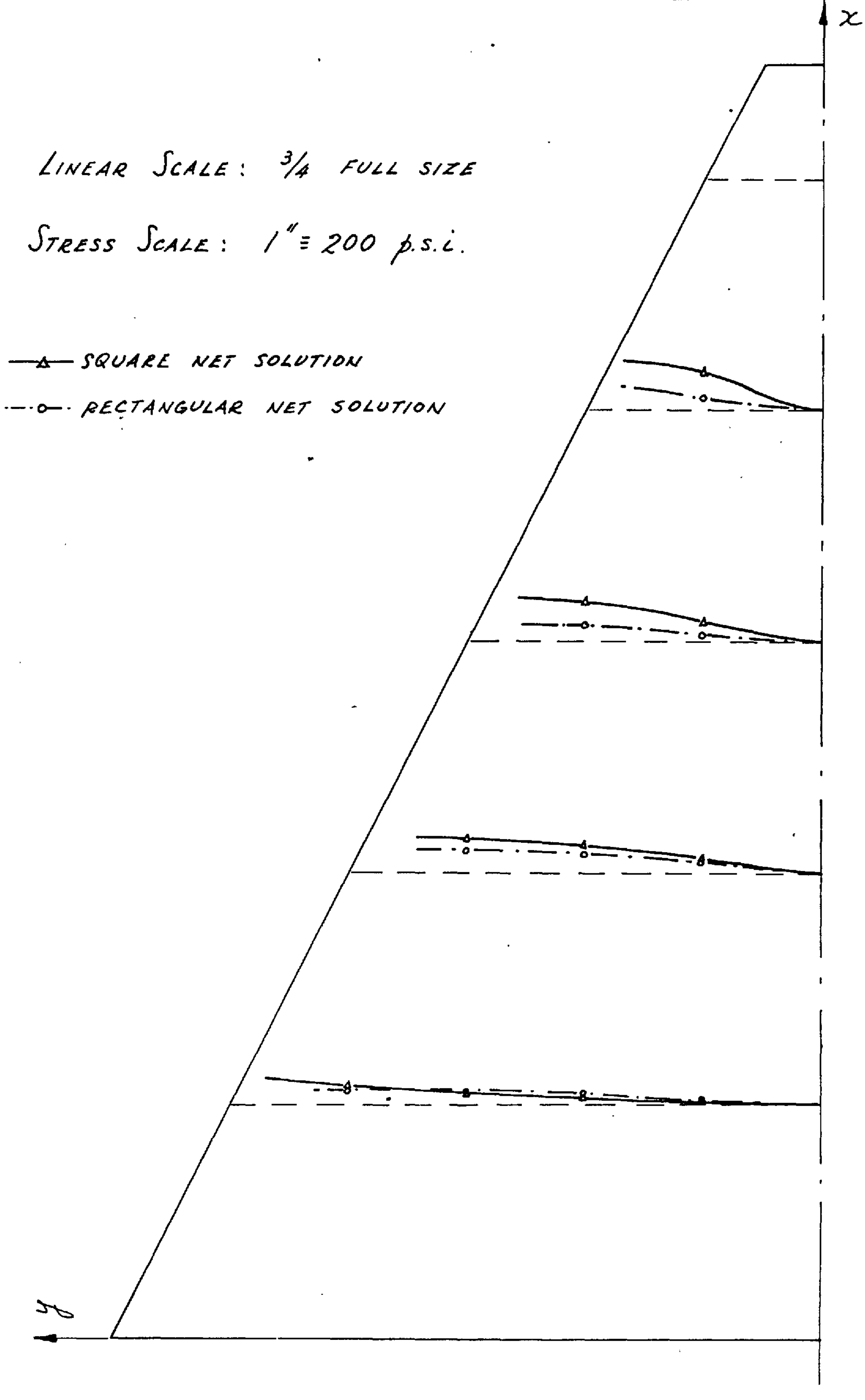

FIG. 4.23 - SQUARE NET FOR MIXED BOUNDARY PROBLEM

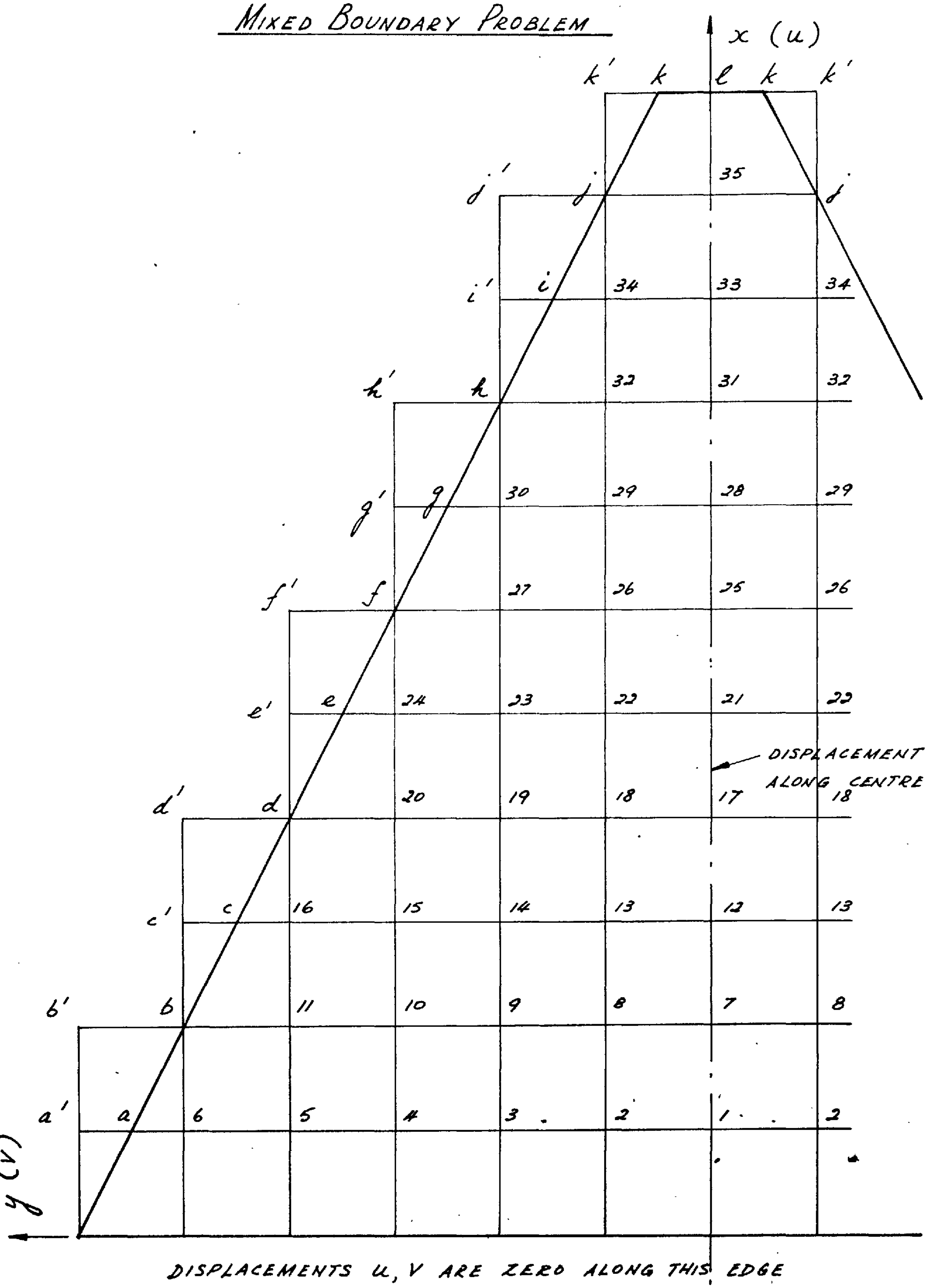

TABLE 5.1 – EXPERIMENTAL STRESSES IN WALL "A". CASE 1

POINT (SEE FIG. 5.9)	OUTER SURFACE VERT. STRESS (p.s.i)	OUTER SURFACE HORIZ. STRESS (p.s.i)	INNER SURFACE VERT. STRESS (p.s.i)	INNER SURFACE HORIZ. STRESS (p.s.i)	MID – PLANE VERT. STRESS (p.s.i)	MID – PLANE HORIZ. STRESS (p.s.i)
1A	-23,628	-13,725	-16,791	1,968	-20,210	-5,879
2A	-16,424	-6,320	-14,852	792	-15,638	-2,764
2B	-14,394	-5,849	-13,521	900	-13,958	-2,475
3A	-8,230	565	-10,646	1,244	-9,438	905
3B	-7,717	601	-10,439	952	-9,078	777
3C	-6,424	-773	-10,585	1,056	-8,505	142
4A	-7,921	-884	-6,866	2,335	-7,394	746
4B	-7,561	-825	-6,765	2,277	-7,163	726
4C	-6,574	-585	-6,931	2,020	-6,753	718
4D	-4,573	-211	-6,736	1,695	-5,655	742
5A	-9,893	-2,770	-2,959	2,874	-6,426	52
5B	-9,117	-3,037	-2,624	-3,004	-5,871	-17
5C	-8,730	-2,153	-3,313	2,001	-6,022	-76
5D	-7197	-598	-3,875	1,504	-5,536	453
5E	-5,508	1,273	-6,671	-1,585	-6,090	-156
6A	-8,012	-3,085	-3,007	1,059	-5,510	-1,013
6B	-7,973	-3,417	-2,874	926	-5,424	-1,246
6C	-8,626	-3,063	-3,482	179	-6,054	-1442
6D	-8,103	-2,316	-3,966	-734	-6,035	-1,525
6E	-7,236	-1,020	-4,550	-1,591	-5,893	-1,306
6F	-7,084	-32	-4,618	-2,199	-5,851	-1,116
7A	-1,507	-104	-8,685	-5,294	-5,096	-2,699
7B	-555	-1,052	-8,555	-5,846	-4,555	-3,449
7C	-237	-2,134	-7,356	-5,775	-3,797	-3,955
7D	-1,065	-2,533	-6,320	-4,340	-3,693	-3,437
7E	-2,517	-3,625	-5,453	-3,780	-3,985	-3,703
7F	-3556	-4914	-5,239	-4,628	-4,398	-4,771

TABLE 5.2 – EXPERIMENTAL STRESSES IN WALL "B". CASE 1.

POINT (SEE FIG. 5.9)	OUTER SURFACE STRESS (p.s.i.)		INNER SURFACE STRESS (p.s.i.)		MID-PLANE STRESS (p.s.i.)	
	VERTICAL	HORIZONTAL	VERTICAL	HORIZONTAL	VERTICAL	HORIZONTAL
1A	−18,701	−8,574	−28,870	−2,852	−23,786	−5,713
2B	−14,911	−5,417	−14,518	−728	−14,715	−3,073
2A	−14,687	−4,966	−18,253	−2,244	−16,470	−3,605
2B′	−13,670	−3,271	−14,151	−1,942	−13,911	−2,607
3C	−5,879	−1,786	−4,427	−3,703	−5,153	−2,745
3B	−6,710	−744	−5,729	−3,332	−6,220	−2,038
3A	−7,499	−916	−5,911	−2,770	−6,705	−1,843
3B′	−7,106	−685	−7,363	−3,566	−7,235	−2,126
3C′	−7,369	−1,354	−7,058	−4,209	−7,214	−2,782
4D	−2,640	−3,160	−890	−4,573	−1,765	−3,867
4C	−2,345	−1,890	−2,709	−4,450	−2,527	−3,170
4B	−2,007	−786	−3,569	−4,180	−2,788	−2,447
4A	−1,874	−244	−3,797	−3,956	−2,836	−2,100
4B′	−1,871	−331	−3,742	−3,966	−2,807	−2,149
4C′	−2,066	−1,069	−3,277	−3,797	−2,672	−2,433
4D′	−2,251	−2,364	−2,744	−3,988	−2,498	−3,176
5E	−3,491	−4,894	−2,602	−1,380	−3,047	−3,137
5D	−750	−2,173	−1,030	−1,936	−890	−2,055
5C	679	−383	−1,533	−2,235	−427	−1,309
5B	1,172	945	−1,595	−1,371	−212	−213
5A	1,806	1,669	−1,442	−676	182	497
5B′	1,793	1,046	−1,994	−1,903	−101	−429
5C′	513	−1,023	−2,007	−2,527	−747	−1,775
5D′	−39	−1,868	−2,956	−4,199	−1,498	−3,034
5E′	−422	−130	−3,621	−4,638	−2,022	−2,384
6F	−3,108	−6,252	−1,475	289	−2,292	−2,982
6E	−685	−1,091	−900	140	−793	−476
6D	1,004	1,367	−552	−169	226	599
6C	2,140	3,449	−630	−429	755	1,510
6B	2,533	4,456	−1,341	−818	596	1,819
6A	2,702	5,008	−1,861	−978	421	2,015
6B′	2,059	3,573	−1,426	156	317	1,865
6C′	1,241	1,851	−1,004	578	119	1,215
6D′	1,146	2,030	−1,231	510	−43	1,270
6E′	88	676	−1,981	−984	−947	−154
6F′	−1,410	−3,082	−1,955	−2,069	−1,683	−2,576
7F	−253	1,101	3,670	1,410	1,709	1,256
7E	1,897	6,236	1,556	−117	1,727	3,060
7D	2,904	11,494	939	−598	1,922	5,448
7C	2,920	11,351	−1,273	−2,157	824	4,597
7B	1,637	10,520	−3,975	−4,157	−1,169	3,182
7A	302	9,523	−6,252	−5,437	−2,975	2,043
7B′	−2,634	11,747	−3,975	−471	−3,305	5,638
7C′	2,137	13,618	1,312	10,419	1,725	12,019
7D′	133	7,999	3,742	9,860	1,938	8,930
7E′	−539	2,488	5,908	8,574	2,685	5,531
7F′	−1,562	−1,361	4,781	2,926	1,610	783

TABLE 5.3 – EXPERIMENTAL STRESSES IN WALL "C". CASE 1.

POINT (SEE FIG. 5.9)	OUTER SURFACE VERT. STRESS (p.s.i)	OUTER SURFACE HORIZ. STRESS (p.s.i)	INNER SURFACE VERT. STRESS (p.s.i)	INNER SURFACE HORIZ. STRESS (p.s.i)	MID-PLANE VERT. STRESS (p.s.i)	MID-PLANE HORIZ. STRESS (p.s.i)
1A	-24,073	-16,161	-19,464	744	-21,769	-7,709
2A	-16,733	-6,265	-15,658	370	-16,196	-2,948
2B	-14,443	-5,333	-15,180	101	-14,812	-2,616
3A	-8,841	497	-10,049	1,367	-9,445	932
3B	-8,139	179	-10,260	773	-9,200	476
3C	-8,899	-1,731	-10,815	101	-9,857	-815
4A	-7,847	-409	-6,418	2,351	-7,133	971
4B	-7,541	-377	-6,119	2,267	-6,830	945
4C	-7,675	-1,007	-5,892	1,952	-6,784	473
4D	-7,399	-1,452	-5,086	1,783	-6,243	166
5A	-7,908	-1,578	-4,255	1,715	-6,082	69
5B	-8,146	-1,384	-4,307	1,637	-6,227	127
5C	-7,788	-1,189	-3,897	1,526	-5,843	169
5D	-8,081	-1,276	-3,936	630	-6,009	-323
5E	-7,723	-1,169	-3,927	750	-5,825	-210
6A	-5,651	-1,335	-5,456	-302	-5,554	-819
6B	-6,171	-1,582	-5,102	-490	-5,637	-1,036
6C	-6,606	-1,565	-4,635	-406	-5,621	-986
6D	-6,593	-1,621	-4,339	-406	-5,471	-1,014
6E	-7,191	-1,832	-3,959	-614	-5,575	-1,223
6F	-8,769	-2,666	-3,508	-1,361	-6,139	-2,014
7A	474	585	-13,306	-4,989	-6,416	-2,202
7B	2,429	237	-11,929	-4,628	-4,750	-2,196
7C	3,254	-926	-9,867	-4,914	-3,307	-2,920
7D	4,859	-1,471	-7,551	-5,450	-1,346	-3,461
7E	5,057	-822	-6,577	-5,833	-760	-3,328
7F	3,729	-341	-5,151	-6,281	-711	-3,311

TABLE 5.4 – EXPERIMENTAL STRESSES IN BASE PLATE. CASE 1.

POINT (SEE FIG. 5.9)	OUTER SURFACE LONG. STRESS (p.s.i)	OUTER SURFACE TRANS. STRESS (p.s.i)	INNER SURFACE LONG. STRESS (p.s.i)	INNER SURFACE TRANS. STRESS (p.s.i)	MID-PLANE LONG. STRESS. (p.s.i)	MID-PLANE TRANS. STRESS (p.s.i)
1A	21,832	7,814	16,090	-13,972	18,961	-3,079
1B	20,471	7,226	7,730	6,034	14,101	6,630
1C	20,474	5,781	-4,891	-5,908	7,792	-64
1D	20,435	318	-45,752	-48,691	-12,659	-24,187
2A	4,972	-5,268	3,949	12,991	4,461	3,862
2B	8,295	-3,933	12,127	-438	10,211	2,186
2C	9,461	-2,429	11,237	3,417	10,349	494
2D	11,887	312	5,287	22,241	8,587	11,277
3A	4,216	-7,857	7,847	14,177	6,032	3,160
3B	6,772	-5,840	15,132	325	10,952	-2,758
3C	9,445	-1,611	15,024	5,304	12,235	1,847
3D	12,933	5,700	19,110	30,864	16,022	18,282
4A	8,935	-3,767	13,056	578	10,996	-1,595
4B	10,565	-2,095	12,270	1,578	11,418	-259
4C	11,773	425	11,397	-809	11,585	-192
4D	12,722	3,543	9890	-8,194	11,306	-2,326
5A	17,606	6,236	1,903	5,294	9,755	5,765
5B	16,921	3,787	4,920	669	10,921	2,228
5C	15,356	3,196	8,503	2,761	11,930	2,979
5D	13,414	4,372	14,960	12,358	14,187	8,365

TABLE 5.5—EXPERIMENTAL STRESSES IN WALL "A." CASE 2.

POINT (SEE FIG. 5.9)	OUTER SURFACE VERT. STRESS (p.s.i)	OUTER SURFACE HORIZ. STRESS (p.s.i)	INNER SURFACE VERT. STRESS (p.s.i)	INNER SURFACE HORIZ. STRESS (p.s.i)	MID-PLANE VERT. STRESS (p.s.i)	MID-PLANE HORIZ. STRESS (p.s.i)
1A	-22,361	-3,261	-13,196	1,296	-17,779	-983
2A	-17,428	-2,056	-12,907	792	-15,168	-632
2B	-16,973	-2,507	-12,455	-250	-14,714	-1,379
3A	-10,205	-598	-11,026	481	-10,616	-59
3B	-9,834	-1,221	-10,835	-348	-10,335	-785
3C	-8,275	-747	-10,218	136	-9,247	-306
4A	-8,243	-737	-7,681	1,497	-7,962	380
4B	-7,866	-857	-7,740	1,302	-7,803	223
4C	-6,522	-805	-7,464	857	-6,993	26
4D	-4,849	-825	-7,233	159	-6,041	-333
5A	-8,993	-2,144	-4,060	2,449	-6,527	153
5B	-8,535	-1,799	-3,102	2,595	-5,819	398
5C	-8,133	-1,734	-4,031	1,575	-6,082	-80
5D	-6,739	-841	-4,596	403	-5,668	-219
5E	-3,547	2,105	-4,742	-1,442	-4,145	332
6A	-7,957	-2,124	-3,007	1,738	-5,482	-193
6B	-7,990	-2,046	-2,725	1,708	-5,358	-169
6C	-7,701	-1,838	-3,336	1,049	-5,519	-395
6D	-7,015	-1,159	-3,920	195	-5,468	-482
6E	-5,983	-286	-4,469	-1,124	-5,226	-705
6F	-5,057	822	-4,745	-2,325	-4,901	-752
7A	-1,523	805	-7,460	-1,494	-4,492	-345
7B	-1,608	1,013	-8,110	-2,053	-4,859	-520
7C	-1,738	-380	-7,499	-1,397	-4,619	-889
7D	-2,585	-549	-6,356	-1,520	-4,471	-1,035
7E	-3,670	-1,117	-5,258	-1,010	-4,464	-1,064
7F	-4,096	-1,835	-5,232	-526	-4,664	-1,181

TABLE 5.6 – EXPERIMENTAL STRESSES IN WALL "B". CASE 2.

POINT (SEE FIG. 5.9)	OUTER SURFACE STRESS (p.s.i.)		INNER SURFACE STRESS (p.s.i.)		MID-PLANE STRESS (p.s.i.)	
	VERTICAL	HORIZONTAL	VERTICAL	HORIZONTAL	VERTICAL	HORIZONTAL
1A	-685	-799	2,530	7,252	923	3,227
2B	1,673	-318	3,222	3,810	2,448	1,746
2A	-344	130	1,312	3,345	484	1,738
2B'	-2,368	-513	-110	4,092	-1,239	1,790
3C	4,605	221	5,330	3,183	4,968	1,702
3B	1,770	6	2,598	2,147	2,184	1,077
3A	-299	88	247	-162	-26	-37
3B'	-2,183	-104	-1,228	422	-1,206	159
3C'	-5,158	-94	-3,910	-747	-4,534	-421
4D	3,780	-562	5,226	3,329	4,503	1,384
4C	2,952	13	3,742	2,611	3,347	1,312
4B	1,890	396	2,439	1,627	2,165	1,012
4A	172	81	468	-299	320	-109
4B'	-1,608	338	-1,397	-809	-1,503	-238
4C'	-3,128	-6	-3,634	-2,550	-3,381	-1,278
4D'	-4,700	-425	-5,742	-4,339	-5,221	-2,382
5E	637	-1,400	4,303	3,488	2,470	1,044
5D	1,634	-448	3,449	2,904	2,542	1,228
5C	1,695	338	2,247	2,861	1,971	1,100
5B	1,708	961	1,192	1,010	1,450	986
5A	861	792	45	-45	453	374
5B'	94	1,179	-1,289	-1,039	-598	70
5C'	-1,062	-383	-2,702	-2,296	-1,882	-1,340
5D'	-1,916	-286	-4,258	-3,534	-3,087	-1,910
5E'	-2,913	-1,829	-4,885	-3,459	-3,899	-2,644
6F	-276	-909	1,630	2,647	677	869
6E	718	425	1,595	2,046	1,157	1,236
6D	1,595	1,371	1,198	1,130	1,397	1,251
6C	1,491	1,513	783	828	1,137	1,171
6B	1,851	1,919	227	451	1,039	1,185
6A	1,793	2,312	-682	175	556	1,244
6B'	1,228	1,906	-1104	-335	62	786
6C'	520	1,130	-1,280	-331	-380	400
6D'	-195	325	-1,169	26	-682	176
6E'	-913	-867	-1,241	-201	-1,077	-534
6F'	-2,231	-2,683	-1,228	-549	-1,730	-1,616
7F	4,933	3,621	-3,904	-2,644	515	489
7E	5,210	4,531	-2,670	-1,991	1,270	1,270
7D	5,044	5,248	-1,403	-1,604	1,821	1,822
7C	6,077	6,418	-981	-1,478	2,548	2,470
7B	4,209	5,404	-1,919	-494	1,145	2,455
7A	2,543	3,131	-1,523	422	510	1,777
7B'	2,384	3,969	-412	2,235	986	3,102
7C'	1,949	3,303	565	2,826	1,257	3,065
7D'	906	2,397	2,845	4,313	1,876	3,355
7E'	577	1,234	4,550	5,274	2,464	3,254
7F'	419	893	6,489	8,162	3,454	4,528

TABLE 5.7 - EXPERIMENTAL STRESSES IN WALL "C". CASE 2.

POINT (SEE FIG. 5.9)	OUTER SURFACE VERT. STRESS (p.s.i)	OUTER SURFACE HORIZ. STRESS (p.s.i)	INNER SURFACE VERT. STRESS (p.s.i)	INNER SURFACE HORIZ. STRESS (p.s.i)	MID-PLANE VERT. STRESS (p.s.i)	MID-PLANE HORIZ. STRESS (p.s.i)
1A	20,871	3,693	13,813	-1,108	17,342	1,293
2A	16,648	2,114	13,056	-97	14,852	1,009
2B	17,015	4,583	14,404	841	15,710	2,712
3A	10,218	455	10,705	13	10,462	234
3B	10,224	1,929	11,043	646	10,634	1,288
3C	6,765	1,410	10,728	2,319	8,747	1,865
4A	6,262	429	8,269	-728	7,266	-150
4B	6,129	477	8,233	-357	7,181	60
4C	5,950	572	8,003	341	6,977	457
4D	5,492	607	8,600	2,114	7,046	1,361
5A	6,859	1,910	6,057	-1,695	6,458	108
5B	6,937	1,491	5,625	-1,475	6,281	8
5C	6,414	741	5,706	-624	6,060	59
5D	5,125	-211	5,817	708	5,471	249
5E	2,358	-1,936	5,645	2,572	4,002	318
6A	9,448	3,342	1,270	-2,709	5,359	317
6B	9,074	2,994	1,491	-2,082	5,283	456
6C	8,249	2,124	1,666	-2,092	4,958	16
6D	3,732	854	2,244	-380	2,988	237
6E	5,775	-396	3,228	922	4,502	263
6F	5,486	-1,929	4,774	2,423	5,130	247
7A	13,790	4,635	-4,836	-880	4,477	1,878
7B	13,758	5,216	-5,521	-1,679	4,119	1,769
7C	14,654	6,223	-4,989	-1,871	4,833	2,176
7D	16,606	7,113	-3,222	-2,157	6,692	2,478
7E	17,421	6,889	201	1,241	8,811	4065
7F	16,626	6,203	3,254	2,757	9,940	4,480

TABLE 5.8 – EXPERIMENTAL STRESSES IN BASE PLATE. CASE 2.

POINT (SEE FIG. 5.9)	OUTER SURFACE LONG. STRESS. (p.s.i)	OUTER SURFACE TRANS. STRESS (p.s.i)	INNER SURFACE LONG. STRESS (p.s.i)	INNER SURFACE TRANS. STRESS (p.s.i)	MID-PLANE LONG. STRESS (p.s.i)	MID-PLANE TRANS. STRESS (p.s.i)
1A	–2,598	–789	8,951	3,754	3,177	1,483
1B	–432	516	5,197	4,881	2,383	2,699
1C	2,800	2,621	3,274	5,534	3,037	4,078
1D	7,324	5,382	3,430	6,142	5,377	5,762
2A	–2,718	–4,778	3,082	–4,709	182	–4,744
2B	–1,647	–3,774	3,644	–809	999	–2,292
2C	896	–643	3,777	1,179	2,337	268
2D	4,147	3,943	3,098	7,278	3,623	5,611
3A	–2,644	–5,106	2,592	3,972	–26	–567
3B	–877	–3,569	3,323	–315	1,223	–1,942
3C	818	–1,283	4,274	1,741	2,546	–1,512
3D	3,124	1,747	4,440	7,334	3,782	4,541
4A	770	–1,829	2,816	2,498	5,258	335
4B	1,458	–1,121	2,933	2,956	2,196	918
4C	2,757	630	2,322	–120	2,540	255
4D	4,164	3,033	1,663	–5,391	2,914	–1,179
5A	7,373	2,920	–4,713	13	1,330	1,467
5B	6,538	2,696	–2,452	–1,276	2,043	710
5C	4,109	1,101	994	1,335	2,552	1,218
5D	1,884	–2,140	1,351	5,128	1,618	1,494

TABLE 5.9 – EXPERIMENTAL STRESSES IN WALL "A". CASE 3.

POINT (SEE FIG. 5.9)	OUTER SURFACE VERT. STRESS (p.s.i)	OUTER SURFACE HORIZ. STRESS (p.s.i)	INNER SURFACE VERT. STRESS (p.s.i)	INNER SURFACE HORIZ. STRESS (p.s.i)	MID-PLANE VERT. STRESS (p.s.i)	MID-PLANE HORIZ. STRESS (p.s.i)
1A	−19,796	−1,124	−7,889	2,170	−13,843	523
2A	−15,869	−520	−10,445	1,127	−13,157	304
2B	−15,931	−1,010	−7,454	1,270	−11,693	130
3A	−9,896	29	−11,793	572	−10,845	301
3B	−10,351	−406	−11,338	325	−10,845	−41
3C	−9,178	−136	−10,932	−81	−10,055	−69
4A	−8,665	−864	−8,262	1,910	−8,464	523
4B	−8,292	−900	−8,233	1,712	−8,263	406
4C	−7,187	−565	−8,298	1,013	−7,743	224
4D	−5,557	−244	−8,431	−292	−6,994	−268
5A	−10,318	−2,725	−3,930	2,871	−7,124	73
5B	−10,192	−2,598	−4,147	2,452	−7,170	−73
5C	−6,895	−1,449	−4,112	1,699	−5,504	125
5D	−7,233	−520	−4,586	140	−5,910	−190
5E	−4,976	2,053	−6,073	−2,524	−5,525	−236
6A	−8399	−2,907	−3,654	776	−6,027	−1066
6B	−8,584	−3,020	−3,615	523	−6,100	−1,249
6C	−8,594	−2,965	−3,501	114	−6,048	−1,126
6D	−7,882	−2,072	−4,018	−896	−5,950	−1,484
6E	−6,554	−815	−4,589	−2,101	−5,572	−1,458
6F	−5,804	299	−5,060	−3,072	−5,432	−1,387
7A	650	198	−8,889	−4,027	−4,120	−1,915
7B	552	−127	−8,516	−3,767	−3,982	−1,947
7C	−507	−890	−7,964	−3,894	−4,236	−2,392
7D	−3,241	−2,900	−6,161	−2,816	−4,701	−2,858
7E	−5,661	−4,079	−4,716	−2,907	−5,189	−3,493
7F	−6,184	−4,826	−4,362	−3683	−5,273	−4,255

TABLE 5.10 - EXPERIMENTAL STRESSES IN WALL "B". CASE 3.

POINT (SEE FIG. 5.9)	OUTER SURFACE STRESS (p.s.i.)		INNER SURFACE STRESS (p.s.i.)		MID-PLANE STRESS (p.s.i.)	
	VERTICAL	HORIZONTAL	VERTICAL	HORIZONTAL	VERTICAL	HORIZONTAL
1A	-325	-393	3,313	8,376	1,829	3,992
2B	1,751	-58	3,063	3,290	2,407	1,616
2A	133	247	2,157	4,281	1,145	2,264
2B'	-1,877	607	-1,059	2,332	-1,468	1,470
3C	4,553	-533	5,323	1,030	4,938	249
3B	2,059	-406	2,858	870	2,459	232
3A	601	36	812	-403	707	-184
3B'	-1,494	224	-1,848	-1,717	-1,671	-747
3C'	-3,888	-179	-4,057	-2,030	-3,973	-1,105
4D	4,024	-338	5,918	2,978	4,921	1,320
4C	3,423	-374	4,843	1,679	4,133	653
4B	2,514	-266	3,404	533	2,959	134
4A	1,257	-325	1,585	-698	1,422	-512
4B'	-221	-244	-916	-2,046	-569	-1,145
4C'	-2,092	-195	-2,982	-2,439	-2,537	-1,317
4D'	-3,894	84	-5,499	-4,031	-4,697	-1,974
5E	2,852	-312	3,446	2,611	3,149	1,150
5D	1,754	-146	4,076	3,124	2,915	1,406
5C	1,387	393	3,677	2,887	2,532	1,640
5B	1,819	935	3,001	1,825	2,410	1,380
5A	2,374	1,988	1,932	438	2,153	1,213
5B'	1,578	1,598	386	-471	982	564
5C'	393	1,004	-841	-1,406	-617	-201
5D'	-942	10	-2,994	-2,384	-1,968	-1,187
5E'	-2,205	-1,143	-5,365	-3,105	-3,785	-2,124
6F	-1,319	-1,432	-448	1,634	-884	101
6E	331	1,280	1,630	1,676	981	1,478
6D	1,929	3,150	1,306	1,192	1,618	2,171
6C	2,394	4,001	1,172	945	1,782	2,473
6B	1,341	2,803	403	741	872	1,772
6A	2,939	5,109	952	1,293	1,946	3,201
6B'	2,748	4,963	-448	1,634	1,150	3,299
6C'	2,140	4,128	-789	1,764	676	2,946
6D'	1,260	2,595	-841	1,010	210	1,803
6E'	-192	825	-1,345	32	-769	429
6F'	-2,744	-4,372	-2,540	-2,540	-2,642	-3,456
7F	2,228	5,395	-1,494	-71	367	2,662
7E	3,865	8,841	97	-650	1,981	4,096
7D	7,658	12,585	-1,744	-1,858	2,957	5,364
7C	7,775	12,975	-2,540	-2,540	2,618	5,218
7B	5,236	10,435	-3,888	-2,124	674	4,156
7A	2,309	8,954	-3,274	1,156	-483	5,055
7B'	737	8,243	-2,189	4,433	-726	6,338
7C'	1,205	9,003	-1,046	6,551	80	7,777
7D'	1,211	9,802	1,653	8,344	1,432	9,073
7E'	1,150	6,687	2,299	5,622	1,720	6,155
7F'	-185	2,303	1,890	2,345	853	2,324

TABLE 5.11 – EXPERIMENTAL STRESSES IN WALL "C". CASE 3.

POINT (SEE FIG. 5.9)	OUTER SURFACE VERT. STRESS (p.s.i)	OUTER SURFACE HORIZ. STRESS (p.s.i)	INNER SURFACE VERT. STRESS (p.s.i)	INNER SURFACE HORIZ. STRESS (p.s.i)	MID-PLANE VERT. STRESS (p.s.i)	MID-PLANE HORIZ. STRESS (p.s.i)
1A	20,871	3,693	13,813	-1,108	17,342	1,293
2A	16,648	2,114	13,056	-97	14,852	1,009
2B	17,015	4,583	14,404	841	15,710	2,712
3A	10,218	455	10,705	13	10,462	234
3B	10,224	1,929	11,043	646	10,634	1,288
3C	6,765	1,410	10,728	2,319	8,747	1,865
4A	6,262	429	8,269	-728	7,266	-150
4B	6,129	477	8,233	-357	7,181	60
4C	5,950	572	8,003	341	6,977	457
4D	5,492	607	8,600	2,114	7,046	1,361
5A	6,859	1,910	6,057	-1,695	6,458	108
5B	6,937	1,491	5,625	-1,475	6,281	8
5C	6,414	741	5,706	-624	6,060	59
5D	5,125	-211	5,817	708	5,471	249
5E	2,358	-1,936	5,645	2,572	4,002	318
6A	9,448	3,342	1,270	-2,709	5,359	317
6B	9,074	2,994	1,491	-2,082	5,283	456
6C	8,249	2,124	1,666	-2,092	4,958	16
6D	3,732	854	2,244	-380	2,988	237
6E	5,775	-396	3,228	922	4,502	263
6F	5,486	-1,929	4,774	2,423	5,130	247
7A	13,790	4,635	-4,836	-880	4,477	1,878
7B	13,758	5,216	-5,521	-1,679	4,119	1,769
7C	14,654	6,223	-4,989	-1,871	4,833	2,176
7D	16,606	7,113	-3,222	-2,157	6,692	2,478
7E	17,421	6,889	201	1,241	8,811	4,065
7F	16,626	6,203	3,254	2,757	9,940	4,480

TABLE 5.12 - EXPERIMENTAL STRESSES IN BASE PLATE. CASE 3.

POINT (SEE FIG. 5.9)	OUTER SURFACE LONG. STRESS (p.s.i)	OUTER SURFACE TRANS. STRESS (p.s.i)	INNER SURFACE LONG. STRESS (p.s.i)	INNER SURFACE TRANS. STRESS (p.s.i)	MID-PLANE LONG. STRESS (p.s.i)	MID-PLANE TRANS. STRESS (p.s.i)
1A	16,366	3,413	22,033	-5,093	19,200	-840
1B	15,460	4,316	10,117	3,222	12,789	3,769
1C	16,070	3,706	-7,869	-8,435	4,101	-2,365
1D	20,075	3,007	-45,447	-37,987	-12,686	-17,490
2A	8,327	-4,898	4,099	13,478	6,213	4,290
2B	8,126	-559	11,770	-1,140	9,948	-850
2C	9,549	-399	11,488	4,820	10,519	2,211
2D	12,270	4,969	11,465	25,593	11,868	15,281
3A	5,313	-8,405	9,419	13,534	7,366	2,565
3B	7,993	-4,053	13,875	-1,384	10,934	-2,719
3C	10,383	416	16,337	5,261	13,360	2,839
3D	11,923	3,832	20,611	25,132	16,267	14,482
4A	10,650	-2,394	12,062	-1,049	11,356	-1,722
4B	11,475	-844	11,907	968	11,691	62
4C	13,111	1,923	12,559	1,754	12,835	1,839
4D	14,388	5,050	12,712	-263	13,550	2,394
5A	18,259	6,730	5,421	8,133	11,840	7,432
5B	16,457	4,589	5,197	1,578	10,827	3,084
5C	16,236	3,670	8,379	3,225	12,308	3,448
5D	18,935	5,460	11,088	10,312	15,012	7,886

FIG. 5.1 — STEEL MODEL TRUSS

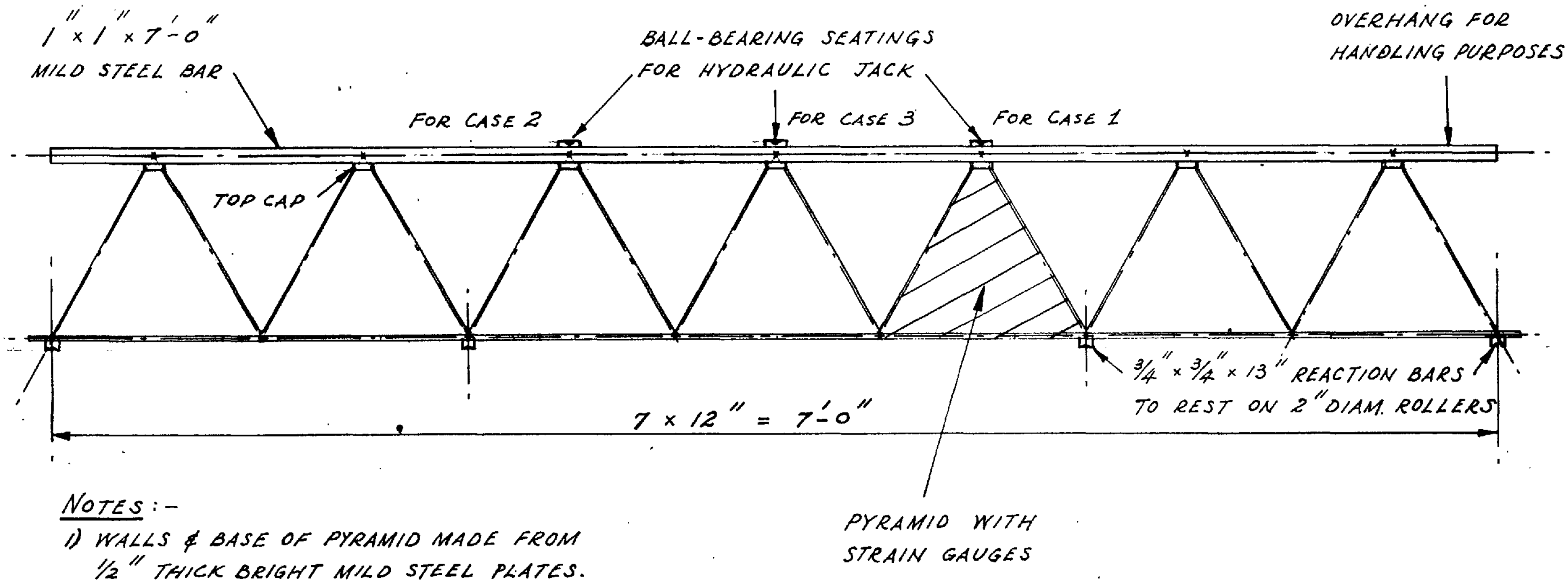

NOTES :-

1) WALLS & BASE OF PYRAMID MADE FROM 1/2" THICK BRIGHT MILD STEEL PLATES.
2) FOR DETAILS OF WELDING, SEE FIG. 5.2.

FIG. 5.2 – WELDING DETAILS

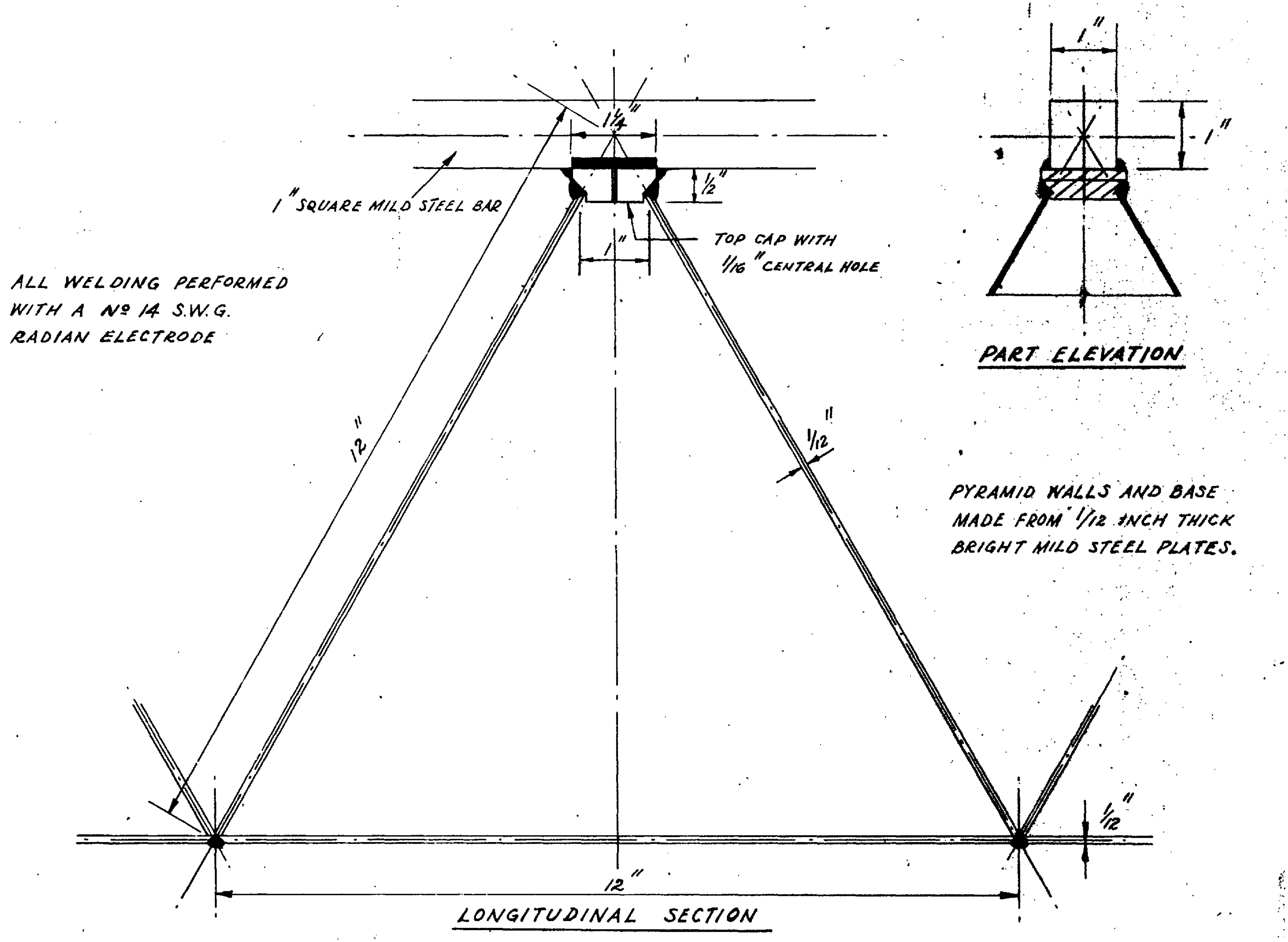

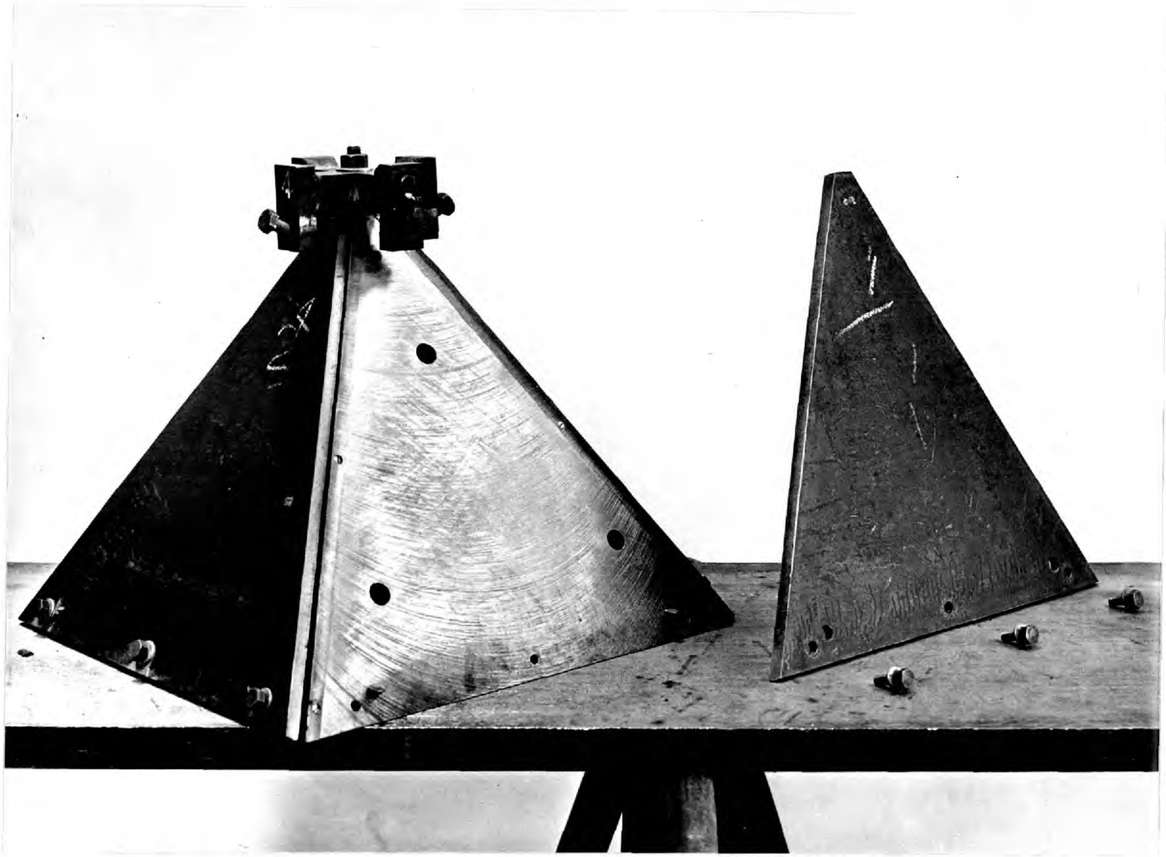

Fig. 5.3 - Jig for welding of pyramid walls.

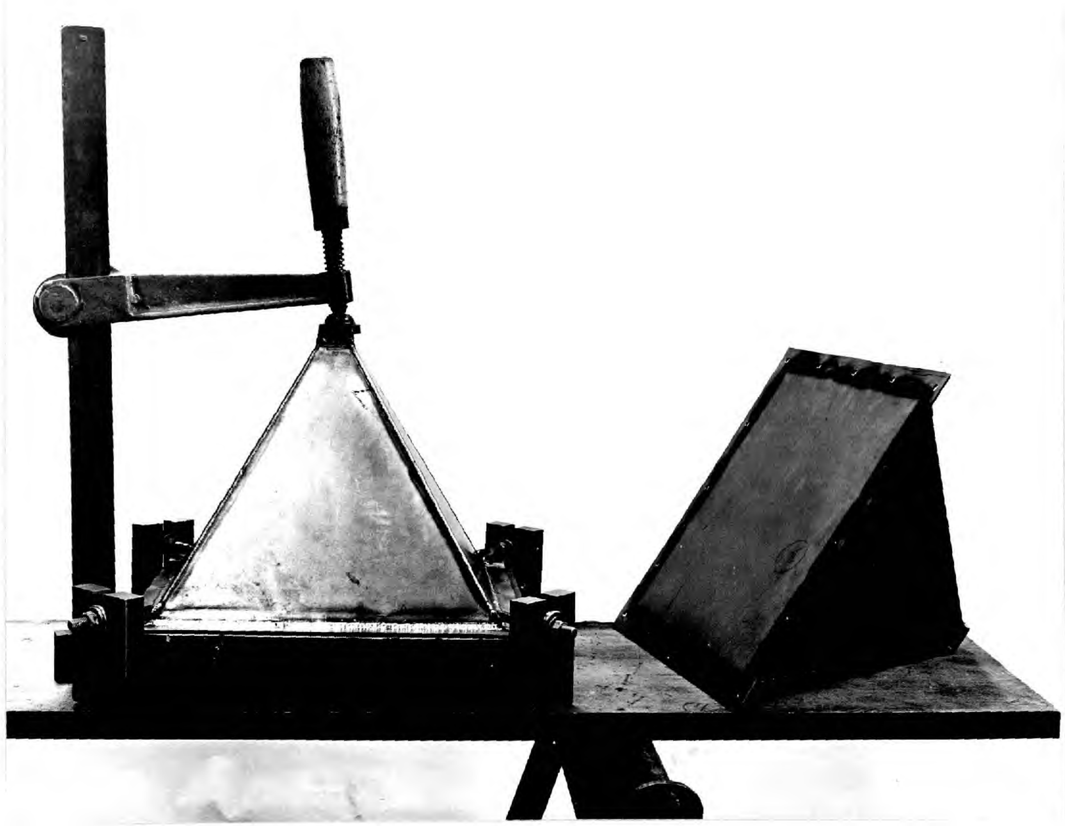

Fig. 5.4 - Set-up for welding of base plates to pyramids.

FIG. 5.5 - LOCATION OF STRAIN GAUGES

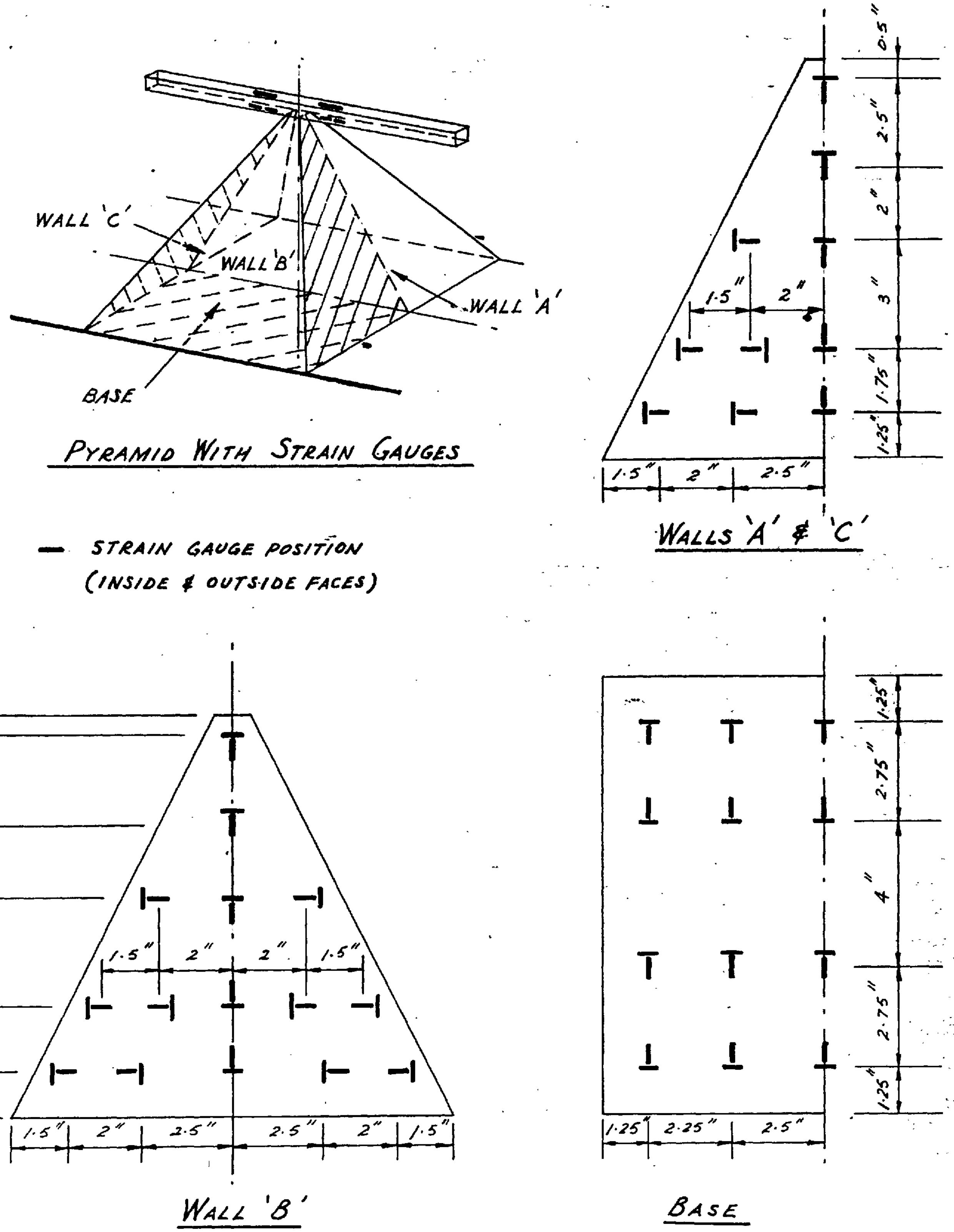

FIG. 5.6 — LOADING CASES FOR STEEL TRUSS MODEL

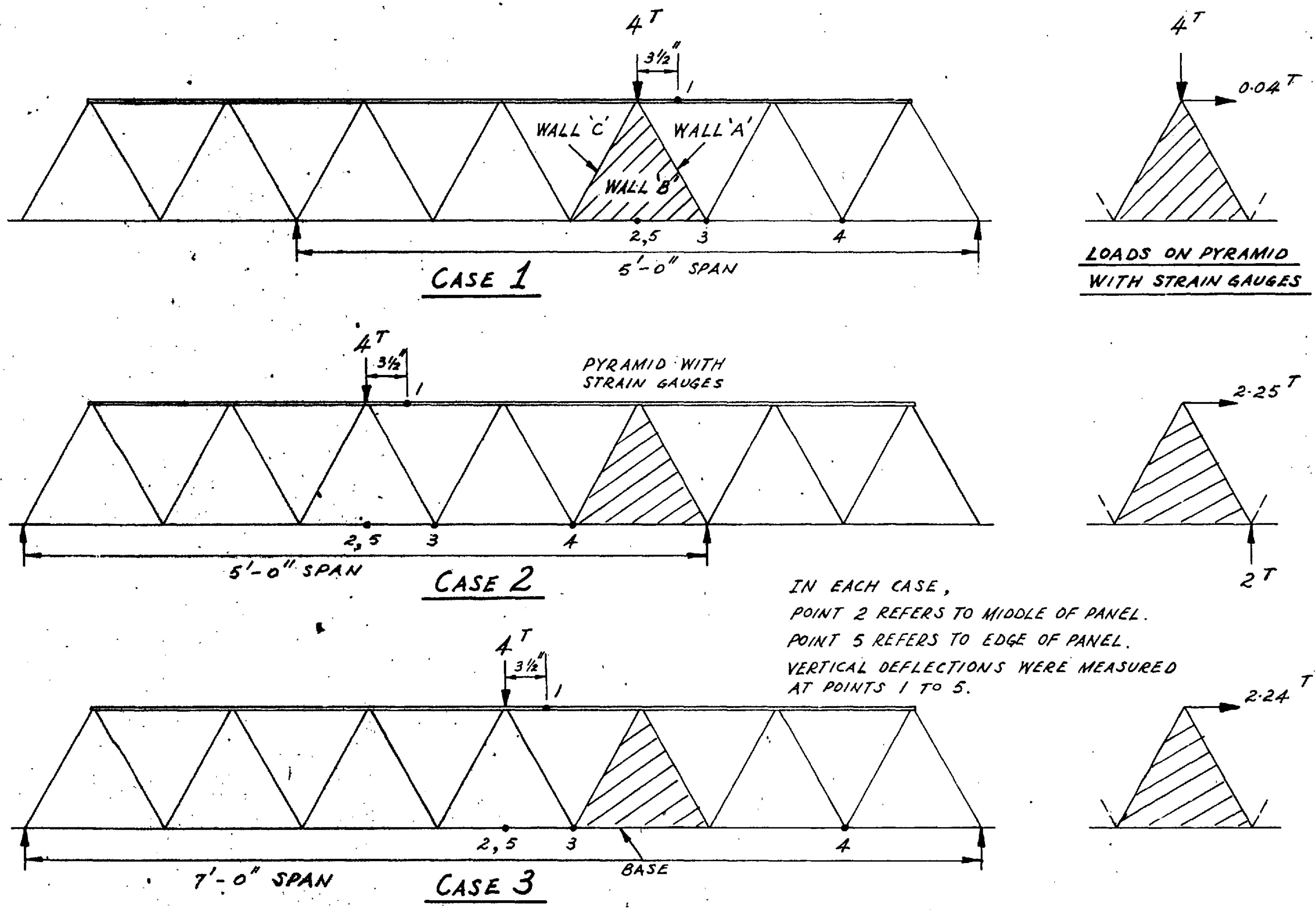

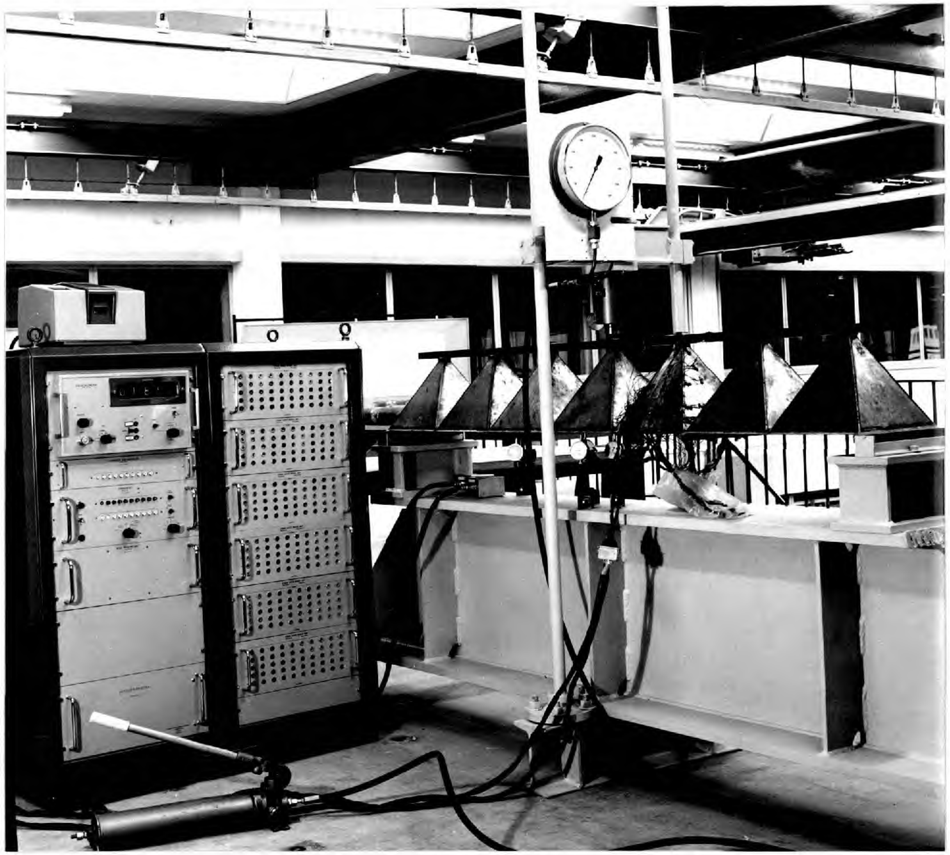

Fig. 5.7 - Test on steel model; Loading case 3.

'Solartron' shown at left of picture.

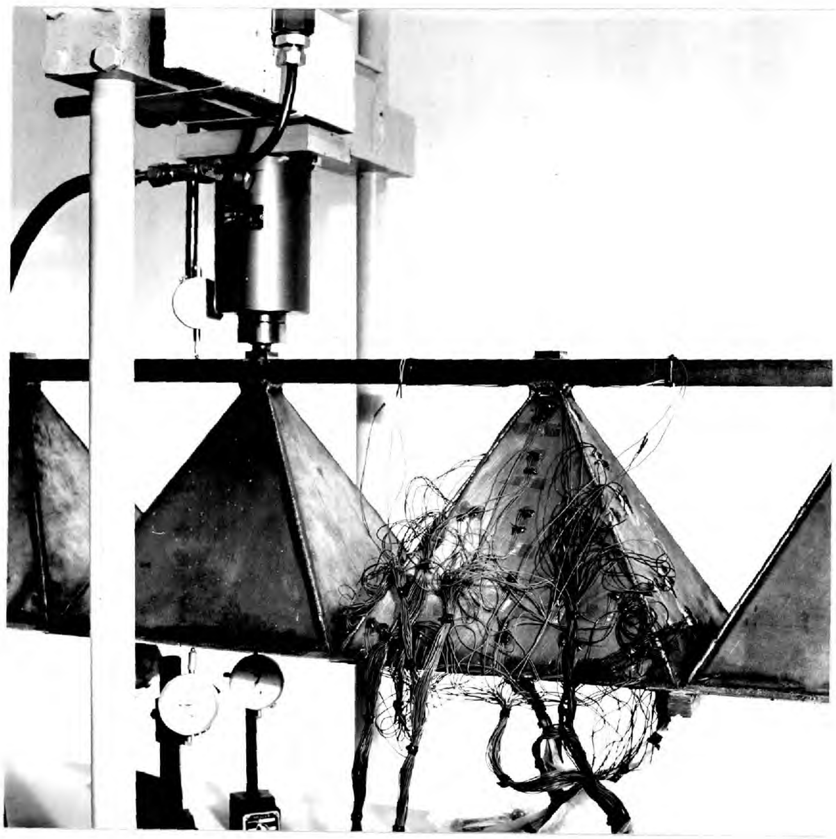

Fig. 5.8 - Test on steel model.

Close-up of pyramid with strain gauges.

FIG. 5.9 - REFERENCE DIAGRAMS FOR TABLES 5.1 TO 5.12.

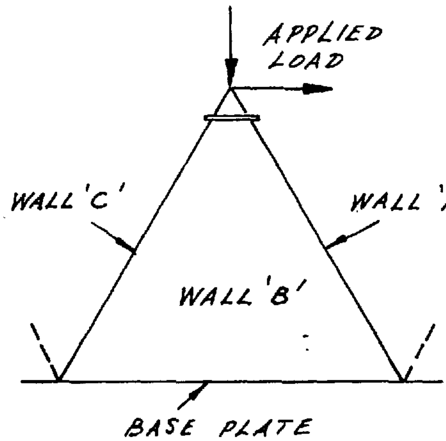

FOR LOADING CASES, SEE FIG. 5.6.

SIGN CONVENTION : TENSILE STRESSES POSITIVE

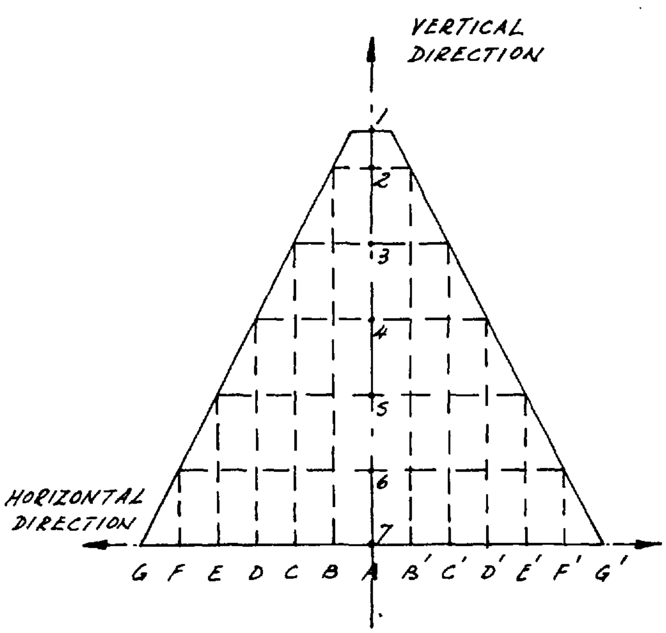

PYRAMID WALLS

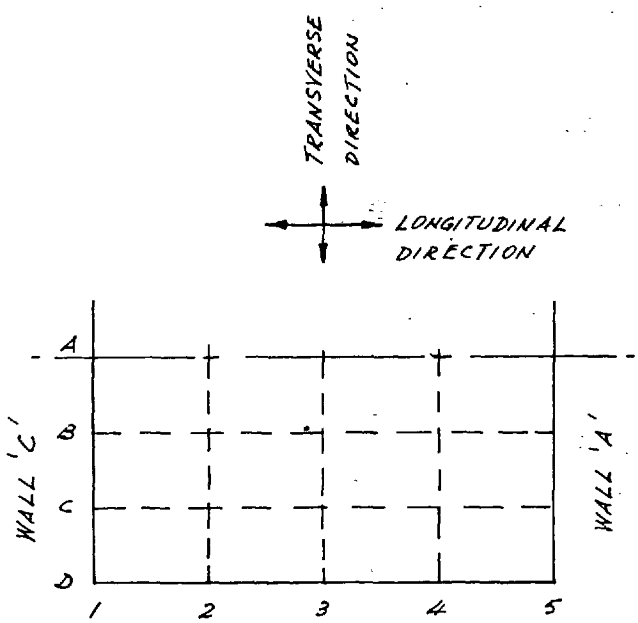

BASE PLATE

FIG. 5.10 — MID-PLANE STRESS DISTRIBUTION IN WALL 'A'. CASE 1.

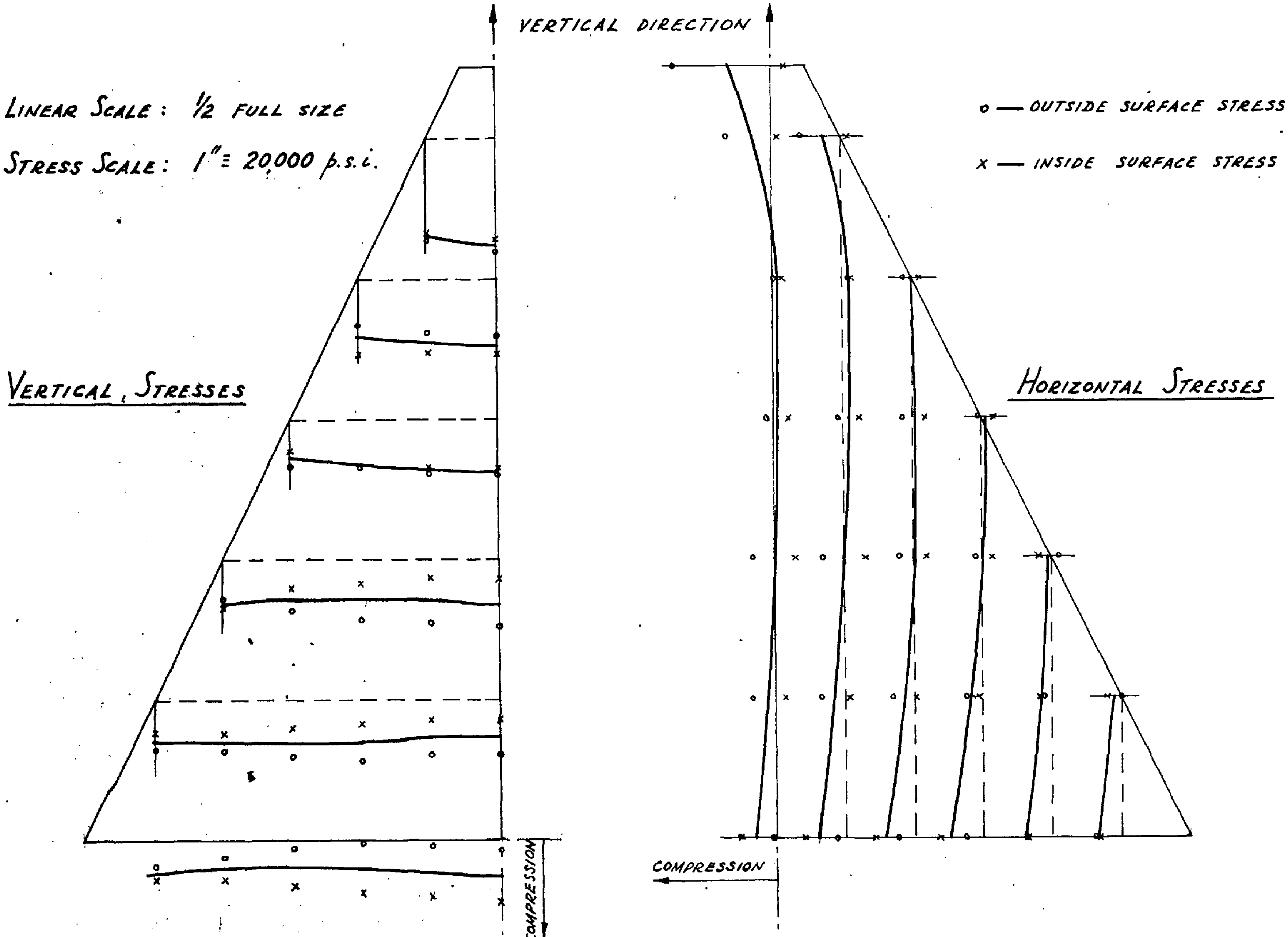

FIG. 5.11 — VERTICAL MID-PLANE STRESS DISTRIBUTION IN WALL 'B'. CASE 1.

LINEAR SCALE: ½ FULL SIZE

STRESS SCALE: 1" ≡ 20,000 p.s.i.

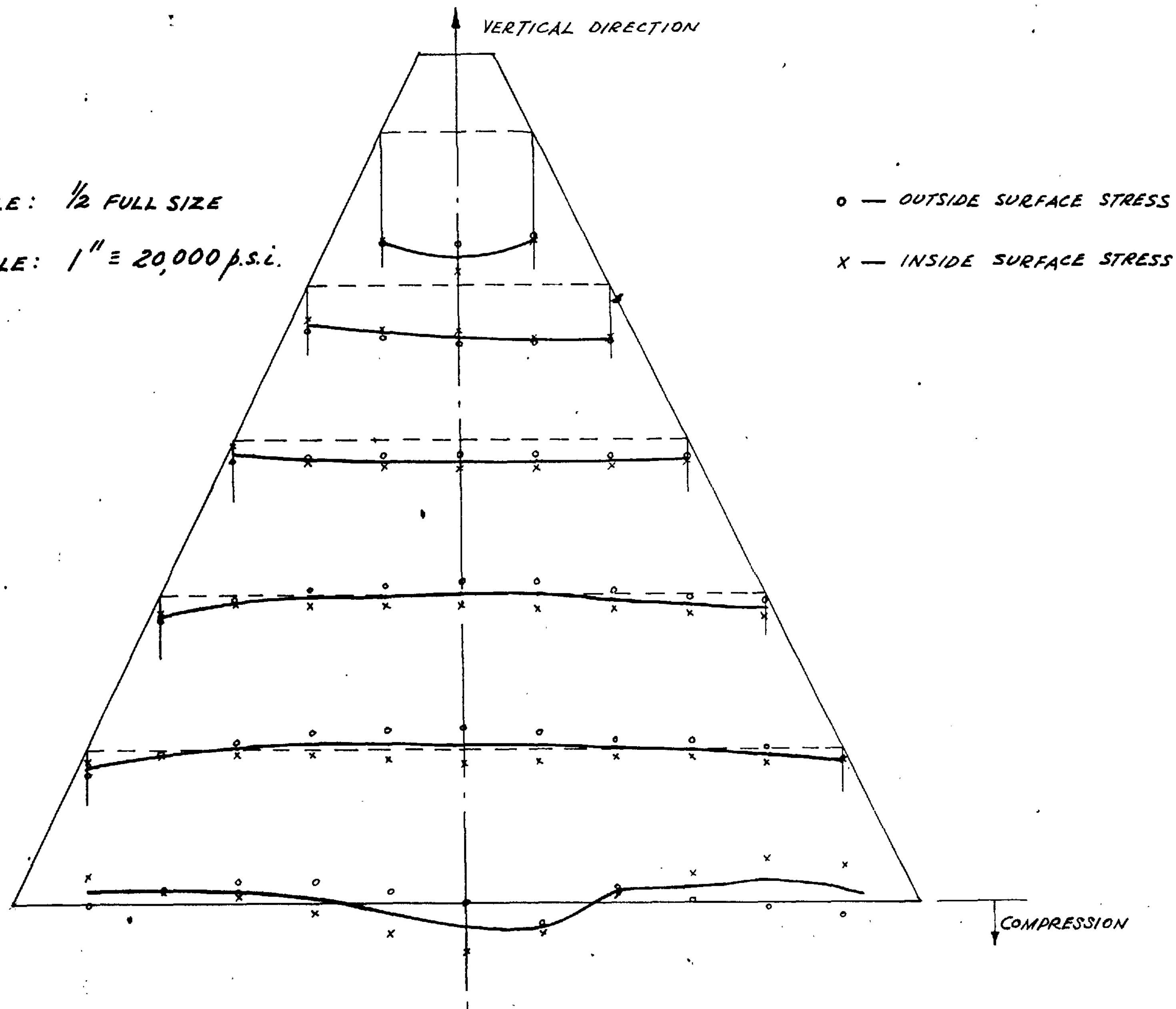

FIG. 5.12 — HORIZONTAL MID-PLANE STRESS DISTRIBUTION IN WALL 'B'. CASE 1

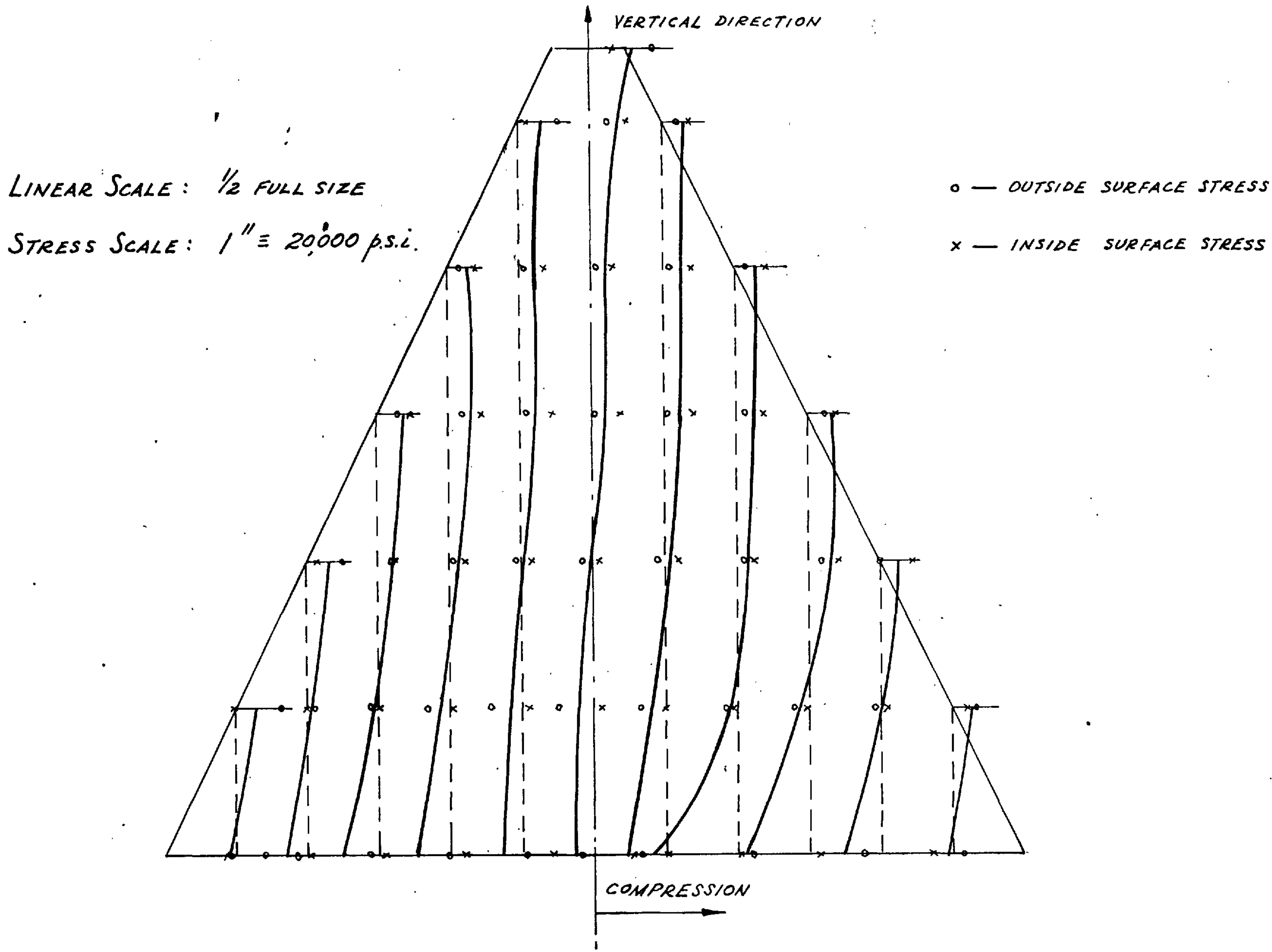

FIG. 5.13 – MID-PLANE STRESS DISTRIBUTION IN WALL 'C'. CASE 1.

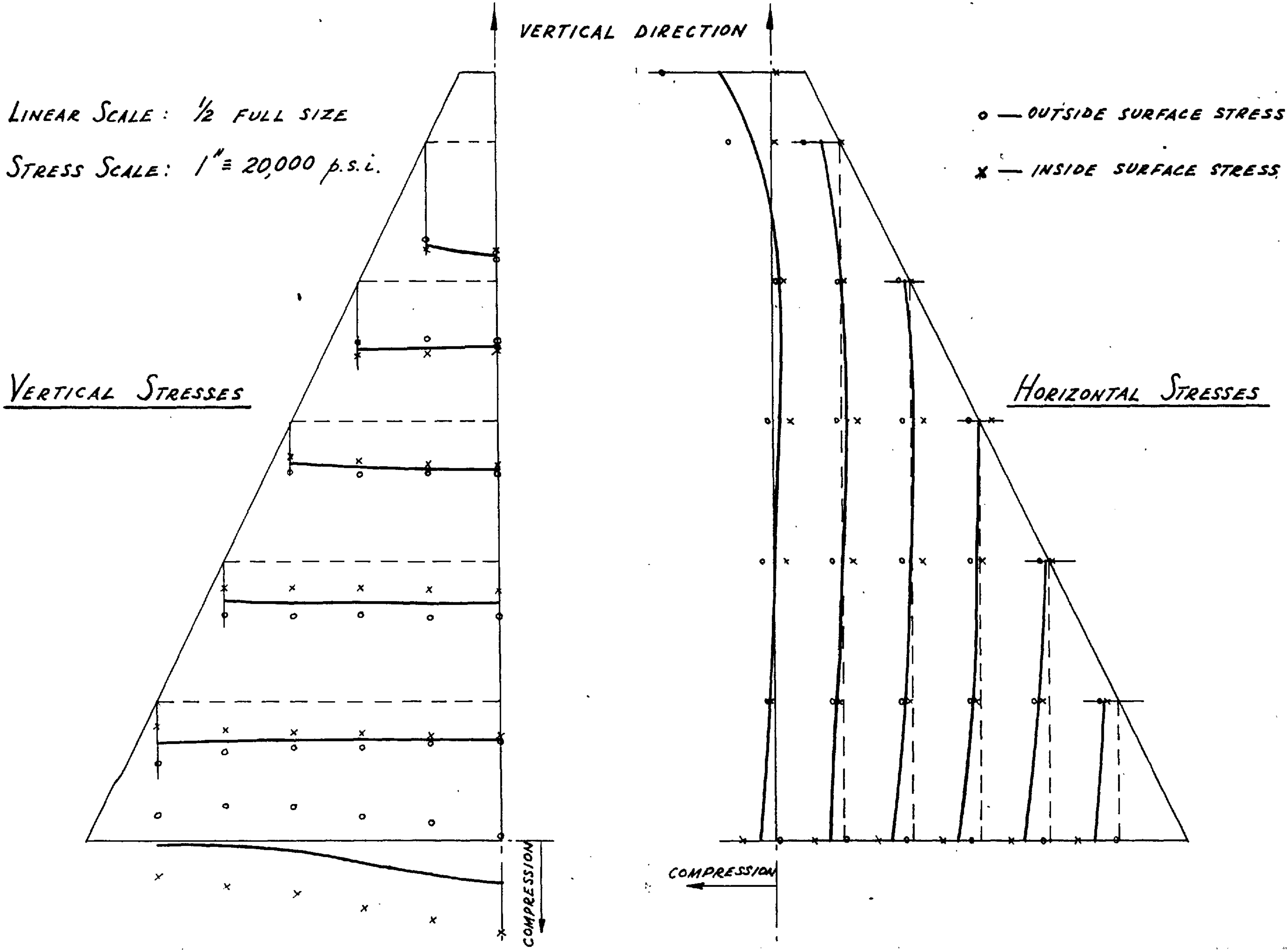

FIG. 5.14 – MID-PLANE STRESSES IN BASE PLATE. CASE 1.

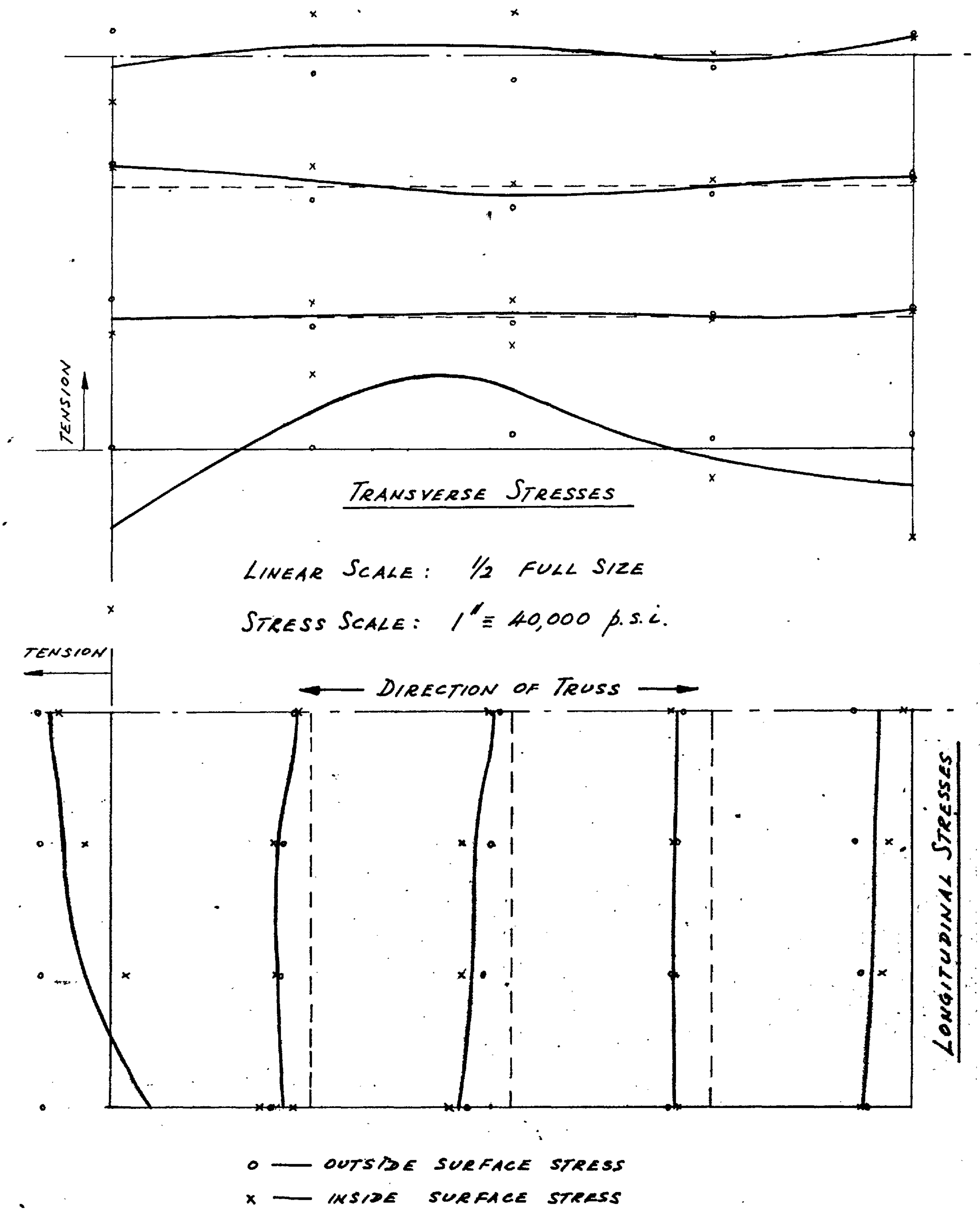

Fig. 5.15 – Mid-Plane Stress Distribution in Wall 'A'. Case 2.

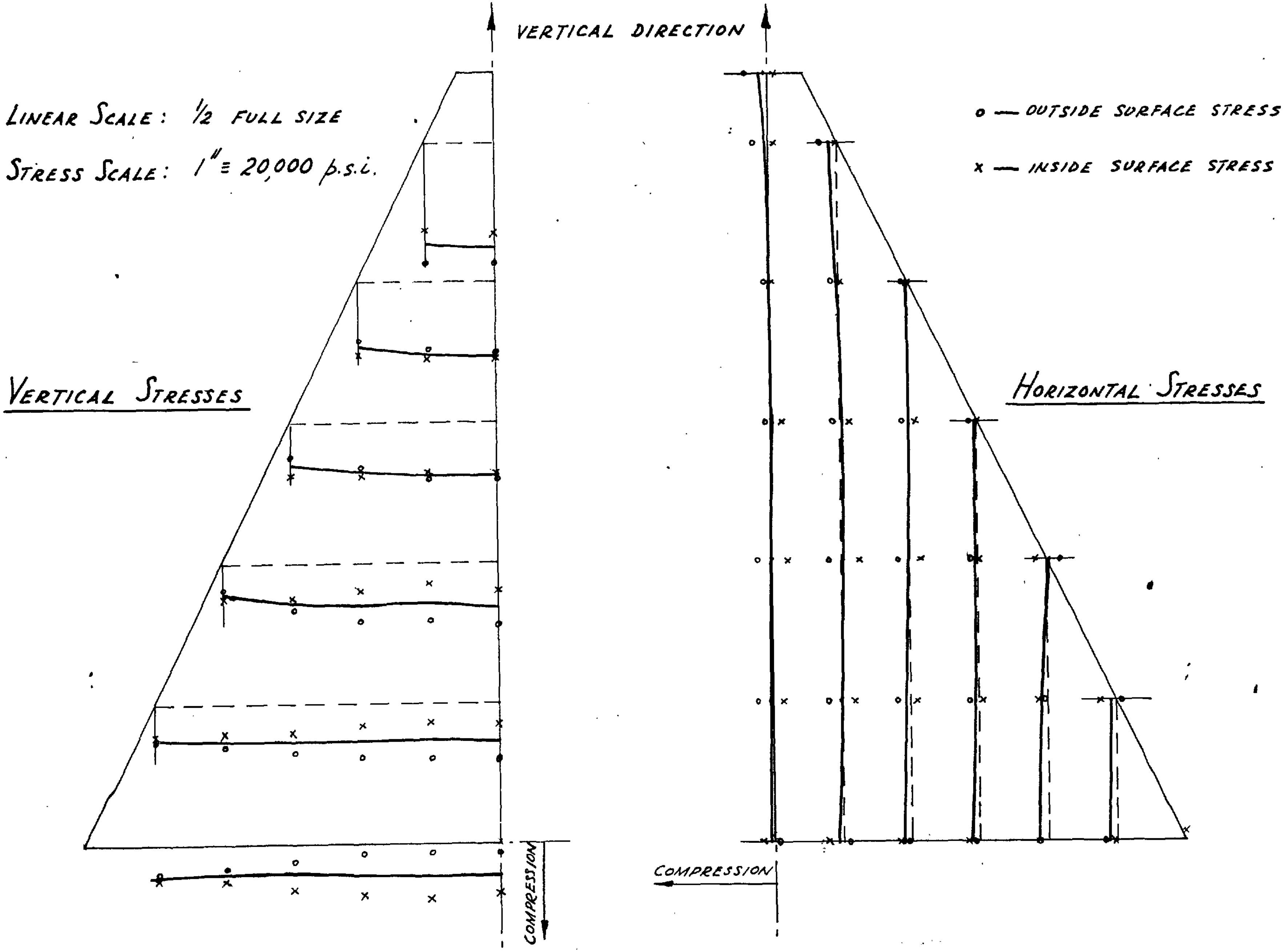

FIG. 5.16 – VERTICAL MID-PLANE STRESS DISTRIBUTION. IN WALL 'B'. CASE 2.

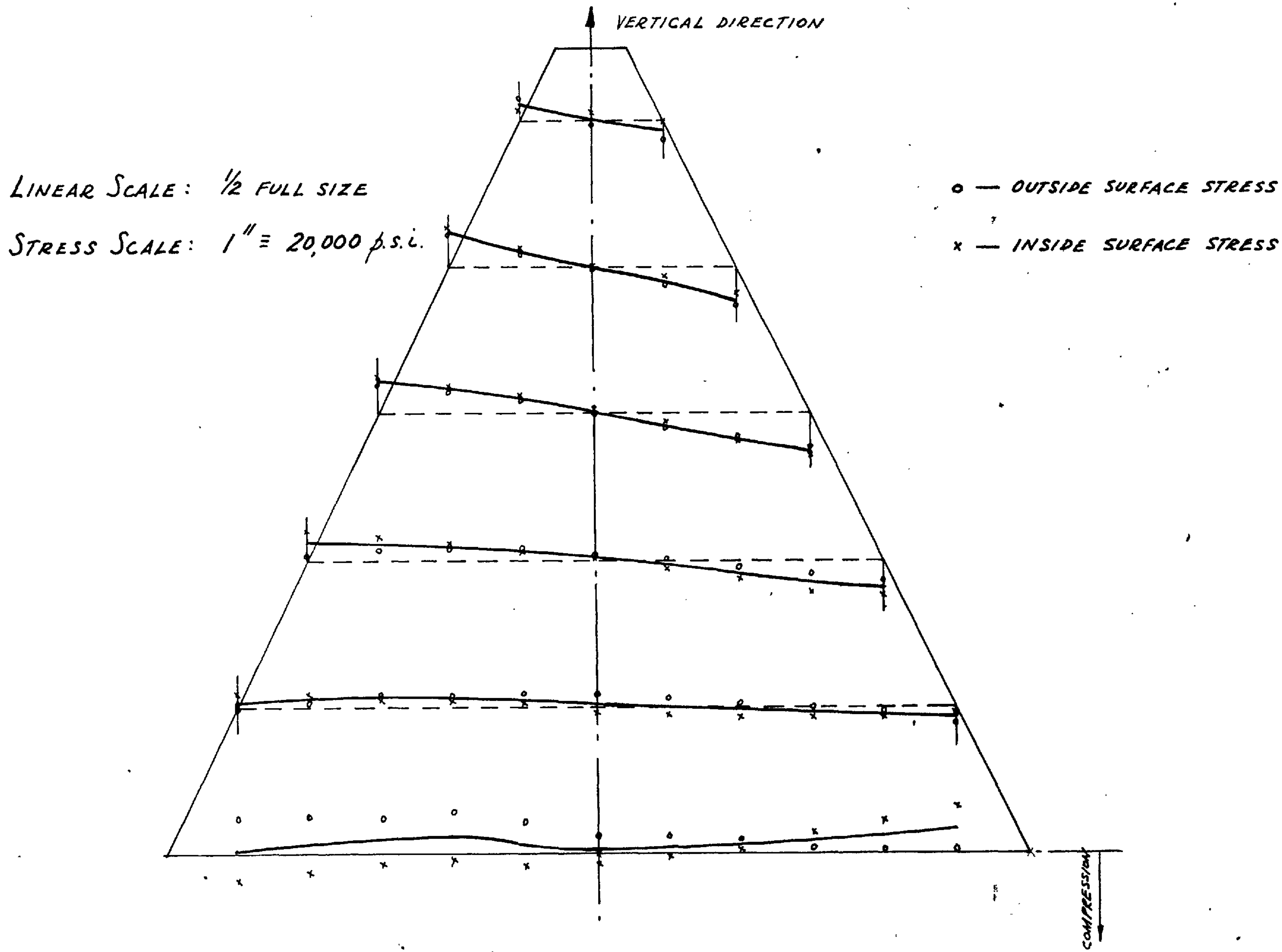

FIG. 5.17 — HORIZONTAL MID-PLANE STRESS DISTRIBUTION IN WALL 'B'. CASE 2.

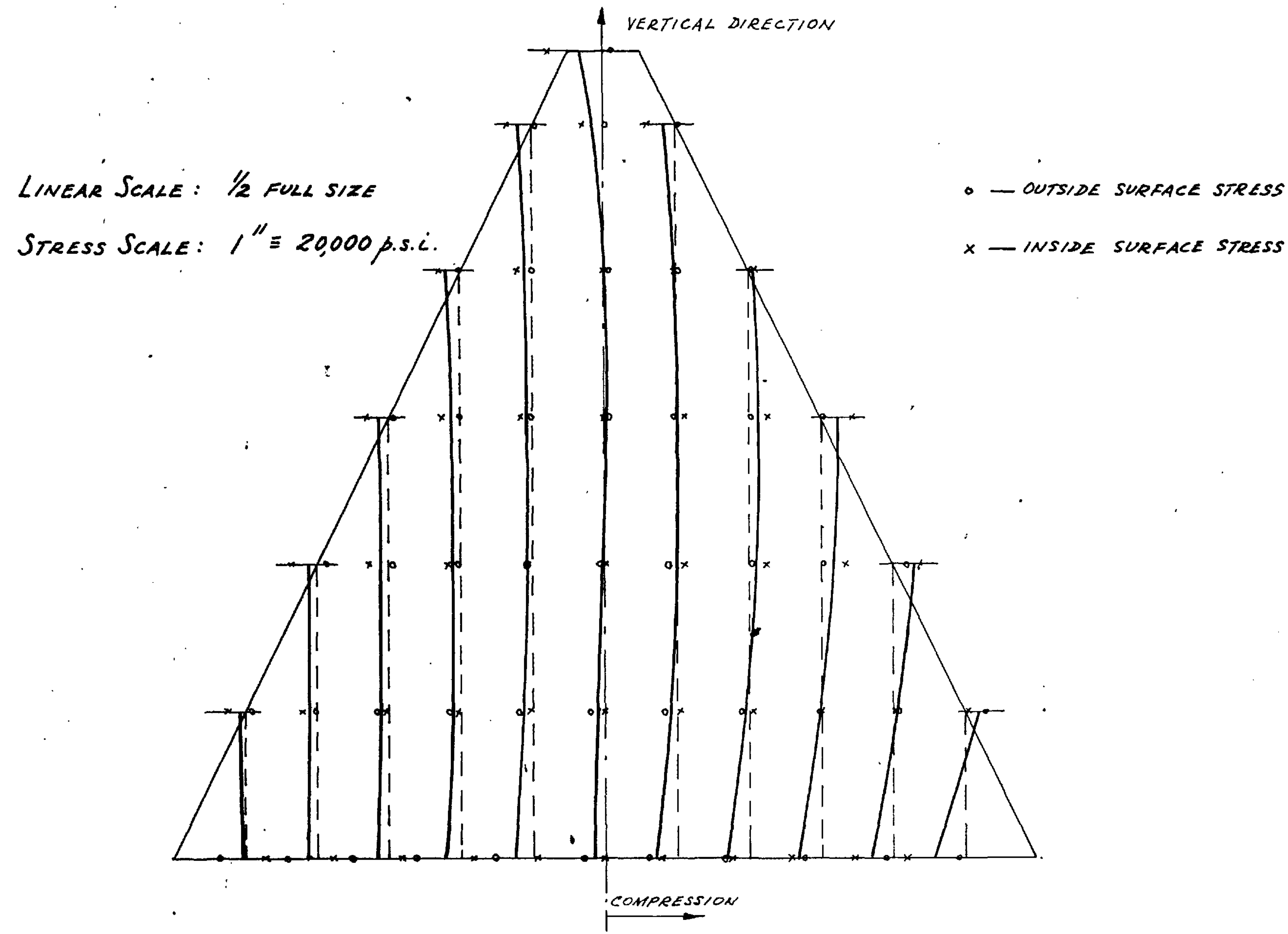

FIG. 5.18 – MID-PLANE STRESS DISTRIBUTION IN WALL 'C'. CASE 2.

LINEAR SCALE: 1/2 FULL SIZE

STRESS SCALE: 1" ≅ 20,000 p.s.i.

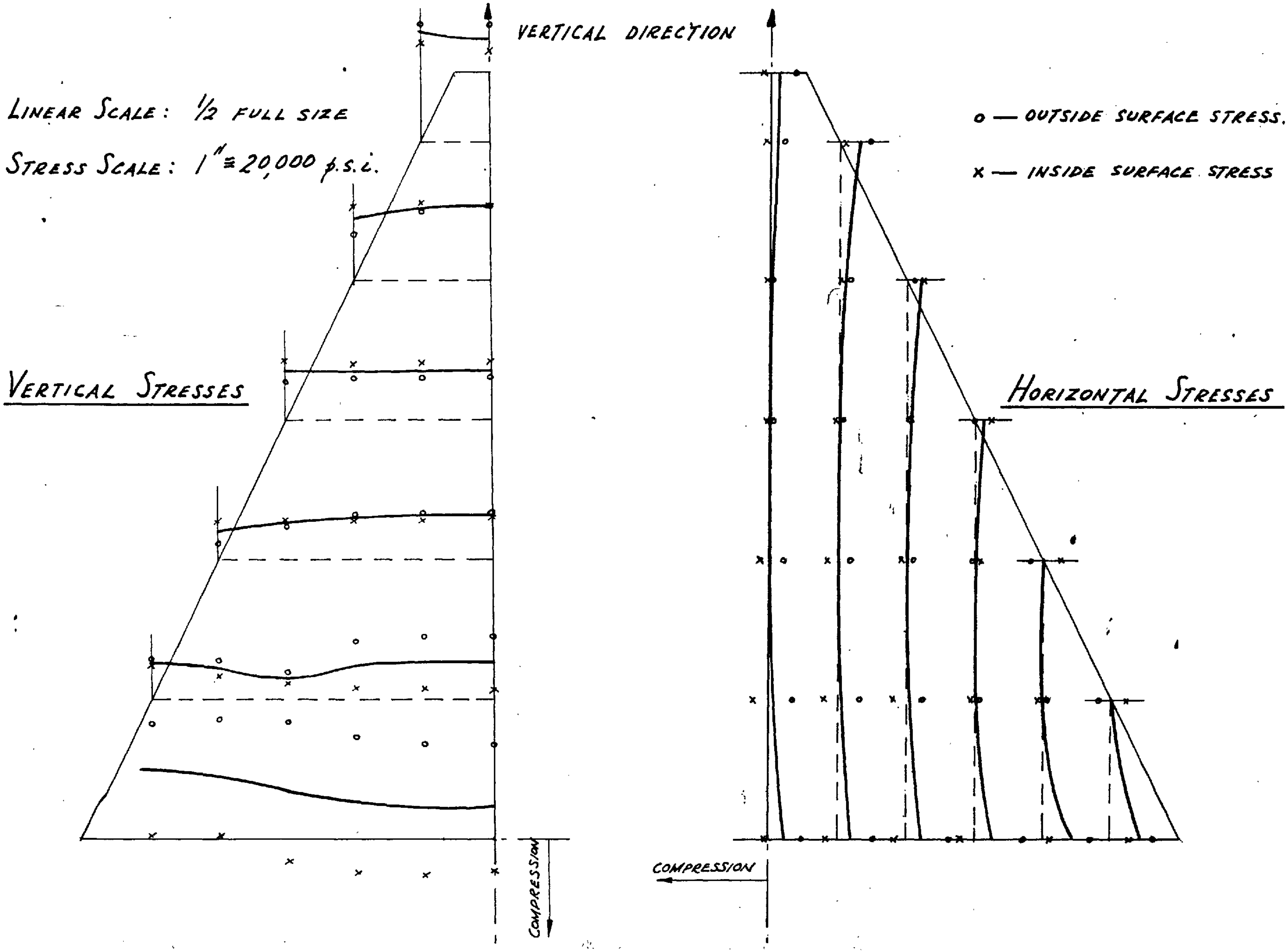

FIG. 5.19 – MID-PLANE STRESSES IN BASE PLATE. CASE 2.

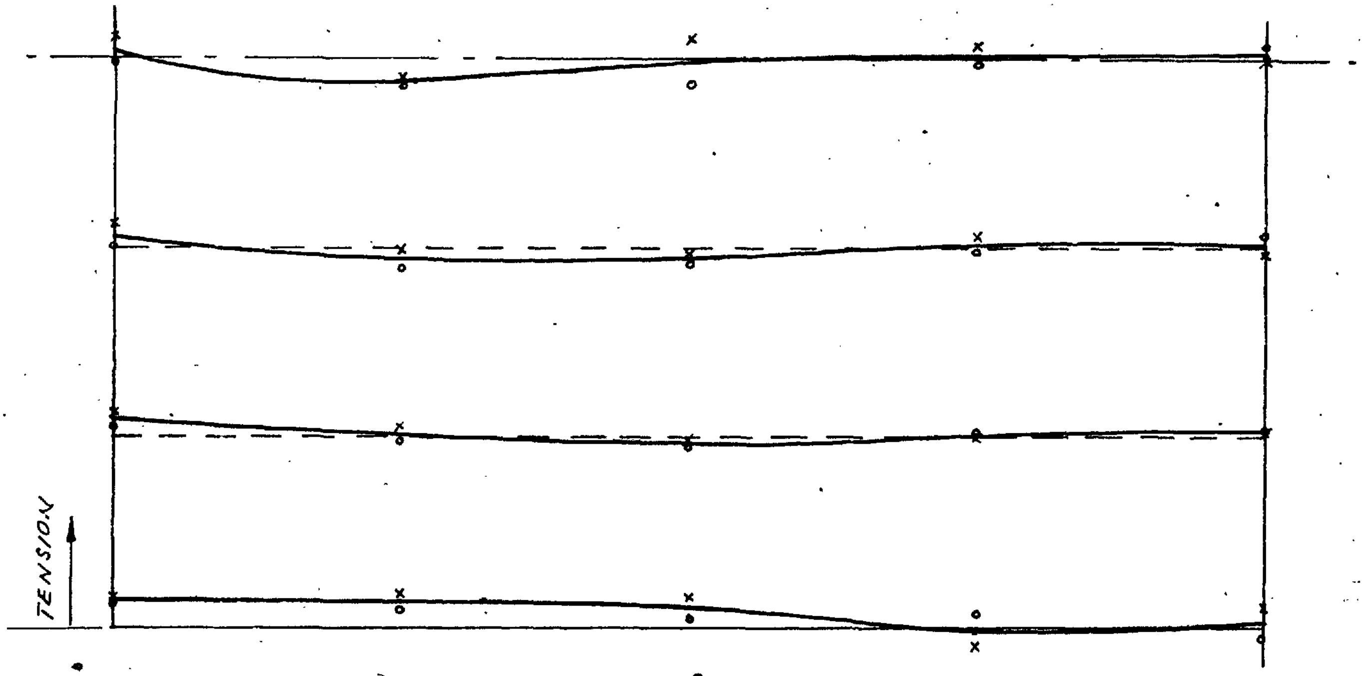

TRANSVERSE STRESSES

LINEAR SCALE: ½ FULL SIZE

STRESS SCALE: 1" ≡ 40,000 p.s.i.

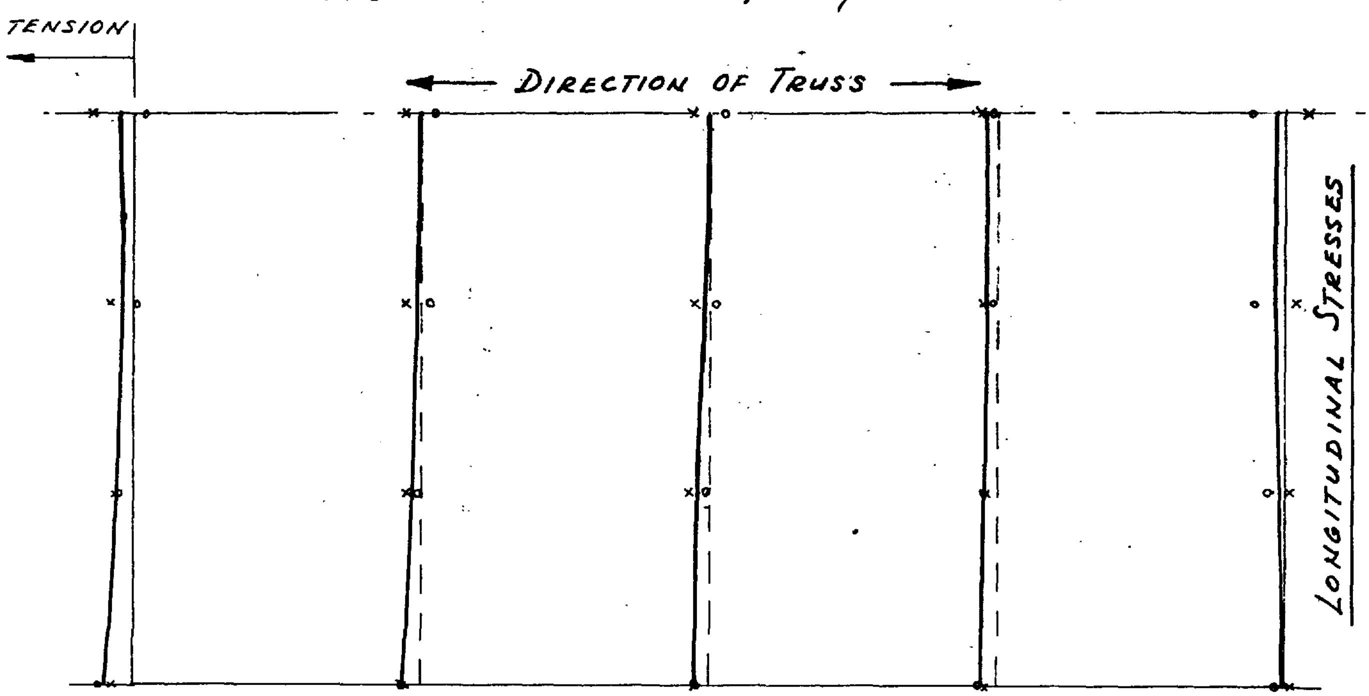

LONGITUDINAL STRESSES

o —— OUTSIDE SURFACE STRESS

x —— INSIDE SURFACE STRESS

Fig. 5.20—Mid-Plane Stress Distribution In Wall 'A'. Case 3.

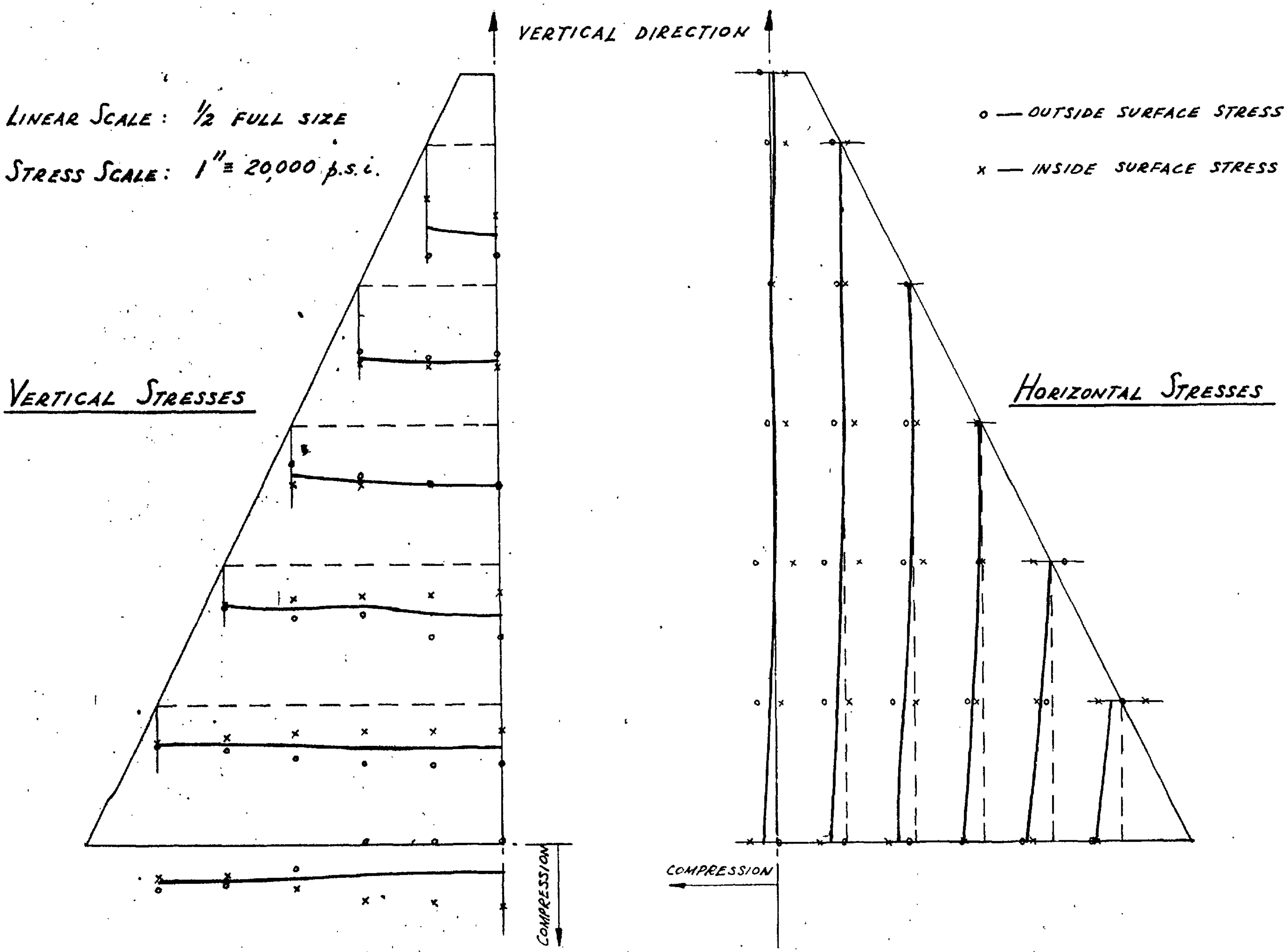

FIG. 5.21—VERTICAL MID-PLANE STRESS DISTRIBUTION IN WALL 'B'. CASE 3.

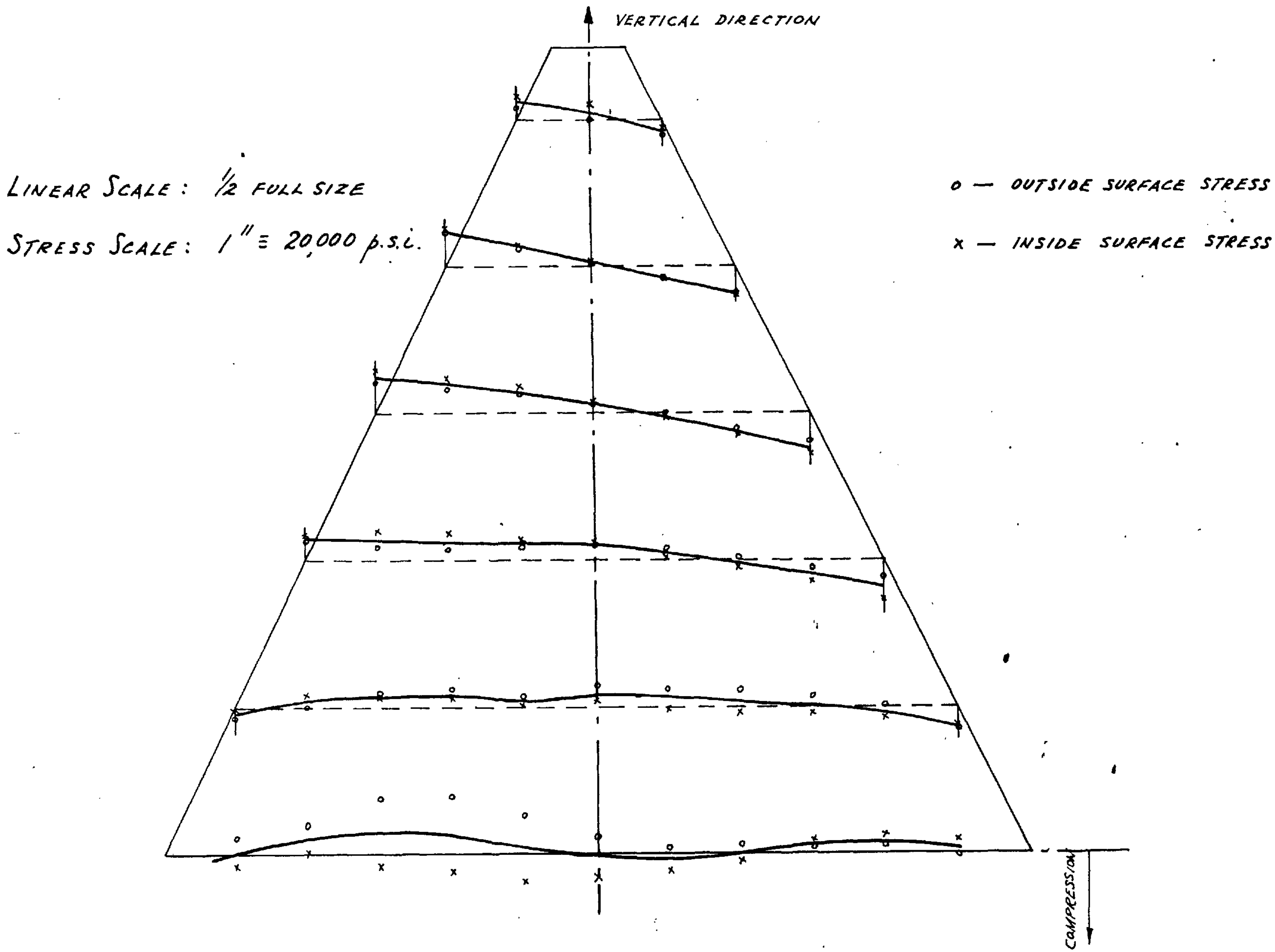

FIG. 5.22 — HORIZONTAL MID-PLANE STRESS DISTRIBUTION IN WALL 'B'. CASE 3.

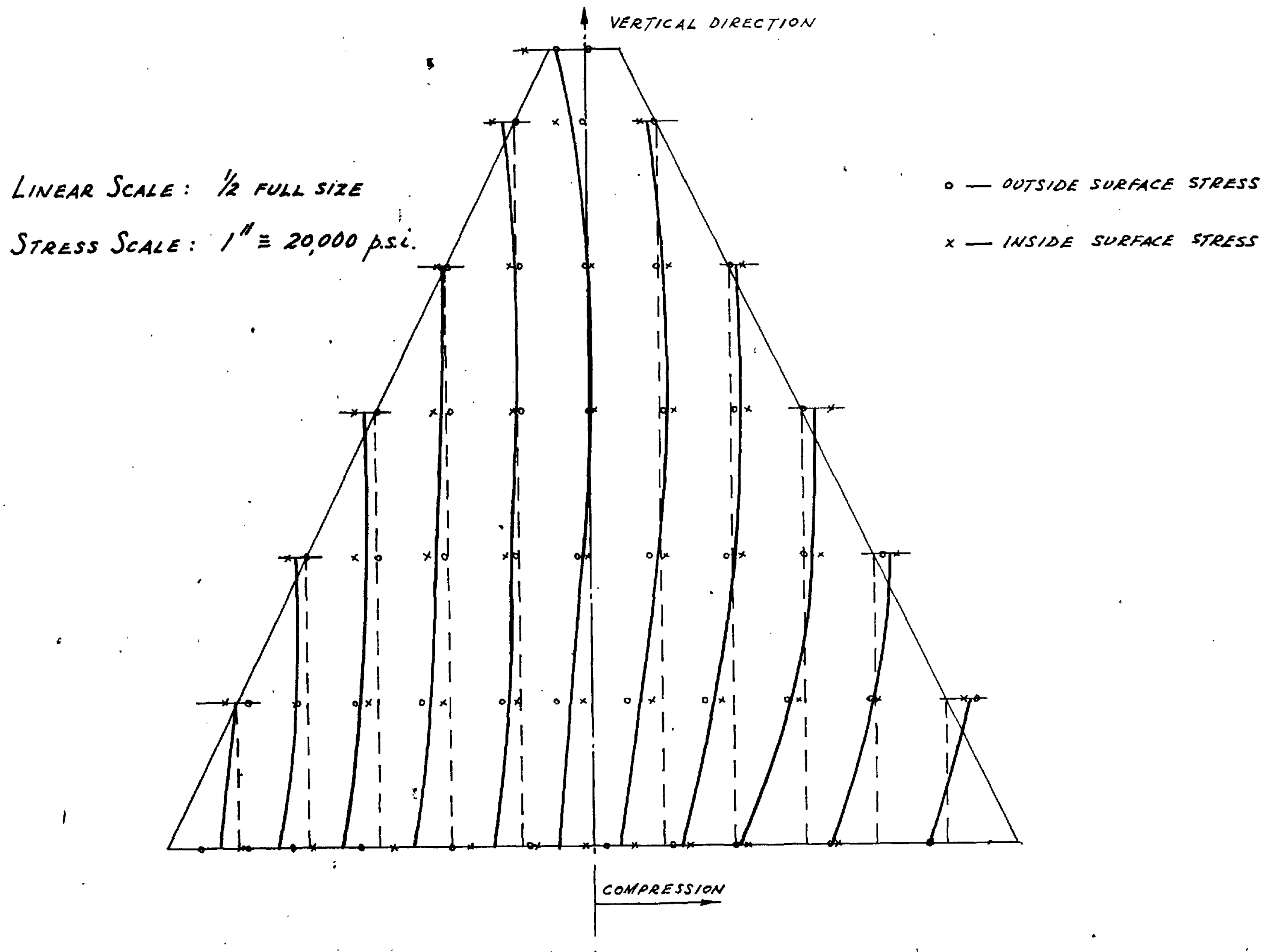

FIG. 5.23 – MID.-PLANE STRESS DISTRIBUTION IN WALL 'C'. CASE 3.

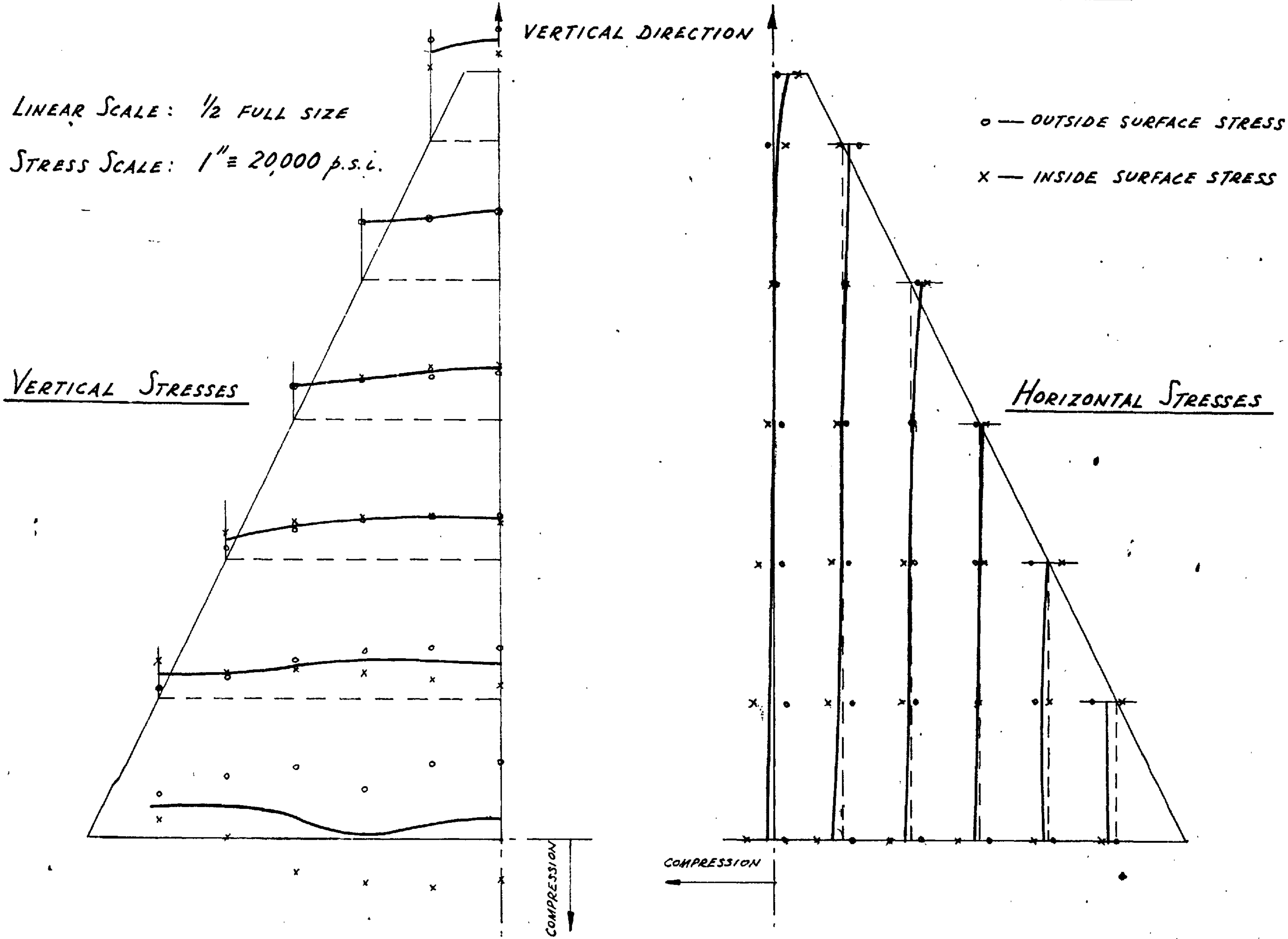

Fig. 5.24 – Mid-Plane Stresses In Base Plate. Case 3.

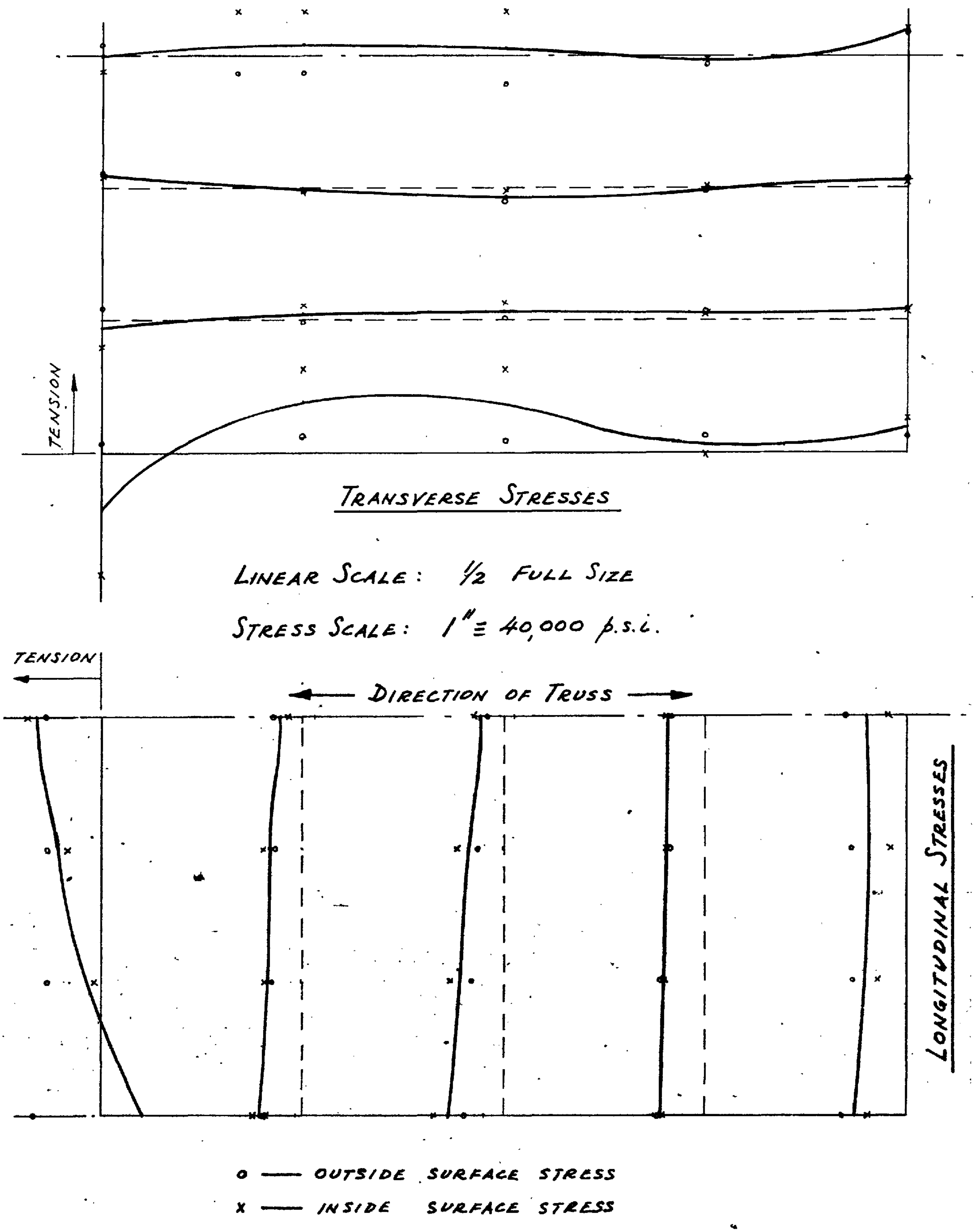

FIG. 5.25 - LOAD-DEFLECTION GRAPHS. CASE 1.

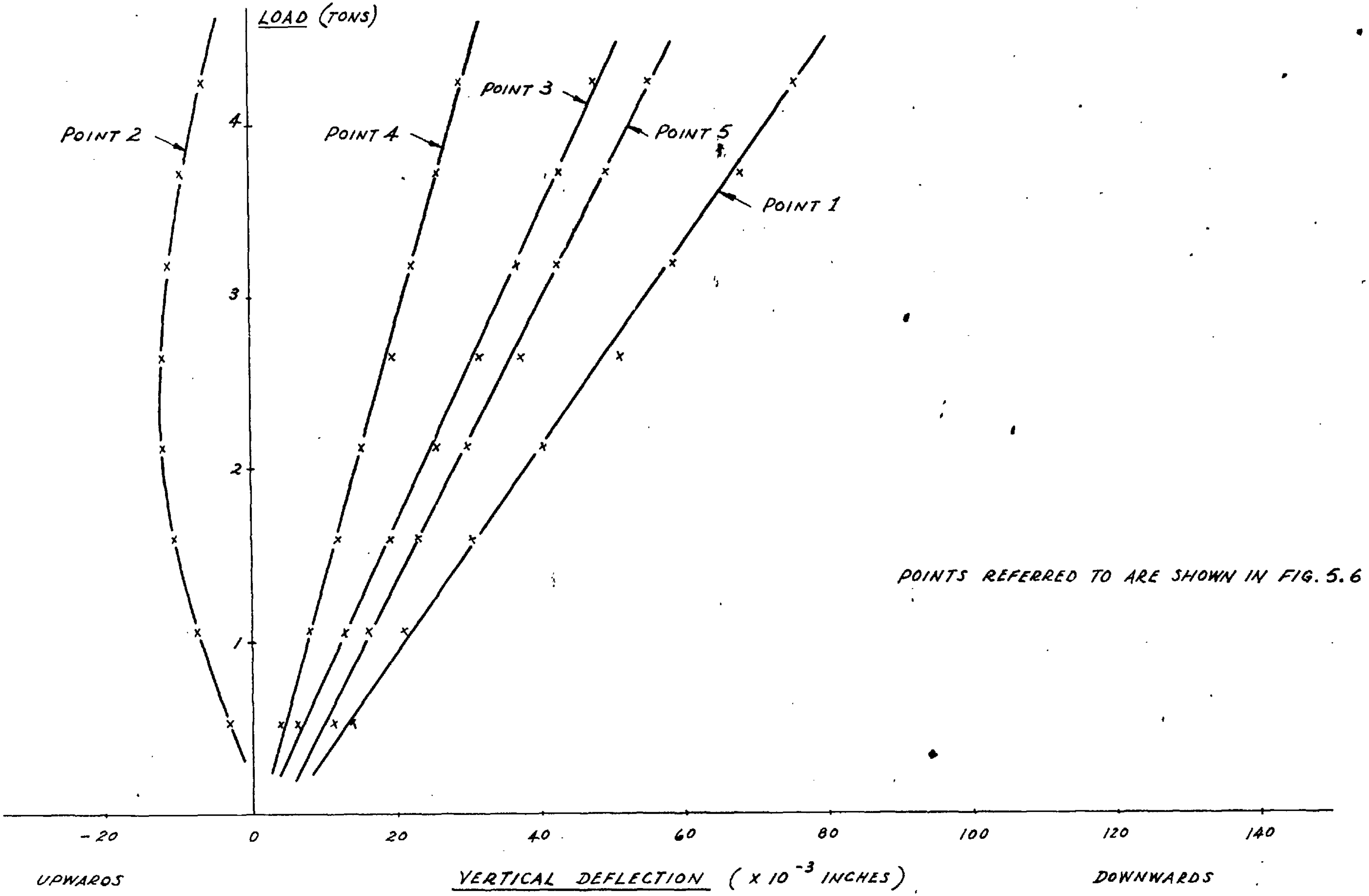

FIG. 5.26 – LOAD-DEFLECTION GRAPHS. CASE 2.

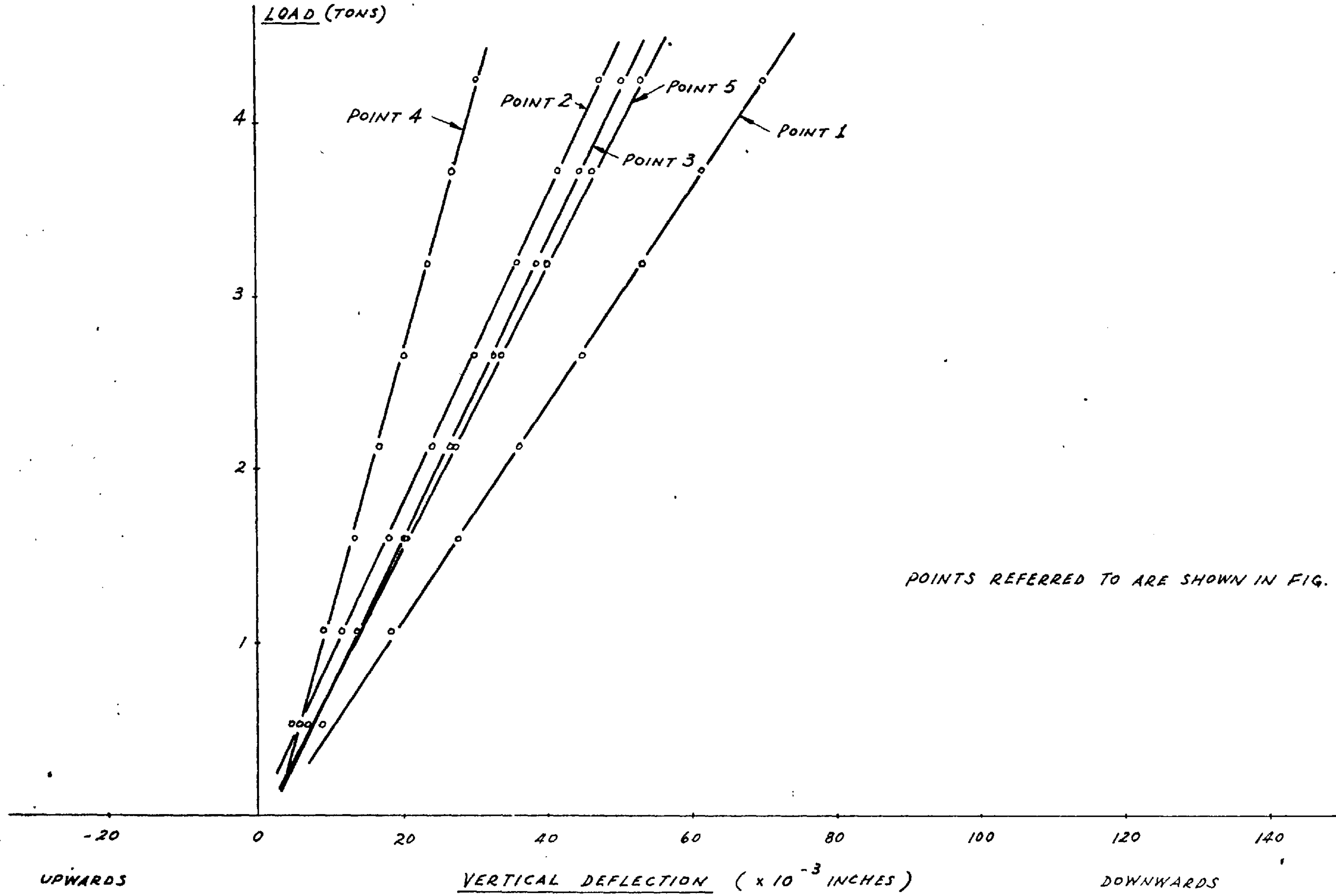

POINTS REFERRED TO ARE SHOWN IN FIG. 5.6

FIG. 5.27 – LOAD-DEFLECTION GRAPHS. CASE 3.

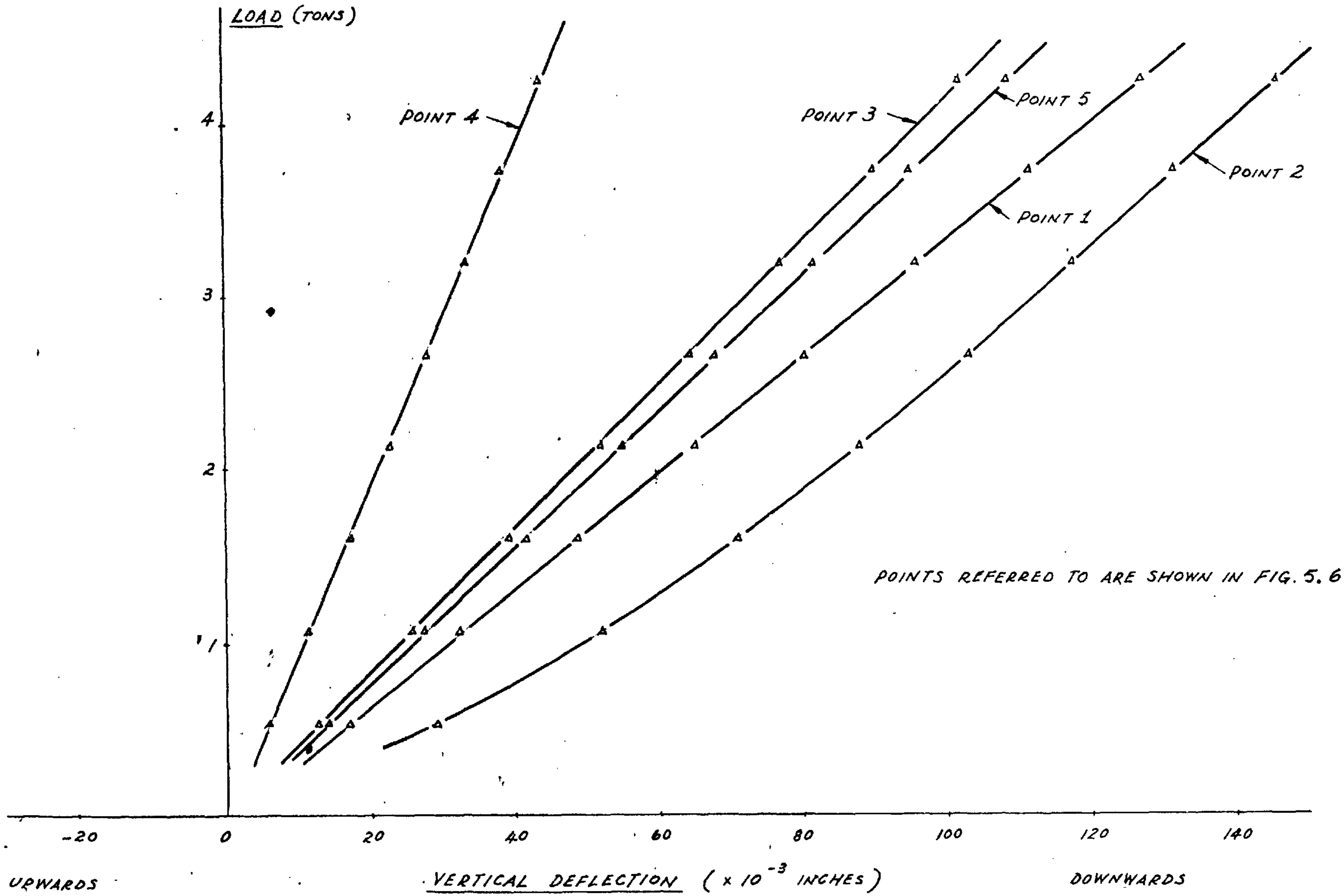

Fig. 6.1 - Trapezoidal Plate and Loading
(From Paper by B. Klein)

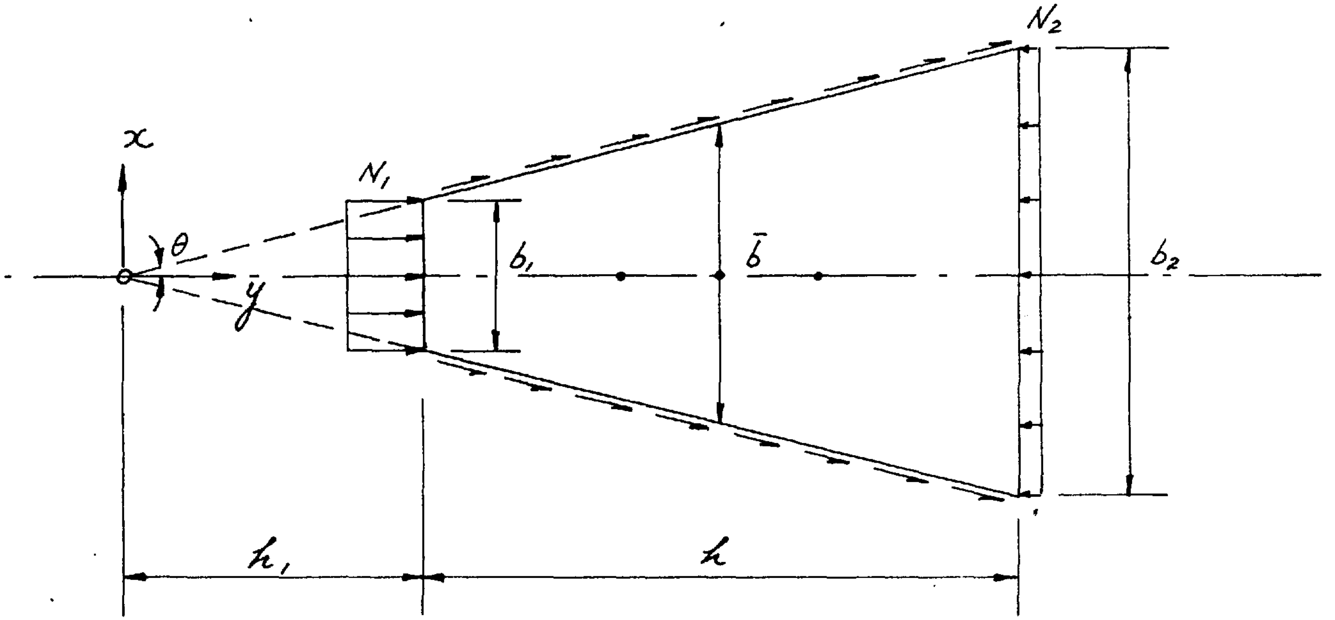

t = plate thickness.